IN VITRO TOXICITY ASSESSMENT OF DUST EMISSIONS FROM SIX SOUTH AFRICAN GOLD MINE TAILINGS SITES

Charlene Andraos

A thesis submitted to the
Faculty of Health Sciences,
School of Pathology,
Molecular Medicine and Haematology Section,
University of the Witwatersrand,
in fulfilment of the requirements for the degree of
Doctor of Philosophy

Johannesburg, 2019

DECLARATION

I, Charlene Andraos (student number: 585802), declare that this thesis is my own, unaided work. It is being submitted for the Degree of Doctor of Philosophy at the University of the Witwatersrand, Johannesburg. It has not been submitted before for any degree or examination at any other University.

_____
(Signature of candidate)

_____day of_____20_____in_____

PRESENTATIONS ARISING FROM THIS STUDY

2018: 6th NanoSafe Conference, Grenoble, France, 5 – 9 November. Oral presentation: "Non-Cancer and Cancer Risk of Communities Surrounding Gold Mine Dumps in South Africa due to Nano-Sized Silica Dust Inhalation".

2016: XIV International Congress of Toxicology, Merida, Mexico, 2 – 5 October. Poster presentation: "Possible Non-Cancer and Cancer Risk of Communities Surrounding Gold Mine Tailings Storage Facilities in Gauteng and North-West due to Silica Dust Inhalation".

2016: 7th Postgraduate Cross Faculty Symposium, Wits Medical School, South Africa, 1 March. Oral presentation: "*In Vitro* Toxicity Assessment of Dust Emissions from South African Gold Mine Tailings Sites".

2015: 7th International Symposium on Nanotechnology: Occupational and Environmental Health, Legend Golf & Safari Resort, Limpopo, South Africa, 18 - 23 October. Poster presentation: "The Use of Conventional Tests and Fluorescence Dyes in the Assessment of the Toxicity of Plasmonic Gold and Silver Nanoparticles: A Cautionary Note". Oral presentation: "*In Vitro* Toxicity Assessment of Dust Emissions from South African Gold Mine Tailings Sites".

2014: Official opening ceremony of the Phillip V. Tobias Health Sciences Building at Wits Medical School, South Africa, 29 October. Poster presentation: "Mechanisms of Interference of Engineered and Incidental Nanoparticles with Conventional Assay Systems".

2014: Wits Faculty of Health Sciences Research Day and Postgraduate Expo, Wits Medical School, South Africa, 16 September. Poster presentation: "Mechanisms of Interference of Engineered and Incidental Nanoparticles with Conventional Assay Systems".

2014: 53rd Annual Society of Toxicology (SOT) meeting, Phoenix, Arizona, USA, 23 – 27 March. Poster presentation: "*In Vitro* Toxicity Assessment of Dust Emissions from South African Gold Mine Dumps".

2013: 10th International Particle Toxicology Conference, Düsseldorf, Germany, 4 - 7 June. Poster presentation: "Mechanisms of Interference of Engineered and Incidental Nanoparticles with Conventional Assay Systems".

2011: 2nd Biennial Conference of the African Federation of Clinical Chemistry (AFCC), hosted by the Clinical Chemists Association of Kenya (CCAK) in collaboration with the Toxicology Society of South Africa (TOXSA), Kenya, 28 – 30 September. Oral presentation: "*In Vitro* Toxicity Assessment of Dust Emissions from Six South African Gold Mine Tailings Sites".

2011: Gordon Research Conference, Cellular and Molecular Mechanisms of Toxicity, Proctor Academy, New Hampshire, USA, 7 - 12 August. Oral presentation and poster presentation: "Hazard Identification of Dust Emissions from Six South African Gold Mine Tailings Sites: *In Vitro* Toxicity Assessment".

PUBLICATIONS ARISING FROM THIS STUDY

Publications:

Andraos, C., Dekker, K. and Gulumian, M. (2018a). Ambient PM_{10} and respirable dust levels near gold mine tailings storage facilities in South Africa. *CLEAN–Soil, Air, Water***,** doi: 10.1002/clen.201800103.

Andraos, C., Utembe, W. and Gulumian, M. (2018b). Exceedance of environmental exposure limits to crystalline silica in communities surrounding gold mine tailings storage facilities in South Africa. *Science of the Total Environment,* 619**,** 504-516.

The signed declaration by the student and the co-authors' agreement for the use of these published articles in this thesis is shown in **Appendix A**. Permission from the journals to reuse the content from the articles in this thesis is provided in **Appendix B**.

Technical reports submitted to the Mine Health and Safety Council (MHSC) of South Africa:

SIM 10-08-01: Gulumian, M., **Andraos, C.**, Voyi, K., and Annegarn, H. "Adverse Health Impacts Associated with Dust Emissions from Gold Mine Tailings". Year 1, quarters 1 - 4 and annual report, 2012 - 2013.

SIM 10-08-01: Gulumian, M., **Andraos, C.**, Voyi, K., and Annegarn, H. "Adverse Health Impacts Associated with Dust Emissions from Gold Mine Tailings". Year 2, quarters 1 - 4 and annual report, 2014 - 2015.

SIM 10-08-01: Gulumian, M., **Andraos, C.**, Voyi, K., and Annegarn, H. "Adverse Health Impacts Associated with Dust Emissions from Gold Mine Tailings". Year 3, quarters 1 - 4 and annual report, 2016 - 2017.

SIM 10-08-01: **Andraos, C.** and Gulumian, M. "Adverse health impacts associated with dust emissions from gold mine tailings" Final report and advisory note (Years 1 - 3). 2017.

OTHER PUBLICATION OUTPUTS DURING THE COURSE OF THIS STUDY

Publications:

Gulumian, M. and **Andraos, C.** (2018). In search of a converging cellular mechanism in nanotoxicology and nanomedicine in the treatment of cancer. *Toxicologic Pathology*, 46, 4-13.

Gulumian, M., **Andraos, C.**, Boodhia, K., et al. (2016). Nanotoxicology at the NIOH and its relevance to particle toxicology and occupational health: back to basics. *Occupational Health Southern Africa*, 22, 15-19.

Gulumian, M., Verbeek, J., **Andraos, C.**, et al. (2016). Systematic review of screening and surveillance programs to protect workers from nanomaterials. *PLoS One*, 11, e0166071.

Sanabria, N. M., Vetten, M., **Andraos, C.**, et al. (2014). Gold nanoparticle interference study during the isolation, quantification, purity and integrity analysis of RNA. *PLoS One*, 9, e114123.

Vetten, M. A., Tlotleng, N., Rascher, D. T., Skepu, A., Keter, F. K., Boodhia, K., Koekemoer, L-A., **Andraos, C.** (2013). Label-free *in vitro* toxicity and uptake assessment of citrate stabilised gold nanoparticles in three cell lines. *Particle and Fibre Toxicology*, 10, 50.

Technical Reports:

Gulumian, M., de Jager, P., Masoka, X., Vetten, M., **Andraos, C.**, Boodhia, K., Koekemoer, L., Sanabria, N., Matatiele, P., Singh, E. Nanotechnology in South Africa: A Baseline Study. Commissioned by the Department of Science and Technology (DST), March 2014.

Gulumian, M., Verbeek, J., **Andraos, C.**, Sanabria, N., de Jager, P. Surveillance programmes to protect workers from potential risks of manufactured nanomaterials: a systematic review. Submitted to the World Health Organisation (WHO), November 2015.

ABSTRACT

Decades of mining in South Africa have produced waste material, which was deposited in numerous gold mine tailings storage facilities (TSFs). These TSFs have contributed to air pollution due to the lack of proper rehabilitation measures needed to mitigate erosion. Indeed, human populations residing in close proximity to these TSFs have raised concern about high dust levels and the onset of respiratory-related symptoms possibly caused by tailings emissions.

Currently, South Africa does not have an efficient routine air monitoring system in residential areas of surrounding communities to determine the extent of air pollution. Moreover, it is not as yet known whether these tailings dusts are toxic and could be the cause of such ill effects. In addition, the physicochemical properties that may govern their toxicity have not as yet been identified.

The present study has therefore conducted a risk assessment to:

- **Determine the toxicity of the dust emitted from five TSFs situated in the Gauteng and North West Provinces of South Africa (*Hazard Identification*):** Bulk dust samples were collected from the TSFs and sieved to enrich the airborne particle fraction. Thereafter, physicochemical analysis on these particles were conducted i.e. size distribution analysis, analysis of specific surface area, shape and surface elemental composition, mineral composition, total elemental composition and surface activity. In addition, the potential toxicity of the particles was assessed *in vitro* using two human lung-derived cell lines i.e. BEAS-2B epithelial and U937 monocytic-macrophage cells. Toxicity assessment included label-free toxicity analysis as well as assessment of the degree of cellular internalisation.
- **Assess the levels of PM_{10} and PM_4 dust as well as crystalline silica levels in environmental and personal filter samples (*Exposure Assessment*):** Continuous real-time ambient PM_{10} at residential areas close to three TSFs were recorded and ambient PM_{10} were also collected on filters for silica content analysis. Furthermore, PM_4 was collected from personal samplers attached to school children at schools located at various

distances from all five TSFs for silica content analysis i.e. respirable crystalline silica (RCS).

- **Calculate the potential risk for the surrounding communities *(Risk Characterisation)*:** Cancer and non-cancer endpoints were used to calculate the potential risk of surrounding communities from lifetime exposure to inhalation of RCS.

The results from *Hazard Identification* show that all tailings dusts exhibited *in vitro* toxicity, more so in the BEAS-2B cell line compared to the U937 cell line. This toxicity could have been governed either by their elemental composition or a combination of other physicochemical properties. The results from *Exposure Assessment* showed that the ambient PM_{10} levels in surrounding populations exceeded the current South African limit of 75 µg/m^3 by several fold (i.e. three to four times). Furthermore, the RCS levels collected from PM_4 from surrounding communities exceeded the current international interim RCS limit of 3 µg/m^3.

Finally, *Risk Characterisation* revealed surrounding communities to possibly develop non-cancer adverse health effects as hazard quotients as high as higher than 1 was calculated. Moreover, calculations of cancer adverse health effects also showed possible risk of regulatory concern as more than 1 individual per 1000 could potentially develop cancer when exposed to RCS levels recorded in this study. One site in particular showed an HQ of 11.6 (non-cancer) and the possibility of more than 2 individuals per 1000 to possibly develop cancer.

This study could therefore provide mechanistic evidence to support future epidemiological studies attempting to link tailings dust exposure to adverse health effects. In addition, this study could serve as a starting point for future ambient and personal sampling campaigns and suggests that a RCS interim exposure limit, particularly for South Africa, be established.

ACKNOWLEDGEMENTS

My eternal gratitude goes out to:

My supervisor, Prof Mary Gulumian, for her guidance, patience and support throughout the duration of this project.

The Mine Health and Safety Council of South Africa for the funding provided for this study. This project was a collaborative effort between the National Institute for Occupational Health (NIOH), the University of Pretoria and the University of Johannesburg. Collection of bulk dust samples and collection of ambient PM_{10} and PM_4 on filters were conducted by Dr Ojelede and Dr Nkozi.

My parents, Billy and Adri, for their unconditional support and encouragement, not only during my PhD studies but throughout my scientific career and life in general. This would not have been possible without you.

CONTENTS

ABBREVIATIONS

µm, micrometer
•OH, hydroxyl radical
ACGIH, American Conference of Governmental Industrial Hygienists
AGA, Anglo Gold Ashanti
AM, alveolar macrophage
AMD, acid mine drainage
AMP, adenosine monophosphate
AP-1, activator protein-1
APD, avalanche photodetector
APS, aerodynamic particles sizer
AQA, Air Quality Act
AQM, Air Quality Management
AQMP, Air Quality Management Plan
As, arsenic
ASTER, Advanced Spaceborne Thermal Emission and Reflection Radiometer
AT, averaging time
ATCC, American Type Culture Collection
ATP, adenosine Triphosphate
ATSDR, Agency for Toxic Substances and Disease Registry
Au, gold
Ba, barium
BDL, below detection limit
BEAS-2B, human bronchial epithelial cell line
BET, Brunauer-Emmett-Teller
BMD, benchmark dose
BMC, benchmark concentration
BTF, Brakpan tailings facility
C, carbon
CA, concentration in air
$CaCO_3$, calcium carbonate
CB, carbon black
CCME, Canadian Council of Ministers of the Environment
Cd, cadmium
CD14, cluster of differentiation 14
CDC, Centre for Disease Control and Prevention
CFA, coal fly ashes
CGR, Crown Gold Recoveries
CGS, Council for Geoscience
CI, cell index
CIL, carbon-in-leach
CIP, carbon-in-pulp
CN, cyanide
Co, cobalt

CO_2, carbon dioxide
CoGTA, Department of Cooperative Governance and Traditional Affairs
Comet, single-cell gel electrophoresis
CPC, condensation particle counter
Cr, chromium
CSF, cancer slope factor
Cu, copper
CuO, copper oxide
CWP, coal workers' pneumoconiosis
CYP, cytochrome P450
DAC, Department of Arts and Culture
DAFF, Department of Agriculture, Forestry and Fisheries
DANCED, Danish Co-operation for Environment and Development
DEA, Department of Environmental Affairs
DEP, diesel exhaust particulate
dH_2O, distilled water
DHS, Department of Human Settlement
DMA, Differential Mobility Analyser
DMPO, 5,5-Dimethyl-1-Pyrroline-N-Oxide
DMR, Department of Mineral Resources
DP, Department of Police
DPBS, Dulbecco's phosphate buffered saline
DRD, Durban Roodepoort Deep
DRD&LR, Department of Rural Development and Land Reform
DST, Department of Science and Technology
DWA, Department of Water Affairs
E, east
EC, exposure concentration
ECM, extracellular matrix
ED, exposure duration
EDTA, ethylene diamine tetra acetic acid
EF, exposure frequency
ENE, east-northeast
EPA, Environmental Protection Agency
EPFR, environmentally persistent free radical
ERPM, East Rand Proprietary Mines
ESE, east-southeast
ESR, electron spin resonance
ET, exposure time
FBS, foetal bovine serum
FDA, Food and Drug Administration
Fe, iron
Fe^{+2}, ferrous iron
Fe^{+3}, ferric iron
$FeCl_2$ ferrous chloride
FeO, iron oxide

$Fe(OH)_2$, iron (II) hydroxide
FeS_2, pyrite
$FeSO_4$, ferrous sulfate
GCRO, Gauteng City-Region Observatory
GDACE, Gauteng Department of Agriculture Conservation and Environment
GDARD, Gauteng Department of Agriculture and Rural Development
GDCS, Gauteng Department of Community Safety
GDEDP, Gauteng Department of Economic Development and Planning
GDHSD, Gauteng Department of Health and Social Development
GDLGH, Gauteng Department of Local Government and Housing
GIS, Geographical Information System
GOP, Gauteng Office of the Premier
GPDMC, Gauteng Provincial Disaster Management Centre
GSD, geometric standard deviation
H_2O_2, hydrogen peroxide
HCl, hydrochloric acid
Hf, hafnium
HF, hydrofluoric acid
Hg, mercury
Hg^0, mercury
Hg^{+1}, mercurous mercury
Hg^{+2}, mercuric mercury
HI, hazard index
HIS, hyperspectral imaging system
HNO_3, nitric acid
HQ, hazard quotient
IARC, International Agency for Research on Cancer
ICP-AES, inductively coupled plasma atomic emission spectroscopy
ICP-MS, inductively coupled plasma mass spectroscopy
ICRP, International Commission on Radiological Protection
Ig, immunoglobulin
IL, interleukin
Ir, iridium
IRIS, Integrated Risk Information System
IURs, inhalational unit risks
Kr, krypton
LDH, lactate dehydrogenase
LOAEL, lowest observed adverse effect level
LRR, leucine-rich-repeat
MAK, Maximale Arbeitsplatz Konzentration
MAPK, mitogen-activated protein kinase
MCE, mixed cellulose ester
Mg, magnesium
MHSC, Mine Health and Safety Council, South Africa
MI, myocardial infarction
MMAD, median mass aerodynamic diameter

Mn, manganese
MnO, manganese oxide
MnO_2, manganese dioxide
Mo, molybdenum
MPRDA, Mineral and Petroleum Resources Development Act
MRA, Mine Residue Area
MTT, 3-(4,5-Dimethyl-2-thiazolyl)-2,5-diphenyl-2H-tetrazolium bromide
N, north
N_2, nitrogen
NAAQS, South African National Ambient Air Quality Standard
NACHT, NAIP (neuronal apoptosis inhibitory protein), CIITA (MHC class II transcription activator), HET-E (incompatibility locus protein from *Podospora anserina*) and TP1 (telomerase-associated protein)
NAD+, oxidized nicotinamide adenine dinucleotide
NAD(P)H, reduced nicotinamide adenine dinucleotide (phosphate)
Nb, niobium
NCI, normalised CI
NDMC, National Disaster Management Centre
NE, northeast
NEMA, National Environment Management Act
NF-κB, nuclear factor-κB
Ni, nickel
NIH, National Institutes of Health
NLRP3, NACHT, LRR and PYD domains-containing protein 3
Nm, nanometer
NNE, north-northeast
NNR, National Nuclear Regulator
NNW, north-northwest
NOAEL, no observed adverse effect level
NP, nanoparticle
NQO, NAD(P) H:quinone oxidoreductase
Nrf2/ARE, nuclear factor E2-related factor 2/ antioxidant responsive element
NS, not significant
NTP, National Toxicology Program
NW, northwest
O, oxygen
$^1O_2$, singlet oxygen
$O_2^{\bullet-}$, superoxide anion radical
OEHHA, Office of Environmental Health Hazard Assessment
OSHA, Occupational Safety and Health Administration
PAH, polycyclic aromatic hydrocarbons
Pb, lead
$PbCO_3$, cerussite
PbS, galena
$PbSO_4$, anglesite
Pd, pore diameter

Pd, palladium
PEL, permissible exposure limit
PM, particulate matter
PMA, phorbol-12-myristate-13 acetate
PMS, N-methyl dibenzopyrazine methyl sulphate
PNOC/R, particles not otherwise classified/regulated
POD, point of departure
PPi, pyrophosphate
Pt, platinum
PV, pore volume
PYD, pyrin domain
RBC, red blood cells
RCS, respirable crystalline silica
R*f*C, reference concentration
RfD, reference dose
Rh, rhodium
RLE, rat lung epithelial
ROFA, residual oil fly ash
ROS, reactive oxygen species
RPM, revolutions per minute
RPMI, Roswell Park Memorial Institute
RR, relative risk
RTCA, real-time cell analyser
S, south
SAAQIS, South African Air Quality Information System
SAHRA, South African Heritage Resources Agency
SAM, Spectral Angle Mapper
SAWS, South African Weather Service
Sb, antimony
Sc, scandium
SD, standard deviation
SE, southeast
SEA, State of Environment Report
SEM-EDX, scanning electron microscopy with energy dispersive X-ray spectroscopy
Si, silicon
SiO_2, silica
Si-OH, silanol
SMPS, Scanning Mobility Particle Sizer
Sn, tin
SOD, superoxide dismutase
SP, single plate
SR, scavenger receptor
SSE, south-southeast
SSPD, Small-Scale Powder Disperser
SSW, south-southwest
SW, southwest

Syk, spleen tyrosine kinase
Ta, tantalum
Ti, titanium
TLR, toll-like receptor
TLV, threshold limit value
TM, thematic mapper
TSF, tailings storage facility
TSP, total suspended particle
TWA, time weighted average
U, uranium
U937, macrophage-like monocytic cell line
UFPs, ultrafine particles
UJ, University of Johannesburg
UO_2, uraninite
US, United states
UV-vis, ultraviolet - visible
V, vanadium
W, tungsten
W, west
WHO, World Health Organization
WNW, west-northwest
WSW, west-southwest
XRD, X-ray diffraction
Y, yttrium
Zn, zinc
Zr, zirconium

LIST OF FIGURES

LIST OF TABLES

1. INTRODUCTION

Mining in the goldfields of the Witwatersrand basin formed an integral part of South Africa's rich history. Activities on these mines have however also produced waste material, which has inevitably resulted in the deposition of hundreds of mine tailings storage facilities (TSFs), more commonly known as mine dumps. These TSFs became a fixture on the South African landscape covering approximately 400 km^2 of land. The majority of these TSFs either lay dormant and, due to neglect or poor design, do not exhibit efficient rehabilitation measures or are currently being reclaimed in order to further extract residual gold still present in the tailings material. Whether dormant or reclaimed, these TSFs are subjected to water and wind erosion thereby contributing to water, soil and air pollution. Throughout the years, studies have mainly focused on the contribution of TSFs to acid mine drainage and its effects on the ecosystem. However, studies addressing the contribution of TSFs to air pollution and the effects on the surrounding environment are surprisingly limited, despite the public outcry of surrounding communities complaining of dust-related adverse health effects.

In order to determine whether tailings material emitted from TSFs could pose a risk to communities, the current study sought to assess the inherent toxicity of these tailings particles and whether the toxicity observed could have been governed by their physicochemical properties (discussed under *Hazard Identification*).

The level of exposure of the surrounding communities to these dusts is also important in determining whether tailings material pose a risk and therefore their levels were evaluated in the environmental PM_{10} and personal PM_4 samples collected (discussed under *Exposure Assessment*). It is imperative to note that the mine dust generated from gold mines is likely to contain crystalline silica. Over the years, the focus was mainly on occupationally-based exposures to crystalline silica-containing dusts and it is only in recent years that the focus has been broadened to include non-occupational (or environmental) exposures. Subsequently, in addition to PM levels in the environmental and personal samples, the content of crystalline silica was quantified in the current study. *Risk Characterisation* was then conducted in which the respirable crystalline silica levels obtained from the PM_4 sampling was used to calculate the

possibility of developing cancer and non-cancer adverse health effects in surrounding populations following chronic life-time exposure.

In this thesis, the above presented outline of work conducted is presented in the conventional monograph 'block' format and is divided into the following chapters:

The Literature Review chapter **(Section 2)** contains a description of the history of gold mining in South Africa, the activities of which resulted in the production of tailings waste contributing to air pollution and possibly producing ill effects in the surrounding communities **(Section 2.1)**. The potential for tailings particles to exhibit an inherent toxicity based on their physicochemical properties is then discussed in **Section 2.2**. The potential of tailings particles to reach surrounding environments is subsequently addressed in **Section 2.3** and thereafter the susceptibility of vulnerable populations to this exposure is presented in **Section 2.4**. This is followed with a discussion on the challenges involved in the rehabilitation of these TSFs **(Sections 2.5)** as well as challenges currently faced in the South African legislation and governance **(Section 2.6)**. Finally, the chapter ends with a summary of previously published studies assessing risk of tailings material on surrounding populations **(Section 2.7)** as well as the research question for the current study.

In the Materials and Methods chapter **(Section 3)** the methodologies used for each of the major objectives of this study i.e. *Hazard Identification* **(Section 3.1)**, *Exposure Assessment* **(Section 3.2)** and *Risk Characterisation* **(Section 3.3)** are presented.

In the Results chapter **(Section 4)** a detailed description of the results obtained for each of the major objectives i.e. *Hazard Identification* **(Section 4.1)**, *Exposure Assessment* **(Section 4.2)** and *Risk Characterisation* **(Section 4.3)** are provided.

In the Discussion chapter **(Section 5)** an interpretation of the results in *Hazard Identification* **(Section 5.1)**, *Exposure Assessment* **(Section 5.2)** and *Risk Characterisation* **(Section 5.3)** are presented. This chapter ends with the limitations of this study as well as recommendations.

In the Conclusion chapter **(Section 6)**, a summary of the major findings of this study is presented.

2. LITERATURE REVIEW

2.1. Mining

2.1.1. History of mining in South Africa

South Africa consists of several well-known gold fields including the Witwatersrand gold field, Potchefstroom gold field, Klerksdorp gold field and Southern Free State gold field **(Figure 2-1)**. The Witwatersrand gold field, discovered in 1886, consists of the West Rand, Central Rand and East Rand **(Figure 2-1)** and is the largest gold field in the world, extending over 300 km and covering 1600 km^2 (Chevrel et al., 2003). This gold field dominates the gold mining industry for the past 120 years (Frimmel, 2005). Together, these gold fields have produced 50 055 tonnes of gold since the start of the industry to 2004, accounting for approximately 33% of all the gold estimated to be above the earth's surface (Frimmel, 2005).

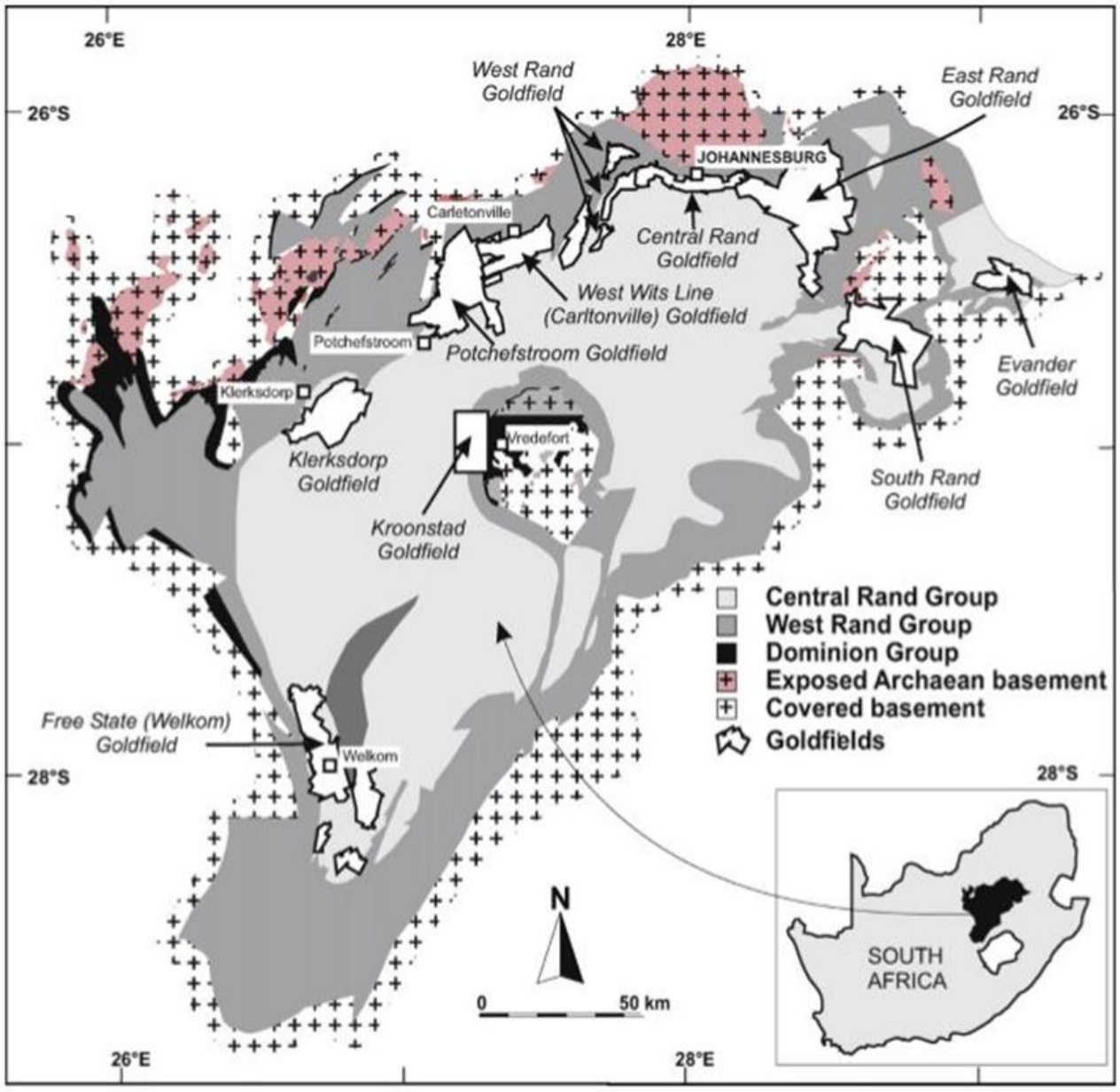

Figure 2-1: Gold fields in South Africa. Obtained from Dankert and Hein (2010).

2.1.2. Process of gold extraction during mining in South Africa

Gold ore in the Witwatersrand gold field is present in the form of conglomerates, which are sedimentary rocks consisting of ~ 80% quartz within a fine-grained matrix of naturally cementing material i.e., 1) micaceous minerals such as sericite, pyrophyllite, muscovite, chlorite and chloritoid ranging from 10 to 30%; 2) pyrite (FeS_2) ranging from 3 to 4%; 3) sulphides such as pyrrhotite, chalcopyrite, pentlandite, galena, cobaltite, sphalerite, gersdorffite, linnacite and

arsenopyrite ranging from 1 to 2%; 4) primary minerals such as chromite, rutile, garnet, zircon, xenotime, ilmenite and tourmaline; 5) secondary minerals such as anatase and skutterudite ranging from 1 to 2%; 6) alteration products such as goethite and leucoxene and 7) radioactive elements such as uraninite (UO_2) (Sutton, 2012, Anhaeusser et al., 1987, Liebenberg, 1956, Rosner, 1999). The section below discusses some of the techniques that were (or still are) used in South Africa to recover gold from the matrix material.

Amalgamation

Amalgamation was the primary method of gold recovery in South Africa and entailed crushing the gold bearing ore as fine as talcum powder and then hydrating it to form a viscous pulp. The pulp was passed over mercury (Hg)-coated copper (Cu) plates, which allowed the gold to sink through the pulp and make contact with the Hg to form an amalgam. The amalgam was scraped off the plates to liberate the gold (Nsimba, 2009). The major disadvantage of this technique was the use of the highly toxic Hg, which led to devastating adverse consequences for human health and the environment. In addition, this method became less efficient due to the reaction of Hg with sulphur, making it less selective for gold.

Cyanidation

Cyanidation is more popular than amalgamation although it is still controversial based on the use of the highly toxic element, cyanide (CN). Briefly, gold ore is first ground to a fine powder in large rotary mills or milling circuits. Leaching reagents in the form of CN and an oxidant e.g. oxygen (O) as well as water is added to the fine ore in a series of agitated leach reactors to form pulp. The pulp is filtered to remove the fine matter and the leached gold is precipitated out of solution by adding zinc (Zn). The solution is then filtered again to remove the Zn-gold precipitate. These steps are costly and not very effective as gold is lost during both filtration steps. Consequently, the carbon-in-pulp (CIP) process was developed in the 1970s during which gold can be recovered by using activated carbon to adsorb the gold directly from the pulp thereby avoiding further loss of gold through filtration. Once all or most gold has been recovered from the pulp, the pulp, which at this stage is known as tailings material, is pumped to tailings slimes dams also known as tailings storage facilities (TSFs), for disposal. The carbon containing the adsorbed gold is washed with a solution of dilute hydrochloric acid (HCl). This removes calcium

carbonate ($CaCO_3$) precipitates and cleanses the carbon pores. Thereafter, the carbon is eluted with sodium cyanide (NaCN) and sodium hydroxide (NaOH) at high temperatures to allow the gold to desorb from the carbon back into the solution where it is recovered. Variations of the CIP have been developed. For example, in the carbon-in-leach (CIL) method, leaching and adsorption are performed in the same series of tanks, thereby reducing the cost considerably. These methods are discussed in more detail in Stange (1999).

2.1.3. Waste produced by gold extraction

The types of solid waste generated during gold extraction vary in their physical and chemical composition and include (Bolan et al., 2017):

- Overburden, which is rock that is removed to allow access to the mineral-containing ore,
- Waste rock, which is material that is economically unviable,
- Slags, which is non-metallic by-products from metal smelting,
- Sludge, which is solids that have been removed from the mine water as well as chemicals that have been added to improve the extraction process,
- Tailings material

There are two main types of tailings material namely sand and slime. Tailings sand is approximately 200 µm in diameter and was produced during the gold extraction process when stamp mills were used to crush the ore when gold mining was in its infancy (Bailey and Stanley, 1987, Stanley, 1987). The tailings sand was deposited mechanically on TSFs using coco-pans (Thomas, 1968). Tailings slime, on the other hand, is fine slurry with a diameter of approximately 70 µm, which was produced during the more advanced cylindrical or tube milling, thereby enabling the ore to be reduced to a much finer size further liberating the gold (Funke, 1990). As a consequence, tailings slimes contain smaller amounts of lower grade gold compared to that of sand tailings (DRDGold, 2014). Tailings slimes are deposited on TSFs hydraulically using paddock systems (Funke, 1990).

Mining on the Witwatersrand gold field alone is reported to have generated 200 000 tonnes of waste per ton of gold (Anglogold, 2004). As a consequence, mining has given rise to more than 270 TSFs (Rösner, 2001, Anglogold, 2004), many of which are located in the Central Rand of

the Witwatersrand (Phakedi, 2011), covering a total area of 400 km^2 and comprising of about 6 billion tonnes of gold and uranium tailings (Chevrel et al., 2003).

Different terminologies are used to refer to different types of waste. For example, tailings deposits are also known as tailings dumps, tailings dams, tailings disposal facilities (TDFs), TSFs and mine residue deposits or mine residue areas (MRAs). MRAs, in the case of Sutton (2012), is used to refer to all the waste produced during mining and includes tailings deposits, waste rock dumps, open cast excavations and quarries, water storage facilities and return water dams, tailings spillage sites, generally near TDF dams and footprints left after the re-mining of TDFs, mine waste, urban waste, spillage, industrial waste, etc. within the boundaries of former mine properties (GDARD, 2009a). For the purposes of this thesis, the term TSF will be used to refer to sand and slimes tailings dumps only and does not include other forms of mine waste.

2.1.4. Complaints of surrounding communities and environmental pollution

Although some would consider the presence of these TSFs as historical landmarks signifying the success of the gold mine industry in South Africa for the past 120 years, most consider their mere presence a nuisance and, more importantly, a health risk for the ecosystem. This is mainly contributed to the increase in awareness by members of the public responding to improper disposal of mine waste and other hazardous waste that resulted in undesirable health and environmental consequences (Phakedi, 2011). In Gauteng, a large proportion of the population lives beside abandoned mining waste where population densities reach levels higher than 6 261 individuals per km^2 (GCRO, 2018).

Due to wind and water erosion, tailings particles are easily transported to surrounding communities by air as suspended dust particles (particulate matter, PM) or by soil and/or water contamination. Several complaints from surrounding communities regarding tailings pollution have been recorded throughout the years. For example, complaints recorded by the Crown Mines Dust Monitoring Forum from 1995 to 2010 have shown the highest frequency of complaints to occur in August and September, coinciding with the dryer, windier South African climate. As much as 28% of these complaints involved health concerns caused by tailings dust exposure (Oguntoke and Annegarn, 2014). Wright et al. (2014) observed a similar occurrence in which

communities surrounding TSFs in the Witwatersrand area complained about health effects caused by dust emitted from TSFs. Despite the fact that a great number of health complaints has been recorded by the surrounding communities and despite studies showing associations between PM levels and symptoms/disease (discussed further in the subsequent sections), it is not yet clear what the correlation is between exposure to tailings PM and the onset of disease.

2.2. Potential toxicity of tailings material

For tailings material to have an adverse outcome on the ecological system, it must exhibit an inherent potential to be hazardous or toxic to the environment. The degree of toxicity of particles in general is governed by their physicochemical properties (Valavanidis et al., 2008), of which some are discussed below.

2.2.1.Particle size

The crushing and grinding of ore will undoubtedly create particles of small sizes and with the advancement of the refining procedures to extract more gold, these particles will more than likely further decrease in size. In general, the size of tailings particles is dependent on the characteristics of the ore from which the desired mineral is extracted as well as the milling process and is generally described in terms of clay (< 0.002 mm), silt (0.002-0.05 mm), sand (0.05-2 mm) and gravel (> 2 mm) content (Sarsby, 2000). Gold tailings generally fall under the sandy-silt class (Sarsby, 2000) and this was also confirmed for the gold tailings from the Witwatersrand (Nengovhela et al., 2006).

Size, in particular the median mass aerodynamic diameter (MMAD), is defined as the aerodynamic diameter of a particle in which 50% of the aerosol mass is greater than the specified cut-point and the other 50% is smaller (Lewis and Copley, 2011). MMAD is a good indicator for predicting lung deposition, and therefore predicted toxicity, and is often reported together with the geometric standard deviation (GSD), which indicates the spread around the MMAD (Gardenhire, 2015).

The typical mass-based, size distribution of PM is as follows:

1. The **inhalable** fraction **(Figure 2-2)**, which includes the total suspended particles (TSP) in the atmosphere is the total airborne particles. This fraction, which also evidently consists of all the other smaller fractions discussed below, is inhaled through the head airways, also known as the extra-thoracic region, which includes the nose, pharynx, mouth and larynx **(Figure 2-3)** (CEN, 1993, ICRP, 1994, Brown et al., 2013). The inhalable fraction also contains the extra-thoracic fraction, which is the mass fraction of inhaled particles that do not penetrate beyond the larynx (CEN, 1993).
2. The **thoracic** fraction **(Figure 2-2)** is the total airborne particles penetrating beyond the larynx in the **tracheobronchial** region also known as the conducting airways, which includes the trachea, stem bronchi and terminal bronchioles **(Figure 2-3)** (ICRP, 1994, Brown et al., 2013, CEN, 1993). Particulate matter with an MMAD $\leq$ 10 μm (PM_{10}) is the particle size having 50% penetration for the thoracic fraction and is often referred to as the coarse fraction (CEN, 1993, ACGIH, 2005, Brown et al., 2013).
3. The **respirable** fraction **(Figure 2-2)** is the total airborne particles penetrating the **alveolar or gas-exchange region** also known as the pleural or parenchymal region, which consists of the bronchi, respiratory bronchioles and alveoli **(Figure 2-3)** (ICRP, 1994, Brown et al., 2013). Relative to total airborne particles, the particle size having 50% penetration for the respirable fraction is 4.0 μm (PM_4; MMAD $\leq$ 4 μm) (CEN, 1993, ACGIH, 2005, Brown et al., 2013).
4. The **fine** and **ultrafine** particle fractions **(Figure 2-2)** represent those particles with an MMAD $\leq$ 2.5 μm ($PM_{2.5}$) and $\leq$ 0.1 μm ($PM_{0.1}$), respectively. The $PM_{0.1}$ fraction contains nanoparticles (NPs) or ultrafine particles (UFPs) with diameters $\leq$ 100 nm. It has been suggested that UFPs may be more toxic, as shown in animal-based *in vivo* and *in vitro* toxicological studies (Donaldson et al., 2001), compared to the other size fractions, for the following reasons:
    a. They have the potential to escape broncho-mucociliary action and clearance by alveolar macrophages. In addition, these NPs may penetrate deep within the alveoli, enter the circulation and exert their toxic effects in distal organs (Nemmar et al., 2002, Oberdörster et al., 2004);

b. They have a greater surface area to mass ratio compared to larger particles (discussed in more detail in **Section 2.2.2**), thereby providing a larger area for adsorption of toxic metals and providing a higher surface activity for interaction with biological surfaces;
c. Due to their small size, UFPs form a small proportion of the total mass of $PM_{2.5}$ and PM_{10}, but may comprise a large majority of the total particle count.

Due to the points listed above, it has been suggested that UFPs may be responsible for the observed health effects of PM_{10} and $PM_{2.5}$. However, apart from single studies suggesting that UFPs could lead to adverse health effects (e.g. Frampton (2007) and those listed in **Table 2-1**), there is currently no conclusive epidemiological evidence to date to confirm such a causal link between exposure to UFPs and observed health effects (Ohlwein et al., 2019). This lack of evidence may be due to factors such as study heterogeneity, limited accounting for UFP spatial variation, and lack of significant findings from multi-pollutant models, as suggested in the review by Heinzerling et al. (2016).

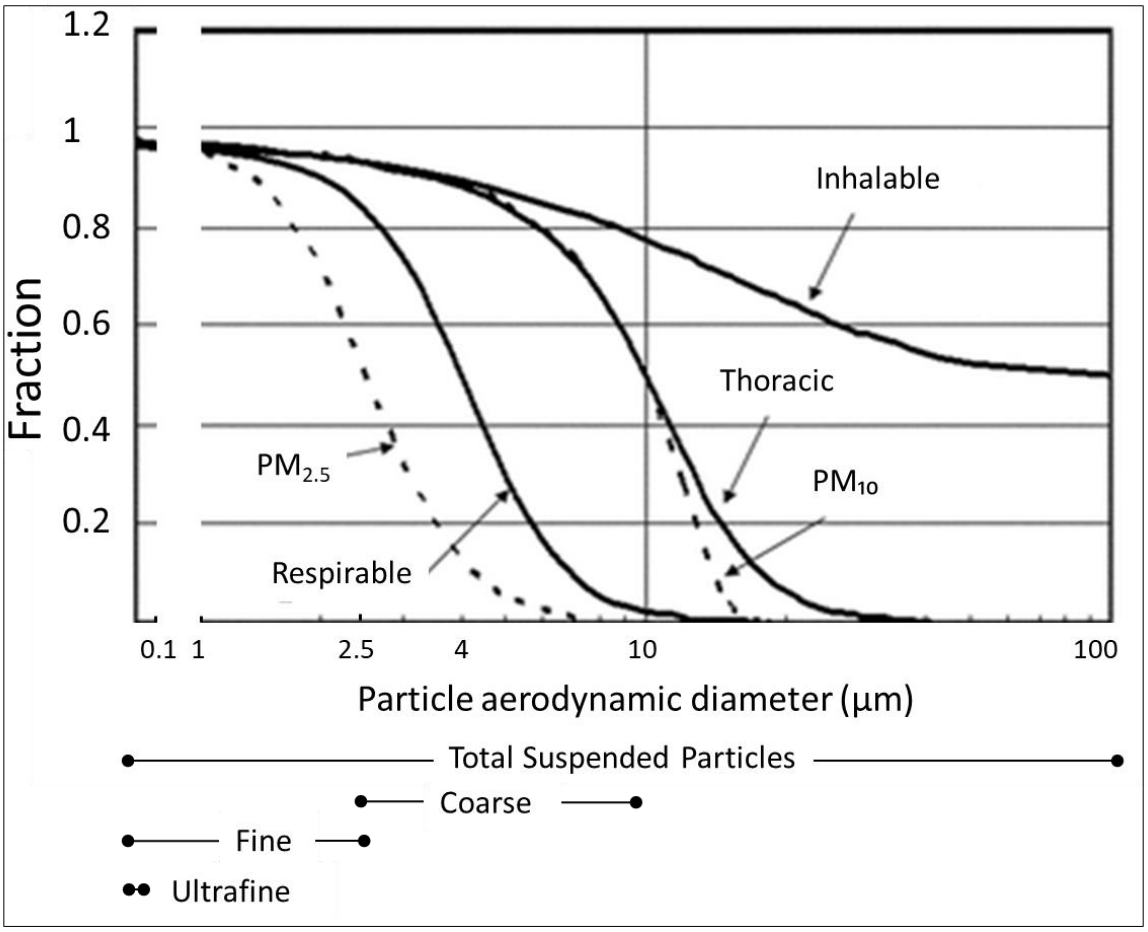

Figure 2-2: Typical size distribution of atmospheric aerosols. Adapted from Vincent (2005).

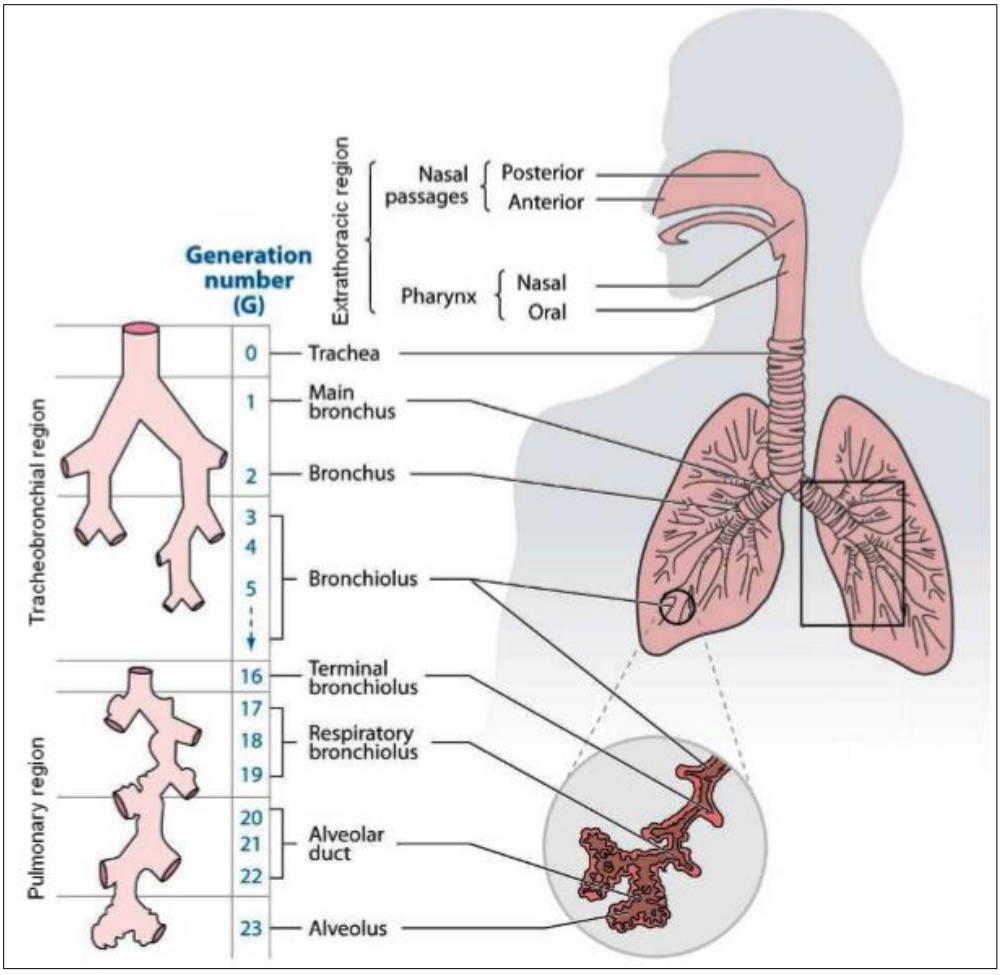

Figure 2-3: The human respiratory tract model. The tracheobronchial region extends from generation 0 (trachea) to 16 (terminal bronchioles) and pulmonary or alveolar region extends from generation 17 (respiratory bronchioles) to 23 (alveolus) (Hussain et al., 2011).

Evidently, smaller and larger particles will exhibit different toxicological properties due to their differences in their deposition patterns in the respiratory tract **(Figure 2-4)**. For example, dusts that mainly deposit in the deeper areas of the respiratory system may be responsible for pneumoconiosis (i.e. silicosis) in coal miners, whereas larger particles may be responsible for the development of bronchitis and reduction of ventilator capacity (Morgan, 1978). Therefore, sampling of PM at all the size ranges e.g. ($PM_{0.1}$ – PM_{10}) may not correlate with observed health effects if the risk is associated only with one specific size-range e.g. those particles that enter the thorax or alveolar region (Brown et al., 2013). A summary of some studies that have associated

different-sized PM fractions to diseases is provided in **Table 2-1** as examples of the effects of size**.**

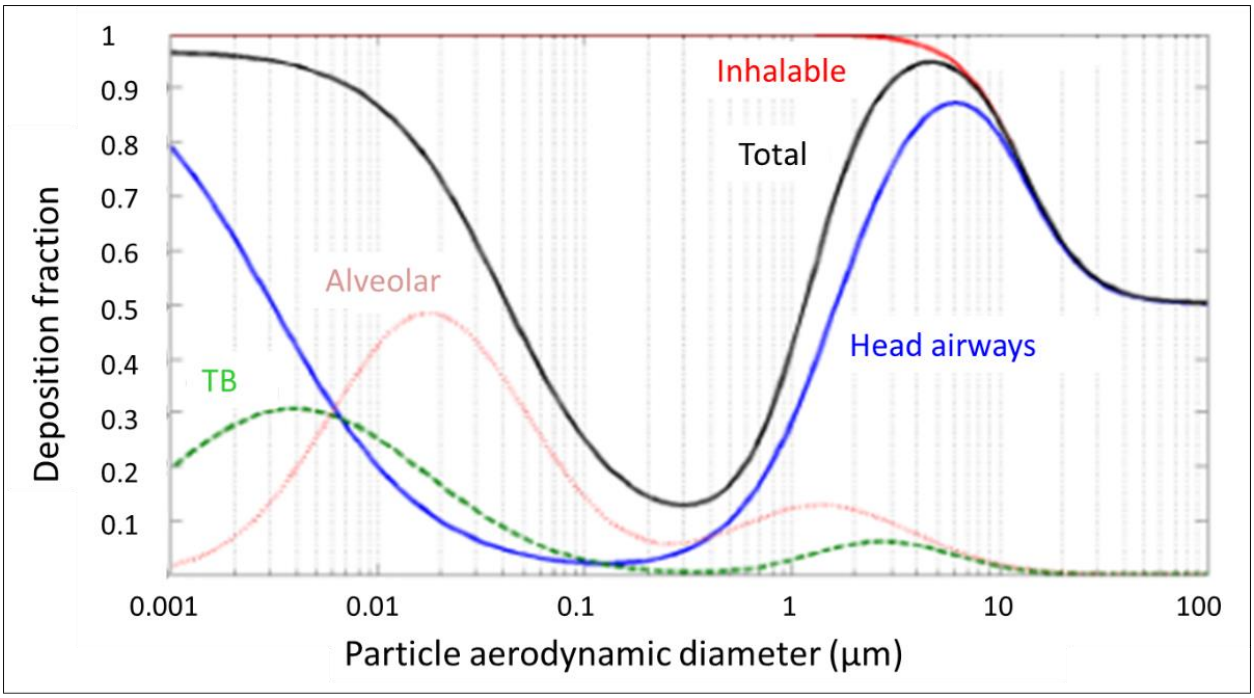

Figure 2-4: The ICRP deposition model. Adapted from ICRP (1994).

Table 2-1: Different-sized PM fractions from environmental air pollution studies and their associated diseases or symptoms.

PM fraction	Disease/Symptom	Exposure; Percent Increases in Mortality (95% CI)	Reference
$PM_{0.1}$	Ischemic heart mortality	1.06 (1.03-1.09)[#^]	(Ostro et al., 2015)
	Wheeze	2.46 (1.04 - 5.84)[^]	(Andersen et al., 2008)
	Exacerbation of skin symptoms in children with atopic dermatitis	3.1 (0.2–6.1) 28–140/m^3	(Song et al., 2011)
	Prevalence of inhaled short-acting β_2-agonists agonist (asthma) use	1.08 (0.96–1.21)[^]	(Von Klot et al., 2002)
$PM_{2.5}$*	All-cause mortality	13 (4.2–23)[≈]; 6.6 (3.5–9.8)[≈]; 1.06** (1.02-1.11)[≈]; 14 (5.4–23)[≈]; 6.2 (1.6–11)[≈]; 4 (1–7)[≈],1 (-0.6-2.6)[≈]; 7 (3–10)[≈]; 17 (5–30)[≈]; 12 (-8-38)[≈]; 16 (7–26)[≈]; 6 (-6-22)[≈]; 11 (9–13)[≈]; 5.6 (3.5–7.8)[≈]	(Dockery et al., 1993, Krewski et al., 2004, Laden et al., 2006, Eftim et al., 2008, Pope III et al., 1995, Pope III et al., 2002, Pope et al., 2004, Jerrett et al., 2005, Krewski et al., 2009, Lipfert et al., 2006a, Lipfert et al., 2006b, Enstrom, 2005, Filleul et al., 2005, Gehring et al., 2006)
	Cardiopulmonary Mortality	18 (6.0 –32)[≈]; 12 (6.7–17)[≈]; 1.09** (1.03-1.16)[≈]; 19 (6.5–33)[≈]; 9.3 (3.3–16)[≈]; 5 (-2-12)‡[≈]; 12 (-3–30)[≈]; 52 (9–115)[≈]; 13 (9.5–16)[≈]	(Beelen et al., 2008, Krewski et al., 2009, Pope III et al., 2002, Dockery et al., 1993, Krewski et al., 2004, Pope III et al., 1995, Pope et al., 2004, Jerrett et al., 2005, Filleul et al., 2005, Gehring et al., 2006)
	Cardiovascular mortality	13 (8.1–18)[≈]; 12 (8–15)[≈]; 42 (6–90)[≈]; 28 (13–44)[≈]; 76 (25–147)[≈]; 24 (9–41)†[≈]	(Laden et al., 2006, Krewski et al., 2004, Pope et al., 2004, Pope III et al., 2002, Miller et al., 2007, Chen et al., 2005)
	Ischemic heart mortality	18 (14–23)[≈]; 39 (12–73)[≈]; 24 (20–29)[≈]	(Pope et al., 2004, Pope III et al., 2002, Jerrett et al., 2005, Krewski et al., 2009)
	Ischemic heart mortality	1.19 (1.08-1.31)[≈]	(Ostro et al., 2015)
	Lung cancer mortality	1.14** (1.04-1.23)[≈]	(Pope III et al., 2002)
	Myocardial infarction (MI), stroke, arrhythmia, and heart failure exacerbation	Hours to days	
	Diabetes increased risk of $PM_{2.5}$-related mortality	1.98 (0.54-3.44)	(Alessandrini et al., 2016)

PM fraction	Disease/Symptom	Exposure; Percent Increases in Mortality (95% CI)	Reference
	Cardiac arrhythmia increased risk of $PM_{2.5}$-related mortality	1.65 (0.37-2.95)	(Alessandrini et al., 2016)
	Heart conduction disorders increased risk of $PM_{2.5}$-related mortality	4.22 (0.15-8.46)	(Alessandrini et al., 2016)
PM_{10}	All-cause daily mortality	0.2–0.6% increase per 10 μg/m^3 of PM_{10}	(WHO, 2005, Samoli et al., 2008)
	All cause	0.74 per 14.4 μg/m^3 increase in PM_{10}	(Alessandrini et al., 2016)
	Heart conduction disorders increased risk of PM_{10}-related mortality	4.19 (0.38-8.14)$^{\approx}$	(Alessandrini et al., 2016)

* Most references cited were obtained from Brook et al. (2010)
** Average adjusted mortality Relative Risk (RR)
$^{\#}$ Cu of $PM_{0.1}$
$^{\wedge}$ Odds ratios
$^{\approx\approx}$Based on a 10 μg/m^3 increase in PM

Not only may particle size predict toxicity but it may also determine the retention time of the particle in the air, thus increasing the chances of it being inhaled. For example, smaller particles will remain airborne for longer periods and will travel longer distances compared to their larger counterparts **(Table 2-2)**.

Table 2-2: The estimated retention time of the particle size in each deposition location (Bailey, 1994).

Anatomical region	PM size (µm)	Deposition location	Retention time
Extra-thoracic (Inhalable)	7-10	Nasal passage	1 day; small fraction may be retained for longer
	5-7	Pharynx	Few minutes
Tracheobronchial (Thoracic)	3-5	Trachea	Few minutes
	2-3	Bronchi	Hours to weeks
	1-2.5	Terminal bronchioles	Hours to weeks
Alveolar (Respirable)	0.5-1	Alveoli	50-7 000 days

2.2.2.Surface area and surface activity

The size of a particle also governs the surface area or the quantity of accessible surface and, for a fixed mass of particles, the surface area increases as the particle size becomes smaller (Sager and Castranova, 2009). As all chemical reactions take place at the surface, small particles, with large surface areas generally have a high surface activity. Surface activity is defined as the ability of particles to produce reactive oxygen species (ROS) due to their surface properties. These surface properties may include surface charge, poorly coordinated transition metal ions or dangling bonds, created during homolytic fractures leading to an unpaired electron or during interaction with biomolecules at the cell membranes (Pavan and Fubini, 2016). The ROS will in turn lead to oxidative stress, which in some cases, may lead to adverse effects on cells (Fubini and Fenoglio, 2007, Fubini and Arean, 1999). Therefore, smaller particles with larger surface areas may exhibit a higher toxic potential, compared to larger particles with smaller surface areas. An example provided by Spech et al. (2000) is shown in **Figure 2-5** where the relationship between size, surface area and toxicity is illustrated. **Figure 2-5** shows that the size of the silica crystals is inversely proportional to their surface area **(Figure 2-5A)** and cytotoxic index **(Figure 2-5B)**, which in this case, was measured as the Chromium-51 release, a marker for alveolar macrophage

(AM) injury. As a result, the surface area of the silica crystals was directly proportional to their cytotoxic index **(Figure 2-5C)**.

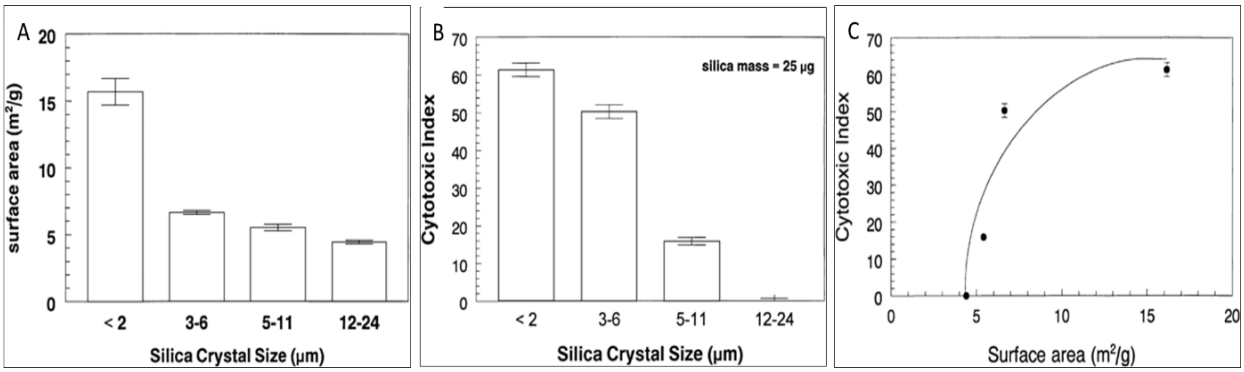

Figure 2-5: Effect of silica crystal size and surface area on the toxicity to AMs. ^{51}Cr-labeled AMs were exposed to silica crystals at a concentration of 250 µg silica/ml for 4 h at 37 °C. (A) surface area versus size, (B) silica crystal ^{51}Cr release as a marker of cell injury (as determined by cytotoxic index) increased in a size-dependent manner in silica-exposed AM cultures, with smaller crystalline particles (i.e., < 2 µm) being the most toxic ($P < 0.05$ by ANOVA with repeated measures with Dunnett's method), (C) surface area compared with cytotoxic index. Results are means ± SE from 3 experiments performed in triplicate. Adapted from Spech et al. (2000).

Often, the relationship between size, surface area and surface activity is clear cut and directly inter-dependent for homogeneous particles with smooth surfaces. However, this relationship can become complicated for particles with complex surfaces consisting of rough, porous textures and angular shapes with sharp edges, collectively referred to as the micromorphology (discussed below). The relationship can further be complicated by the spatial arrangement and interaction between surface functional groups on, for example, particles consisting of multiple atomic layers, hereafter referred to as surface microtopography (Gulumian, 1999). Therefore, the surface areas and surface activities for micro- (pore diameter < 2 nm) and mesoporous (pore diameter 2 – 50 nm) materials (Groen et al., 2003) as well as anthropogenic (man-made) environmental particles will be dependent on their size as well as micromorphology and microtopography.

2.2.3.Micromorphology and microtopography

Expectedly, tailings particles exhibit an irregular micromorphology with rough, porous textures and very angular shapes with sharp edges (Sarsby, 2000, Rodriguez and Edeskär, 2013) due to the mechanical abrasion and fracturing encountered during mining. Micromorphology has been shown to also govern the surface area as well as surface activity and, hence, toxicity of particles (Turci et al., 2016, Fubini and Fenoglio, 2007). For example, in a study conducted by Turci et al. (2016), the cytotoxic potential of crystalline silica with smooth, intact surfaces and ordered crystal lattices were compared to that of fractured crystalline silica with disordered crystal lattices. The authors found that fracturing led to an increase in surface area from 0.3 to 9.5 m^2/g. This increase in surface area was not due to the decrease in particle size, but rather from the generation of irregular surfaces during fracturing. These irregular surfaces were shown to strongly interact with the membranes of red blood cells (RBC) and liposomes inducing lysis and cellular stress in the RAW 264.7 macrophage cell line. In addition, compared to intact particles, the fractured particles showed a higher degree of surface ROS generation, which was mainly due to the cleavage of the silicon-oxygen (Si-O-Si) bonds. The authors concluded that the fracturing of silica particles led to a disorganization of the silanol (Si-OH) surface moieties, resulting in reactive silanol patches, which increased the biological activity and toxicity of the particles. Therefore, even though it was originally believed that the crystallinity of silica was solely responsible for its pathogenicity, this view has recently changed in light of recent findings emphasizing the importance of micromorphology and microtopography in governing the arrangement of surface functional groups (i.e. silanols), which ultimately determines the degree of pathogenicity (Pavan and Fubini, 2016).

2.2.4.Chemical composition

As mentioned earlier, gold deposits within the conglomerates of the Witwatersrand gold fields naturally co-occur with approximately 80% quartz associated with various phyllosillicates (Rosner, 1999), FeS_2, uranium (U) complexes (e.g. UO_2) as well as metals such as magnesium (Mg), Cu, Zn, manganese (Mn), arsenic (As), nickel (Ni), chromium (Cr), cobalt (Co) and lead (Pb) (Merkel and Arab, 2014, Sutton, 2012, Feather and Koen, 1975, Liebenberg, 1972). If not extracted together with gold to be utilized in other downstream production processes, both Fe_2S and UO_2 are disposed in tailings material (Sutton, 2012). Moreover, other additional elements

such as Hg and CN, Mn, tin (Sn) and vanadium (V) make their way into tailings deposits as they are added during the gold extraction process (Mphephu, 2001). Indeed, Nengovhela et al. (2006) showed that tailings samples collected from five TSFs in the Witwatersrand basin consisted of the following minerals: FeS_2, jarosite, chloritoid, K-Feldspar, quartz, mica, chlorite, pyrophyllite, clay and gypsum, with quartz and chloritoid being the most and second most abundant minerals, respectively, as well as several different elements such as Al, Ca, Fe, Zn, Ni, Co, Mg and Na. The presence of these elemental contaminants in the resultant tailings, of which some have a direct effect on surface activity and toxicity of particles, is therefore inevitable. It should be noted that the concentrations of these contaminants in the bulk material may also be markedly different from the concentrations within smaller particle size fractions. For example, the United States Environmental Protection Agency (US EPA) has shown that the percentage of silica in various particle size fractions from Canadian gold mines ranged from 44.3% in the size fraction > 32 µm to 0.9% in the size fraction from 0.5 to 1 µm (EPA, 1996). In South Africa, even though the conglomerates of the Witwatersrand gold fields consist of approximately 80% quartz, the levels of RCS may be much lower. Indeed, Hnizdo and Sluis-Cremer (1993) and Churchyard et al. (2004) have recorded RCS levels of 30% and 12 - 16%, respectively, at various South African gold mines, which is much lower than the quartz levels in the Witwatersrand conglomerates. Some of these contaminants will be discussed briefly below.

Mineral contaminants

Silica (SiO_2), CAS#: 7631-86-9

Silica comprises a group of minerals consisting of Si and O. All silica minerals share a $[SiO4]^{4-}$ three dimensional tetrahedron structure but differ by their spatial arrangement, which results in several different polymorphs (Turci et al., 2016). These polymorphs are categorised into two main groups i.e. crystalline and amorphous (NTP, 2005). With crystalline silica, the $[SiO4]^{4-}$ tetrahedron units are arranged in definite regular patterns (Parmeggiani, 1983), while amorphous silica does not have any definite arrangements. There are seven crystalline polymorphs of which the three major forms are quartz, tridymite and cristobalite. Each of these polymorphs exist in α and β phases, which is stable at low and high temperatures, respectively (Yoder, 2006). The crystal structure of both α and β phases of quartz is hexagonal; however, the β phase is slightly more symmetrical than the α phase. In contrast, α tridymite is orthorhombic, while β tridymite is

hexagonal and α cristobalite is tetragonal while β cristobalite is isometric. Crystalline silica, α quartz in particular, has long been known to be a toxic component in soils and gold-bearing ore and exerts its toxic effects through the production of ROS such as hydroxyl radicals (•OH) (Vallyathan and Shi, 1997, Fubini, 1998). As stated in Andraos et al. (2018b), "crystalline silica has been classified by the International Agency for Research on Cancer (IARC) as a Group 1 carcinogen (IARC, 2012a), based on the fact that chronic occupational exposure to high levels of crystalline silica dust for prolonged periods may produce carcinogenic adverse health effects such as lung cancer (Vida et al., 2010). Occupational exposure to crystalline silica may also lead to non-cancer adverse health effects such as pulmonary silicosis (type of lung fibrosis) (Craighead, 1988), chronic obstructive pulmonary disease, chronic bronchitis, emphysema, small airways disease (Hnizdo and Vallyathan, 2003), tuberculosis/silicotuberculosis (Akugizibwe, 2014), autoimmune diseases (rheumatoid arthritis, scleroderma, systemic lupus erythematosus) (Steenland and Goldsmith, 1995) and kidney disease (Vupputuri et al., 2012). Acute occupational exposures to high concentrations of crystalline silica have shown to cause cough, shortness of breath, and pulmonary alveolar lipoproteinosis (acute silicosis) (Chapman, 1932)".

It is also possible to be exposed to crystalline silica in non-occupational settings although research addressing non-occupational exposures is still rather limited. It has been suggested that non-occupational exposures to crystalline silica near silica-dust generating sources may lead to increased susceptibilities to certain diseases comparable to those of occupational origin. The US EPA (EPA, 1996) and Bhagia (2012) summarise these environmental scenarios in which non-occupational silica exposures have been documented. For example, according to the US EPA, activities or scenarios, which may result in the environmental release of silica include emissions from: (1) construction and demolition activities; (2) unpaved and paved roads; (3) ceramic, brick, and clay industries; (4) metallurgic activities; (5) quarries and mining; (6) agricultural operations; (7) power plants; (8) forest fires; and (9) general wind erosion. It is apparent from this list of potential sources that many occupationally related activities may result in environmental exposures to surrounding communities. Indeed, Bhagia (2009) recorded average quartz concentrations in the surrounding residential areas of a slate pencil industry as high as 41.07–57.22 $\mu g/m^3$, compared to 3.51 $\mu g/m^3$ at a control site 5 km away. For the agricultural setting, particularly in South Africa, it was suggested that farmers and farm workers may not

only be exposed daily to silica via their occupational activities but may also be exposed environmentally as both farmers and farmworkers generally inhabit the farms where they work (Swanepool et al. 2010, Swanepool et al. 2011, Swanepool, 2012), or stay closely within the vicinity of the farms (Bhagia, 2012). Therefore, exposure to silica outside of their working hours may contribute to their overall cumulative silica exposure. Indeed, silicosis has been recorded in agricultural workers (Schenker, 1998). In more extreme settings, environmental exposures to silica may occur in environmental settings located far from industrial activities but where the crystalline silica content of environmental dust is high and dust storms are common (Norboo et al. 1991, Saiyed et al. 1991, Patial, 1999).

Pyrite (FeS_2), CAS#: 1309-36-0

Pyrite, also known as fool's gold (Rickard, 2015), is the most common and abundant, naturally occurring, iron (Fe) sulphide mineral and has been shown to result in lung injury. For example, Huang et al. (2005) found a significant correlation between bioavailable Fe released from coal, which generally exhibits a high FeS_2 concentration, and the prevalence of coal workers' pneumoconiosis (CWP). Huang et al. (2005) also showed that coal miners from regions containing higher bioavailable Fe levels had a higher prevalence of CWP, COPD, and asthma, compared to miners from regions where bioavailable Fe levels were low. In addition, other studies have shown that coal samples with higher Fe levels induced higher levels of pro-inflammatory cytokines and alterations of lung cell genes (Zhang et al., 2002, Hu et al., 2003, Zhang and Huang, 2003, Cohn et al., 2006a). The mechanism of toxicity of FeS_2 is known to involve the production of hydrogen peroxide (H_2O_2), which, in turn, is converted to •OH on the FeS_2 surface, possibly by reacting with ferrous Fe via a Fenton reaction mechanism (Cohn et al., 2006b, Cohn et al., 2004, Borda et al., 2001, Ahlberg and Broo, 1997, Cohn et al., 2006a).

Other elemental contaminants

It is well known that certain elements in their correct quantities are critical to normal human development but could become toxic depending on the concentration and/or route of exposure. The Agency for Toxic Substances and Disease Registry (ATSDR) (ATSDR, 2016), a federal public health agency of the U.S. Department of Health and Human Services, provides up to date, peer-reviewed, toxicological profile information sheets, known as ToxProfiles, of the most

common toxic substances based on health and toxicological scientific knowledge. In order to obtain an idea of the possible inherent toxicity of tailings based on their elemental profile, the data of the ToxProfiles (as well as references listed therein) of the elements known to be present in tailings are summarised in the following section. ToxProfiles appeared to serve as a good review of literature as it provided singular studies addressing health impacts based on different exposure routes. Only the inhalation exposure route has been considered for the purposes of this thesis. Therefore, the studies listed in ToxProfiles addressing health impacts via the inhalation route were referenced in this section of the thesis.

Mercury (Hg), CAS#: 7439-97-6

Mercury occurs naturally in the environment mainly in the form of metallic or elemental Hg (Hg^0), which is released into the air by natural processes. When mercury binds to other chemicals, it may adopt different valence states of either Hg^{+1} (mercurous Hg) or Hg^{+2} (mercuric Hg). Once inside the body, mercury exerts its toxic effects by binding to thiol or sulfhydryl groups of proteins thereby inactivating various enzymes, structural proteins and transport processes (Bulger, 1986) as well as altering cell membrane permeability through the formation of mercaptides (i.e. metal thiolates) (Sahaphong and Trump, 1971). The disruption of the thiol groups of proteins by mercury is also shown to promote oxidative stress, lipid peroxidation, mitochondrial dysfunction, and changes in heme metabolism (Zalups and Lash, 1994).

<u>Toxicity associated with inhalation exposure (obtained from ToxProfiles)</u>

Metallic Hg is easily absorbed through the lungs via rapid diffusion. Inhalation of Hg mainly occurs in the form of metallic or organic Hg vapour, which may cause symptoms such as cough, dyspnea, and tightness or burning pains in the chest (Bluhm et al., 1992, Soni et al., 1992, Taueg et al., 1992), airway obstruction, restriction, hyperinflation (Snodgrass et al., 1981), and decreased vital capacity (Lilis et al., 1985, McFarland and Reigel, 1978). Cases of very high acute exposures have led to death through respiratory failure (Soni et al., 1992, Taueg et al., 1992). Other target organs that are also compromised following inhalation exposure to inorganic and organic Hg (in the form of vapour or Hg-containing dust) are the kidneys and the central nervous system, respectively. Neurological symptoms include tremors of hands and body, emotional lability i.e. irritability and nervousness, insomnia, memory loss, neuromuscular

changes, headaches, polyneuropathy and cognitive impairment (Adams et al., 1983, Bluhm et al., 1992). Damage to the kidneys has been reported to range from mild transient proteinuria (Bluhm et al., 1992, Soni et al., 1992) to acute renal failure (Bluhm et al., 1992, Soni et al., 1992, Rowens et al., 1991).

Copper (Cu), CAS#: 7440-50-8

Copper is an essential nutrient for humans and animals at low levels of intake and is incorporated into a number of metallo-enzymes (e.g. cytochrome c oxidase, superoxide dismutase (SOD) and ferroxidases) involved in the reduction of activated oxygen species, hemoglobin formation, drug/xenobiotic metabolism, carbohydrate metabolism, catecholamine biosynthesis, the cross-linking of collagen, elastin, and hair keratin as well as the antioxidant defence mechanism. Copper occurs naturally as cuprous (Cu^{+}) and cupric (Cu^{+2}) ionic states in rock, soil, water, sediment, and, at low levels, in air as well as in all plants and animals. When Cu is released into the environment, it can become strongly attached to the organic material and other components such as clay and sand in the top layers of soil. Therefore, most Cu compounds found in air, water, sediment, soil and rock are strongly attached to dust and dirt or imbedded in minerals.

<u>Toxicity associated with inhalation exposure (obtained from ToxProfiles)</u>

Workers exposed to Cu dust have reported a number of symptoms, some of which are suggestive of respiratory irritation (coughing, sneezing, thoracic pain, and runny nose) and some that include anorexia, nausea, and occasional diarrhoea, hepatomegaly, eye irritation, headache, vertigo, and drowsiness (Askergren and Mellgren, 1975, Suciu et al., 1981). In a study of over 6,700 male workers at a Chinese copper mine, significant increases in the risk of stomach and lung cancer were observed (Chen et al., 1993). However, smoking status, along with exposure to radioactivity, silica, Fe, and As may also have contributed to the increased cancer risk.

Zinc (Zn), CAS#: 7440-66-6

Zinc is an essential nutrient for humans and animals as is necessary for the function of metalloenzymes, including alcohol dehydrogenase, alkaline phosphatase, carbonic anhydrase, leucine aminopeptidase, SOD and DNA- and RNA polymerases, which in turn are necessary for nucleic acid, protein, and membrane metabolism, as well as cell growth and division. Zinc also

plays an essential role in the maintenance of nucleic acid structure of genes (Zn finger phenomenon). Zinc is found in the air, soil and water and is relatively abundant in all foods. Zinc is known to readily combine with other elements, such as chlorine, oxygen, and sulphur to form Zn compounds.

Toxicity associated with inhalation exposure (obtained from ToxProfiles)

Symptoms from inhalation of zinc oxide UFPs include pulmonary function impairment (Brown, 1988, Malo et al., 1990), dryness of the throat and coughing (Drinker and Drinker, 1928), substernal chest pain, cough, and dyspnoea (Rohrs, 1957) as well as an increase in bronchiolar leukocytes and inflammation and tissue damage in the lung periphery (Brown, 1988, Vogelmeier et al., 1987). Collectively, these symptoms are also known as metal fume (or dust) fever. In support of the association of Zn with adverse health effects, Blanc et al. (1991) have observed significant correlations between the concentration of airborne Zn and the proportion of activated T cells including helper cells, inducer cells, suppressor cells and killer cells in a group of 14 welders.

Manganese (Mn), CAS ID #: 7439-96-5

Manganese is a naturally occurring essential element required for the formation of healthy cartilage and bone as well as wound healing and comprises approximately 0.1% of the earth's crust. Manganese is found mainly as oxides, carbonates and silicates in combination with other minerals with Mn dioxide (MnO_2) as the most common naturally-occurring form that exists in nature.

Toxicity associated with inhalation exposure (obtained from ToxProfiles)

Inhalation of particulate manganese compounds in individuals under occupational conditions can lead to lung inflammation and irritation characterised by an infiltration of phagocytic macrophages and leukocytes, localised oedema, pneumonia (Davies, 1946), cough, bronchitis, pneumonitis and minor reductions in lung function (Boojar and Goodarzi, 2002, Abdel-Hamid et al., 1990, Akbar-Khanzadeh, 1993). Occupational inhalation exposure to high levels of Mn compounds may also affect the neurological system, leading to the syndrome known as 'manganism' (Bast-Pettersen et al., 2004, Blond and Netterstrom, 2007, Bouchard et al., 2005).

There is also some evidence that respiratory effects may occur not only in occupational settings but also in residential populations near ferromanganese factories (Kagamimori et al. 1973; Nogawa et al. 1973; WHO 1987).

Antimony (Sb), CAS#: 7440-36-0

Antimony is a metal of which small amounts are found in the earth's crust. The ATSDR report states that "Antimony enters the environment during the mining and processing of its ores and in the production of antimony metal, alloys, antimony oxide, and combinations of antimony with other substances". Antimony ends up in the soil or sediment, where it attaches strongly to particles that contain Fe, Mn, or aluminium (Al).

Toxicity associated with inhalation exposure (obtained from ToxProfiles)

Altered respiratory effects (e.g. airway obstruction, bronchospasm, hyperinflation, chronic bronchitis, emphysema, inactive tuberculosis, irritation and pleural adhesions, which are fibrotic bands that span between the parietal and visceral layers of the pleura) (Cooper et al., 1968, Potkonjak and Pavlovich, 1983, Bogen and Pasternack, 1954) as well as gastrointestinal disorders (e.g. abdominal pain, diarrhoea, vomiting, and ulcers) (Brieger et al., 1954) have been observed in factory workers exposed to airborne antimony.

Arsenic (As), CAS#: 7440-38-2

Arsenic is a natural element present in the Earth's crust, water, air, plants and animals. Arsenic exhibits a high capacity for soil binding, particularly to Fe and Mn oxides. IARC, which is part of the World Health Organization (WHO), the US National Toxicology Program (NTP; which forms part of the National Institutes of Health (NIH), the Centers for Disease Control and Prevention (CDC), the Food and Drug Administration (FDA) and the US EPA, which maintains the Integrated Risk Information System (IRIS), an electronic database of human health effects from exposure to substances) all classify pure arsenic and inorganic arsenic as "known to be human carcinogen" based on evidence from human studies that it can cause cancer of the lung, bladder, kidney, skin and liver (IRIS, 2002). On the other hand, organic As compounds are classified as "not classifiable as to their carcinogenicity in humans" (ACS, 2016).

Toxicity associated with inhalation exposure (obtained from ToxProfiles)

Workers exposed to airborne As dusts often experience mucous membrane irritation, laryngitis, bronchitis, rhinitis and perforation of the nasal septum (Morton and Caron, 1989, Pinto and McGill, 1953, Sandström et al., 1989). Non-malignant deaths resulting from emphysema (Lee-Feldstein, 1986, Lubin et al., 2000, Welch et al., 1982) or pneumoconiosis (Xiang-Zhen et al., 1993) in workers exposed to airborne As have also been observed, although these conditions were possibly the result of the airborne particles *per se* and not the As content. Inhaled inorganic As may also produce effects on the cardiovascular system (e.g. Raynaud's phenomenon and increased vasospasticity) (Lagerkvist et al., 1986). Several case studies have reported nausea, vomiting, and diarrhoea in workers with acute As poisoning following occupational inhalation exposure (Morton and Caron, 1989, Pinto and McGill, 1953, Beckett et al., 1986, Ide and Bullough, 1988).

Nickel (Ni), CAS#: 7440-02-0

Nickel occurs naturally in soils and the form of Ni emitted to the atmosphere is dependent upon the source. Complex Ni oxides, Ni sulphate, and metallic Ni are associated with combustion, incineration, and smelting and refining processes. Background levels of Ni in soils vary widely depending on local geology and anthropogenic inputs, but concentrations typically range between 4 and 80 ppm.

Toxicity associated with inhalation exposure (obtained from ToxProfiles)

A study found an increased risk of moderate pulmonary fibrosis in Ni refinery workers (Berge and Skyberg, 2003). Other symptoms that have also been documented from occupational exposure to Ni included asthma (Dolovich et al., 1984, Shirakawa et al., 1990), increased urinary β-2-microglobulin levels (Sunderman Jr and Horak, 1981), increased immunoglobulin G (IgG), IgA, and IgM levels and decreased IgE levels (Bencko et al., 1982, Bencko et al., 1986) and an increased risk of sinonasal and/or lung cancer according to the International Committee on Nickel Carcinogenesis in Man (Doll et al., 1990), Department of Health and Human Services (NTP, 2002), IARC (IARC, 1990) and the US EPA (IRIS, 2005).

Chromium (Cr), CAS#: 7440-47-3

Chromium is a naturally occurring element found in the Earth's crust, volcanic dust and gases as well as in animals and plants. The stable, inactive inorganic trivalent (III) state of Cr is an essential nutrient that is converted to physiologically active forms by humans and animals, and play a critical role in metabolism (Anderson 1981). It is difficult to distinguish between the toxic effects caused by Cr (III) and the other physiologically active forms in the body due to the rapid interchangeable conversion between the different ionic states (Petrilli et al., 1986, Samitz, 1970).

Toxicity associated with inhalation exposure (obtained from ToxProfiles)

The respiratory tract in humans is a major target of inhalation exposure to Cr compounds. Chronic exposure may lead to sinonasal and lung cancer and Cr (VI) has been classified as a Type I carcinogen (IARC, 2012b). Acute exposure may lead to asthma, decreased forced expiratory lung volume, erythema of the face, nasopharyngeal pruritus (severe itching), nasal blocking, coughing and wheezing (Olaguibel and Basomba, 1988). Olfactory cleft obstruction, dry nose, nasal obstruction, nasal crusting, nasal septum perforation and nasal septum ulcers were significantly increased in workers at chromium plating factories exposed to Cr (VI) and/or Cr (III), compared to an unexposed control group (Kitamura et al., 2003, Kuo et al., 1997).

Cobalt (Co), CAS#: 7440-48-4

Cobalt is a naturally-occurring element that has properties similar to those of Fe and nickel. In soils, Co generally has low mobility and strong adsorption. However, its mobility increases in moist, acidic soils. As a component of cyanocobalamin (vitamin B_{12}), cobalt is essential in the body. Cobalt is a ubiquitous element within the body but is available at the highest concentrations in the liver.

Toxicity associated with inhalation exposure (obtained from ToxProfiles)

The effects of chronic occupational exposure to airborne Co compounds include respiratory irritation, diminished pulmonary function, wheezing, asthma, pneumonia, and fibrosis (Anttila et al., 1986, Deng et al., 1991, Sundaram et al., 2001, Zanelli et al., 1994)

Lead (Pb), CAS# 7439-92-1

Lead occurs naturally in the Earth's crust at about 15–20 mg/kg. The predominant forms of Pb in the environment are inorganic Pb compounds (i.e. salts, oxides and sulphides) and the most important Pb containing ores are galena (PbS), anglesite ($PbSO_4$), and cerussite ($PbCO_3$). Lead differs from other elements in that its toxic effects are the same regardless of the route of entry into the body. Therefore, the information below is not just only applicable to inhalation exposure but to all routes of exposure.

Toxicity to Pb exposure

The available literature shows a potential association between Pb exposure and cerebrovascular disease (Fanning, 1988, Malcolm and Barnett, 1982, Michaels et al., 1991), gastrointestinal (e.g. colic) (Janin et al., 1984)), hematologic (e.g. anaemia) (Schwartz et al., 1990)), and/or neurologic symptoms (McDonald and Potter, 1996), alterations in pulmonary function (Bagci et al., 2004), cardiovascular changes (cardiac conduction and rhythm) (Böckelmann et al., 2002, Cheng et al., 1998) and renal damage (Rastogi, 2008). The most well-recognized symptoms of Pb exposure, however, are those observed in children, which include gastrointestinal symptoms (e.g. abdominal pain, vomiting and constipation) at blood Pb levels as low as 20 µg/d*l* as well as symptoms relating to the central nervous system (e.g. impaired intellectual development) at blood Pb levels higher than 100 µg/d*l* (WHO, 2010). It appears as though there is not a level below which damage in children has not been observed. For example, neurobehavioural damage has been recorded at blood Pb levels as low as 5 µg/d*l* (WHO, 2010).

Cyanide (CN), CAS#: 74-90-8

The CN compounds most commonly found in the environment include NaCN, potassium cyanide and gaseous hydrogen cyanide. The toxicity of CN is dependent on the ease with which the CN anion (CN-) is released. For example, CN salts that are not bound to any metals are toxic, whereas Fe-containing CN compounds do not release CN readily and are therefore nearly nontoxic. Cyanide binds to the metallic cofactor in metalloenzymes, in particular Cytochrome c oxidase, thereby inhibiting enzyme function and leading to the impairment of oxygen use by tissues.

Toxicity associated with inhalation exposure (obtained from ToxProfiles)

Inhalation of sufficient concentrations of hydrogen cyanide (HCN) gas results is rapid death and was therefore used in gas chamber executions (Wexler et al., 1947). Occupational exposures to CN have been shown to cause dyspnoea (Chen and Rose, 1952, El Ghawabi et al., 1975), nasal irritation (McNerney and Schrenk, 1960), precordial pain, which is a pain felt in the centre or left side of the chest (El Ghawabi et al., 1975), nausea and vomiting (Blanc et al., 1985, El Ghawabi et al., 1975).

Iron (Fe), CAS#: 7439-89-6

Iron is the fourth most abundant element on earth and can occur in either the divalent (Fe^{+2}, ferrous) or trivalent (Fe^{+3}, ferric) valence states, which is determined by the pH and redox potential of the environment (Schulte, 2004, EPA, 2003). Iron readily binds to other silicate minerals and elements to form Fe oxides and hydroxides such as FeS_2 (as discussed earlier), ferrous sulphate ($FeSO_4$), ferrous chloride ($FeCl_2$), Fe (II) hydroxide ($Fe(OH)_2$) etc. Iron oxides, in turn, have been shown to adsorb many elements and participate in the attenuation of toxicity of most trace and heavy metals (EPA, 2003). Iron plays a central role in biology by participating in redox reactions and is therefore a powerful catalyst for the formation of •OH via the Fenton reaction. Under normal conditions, cellular organelles such as the mitochondria produce significant amounts of ROS (discussed in more detail later in **Section 2.2.5**). The cellular ROS concentration is kept in equilibrium by the cellular antioxidants as well as by strict modulation of cellular Fe concentrations (Hershko, 2007).

Toxicity associated with inhalation exposure

The occupational inhalation of iron-containing dust or fumes, generally in the welding, iron ore mining and steel industries, often results in a condition known as siderosis, which is a benign form of pneumoconiosis (Doherty et al., 2004) as well as symptoms such as cough and shortness of breath (NJDoH, 2007). Exposure to iron-containing dust or fumes does not necessarily lead to lung cancer but it has been shown that co-exposure of iron-containing dusts with silica, radon gas, diesel exhaust particulate (DEP), corn oils and products of synthetic resins increase the risk of developing cancer (NIOSH, 1989) or mixed dust pneumoconiosis (Nemery, 1990). Inhalation

of iron-containing dust has also been shown to result in severe pneumonia (Khiroya and Turner, 2015).

Radioactive contaminants

Tailings have received a large degree of negative attention, particularly due to the presence of the radioactive contaminant, uranium.

Uranium (U), CAS#: 7440-61-1

Uranium is an alpha-emitting, radioactive, heavy actinide metal and occurs naturally in rock and soil. There are three basic categories of U isotope mixtures i.e. natural, enriched and depleted, each of which consists of different percentages of U-238 (238U), 235U and 234U. When an atom of these isotopes decays, it emits an alpha particle to form a radioactive isotope of another element. This process continues until a stable, non-radioactive isotope of Pb (or bismuth in the case of 233U) is reached. The toxicity of U varies according to its chemical form and route of exposure. For example, oral and dermal exposure to natural and depleted U results in health effects due to their chemical (and not radiological) nature, while inhalation exposure may result in health effects due to their radiological nature.

Toxicity associated with inhalation exposure

In general, soluble U compounds that are inhaled are easily absorbed from the lungs into the bloodstream and are therefore more toxic in distal organs compared to within the lung itself (Tannenbaum et al., 1946). Conversely, inhaled, insoluble U compounds are more toxic to the lungs due to the longer retention time within the lung tissue.

Certain epidemiological studies have not shown significant associations between mortality and exposure to uranium in populations living near U mining and milling operations (Boice Jr et al., 2007a, Boice Jr et al., 2003, Boice Jr et al., 2007b), while other studies have reported increased deaths from cancers of the respiratory tract in U miners (Hornung et al., 1998, Howe and Stager, 1996, Tomasek et al., 2008, Woodward et al., 1991). In acute exposures to U, respiratory diseases may be limited to interstitial inflammation of the alveolar epithelium, which may eventually lead to pulmonary fibrosis although it has been suggested that the toxicity may also be

aggravated by the toxicity of the particles itself and not U *per se* (Cooper et al., 1982, Dungworth et al., 1989, Wedeen, 1991).

2.2.5.Mechanisms leading to toxicity

It is quite evident from the above sections that a common adverse health effect that is shared among toxic inhaled particles is the induction of oxidative stress, through the formation of ROS, which include •OH, superoxide anion radicals ($O_2^{\bullet -}$), H_2O_2, and singlet oxygen ($^1O_2$).

Oxidative mechanisms

As illustrated in **Figure 2-6**, ROS may be generated directly via the activity potential on the particles' surfaces through their surface-area, through surface functional groups, through redox active metals or through the bioactivation of soluble organic constituents such as polycyclic aromatic hydrocarbons (PAHs) and quinones through metabolizing enzymes such as cytochrome P450 (CYP) and reduced nicotinamide adenine dinucleotide (phosphate) (NAD(P)H): quinone oxidoreductase (NQO) (Øvrevik et al., 2015). According to Fubini and Fenoglio (2007), the most common mechanisms of free radical generation are:

(1) the reaction of endogenous hydrogen peroxide (H_2O_2) with surface-bound transition metal ions through Fenton or Haber-Weiss reactions leading to the generation of highly reactive •OH **(Figure 2-6)**, which is by far the most damaging radical, compared to all the other types of ROS. The •OH radicals are able to rapidly react and therefore damage most biological molecules thereby causing DNA damage (Imlay and Linn, 1988, Imlay et al., 1988) and lipid peroxidation (Mylonas and Kouretas, 1999, Gulumian, 1999, Gulumian, 2000);

(2) a surface homolytic rupture of a C–H bond, which generates C-centered radicals in peptides, proteins, etc.

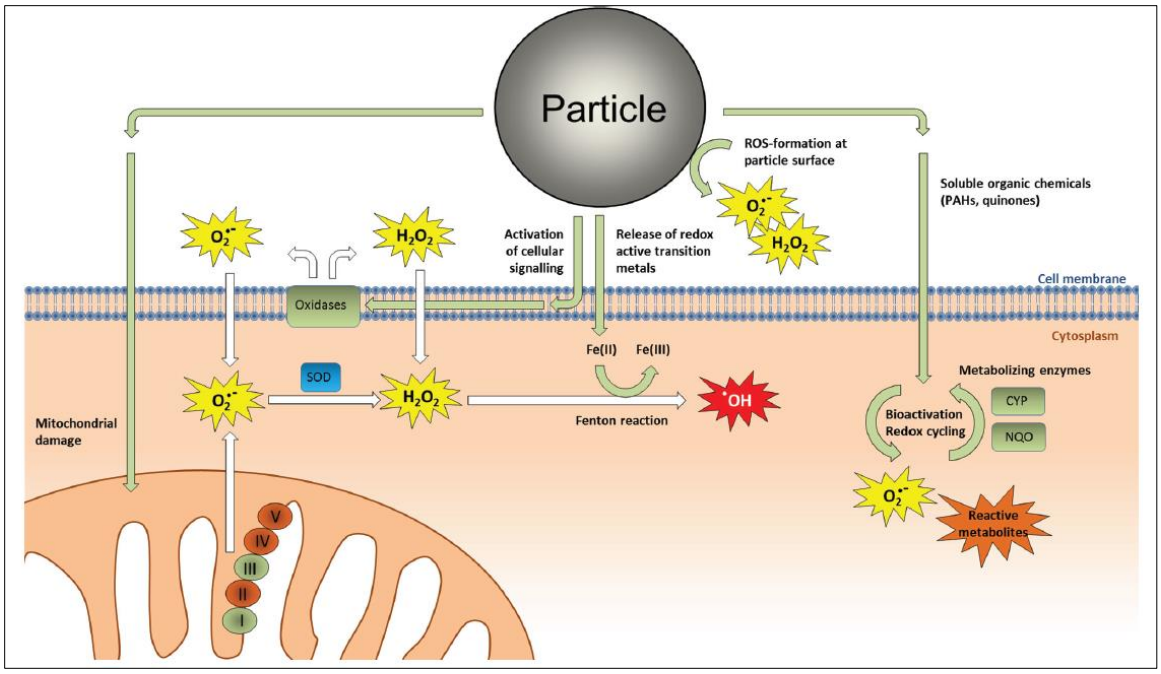

Figure 2-6: Inhaled PM may lead to ROS formation via several routes. Obtained from Øvrevik et al. (2015).

ROS may also be generated from the redox cycling of environmentally persistent free radicals (EPFRs) associated with PM. EPFRs are formed when an organic precursor chemisorbs onto a redox metal site on the particle surface (e.g., CuO or Fe_2O_3) leading to the reduction of the metal via electron transfer and thus the generation of a surface bound EPFR (Gehling et al., 2014, Dellinger et al., 2007).

The 'ROS hypothesis' has therefore been established, based on the different mechanisms by which particles alone may produce ROS, and suggests that, as stated by (Øvrevik et al., 2015), "the ability of particles to induce ROS formation in abiotic/cell-free environments, such as water, buffers, or cell culture medium can predict a particle's relative potential to induce toxicity in cells, animals and humans". For this reason, several researchers have used the ability of particles to induce ROS formation in the absence of cells as "a screening method to assess the biological reactivity of particles (Borm et al., 2007, Ayres et al., 2008)" (Øvrevik et al., 2015).

ROS may be generated not only at the particle surface, but also indirectly by the cells interacting with the particles, which consequently leads to inflammation and oxidative stress. Pulmonary

epithelial cells and resident macrophages are considered the primary targets of inhaled particulates (Øvrevik et al., 2015). In particular, activation of intracellular signalling pathways may trigger production of $O_2^{\bullet -}$ and H_2O_2 through the activation of membrane bound oxidases, and damage to mitochondria may lead to $O_2^{\bullet -}$ production and consequently H_2O_2 through SOD (Øvrevik et al., 2015).

The paradigm in which the formation of ROS may occur directly from the particle or indirectly from the particle-exposed cells is known as the 'oxidative stress paradigm'. Also encompassing this paradigm is the cell's response to oxidative stress. For example, at low levels of oxidative stress, the cells increase their antioxidant levels and restore redox homeostasis through activation of the ROS-sensitive nuclear factor E2-related factor 2/ antioxidant responsive element (Nrf2/ARE) pathway. At intermediate levels of oxidative stress, the mitogen-activated protein kinase (MAPKs) and central proinflammatory transcription factors such as nuclear factor-κB (NF-κB) and activator protein-1 (AP-1) are activated, resulting in the up-regulation of proinflammatory genes. At high levels, apoptosis or necrosis is initiated by oxidative stress resulting in the disruption of the electron transport chain (Øvrevik et al., 2015).

Although oxidative stress mechanisms have been suggested as the major toxicological pathway of particles, numerous studies have failed to find an association between the ability of particles to generate ROS and toxicological endpoints, suggesting the role of non-oxidative mechanisms (Øvrevik et al., 2015), which is discussed below.

Non-oxidative mechanisms

Particles may enter the cell via phagocytosis leading to the destruction of lysosomal membranes, lysosomal leakage and activation of the NLRP3 inflammasome [NACHT, leucine-rich-repeat (LRR) and pyrin domain (PYD)-containing protein 3] with subsequent cleavage/release of interleukin-1β (IL-1β) **(Figure 2-7)**. Proteins of the NACHT family [NAIP (neuronal apoptosis inhibitory protein), CIITA (MHC class II transcription activator), HET-E (incompatibility locus protein from *Podospora anserina*) and TP1 (telomerase-associated protein) play a critical role in the innate immune system (Damiano et al., 2004). Particles may also interact directly with cholesterol in lipid rafts, leading to lipid sorting and Spleen tyrosine kinase (Syk)-activation. Syk

activation in turn induces both IL-1β-transcription and cleavage of pro-IL-1β to mature IL-1β through combined activation of NF-κB and ROS-mediated stimulation of the NLRP3/caspase-1. In this instance, ROS act as a central secondary messenger, therefore, even non-oxidant mediated triggering mechanisms are able to activate downstream redox-regulated events. Particles have also been reported to bind the cluster of differentiation 14 protein (CD14), which may stimulate cytokine responses through activation of Toll-like receptor (TLR) 4-mediated activation of NF-κB and MAPK signalling. Particles have also been shown to bind scavenger receptors (SRs), resulting in pro- and anti-inflammatory effects (Øvrevik et al., 2015).

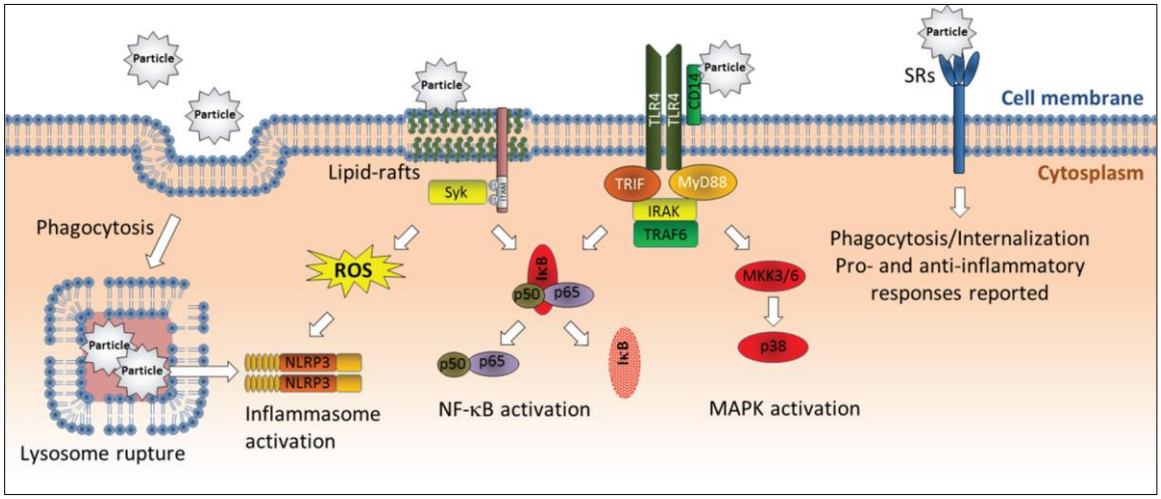

Figure 2-7: Non-oxidant-related mechanisms triggered by inhaled PM. Obtained from Øvrevik et al. (2015).

2.3. Exposure pathways of tailings material to surrounding environments

It is important to note that there will not be any adverse health effects to toxic particles if the exposure to the particle is not possible. With regards to tailings material, several research studies and governmental reports have reported on the several exposure pathways of tailings material to receptor environments. According to the Gauteng Department of Agriculture and Rural Development (GDARD), formerly known as the Gauteng Department of Agriculture Conservation and Environment (GDACE), there are three main issues relating to TSFs:

1. Air-quality, with particular reference to airborne dust and radioactive pollutants emitted from TSFs;

2. Water-flux and water-quality, including issues related to acid mine drainage (AMD), and the transport of radioactive materials and;
3. Geotechnical safety concerns including dangers of sink holes, ground instability and collapse as well as open, unsealed mine shafts (GDARD, 2012).

Each of these issues will be discussed briefly below.

2.3.1.Air pollution

Air pollution has a greater potential to transport contaminants, relative to water and soil pollution, since air is not confined or hindered by topographic boundaries. Air pollution also occurs at a much faster rate than water or soil pollution as it is transported by rapid and uncontrollable wind speeds (Csavina et al., 2012). In addition, air pollution has the potential to contribute to both water and soil pollution as these suspended tailings particles may be washed out during rainfall and contaminate surrounding soils and water as well as vegetation.

Air pollution from un-vegetated abandoned TSFs and poorly managed active TSFs typically occurs during incidents of high wind speeds (GDARD, 2009b) and it has been suggested that the total erosive losses by unprotected TSFs can reach approximately 400 tonnes of dust per hectare per annum (four-year average) (Blight, 1989), of which a significant portion may be airborne (Sutton, 2012). This erosion rate calculated by Blight (1989) seems quite excessive. However, a typical TSF of 50 hectares in size and averaging a height of 15-20 m contain approximately 25 million tonnes of milled tailings (Mrost, 1974), therefore putting the rate of erosion of 400 tonnes of dust per hectare per annum, calculated by Blight (1989), into perspective. Areas located downwind of these sources, i.e. in the direction in which the prevailing wind is blowing, are generally mostly affected (GDARD, 2009b).

The effect of air pollution due to windblown dust from mine tailings dust is twofold in that it presents a nuisance via the soiling of buildings, materials windowsills and cars **(Figure 2-8)** but most importantly carries a health risk (GDARD, 2009b), as depicted in **Figure 2-9**.

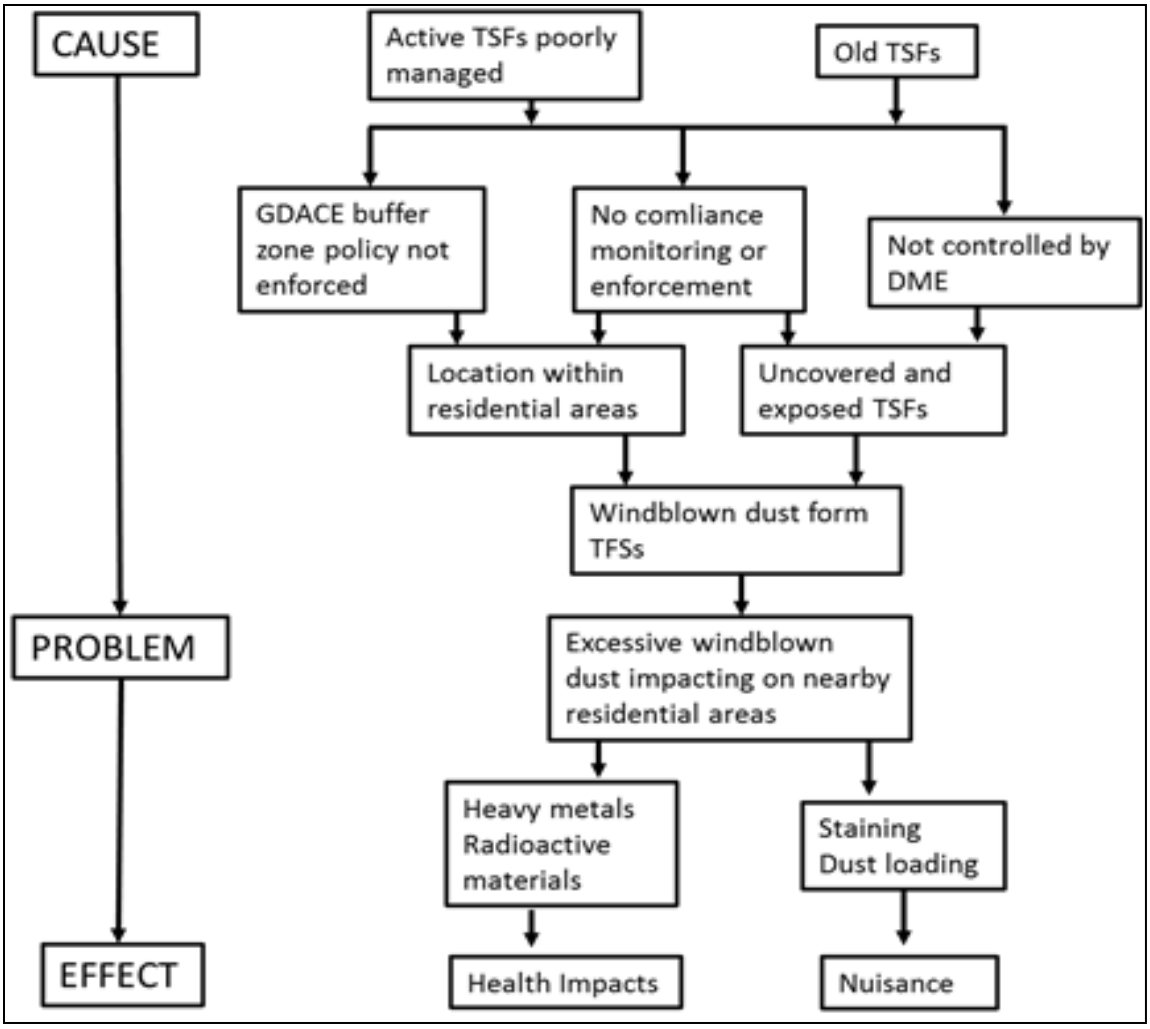

Figure 2-8: Effects of windblown dust from TSFs. Adapted from (GDARD, 2009b).

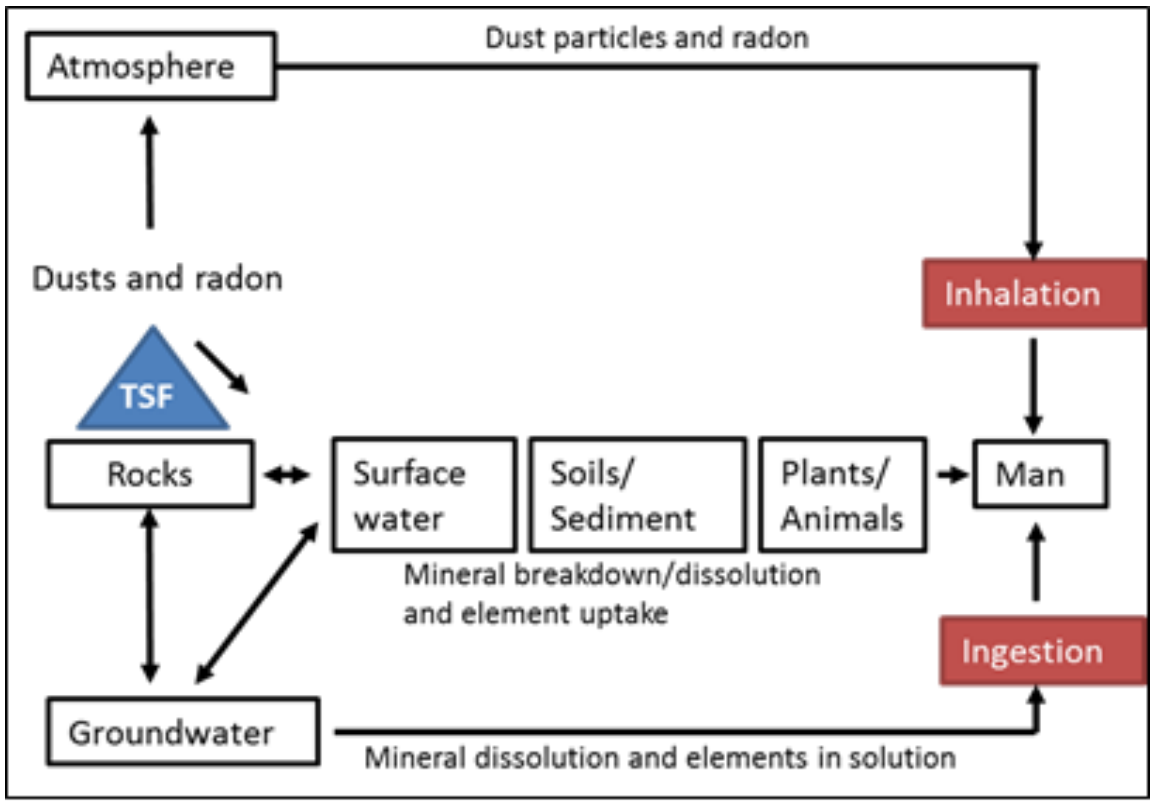

Figure 2-9: Routes of exposure of tailings dust. Adapted from Chevrel et al. (2003).

2.3.2.Water pollution

TSFs affect the surface water drainage system usually in the form of AMD, which is the process of when alkaline slimes turn acidic due to the oxidation of the sulphide minerals in FeS_2 (Bradshaw and Chadwick, 1980). AMD is produced by, (1) the decanting of water contaminated with tailings material from shafts connecting the mine void to the surface or, (2) by erosion, run-off, infiltration and seepage (Chevrel et al., 2003), particularly from older TSFs that are more likely to be located in river beds or over dolomites. The topic of AMD will not be discussed further; however, additional information can be found in the literature (Ochieng et al., 2010, Tutu et al., 2008, McCarthy, 2011, Aucamp and Van Schalkwyk, 2003, Rösner and Van Schalkwyk, 2000).

2.3.3.Mechanical dam wall failures and geotechnical instability

The most widely known TSF mechanical failure is that of the Merriespruit disaster in February of 1994, where the collapse of the dam, as a result of heavy rainfall, led to the deaths of 17

people and 600 000 m^3 of slime entering the residential areas of Merriespruit in Virginia, Free State (Wagener, 1997). Another instance where mechanical dam wall failure led to disastrous consequences is that of the Bafokeng disaster in 1974 during which approximately 2 million m^3 of tailings flowed into the Kwa-Leragane and Elands Rivers, which eventually reached the Vaalkop water reservoir 45 km from the initial TSF site (Blight et al., 1981, Blight, 2010). Fissures and unprotected shafts have also claimed lives, for example, in the case of the Makause site in 2007 where Joyce Shongwe fell to her death (GDARD, 2012). Additional information regarding dam wall failures may be found in Van Niekerk and Viljoen (2005).

2.3.4.Soil pollution

Another source of concern is the fact that the mere presence of TSFs permits exposure to the public via direct contact with the dust through unauthorized entry to the TSF or by living in settlements next to TSFs (GDARD, 2009b).

2.4. Vulnerable receptor environments

Multiple receptor points are affected by TSFs including humans, ecological entities, recreational lands, industrial estates etc. (Chevrel et al., 2003). For the purposes of this thesis, humans as a receptor point will be discussed further:

2.4.1.Children

According to the WHO, the most common route of exposure to dust particles in children is ingestion through hand-to-mouth behaviour. It has been suggested that the amount of soil and house dust ingested by a typical 1-6 year old child is approximately 100 or 200 mg/24 h (WHO, 2010). Children in general are known to be exposed to a higher degree of dust compared to adults because they (1) spend more time outside; (2) have higher breathing rates, compared to that of adults, which in turn results in higher oxygen consumption and possibly particle deposition; (3) consume more, possibly contaminated, water and food per unit body weight; and (4) have higher absorption rates per unit body weight. Apart from the higher exposure to dust by children, children may also be affected to a higher degree to dust pollution due to the fact that they (1) have narrower airways and therefore a higher possibility of airway obstruction; (2) have developmentally immature lungs and immune systems; and (3) have more time to develop

chronic diseases as a consequence of early exposure (Ostro et al., 2009, Moya et al., 2004, Tamburlini et al., 2002, Ryu et al., 1983).

A number of epidemiologic studies have indicated that living near mining waste is a major risk factor for exposure to metals, particularly with children. For example, von Schirnding et al. (2003) showed that the blood Pb levels among the children aged 6-10 years in the Pb mining town of Aggeneys in the Northern Cape, South Africa, averaged around 16 µg/dL, while in the control community of Pella, the mean blood Pb level averaged 13 µg/dL. Similar types of studies were conducted globally:

- A study by Polissar et al. (1990) observed an association between indoor dust with urinary As in an exposed community close to a former copper smelter in Tacoma, Washington. Polissar et al. (1990) suggested that soil ingestion may be a source of exposure in children as their study revealed a stronger relationship between soil As and urinary As in children, compared to that of adults.
- A study by Moreno et al. (2010) revealed that a high percentage of children living in the vicinity of mine tailings at the Taxco mining district in Mexico had a high body burden of Ni (75.4 ± 30.7 µg/L, urine), barium (Ba; 18.4 ± 4.1 µg/L, urine), Mn (5.2 ± 0.7 µg/L, urine), Cr (15.1 ± 4.45 µg/L, urine), Co (18.3 ± 9.7 µg/L, urine), cadmium (Cd; 4.7 ± 2.7 µg/L, urine), As (16.5 ± 8.3 µg/L, urine), Hg (0.7 ± 0.86 µg/L, urine) and Pb (9.4 ± 3.3 µg/dL, blood), which were higher than the reference values.
- In another study conducted in Mexico, Yáñez et al. (2003) found higher As levels in urine (136 µg/g creatinine) and blood Pb levels (11.6 µg/dL) in children living in areas surrounding a mining site and TSFs in Villa de la Paz, compared to a control population in Matehuala (34 µg/g creatinine for As and 8.3 µg/dL for Pb). In accordance with these results, Yáñez et al. (2003) also observed a higher degree of DNA damage in blood cells of the exposed children compared to the control children using the Comet (single-cell gel electrophoresis) assay.
- The New South Wales Government revealed that the blood Pb levels of 85% of children 1 – 4 years of age from the Broken Hill mining community in Australia was higher than 10 µg/dL (NSW, 1993), while Gulson et al. (1994) showed that this elevation in blood Pb levels originated most likely from the TSFs in the Broken Hill area as one of the major

sources and suggested that the ingestion of Pb was probably via hand-to-mouth activities. Furthermore, Gulson et al. (1994) showed that the Pb from soils and dust collected had a high degree of bioavailability therefore corresponding with the elevated blood Pb levels observed.

- Similarly, the following studies have also observed an association between higher levels of toxic metals in children living in (historical) mining and/or smelting communities compared to children in control communities or compared to reference values: Cook et al. (1993), Dutkiewicz et al. (1992), Murgueytio et al. (1997), Hwang et al. (1997) and Loh et al. (2016).

Other studies however did not find an association between metal levels in children and that of mine waste and smelter sites (Danse et al., 1995, Steele et al., 1990, Bjerre et al., 1993, Bussières et al., 2004) and have attributed this lack of association to the lack of bioavailability of metals in tailings dust (Danse et al., 1995).

2.4.2.The poor

Like children, the poor are also more vulnerable to exposure of dust particles mainly due to the fact that they generally suffer from poor health caused by the following factors: poor sanitation, limited access to clean water and inadequate medical assistance as well as an increased likelihood of malnourishment. In addition, poor households are often more likely to be located on the least desirable, cheapest land, like, for instance next to TSFs and they more than likely do not have the option of relocating due to limited financial resources (Sutton, 2012).

2.4.3.The elderly and individuals with existing health problems

Individuals with existing health problems are also particularly vulnerable to dust particles as exposure could lead to the exacerbation of a health problem or to the onset of secondary health problems leading to comorbidity. Similarly, the elderly may also show an increased susceptibility to adverse effects related to dust particles due to pre-existing illnesses such as cardiovascular disease (Goldberg et al., 2013). Other factors that may increase their vulnerability include immunosenescence (gradual deterioration of the immune system due to age) as well as decreased lung function (Simoni et al., 2015, Poland et al., 2014).

It is evident from the above sections that tailings material may carry the potential to be toxic and may reach vulnerable receptor environments through several exposure routes, of which the most difficult to contain is air pollution. The following section addresses the strategies implemented in South Africa to lower air pollution caused by TSFs.

2.5. How to lower air pollution

Apart from monitoring active mining operations, the Department of Mineral Resources (DMR, formerly known as the Department of Minerals and Energy) has an important role to manage active and dormant TSFs **(Figure 2-10)**. The objective for active TSFs is proper dust mitigation through continuous watering as new tailings are deposited while that for older, dormant TSFs is successful reclamation or rehabilitation (GDARD, 2009b).

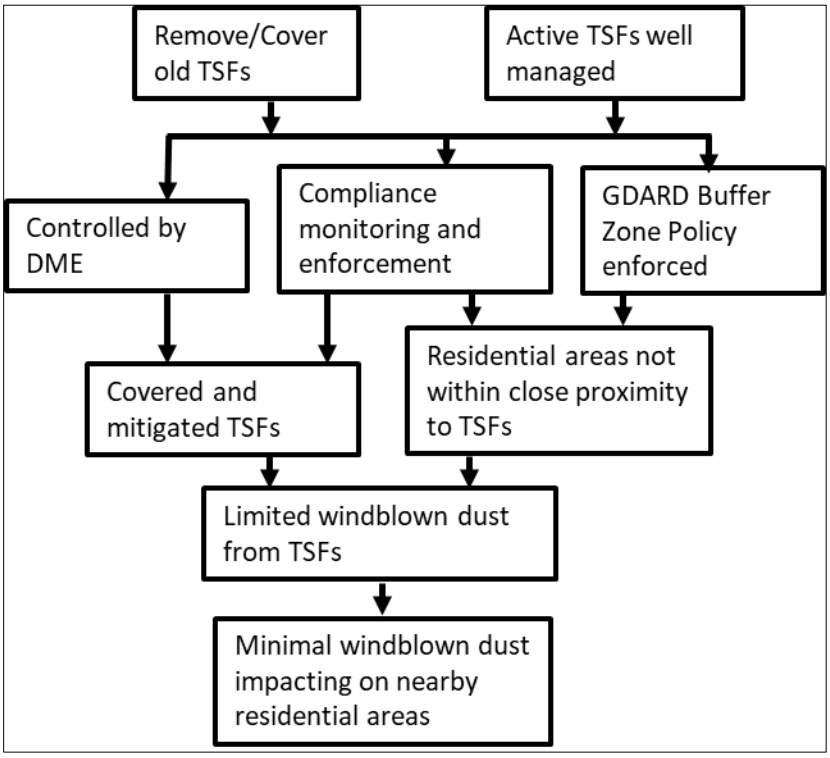

Figure 2-10: Objective tree developed for TSFs. Adapted from (GDARD, 2009b).

2.5.1.Reclamation of TSFs

Reclamation (also known as surface mining) is the extraction of residual gold from tailings material and became a viable option in the 1970s when extraction methodologies had advanced. As a result, some of the landmark TSFs gradually disappeared freeing up valuable land for reuse. Ergo Mining Proprietary Limited is the reclamation operation in South Africa owned and managed by DRDGOLD Limited (DRDGold, 2015) and operates mainly in the central Witwatersrand basin in the Gauteng province **(Figure 2-11)**.

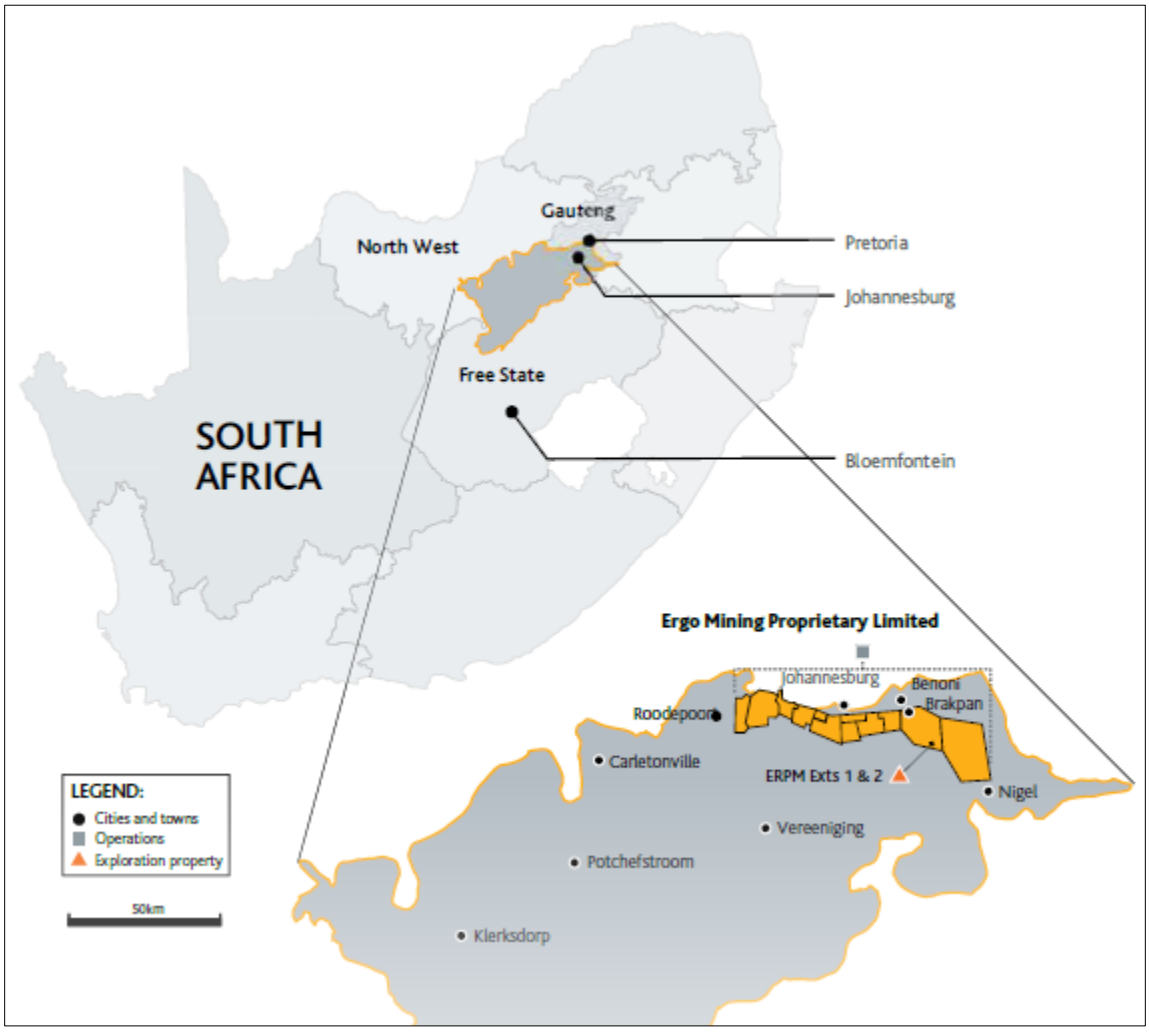

Figure 2-11: Ergo Mining Proprietary Limited operates mainly in the central Witwatersrand basin in the Gauteng Province. Obtained from DRDGold (2015).

During the early years of reclamation, older TSFs, which mainly consisted of sand was reclaimed using front-end loaders that loaded sand onto conveyor belts. The sand was then fed onto a screen where water was added to wash the sand into a sump. The sump was pumped to the plant where the gold was recovered using cyanidation and carbon adsorption (DRDGold, 2014). The majority of sand TSFs have already been reclaimed to date. For newer, slime-containing TSFs, of which hundreds of millions of tonnes are still located in the Wits basin (DRDGold, 2015), reclamation is achieved with monitor guns that direct jets of high-pressure water at the target area. The water dislodges the slime and turns it into slurry that is then channelled to a collection point before being pumped to a metallurgical treatment plant for processing (DRDGold, 2014, DRDGold, 2015).

Tailings reclamation plants within the Witwatersrand basin

The Brakpan (Ergo) reclamation plant, located in Brakpan, currently receives and treats tailings from the Elsburg tailings complex in Boksburg via two feeder lines **(Figure 2-12)**. This plant uses flotation, fine-grind, and a combination of high grade and low grade CIL metallurgical processes to recover gold from slurry. The reclaimed tailings material is deposited on the Brakpan tailings facility (BTF) located 12 km south-west from the plant. The East Rand Proprietary Mines (ERPM) plant, situated near Boksburg, was first established as an underground mining operation but was suspended in 2008 due to safety reasons. The ERPM plant continues as a reclamation plant and holds 65% of ErgoGold through the contribution of its Elsburg Tailings Complex. The Crown and City Deep plants **(Figure 2-12)** operate as milling and pump stations, delivering tailings from the southern and central Witwatersrand to the Brakpan plant via a 50 km pipeline. The much smaller Knights plant **(Figure 2-12)** is currently treating tailings from the Cason TSF, which is one of the last remaining sand TSF in the area, and depositing the residue on the BTF (DRDGold, 2014, DRDGold, 2015).

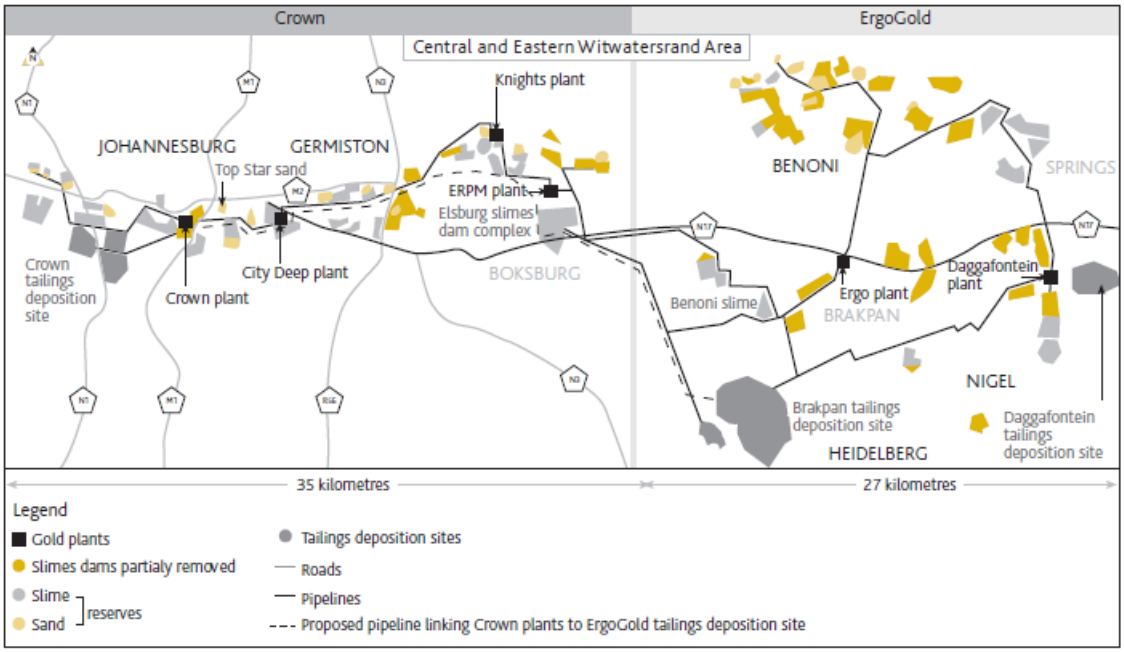

Figure 2-12: Reclamation plants within the Witwatersrand basin. Obtained from DRDGold (2009).

Disadvantages of reclamation

Even though reclamation of TSFs may serve several purposes ranging from the extraction of residual high grade gold to mitigating air pollution as well as freeing up land (known as tailings footprints), for future reuse, it does carry certain disadvantages:

1) Reclamation does not account for the secondary sources of contaminants or leachate that remain in the underlying soil and water sources, which in turn may hinder the use of land. For example, Rösner and Van Schalkwyk (2000) showed that seven TSF footprints were highly acidic (min pH = 3.1) and contained elevated levels of elements including Sn, U, Co, Ni, Pb, V and As among others.
2) Reclamation does not completely eliminate the source of air pollution. In fact, it only moves the source of air pollution from one area to another as reclaimed tailings materials still need to be deposited elsewhere. According to DRDGold, the BTF is the current deposition site for reclaimed tailings within the Witwatersrand area (DRDGold, 2015). Even though DRDGold claims that the BTF is designed such that it causes minimal environmental damage as well as it being located in a less-densely populated area (DRDGold, 2015), the possibility of air pollution cannot completely be ruled out.

3) The disturbance of tailings material through reclamation often introduces new unforeseen problems. For example, during the reclamation process, partially treated acid mine drainage water is mixed with tailings material, thereby introducing air and water into anaerobic tailings and contributing to AMD formation (Mphephu et al., 2003).
4) Of particular concern is the fact that the reclamation process involves refining tailings particles to further liberate the residual gold, thereby creating particles that are smaller in size compared to the initial tailings particles and which contains a higher concentration of elements used for gold extraction. In fact, reclamation companies are considering refining reclaimed tailings a second time (DRDGold, 2015), which will lead to more toxic particles that are even smaller in size.

2.5.2.Rehabilitation of TSFs

In certain instances, it might be more advantageous to remove only the hazardous contaminants, whether organic contaminants or metals, in the tailings material rather than the entire TSF. Technologies developed for organic contaminants include soil vapour extraction and biodegradation etc. whereas technologies for heavy metals include electrokinetic techniques, soil washing techniques and chemical leaching techniques (Xenidis et al., 2003). Electrokinetic techniques make use of an electric field to mobilise metals; Soil washing techniques separate contaminated particles from clean soil via mineral processing methods; Chemical leaching techniques involve dissolution of metals. Although these techniques are a better alternative to TSF reclamation they are in most cases very expensive (Xenidis et al., 2003).

The most common approach is to rehabilitate TSFs by one or a combination of the methods listed below; however, the major drawback with these are cost as the rehabilitated area needs to be maintained on a regular basis for several decades.

Some of the measures to suppress dust and which are currently being used by DRDGold (2015, 2018) include:

- water tanks to spray binding chemicals on all access roads;
- water spraying and irrigation;
- netting on exposed tailings surfaces to reduce wind velocity;

- vegetation on exposed tailings surfaces (discussed below);
- rock cladding (discussed below);
- plans to design future TSFs in such a way that exposed surfaces do not face the direction of prevailing winds.

Vegetation: Vegetation is effective on horizontal surfaces and on low- to intermediate-angled slopes but not on steeper slopes, which are more affected by erosion (GDARD, 2009b). In addition, the sustainability of vegetation cover is often hampered by the characteristics of the tailings material itself such as dryness, acidity, metal toxicity and low nutrient levels etc. (Renault et al., 2001, Renault et al., 2004) as well as secondary factors such as community interference, drought and fires (GDARD, 2009a).

Rock cladding: This non-vegetative alternative, i.e. a 300 mm of fine rock layer, was found to result in an erosion control efficiency of 100%, if the base is levelled and compacted, or ~ 60%, if the base is not compacted (GDARD, 2009a).

Combinations of dust suppression strategies have also proven to be successful. For example, the bio-windbreak method, which involves dust netting (erected in a zigzag pattern to break the wind speed) and establishing vegetation (e.g. self-spreading grass species) in strips under a limited irrigation system (Asikhulume, 2013), is being utilised at the Crown tailings deposition site west of Johannesburg **(see Figure 2-12)**.

According to GDARD, several potential uses for rehabilitated TSFs are possible of which some include the development of grass land with thatch grass for local communities to utilize, agri-business projects, landfill sites for domestic and hazardous waste, areas for the erection of wind turbines and heritage sites (GDARD, 2009a).

2.6. Current legislation and Governance

Section 24 of the Constitution of South Africa Act 108 of 1996 (the Constitution) states that "everyone has the right to an environment that is not harmful to their health or well-being and everyone has the right to have the environment protected, for the benefit of present and future

generations" (SA, 2018). Despite this basic human right, the implementation thereof has been met with challenges. For example, even though complaints have been recorded by the Crown Mines Dust Monitoring Forum due to TSF pollution, as discussed previously, no specific action was taken with respect to 35% of the total complaints received from 1995 to 2010 due to mines refusing to invest resources into solving the pollution problem (Oguntoke and Annegarn, 2014). Similarly, Wright et al. (2014) observed a lack of support from government and mining companies with regards to proper dust mitigation strategies to prevent air pollution.

According to GDARD, if no action is taken to address the air pollution from TSFs, legal action will be taken against local and provincial governments where the Bill of Rights will form the foundation for litigation. Most importantly, failure of action will have a negative impact on the overall health of the residents (GDARD, 2012). The section below addresses a few inhibitory factors identified by GDARD that have been known to hinder the progress for successful mitigation of TSF air pollution.

2.6.1.Too many Acts and Departments involved

GDARD has developed a decision tree consisting of eight questions to assist in the decision making with regards to whether TSFs pose a risk **(Figure 2-13)** (GDARD, 2012). Although the decision tree, in theory, should simplify decision making, the process is complicated by the fact that various national, provincial and municipal governmental agencies are responsible for each question. Moreover, each governmental agency is responsible for more than one question further complicating the process, as illustrated in **(Figure 2-13)**.

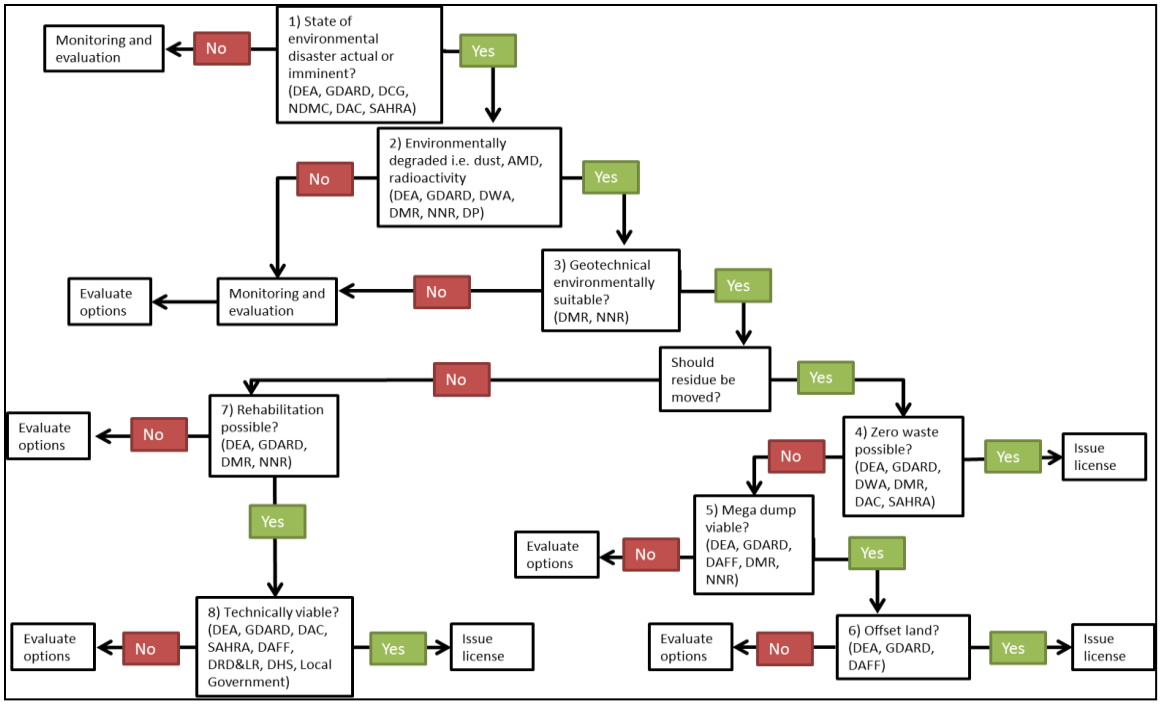

Figure 2-13: Decision tree developed by GDARD. Adapted from GDARD (2012).

The guiding legislation at each question of the decision tree is listed in **Table 2-3**. In addition to the acts mentioned in **Table 2-3**, the following acts are also applicable in the mining fraternity when any occupation or reclamation of TSFs is considered: (1) Constitution of the Republic of South Africa, 1996; Chapter 2; (2) SANS 1929:2005; (3) Atmospheric Pollution Prevention Act, 1965; (4) National Veld and Forest Act, 1998; (5) Various policy documents, Provincial legislation, local by-laws, Common Law, DMR and Department of Water Affairs and Forestry (DWAF) Policy Documents and Guidelines (GDARD, 2009a). It is therefore evident that this will further complicate and hinder the process of dealing with TSFs.

Table 2-3: Guiding legislation at each question of the decision tree. Adapted from GDARD (2012).

MRA Decision	Legislation
State of environmental actual or imminent?	National Environment Management Act (Act No. 107 of 1998) (as amended, including 2010 EIA regulations)
	Disaster Management Act (Act No. 57 of 2002)
	National Heritage Resources Act (Act No. 25 of 1999)
Environmentally degraded (dust, AMD, radioactivity)?	National Environment Management Act (Act No. 107 of 1998) (as amended, including 2010 EIA regulations)
	Environment Conservation Act (Act No. 73 of 1989) (as amended)
	National Environment Management: Biodiversity Act (Act No. 10 of 2004)
	National Environment Management: Protected Areas Act (Act No. 57 of 2003 and 2004) (as amended)
	National Environment Management: Air Quality Act (Act No. 39 of 2004)
	Hazardous Substances Act (Act No. 15 of 1973)
	National Nuclear Regulator Act (Act No. 47 of 1999 and 2006)
	Explosives Act (Act No. 15 of 2003) (as amended including nitrates and other contaminants)
	National Water Act (Act No. 36 of 1998) (as amended, including regulation on use of water for mining and related activities aimed at the protection of water resources)
Geotechnical environmentally suitable?	Mineral and Petroleum Resources Development Act (Act No. 28 of 2002) (as amended, including MPRDA Regulations)
	Mine Health and Safety Act (No. 29 of 1996) (as amended)
	National Nuclear Regulator Act (Act No. 47 of 1999 and 2006)
Zero waste possible?	National Environment Management Act (Act No. 107 of 1998) (as amended, including 2010 EIA regulations)
	National Water Act (Act No. 36 of 1998) (as amended, including regulation on use of water for mining and related activities aimed at the protection of water resources)
	Mineral and Petroleum Resources Development Act (Act No. 28 of 2002) (as amended, including MPRDA Regulations)
	National Heritage Resources Act (Act No. 25 of 1999)
Megadump viable?	National Environment Management Act (Act No. 107 of 1998) (as amended, including 2010 EIA regulations)
	Conservation of Agricultural Resources Act (Act No. 43 of 1983, including top soil conservation measures, no disturbance of land, alien plant control measures)
	National Nuclear Regulator Act (Act No. 47 of 1999 and 2006)
	Mineral and Petroleum Resources Development Act (Act No. 28 of 2002) (as amended, including MPRDA Regulations)
Offset land?	National Environment Management Act (Act No. 107 of 1998) (as amended, including 2010 EIA regulations)
	Conservation of Agricultural Resources Act (Act No. 43 of 1983, including top soil conservation measures, no disturbance of land, alien plant control measures)
Rehabilitation possible?	National Environment Management Act (Act No. 107 of 1998) (as amended, including 2010 EIA regulations)
	National Nuclear Regulator Act (Act No. 47 of 1999 and 2006)
	Mineral and Petroleum Resources Development Act (Act No. 28 of

MRA Decision	Legislation
	2002) (as amended, including MPRDA Regulations)
Technically viable?	National Environment Management Act (Act No. 107 of 1998) (as amended, including 2010 EIA regulations)
	National Heritage Resources Act (Act No. 25 of 1999)
	Conservation of Agricultural Resources Act (Act No. 43 of 1983, including top soil conservation measures, no disturbance of land, alien plant control measures)
	Fertilizers, Farm Feeds, Agricultural Remedies and Stock Remedies Act (Act No.36 of 1947) (as amended)
	Development Facilitation Act (Act No. 67 of 1995) (as amended)
	By-laws

2.6.2.Ownership and responsibility of TSFs not clearly defined

In terms of Section 43(1) of the Mineral and Petroleum Resources Development Act (MPRDA), "any individual or entity that has been granted the permission to mine remains responsible for any environmental liability, pollution or ecological degradation, and management thereof, until the Minister has issued a closure certificate to the holder concerned" (SA, 2018). Furthermore, Section 2(4)(p) of the National Environment Management Act (NEMA), commonly known as the 'polluter pays' principle, specifies that the entity creating TSFs must be responsible for controlling and mitigating further environmental pollution. Despite these Acts, establishing ownership of existing TSFs is currently hindered due to the many ownerless and derelict mines in Gauteng, illegal occupation of land as well as poor management of property ownership (GDARD, 2009a). In addition, the funds allocated for mine closure are often insufficient for the enforcement and long term monitoring of rehabilitation processes. The situation is further complicated by the fact that the Air Quality Act i.e. the National Environmental Management: Air Quality Act (AQA) No 39 of 2004 has placed the responsibility for controlling and mitigating environmental pollution on the shoulders of the provincial and local authorities (GDARD, 2012).

2.6.3.Current Air Quality Management (AQM) not enforced

GDARD has developed the first provincial Air Quality Management Plan (AQMP) in South Africa (GDARD, 2009b) for the Gauteng Province as required by the AQA (GDARD, 2009b). The main aims of the AQMP are as follows: "(i) improve air quality; (ii) reduce negative impacts on human health and the environment; (iii) address the effects of fossil fuels in residential applications; (iv) address the effects of emissions from industrial sources; (v) address effects

from emissions from any point or non-point sources of air pollution; (vi) implement the republic's obligations in respect of international agreements; and, (vii) give effect to best practice in air quality management" (GDARD, 2009b).

Feasible interventions have been developed to address these seven major problems **(Table 2-4)**. One of these interventions involved the establishment of ambient monitoring stations within residential areas adjacent to TSFs to ensure that air pollutants do not exceed the set thresholds. The data obtained from these stations would then be uploaded into the South African Air Quality Information System (SAAQIS) website (discussed in more detail below in **Section 2.6.5**) and then be disseminated to the public as well as stakeholders. However, during an audit, the state of repair of the monitoring stations and infrastructure was found to be poor due to lack of training, time and financial support available to operators (GDARD, 2009b).

Current South African exposure limits to PM and crystalline silica

PM limits

With regards to the PM limits, the South African National Ambient Air Quality Standard (NAAQS) for PM_{10} environmental levels have been set by the Department of Environmental Affairs (DEA) at 75 and 40 µg/m³ as the 24 h average and annual average, respectively, with the 24 h average not be exceeded more than 4 times within a calendar year (DEA, 2009) **(Table 2-4)**. Although not shown in **Table 2-4**, the DEA has also set an environmental standard for $PM_{2.5}$ at 40 µg/m³ (24 h average), which will further be reduced to 25 µg/m³ in the year 2030 (DEA, 2012). Currently, there are no established environmental standards for respirable PM_4 levels in South Africa. The South African DMR, however, has set the current occupational exposure limit (OEL), for respirable PM_4 at 3 mg/m^3 (DMR, 2006). The OEL is defined as "the level to which workers are exposed during their working career that should not cause any adverse health effects to them or their offspring" (Mallon, 2016). Different types of OELs are often set by different international regulatory agencies. For example, the OEL may be defined as a time weighted average (TWA), which is the average, maximum concentration for an airborne substance for an 8 hour work day and 40 hour work week (Mallon, 2016). Different agencies label this 8 h TWA under different terms. For example, the Occupational Safety and Health Administration (OSHA) refer to the 8 h TWA as the permissible exposure limit (PEL) whereas

the American Conference of Governmental Industrial Hygienists (ACGIH) refers to the threshold limit value (TLV). The main difference between the PEL and the TLV is that the PEL is legally enforceable whereas the TLV is only a recommended value. The current PEL and TLV for respirable dusts have been set at 5 mg/m^3 and 3 mg/m^3, respectively (OSHA, 2017b). It should be noted that these South African and international limits are relevant for occupational settings only and are based on inert or nuisance dusts, often labelled as particles not otherwise classified/regulated (PNOC/R) (OSHA, 2017a), which is generally defined as dusts that contain less than 1% quartz (Cherrie et al. 2013). These limits that were set for nuisance dusts may be too high as it was initially accepted that nuisance dust, with its low quartz percentage would have little, potentially reversible, adverse health effects on the lungs. However, as Cherrie et al. (2013) suggested, this notion may be erroneous for the fact that recent epidemiological and toxicological research has proven otherwise. Cherrie et al. (2013), together with the European Institute of Occupational Medicine (IOM), the British Trade Union Congress (TUC) and the German Maximale Arbeitsplatz Konzentration (MAK) Commission suggested that, until further evidence is obtained on the true toxicity of PNOC/R, that current limits be reduced to at least 1 mg/m^3.

It should also be noted that OSHA and ACGIH refer to “respirable” particulates rather than PM_4 particulates. Since the terms “respirable” and “PM_4” are roughly equivalent, they will be used interchangeably throughout this thesis.

Table 2-4: Intervention strategies for TSFs. Adapted from GDARD (2009b).

Intervention strategy	Threshold	Responsible parties
GDARD to develop buffer zone regulations	Record of Decision specifications clearly stating no development within buffer zone	GDARD
Municipalities to develop by-laws to prevent development within GDARD buffer zones	No new residential developments within buffer zone	DEA, GDARD, CoJ, CoT, EMM, WRDM and MDM
Municipalities to develop by-laws requiring monitoring and reporting from mines with active TSFs	Dust fallout within residential areas less than 3 exceedances / year and not more than 2 sequential months) and industrial areas	CoJ, CoT, EMM, WRDM and MDM, mines
Municipalities to establish ambient monitoring stations within residential areas affected by windblown dust from TSFs	PM_{10} 24-h average = 75 µg/m³ & annual average = 40 µg/m³ SO_2 instantaneous = 500 µg/m³, 24-h average = 125 µg/m³ & annual average = 50 µg/m³ NO_2 1-h average = 200 µg/m³ & annual average = 40 µg/m³	GDARD, CoJ, CoT, EMM, WRDM and MDM, mines
Industries to develop mitigation management measures and implementation plans	Percentage vegetation cover up to 1 m from top surface area to be mostly wet	Mines, GDARD, CoJ, CoT, EMM, WRDM and MDM
Closely monitor and manage super dumps	No visual dust from mine tailings removal and dumping	Mines, GDARD, CoJ, CoT, EMM, WRDM and MDM
Removal of dormant TSFs near residential areas	No TSFs near existing residential areas	GDARD, DME
DEA – Department of Environmental Affairs; GDARD – Gauteng Department of Agriculture and Rural Development; GDLG – Gauteng Department of Local Government; GDED – Gauteng Department of Economic Development; CoJ – City of Johannesburg; CoT – City of Tshwane; EMM – Ekurhuleni Metropolitan Municipality; WRDM – West Rand District Municipality; SDM – Sedibeng District Municipality; MDM – Metsweding District Municipality		

Crystalline silica limits

Unlike occupational crystalline silica exposures, there is currently no ambient crystalline silica limit. In the absence of such a limit, several interim limits have been set by various international institutions and state agencies. Interim limits are generally set while awaiting further toxicological and/or epidemiological data in order to calculate a final limit. These interim limits therefore adhere to the precautionary principle i.e. it considers it better to establish a guideline based on incomplete data to ensure human and/or environmental protection than to not establish a guideline at all (CCME, 2016). Indeed proper scientific practice should aim to prevent the incidence of disease rather than to try and reduce the prevalence of disease. These interim limits are available for use by organisations while awaiting further peer review and publication of the final limits. Therefore changes to these interim limits are possible as new literature become available. As stated in Andraos et al. (2018b), “these interim limits are calculated through the

derivation of a point of departure (POD) value (e.g. benchmark dose/concentration (BMD/C), lowest observed adverse effect level (LOAEL) or no observed adverse effect level (NOAEL)) using the epidemiological data from miners exposed to silica. An uncertainty factor is then applied to the POD to account for the general population including sensitive groups such as children and the elderly. For example, using the epidemiological data from white South African miners (Hnizdo and Sluis-Cremer, 1993), the California Office of Environmental Health Hazard Assessment (OEHHA) used benchmark dose modelling to derive a BMC, which was time-adjusted from workplace exposure to an equivalent continuous environmental exposure. The final, time-adjusted BMC value of 9.8 µg/m³ was divided by an uncertainty factor of 3 (i.e. accounting for the general population), leading to a reference interim silica limit of 3 µg/m³ (Collins et al., 2005, OEHHA, 2005). Epidemiological data from other supportive mining studies (Chen et al., 2001, Churchyard et al., 2004, Hughes et al., 1998, Steenland and Brown, 1995) were also used by the OEHHA to calculate reference interim silica limits, which ranged from 3 – 6 µg/m³. Based on these results the OEHHA settled on a reference interim silica limit of 3 µg/m³, specifically for the respirable PM_4 fraction (Collins et al., 2005, OEHHA, 2005). Using a similar approach, the US EPA has set its silica limit for the PM_{10} fraction at 5 µg/m³ (EPA, 1996)". Despite these current international interim limits, South Africa is yet to enforce these limits or set its own limits, which will be addressed in more detail later in this thesis.

These PM and crystalline silica limits discussed above are often referred to as safety limits i.e. below this limit

2.6.4.Buffer zones not enforced

Several projects have been initiated as part of the provincial AQM of which some include the Danish Co-operation for Environment and Development DANCED Report (GDARD, 2009b, Scorgie et al., 2000), Gauteng State of Environment Report (SEA) (GDACE, 2004, GDARD, 2011), GDARD Pilot Study and the GDARD Buffer Zone project (GDARD, 2009b). The latter project, which was also included as one of the intervention strategies for the AQMP **(Table 2-4)** was to set buffer zones for TSFs. Experts and industry representatives were consulted in assisting with establishing these buffer zones. The methodology used was based on "generic information classes, environmental health requirements, desired environmental quality and generic activity

impacts" (GDARD, 2017). Geographical Information System (GIS) Software was used to determine the buffer zones around the areas of interest. For TSFs in particular, the buffer zones suggested were based on the degree of air pollution potentially caused by TSFs. Therefore, wind direction and ambient dust load were taken into account when the buffer zones were determined. A buffer zone distance of 1000 m was recommended for TSFs since, according to GDARD, "beyond this distance dust levels can no longer be distinguished from ambient dust pollution". However, the scientific basis of this statement was not elaborated on in the GDARD report and could not be found elsewhere. Furthermore the GDARD report recommended that, if a buffer zone of 1000 m is not reasonably possible then a buffer zone of 500 m is acceptable, provided that adequate mitigation measures such as proper rehabilitation (e.g. regular wetting) of TSF surfaces is applied (GDARD, 2017). Unfortunately, these buffer zones are merely guidelines and cannot legally be enforced by GDARD, thus allowing occupation of land within these buffer zone restrictions. . Unfortunately, these buffer zones are merely guidelines and cannot legally be enforced by GDARD, thus allowing occupation of land within these buffer zone restrictions.

2.6.5.Information not disseminated properly

As part of the AQM on a national level, the DEA has embarked on the following projects in fulfilment of the AQA:

- National Framework for Air Quality Management APPA Permit Review Project,
- Project Ferro - AQM enforcement initiatives,
- Listed Activities and Minimum Emissions Standard Setting Project
- The residential air pollution initiative Air Quality Management Planning Implementation Manual Project
- The SAAQIS Project (SAAQIS, 2016).

The SAAQIS provides a platform for managing air quality information in South Africa and disseminating collected data to stakeholders and the public (SAAQIS, 2016). However, the current challenge seems to be the lack of uniformity in the way air quality data, in particular ambient and meteorological data, are captured, stored, validated, analysed and reported into SAAQIS (GDARD, 2009b).

It is clear from the sections above that tailings material carries the potential to be toxic and is often one of the main culprits leading to environmental pollution and increased exposure in surrounding communities. Furthermore, mitigating pollution from TSFs appears to be challenging due to several legislative factors that will not be resolved overnight. While current legislation is amended, tailings-related pollution and exposure to communities remain to be unresolved.

2.7. Current available studies

Throughout the years, several studies have addressed the negative environmental impact of TSFs in the Witwatersrand area. Most of these studies involved characterisation of tailings material and the assessment of the extent of environmental pollution produced by TSFs. Certain studies, listed below, have also included 'environmental risk assessment'-based approaches, which is defined as scientifically-based attempts to define the level of risk for the environment. These risk assessment-based approaches, which can be either quantitative or qualitative, can assist with determining priorities for action, selecting the least risky alternative or determining if the benefits outweigh the risks (Sutton, 2012):

Study of Chevrel et al. (2008)

Chevrel et al. (2008) conducted an environmental risk assessment in the Ekurhuleni Metropolitan Municipality of South Africa using Advanced Spaceborne Thermal Emission and Reflection Radiometer (ASTER) as well as data from other resources such as Landsat Thematic mapper (TM), airborne radiometrics, a geological map, a geotechnical map, topographic maps (12 years apart), and field sampling. They applied a simplified risk assessment approach based on scoring 17 parameters related to source, pathway and receptor. Their final scoring was divided into three classes: class 1, requiring further investigation and emergency response; class 2, requiring monitoring, and class 3, not requiring specific work except possible restrictions on urban development.

Study of Sutton (2012)

Sutton (2012) conducted a similar risk assessment approach as that of Chevrel et al. (2008) in the same geographical location by detecting elemental and mineralogical hazards such as Fe-bearing

secondary minerals that are products of FeS_2 oxidation using GIS as well as remote sensing spectral scanners such as ASTER and then assigning relative ratings for hazard severity and land-use vulnerability ranging from 3 to 0; where 3 is high, 2 is medium, 1 is low and 0 is when there is no known hazard or vulnerability described.

Study of Rembuluwani et al. (2014)

Rembuluwani et al. (2014) conducted an environmental risk assessment at an abandoned New Union Gold Mine in Malamulele, Limpopo, South Africa. Their qualitative approach involved visually assessing hazards through visits to the mine sites. The levels of heavy metals in the mine tailings soil and stream sediments were analysed with atomic absorption spectrometry. The hazards were then rated depending on the probability or likelihood of the hazard reoccurring in the future as well as the severity of impact of the hazard.

Study of Oosthuizen et al. (2015)

Unlike the studies mentioned above, Oosthuizen et al. (2015) conducted a 'human' health risk assessment, as opposed to an environmental risk assessment, of airborne metals to a community potentially exposed to tailings dust from TSFs in Kagiso, South Africa. Their study involved sampling particles below 20 μm and determining the metal content by means of Inductively Coupled Plasma Mass Spectroscopy (ICP-MS). The risk of individuals to dust exposure was quantitatively analysed by the calculation of three types of risk estimates: (1) Hazard Quotient (HQ), which describes the potential for developing adverse non-cancerous health effects, (2) Incremental Cancer Risk, which describes the potential for developing cancerous health effects and (3) Hazard Index (HI), which is the total cancer risk for all chemicals to which an individual is exposed.

Study of Kamunda et al. (2016)

Kamunda et al. (2016) conducted a study similar to that of Oosthuizen et al. (2015) in which they conducted a human health risk assessment. They collected soil samples from tailings sites in and around the Witwatersrand region, analysed the elemental composition and calculated the HI and Incremental Cancer Risk values for adults and children living around these tailings sites.

2.8. Research question

Despite these risk assessment-based studies and despite studies showing an association between higher levels of toxic metals in children living in (historical) mining and/or smelting communities compared to children in control communities **(Section 2.4)**, it is still not clear as to whether the physicochemical characteristics of tailings material could lead to adverse health effects when inhaled. Therefore, there appears to be a lack of knowledge linking the predicted toxicity of tailings material to potential adverse health effects in communities using *in vitro* or *in vivo* methodologies. A literature search did not identify a single South African-based study assessing the potential toxicity of tailings material from the Witwatersrand using *in vitro* methodologies. Furthermore, even though it was mentioned that one of the goals of the Gauteng AQM is to monitor air quality with regards to TSF pollution, several challenges have been encountered leading to an inadequate data library within the SAAQIS website and therefore a lack in knowledge with regards to the potential of tailings dust from the TSFs in the Witwatersrand to reach surrounding communities. These knowledge gaps are illustrated in **Figure 2-14**.

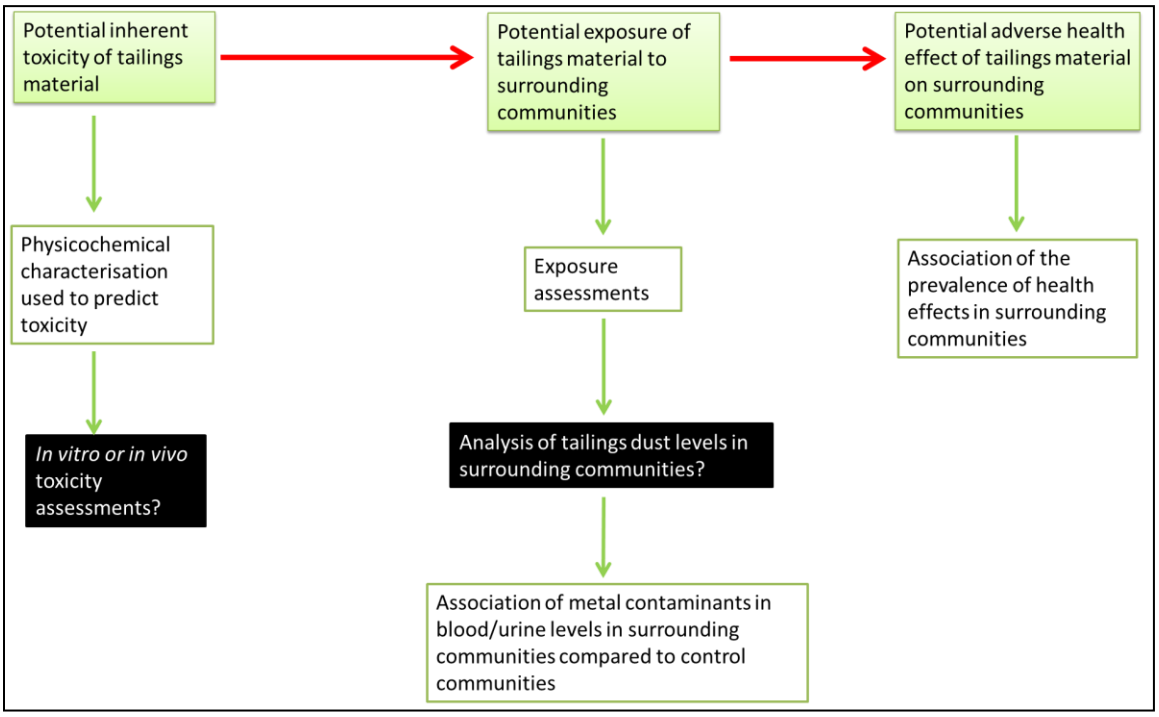

Figure 2-14: Current research gaps.

Based on these gaps in literature the following objectives were set for this project:

- The first goal of this thesis, labelled *Hazard Identification*, was to provide insight into the potential toxicity of tailings particles collected from various TSFs located in the Gauteng and North-West provinces of South Africa by conducting *in vitro* toxicity studies. Within the context of this thesis, it is important to distinguish between 'toxicity' and 'hazard' as these terms are frequently referred to throughout this thesis. *Toxicity* is defined as "any deleterious or adverse biological effect elicited by a chemical, physical, or biological agent" whereas *hazard* is defined as "a potential source of harm" (EPA, 2019). Within human health risk assessment, *Hazard Identification* is conducted to determine whether the chemical, physical or biological agent in question exhibits an inherent potential to be toxic. The toxicity of an agent is generally determined using *in vitro* and/or *in vivo* methodologies. *In vitro* refers to methodologies used in a controlled environment outside of a living organism, whereas *in vivo* refers to methodologies used within a whole, living organism. If it is ascertained that the agent could be toxic then it could be assumed that the agent may pose a health hazard. In addition to conducting *in vitro* toxicity studies, this first goal involved identifying specific physicochemical characteristics of tailings particles i.e. size, surface area, mineral composition, surface and total elemental composition and surface activity that could potentially govern their toxicity.
- The health risk of any hazardous agent depends on the degree of exposure (EPA, 2009). Therefore, the second goal, labelled *Exposure Assessment*, was to determine whether the tailings dusts have the potential to reach surrounding communities by assessing the ambient PM_{10} and personal PM_4 levels and their corresponding crystalline silica levels in communities surrounding the TSFs. For the purpose of this thesis, the crystalline silica obtained from the PM_4 collected on filters will henceforth be referred to as respirable crystalline silica (RCS), while that obtained from the PM_{10} collected on filters will remain crystalline silica.
- The third goal, labelled *Risk Characterisation*, was to calculate the possible non-cancer and cancer adverse health effects of surrounding communities due to lifetime exposure to RCS.

3. MATERIALS AND METHODS

3.1. HAZARD IDENTIFICATION

3.1.1.TSF sites studied

Four TSFs namely Durban Roodepoort Deep (DRD), Crown Gold Recoveries (CGR), ERPM and BTF (hereafter referred to as ERGO), located in Johannesburg and one TSF, namely Anglo Gold Ashanti (AGA), located in Klerksdorp, South Africa **(Figure 3-1)** were selected for this study. The close-up aerial views of each TSF showing the different deposition ponds as well as their characteristics in terms of their size, type of tailings, level of urbanisation, current status, period of reclamation and current rehabilitation measures are shown in **Figure 3-2** and **Table 3-1**, respectively. Initially, it was decided to pair AGA 1 and 2 as one pond and AGA 3 and 4 as the second pond. However, it was later decided that all four ponds would be better represented collectively as one pond. The largest TSF, compared to the other TSFs, is ERGO, with the major deposition pond having a surface area of 8.86 km^2. The DRD and CGR TSFs have the highest and second highest levels of urbanisation with 158 233 and 76 754 individuals, respectively, living within a 2 km radius from the TSFs. For DRD, CGR and ERPM very little buffer separates the TSF from the nearest development. The eastern and western residential developments surrounding ERGO is at least 1 km and 3 km from the TSF, respectively, while the northern and southern side encompasses underdeveloped land and farm land, respectively. The eastern and southern surrounding areas of AGA include mostly farmland, underdeveloped land and the Vaal River, which separates the North-West and Free State Provinces. Residential developments are located approximately 1 – 2 km north, west and south-west from AGA.
It should be noted that the TSFs studied were selected for their:

- Lack of proper remediation to adequately prevent dust erosion
- Density of the surrounding communities
- Large sizes as larger TSFs are anticipated to have a larger impact on the ambient environment and surrounding populations.

Therefore, using these criteria, the worst case scenario was a priority rather than it being representative of TSFs in the region.

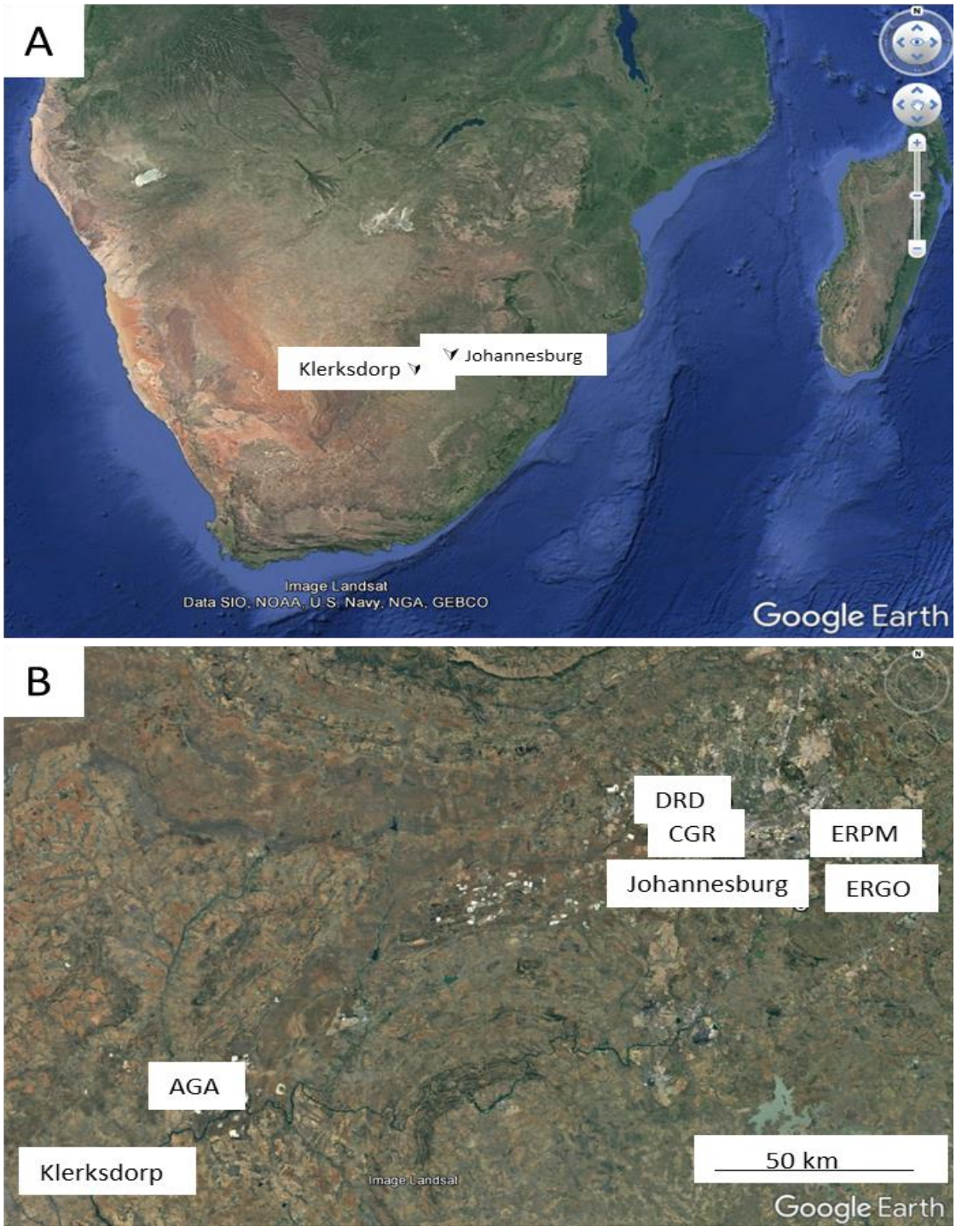

Figure 3-1: TSFs studied. (A) South African continent indicating the two major cities in which the TSFs are located; (B) DRD, CGR, ERPM and ERGO are located in Johannesburg while AGA is located in Klerksdorp. Modified from Andraos et al. (2018b).

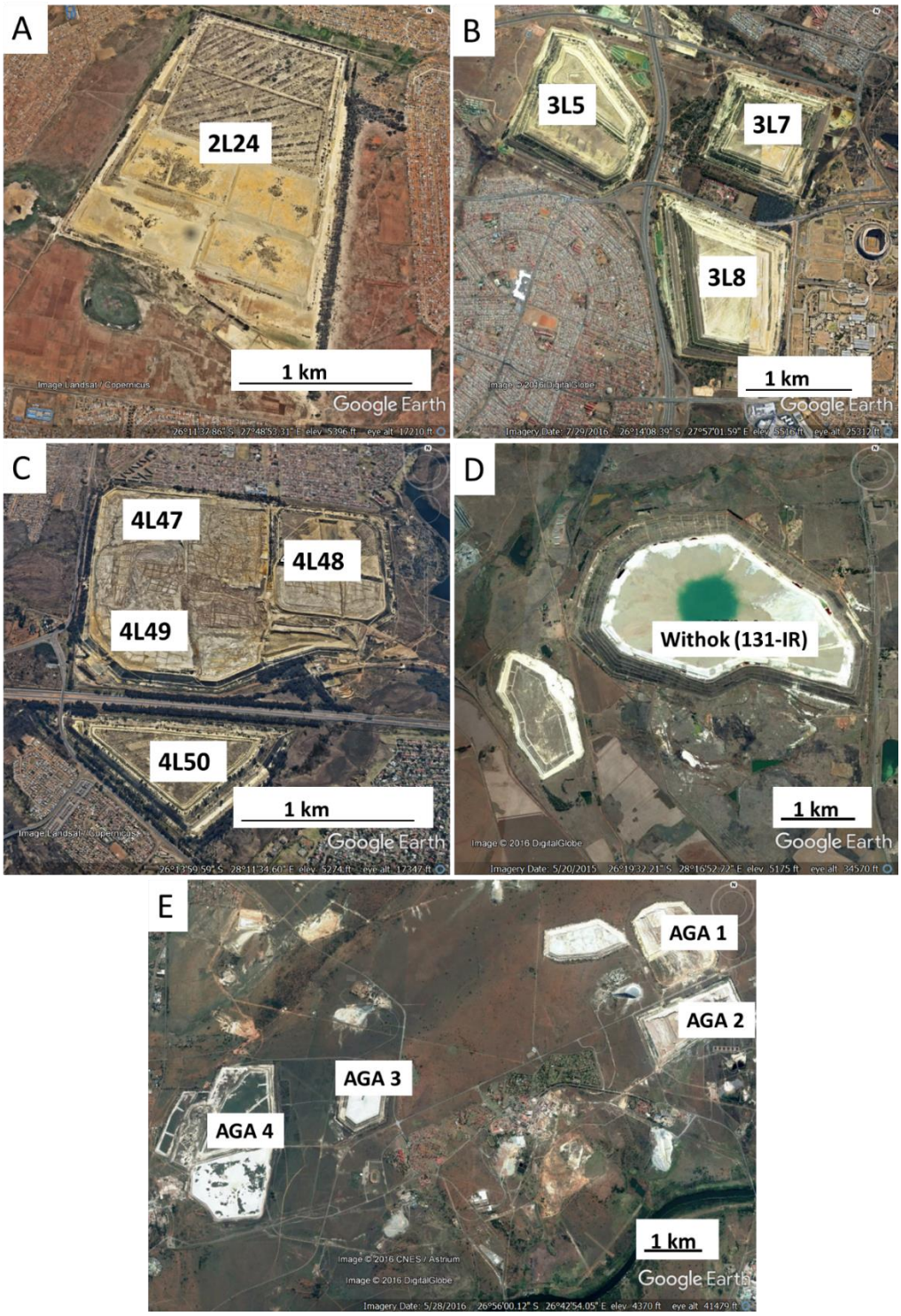

Figure 3-2: Close-up aerial views of the TSFs. (A) DRD; (B) CGR; (C) ERPM; (D) ERGO and (E) AGA. Each TSF is allocated one or more designator number, each of which is discussed in more detail in Table 3-1.

Table 3-1: Characteristics of each of the five TSFs studied.

TSF	Designator numbers	Area (km^2)	Type	# individuals within 2 km radius from TSF	Current status	Period of reclamation	Rehabilitation measures
DRD	2L24	2.55	Slime	158 233 nearest developments within buffer zone)	Dormant	To be reclaimed (Digby Wells report)	Vegetation programme in 2002. Currently mainly uncovered.
CGR	3L5	1.43	Deposition site of reclaimed tailings from smaller TSFs; slime	76 754 (nearest developments within buffer zone)	Active	Dams have to 'dry out' for at least another ten years before re-mining can take place.	Combination of dust netting, limited irrigation and vegetation in 2013.
	3L7	0.98					
	3L8	1.59					
ERPM	4L47	2.94	Slime	36 478 (nearest developments within buffer zone)	Active	Currently being reclaimed	None
	4L48						
	4L49						
	4L50	0.50					
ERGO	Withok (131-IR)	8.86	Deposition site of reclaimed tailings from smaller TSFs; slime	14 359 (nearest developments outside buffer zone)	Active	NA	Surface largely covered with water
	Smaller pond	1.44					None
AGA	1	1.97	Slime	2 171 (nearest developments outside buffer zone)	Active	NA	Vegetation programme initiated in 2002. Programme initiated in 2002 to increase water retention capacity of paddocks. Draw off system installed to allow return water to be re-circulated to minimize water pollution of Vaal river.
	2	1.80					
	3	0.99					
	4	4.46					

3.1.2.Bulk dust collection

Authorisation to sample bulk dust directly from each TSF was granted by the relevant mine managers. Samples were collected randomly on top of the surfaces of the tailings with a shovel approximately 10 cm below the surface in the period from 2011 to 2012. Samples were placed and transported in 5ℓ plastic buckets. A sieve was used to remove large debris if present. The exact position of the bulk dust samples was recorded by means of GPS co-ordinates and Google Earth, as stipulated in **Figure 3-3** and **Table 3-2**, respectively.

Figure 3-3: Bulk dust sampling locations. (A) DRD; (B) CGR; (C) ERPM; (D) ERGO and (E) AGA. The yellow pins indicate the exact positions of the bulk dust sampling locations.

Table 3-2: GPS co-ordinates of the bulk dust sampling locations.

TSF	Sample ID	GPS co-ordinates	
DRD	DRD 01	S 26˚12′13.2″	E 27˚50′34.3″
	DRD 02	S 26˚12′21.7″	E 27˚50′33.0″
	DRD 03	S 26˚12′32.4″	E 27˚50′32.7″
	DRD 04	S 26˚12′31.7″	E 27˚50′07.2″
	DRD 05	S 26˚12′24.3″	E 27˚49′46.9″
	DRD 06	S 26˚12′41.4″	E 27˚50′33.4″
	DRD 07	S 26˚12′38.0″	E 27˚50′20.5″
	DRD 08	S 26˚12′45.5″	E 27˚50′33.7″
	DRD 09	S 26˚12′56.3″	E 27˚50′31.4″
	DRD 10	S 26˚12′55.9″	E 27˚50′22.1″
	DRD 11	S 26˚12′22.5″	E 27˚49′36.2″
	Total		**11**
CGR	CGR 01	S 26˚14′38.9″	E 27˚58′0.23″
	CGR 02	S 26˚14′06.4″	E 27˚57′54.4″
	CGR 03	S 26˚14′41.2″	E 27˚58′21.8″
	CGR 04	S 26˚14′13.3″	E 27˚58′19.3″
	CGR 05	S 26˚13′34.9″	E 27˚57′27.3″
	CGR 06	S 26˚13′24.2″	E 27˚57′01.6″
	CGR 07	S 26˚13′40.6″	E 27˚56′54.2″
	CGR 08	S 26˚13′52.1″	E 27˚57′22.6″
	CGR 09	S 26˚13′40.7″	E 27˚58′05.8″
	CGR 10	S 26˚13′45.3″	E 27˚58′23.6″
	CGR 11	S 26˚14′13.2″	E 27˚58′28.9″
	CGR 12	S 26˚13′57.7″	E 27˚57′19.1″
	CGR 13	S 26˚13′50.8″	E 27˚56′57.7″
	CGR 14	S 26˚13′22.2″	E 27˚57′28.9″
	CGR 15	S 26˚14′39.8″	E 27˚57′50.9″
	CGR 16	S 26˚14′16.6″	E 27˚57′44.0″
	Total		**16**
ERPM	ERPM 01	S 26˚14'49.5"	E 28˚12'51.7"
	ERPM 02	S 26˚14'34.4"	E 28˚12'52.1"
	ERPM 03	S 26˚14'11.9"	E 28˚13'10.3"
	ERPM 04	S 26˚14'09.3"	E 28˚13'07.7"
	ERPM 05	S 26˚14'36.9"	E 28˚13'23.6"
	ERPM 06	S 26˚14'38.3"	E 28˚13'56.9"
	ERPM 07	S 26˚14'45.3"	E 28˚13'44.9"
	ERPM 08	S 26˚14'41.7"	E 28˚13'23.4"
	ERPM 09	S 26˚15'01.4"	E 28˚12'52.0"
	ERPM 10	S 26˚14'23.5"	E 28˚14'01.6"
	ERPM 11	S 26˚15'13.6"	E 28˚12'52.3"
	ERPM 12	S 26˚15'26.1"	E 28˚13'11.1"
	ERPM 13	S 26˚15'13.0"	E 28˚13'26.5"
	ERPM 14	S 26˚15'20.9"	E 28˚13'28.0"
	ERPM 15	S 26˚15'29.7"	E 28˚13'18.4"
	ERPM 16	S 26˚15'22.6"	E 28˚12'57.9"
	ERPM 17	S 26˚14'55.2"	E 28˚12'57.8"
	ERPM 18	S 26˚14'55.4"	E 28˚13'09.6"
	Total		**18**
ERGO	ERGO 01	S 26˚21'20.9"	E 28˚17'25.6"
	ERGO 02	S 26˚22'05.6"	E 28˚17'27.5"
	ERGO 03	S 26˚20'20.0"	E 28˚18'28.8"

TSF	Sample ID	GPS co-ordinates	
	ERGO 04	S 26˚21'21.0"	E 28˚18'58.6"
	ERGO 05	S 26˚21'30.5"	E 28˚19'29.9"
	ERGO 06	S 26˚21'25.5"	E 28˚20'02.1"
	ERGO 07	S 26˚20'13.1"	E 28˚19'17.6"
	ERGO 08	S 26˚21'17.4"	E 28˚20'07.3"
	ERGO 09	S 26˚20'30.3"	E 28˚19'46.5"
	ERGO 10	S 26˚21'01.4"	E 28˚18'09.5"
	Total		**10**
AGA	AGA 01	S 26˚55'49.5"	E 26˚42'23.1"
	AGA 02	S 26˚56'18.4"	E 26˚42'26.0"
	AGA 03	S 26˚56'31.7"	E 26˚41'29.9"
	AGA 04	S 26˚56'41.3"	E 26˚40'46.9"
	AGA 05	S 26˚57'15.1"	E 26˚41'02.4"
	AGA 06	S 26˚57'21.8"	E 26˚40'59.1"
	AGA 07	S 26˚54'01.9"	E 26˚45'34.4"
	AGA 08	S 26˚54'23.9"	E 26˚46'21.5"
	AGA 09	S 26˚54'54.7"	E 26˚46'40.1"
	AGA 10	S 26˚55'24.7"	E 26˚45'50.9"
	AGA 11	S 26˚55'40.5"	E 26˚45'59.9"
	Total		**11**

3.1.3.Physicochemical analysis of tailings bulk dust

3.1.3.1. Size fractionation

Size separation of bulk dust samples was performed using the AS200 Jet sieve shaker (Retsch GmbH, Germany). The principle of the AS200 Jet sieve shaker is based on the newest air jet technology, which is discussed in more detail below:

The different components of the AS200 Jet sieve shaker (RETSCH, 2011) are shown in **Figure 3-4**. In contrast to other methods, air jet sieving is carried out with a single stainless steel mesh sieve at a time. The sieve containing sample material is placed in the nozzle compartment of the AS200 Jet sieve shaker unit and covered with a lid **(Figure 3-4A** and **C)**. A powerful industrial vacuum cleaner generates a strong jet of air in the nozzle compartment **(Figure 3-4B** and **C)**. Fresh ambient air is sucked from under the nozzle through the thin slit of nozzle. The air jet generated by the vacuum can be manually adjusted by using the manual suction force adjuster **(Figure 3-4D)**.

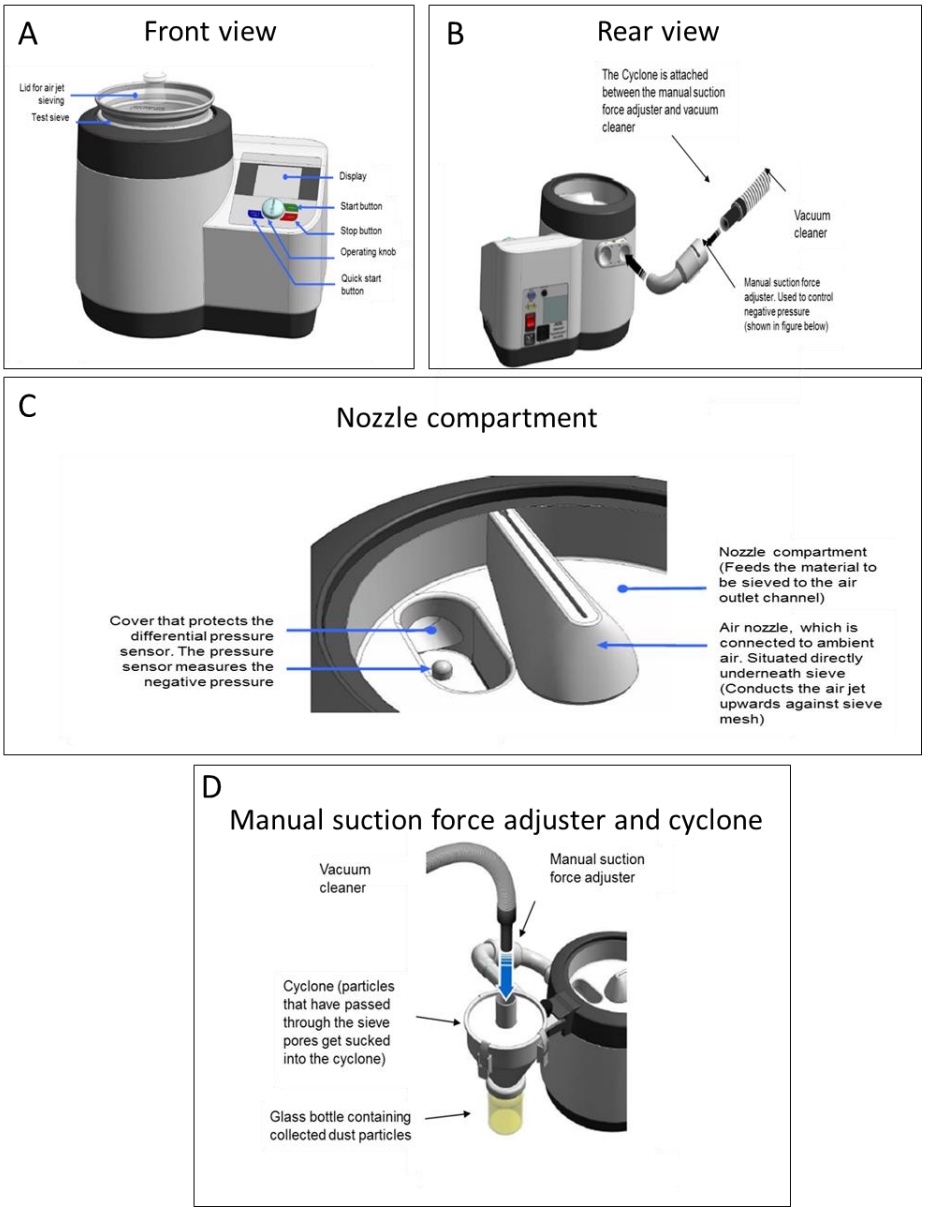

Figure 3-4: Components of the AS200 Air Jet sieve. (A) Front view; (B) Rear view; (C) Nozzle compartment and (D) Manual suction force adjuster and cyclone. Adapted from RETSCH (2011).

The jet of air moving through the slit of the air nozzle rotating below the sieve blows against the sieve mesh **(Figure 3-5)**. The particles are dispersed with each rotation of the air nozzle and are distributed over the complete sieve surface. The inflowing air also causes the particles to impact on the lid which helps to destroy agglomerates. Therefore, a higher speed of inflowing air and number of rotations of the nozzle will result in a higher force of impaction of particles against

the lid. Particles with sizes smaller than the sieve apertures fall through the sieve into the nozzle compartment and are collected by the cyclone **(Figure 3-4D)**.

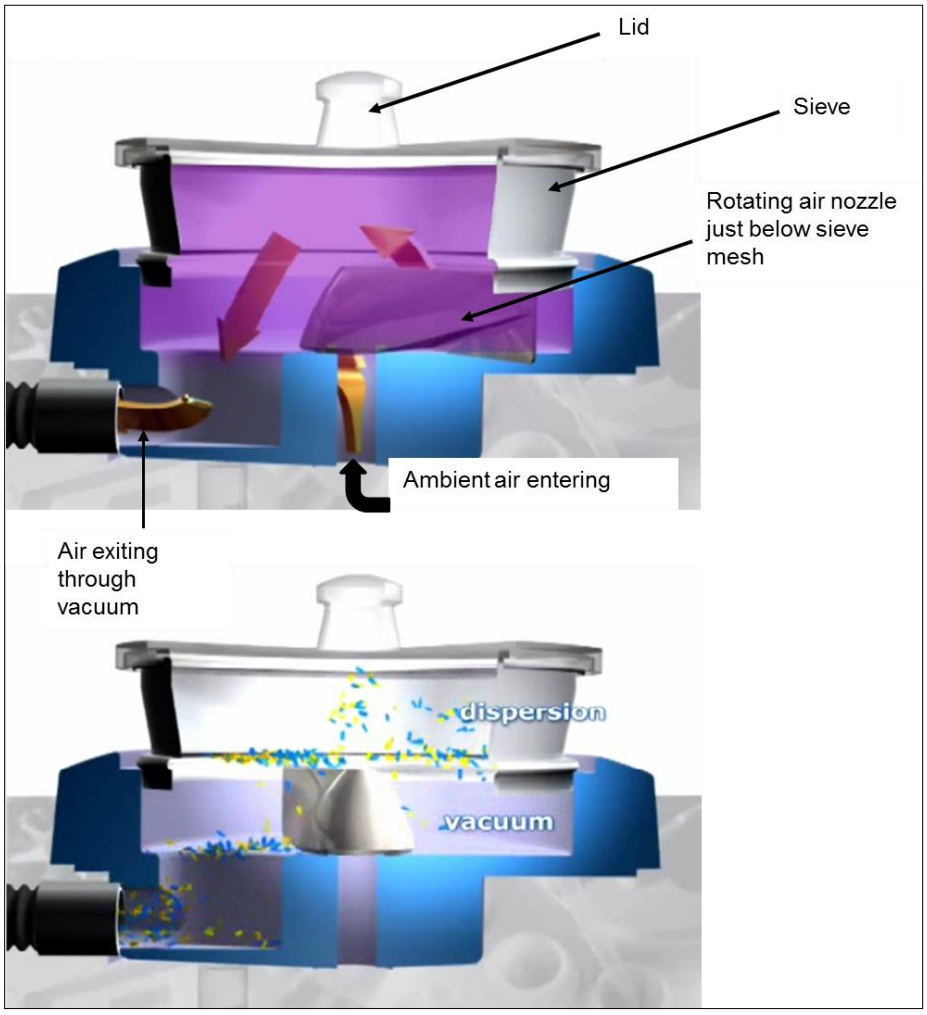

Figure 3-5: Principle of the AS200 Air Jet Sieve. Adapted from RETSCH (2011).

For this study, the sieving process involved first drying the bulk tailings samples on a bench top at room temperature for a minimum of three days. Larger debris such as rock, vegetation etc. were removed from the bulk samples using clean metal tweezers. For each sample, 400 g of bulk material was first sieved using a sieve with an aperture of 100 µm (Retsch GmbH, Germany) to enrich the ≤ 100 µm fraction and therefore eliminate larger particles that might compromise the integrity of the more delicate sieves with smaller apertures. Thereafter, the ≤ 20 µm fraction was further enriched from the ≤ 100 µm fraction using a sieve with an aperture of 20 µm (Retsch

GmbH, Germany). The conditions of each sieving process, as determined through initial optimisation, were as follows: 10 revolutions per minute (RPM), 1 min per sieve run. The ≤ 20 µm sieved tailings bulk dust fraction (which contained the respirable fraction) was stored at room temperature away from sunlight in sterile plastic 50 ml containers until further physicochemical and toxicological analyses.

Certain physiochemical properties of particles, most notably the size, surface area and composition, play an important role in particle induced toxicity. The following section will address the methods used to determine these physicochemical properties of the ≤ 20 µm sieved tailings bulk dust fraction.

3.1.3.2. Size distribution

The tailings dust samples were introduced simultaneously at 1 *l*/min into the Electrostatic Classifier Model 3080 in a Scanning Mobility Particle Sizer (SMPS) configuration, and the Aerodynamic Particles Sizer (APS; Model 3321) using the Small Scale Particle Dispenser (SSPD; Model 3433). The Condensation Particle Counter (CPC; Model 3772) was used to determine the particle concentrations in number of particles per cm^3 of air. The Aerosol Instrument Manager Software (version 8.1.0) was used to collect data and the Data Merge Software (version 1.0.1) was then used to merge the SMPS and APS data files thereby producing single particle size distributions. The following sections will briefly summarise the principle of each of these instruments

Electrostatic Classifier Model 3080

The Electrostatic Classifier **(Figure 3-6)** may be used either as a monodisperse-aerosol generation system or as an integral part of a submicrometer-particle sizing system in an SMPS configuration (TSI, 2001). In an aerosol generation system, the Electrostatic Classifier, together with a Differential Mobility Analyser (DMA, **Figure 3-6**), selects airborne particles of uniform size from a polydisperse source, which results in a monodisperse aerosol. When used in an SMPS configuration, the monodisperse aerosol is transferred from the Electrostatic Classifier to a CPC (discussed in next section), which measures the particle number concentration. The

Electrostatic Classifier is capable of measuring particle size distributions ranging from 2 to 1000 nm (TSI, 2001).

Figure 3-6: Electrostatic Classifier Model 3080 attached to a long Differential Mobility Analyser Model 3081. Adapted from TSI (2001).

In **Figure 3-7A** the principle of the Electrostatic Classifier is illustrated (TSI, 2001). The aerosol first enters through the inlet and the impactor (both located on the front panel, **Figure 3-6**), which removes particles above a known particle size by inertial impaction. A nozzle, which is directed at a flat plate allows the aerosol flow to accelerate as air is drawn through the inlet. Small particles are able to follow the streamlines of the air, thereby avoiding inertial impaction with the plate while larger particles are unable to follow the streamlines and impact on the plate. The cut-point diameter depends on the impactor flow rate and nozzle diameter. The smaller particles that exit the impactor pass through a Krypton(Kr)-85 neutraliser and are introduced to a bipolar charge. An equilibrium charge state is obtained, with known percentages of particles carrying no charge, a single charge, or multiple charges of both positive and negative polarities

(TSI, 2001). Neutralised aerosol particles pass from the neutraliser into the DMA and are classified based on their electrical mobility, which is inversely related to particle size and proportional to number of charges on particles. The DMA **(Figure 3-7B)** contains two concentric metal cylinders. Polydisperse aerosol (containing particles) and sheath air (particle-free) are introduced at the top of the DMA and flow down the annular space between the cylinders. Polydisperse aerosol surrounds the inner core of sheath air. The inner cylinder (known as the collector rod), is maintained at a negative voltage, while the outer cylinder is grounded. This creates an electric field upon which negatively charged particles stick to the outer electrode, neutral particles are removed with the excess flow and transferred to a particle sensor such as a CPC and positive particles are carried downward with sheath airflow while being attracted radially toward the centre electrode. Smaller particles having a high electrical mobility precipitate along the upper portion of the rod while larger particles with a low electrical mobility will precipitate towards the lower end (TSI, 2001).

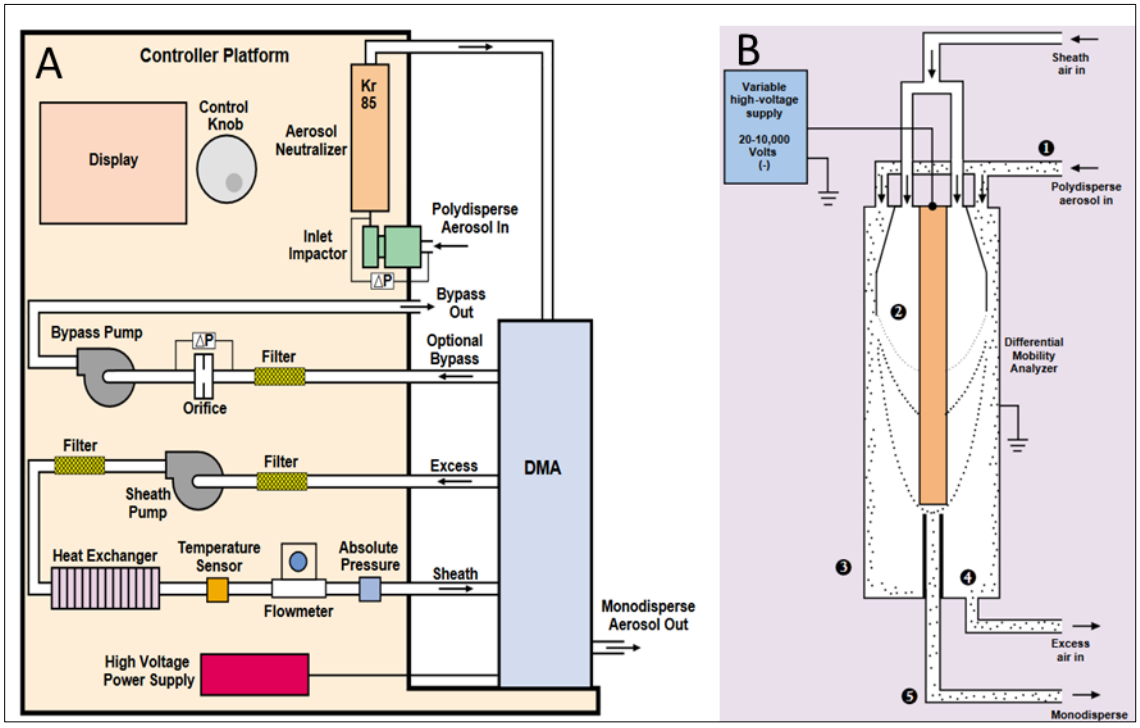

Figure 3-7: Flow schematic of the Electrostatic Classifier Model 3080 (A) and the long Differential Mobility Analyser Model 3081 (B). Adapted from TSI (2001).

The output of the Electrostatic Classifier may be viewed and manipulated using the Aerosol Instrument Manager® Software. The output of the Electrostatic Classifier in an SMPS configuration is shown in **Figure 3-8**. A graph provides a visual illustration of particle size (x-axis) against particle number, particle mass or particle surface area (y-axis). Descriptive statistical parameters such as median, mean, geometric mean, mode and geometric standard deviation for each dose metric are also automatically calculated after each sample run (right bottom corner of **Figure 3-8**).

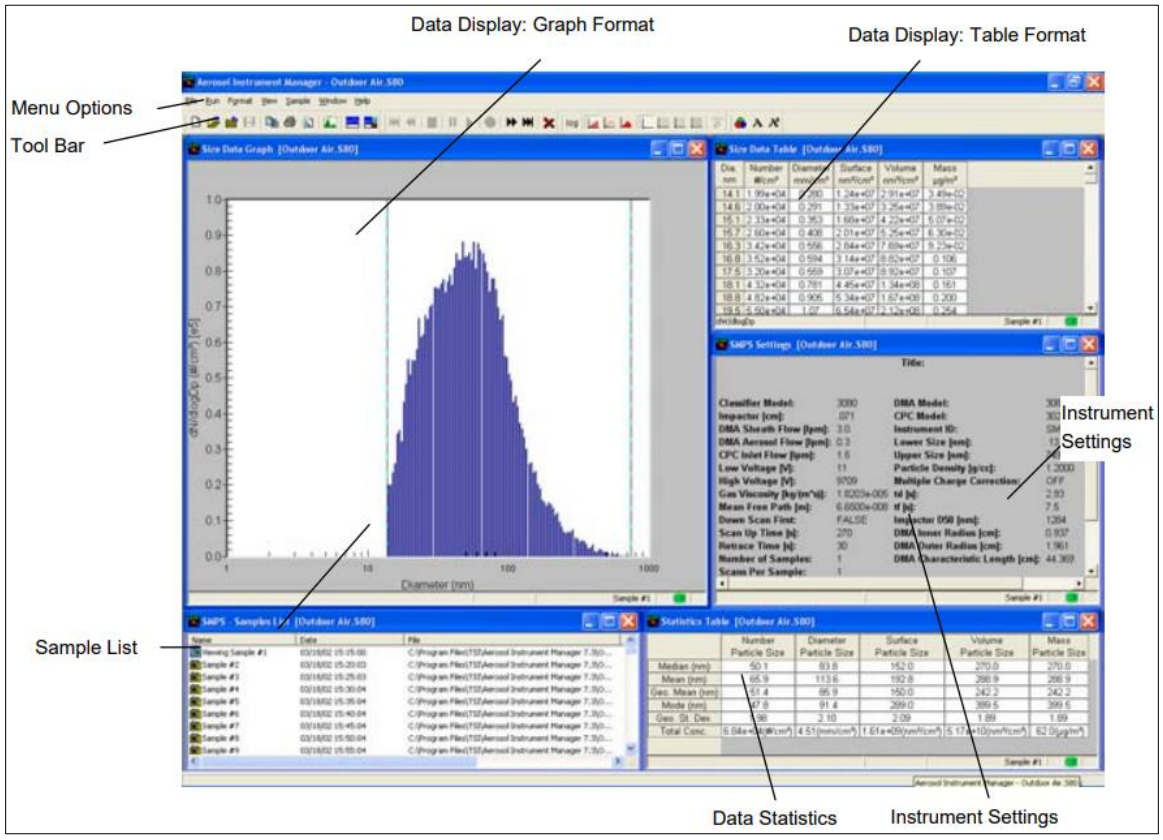

Figure 3-8: Output display of the Electrostatic Classifier Model 3080 using the Aerosol Instrument Manager® Software. Obtained from TSI (2010b).

Condensation Particle Counter (CPC) Model 3772

The CPC **(Figure 3-9A)** detects particles from 10 nm to 20 µm in diameter (TSI, 2007). The aerosol sample e.g. from the DMA is continuously drawn through a heated saturator in which alcohol (e.g. butanol) is vaporized and diffuses into the sample stream **(Figure 3-9B)**. Condensation is initiated by a cooled condenser and particles that are larger than a specified

threshold diameter grows into larger droplets. These droplets pass through an optical detector where they are counted. The detector counts individual pulses produced as each particle (droplet) passes through the sensing zone. An external vacuum pump draws the aerosol sample through the CPC at a constant aerosol flow rate of 1 *l*/min (TSI, 2007).

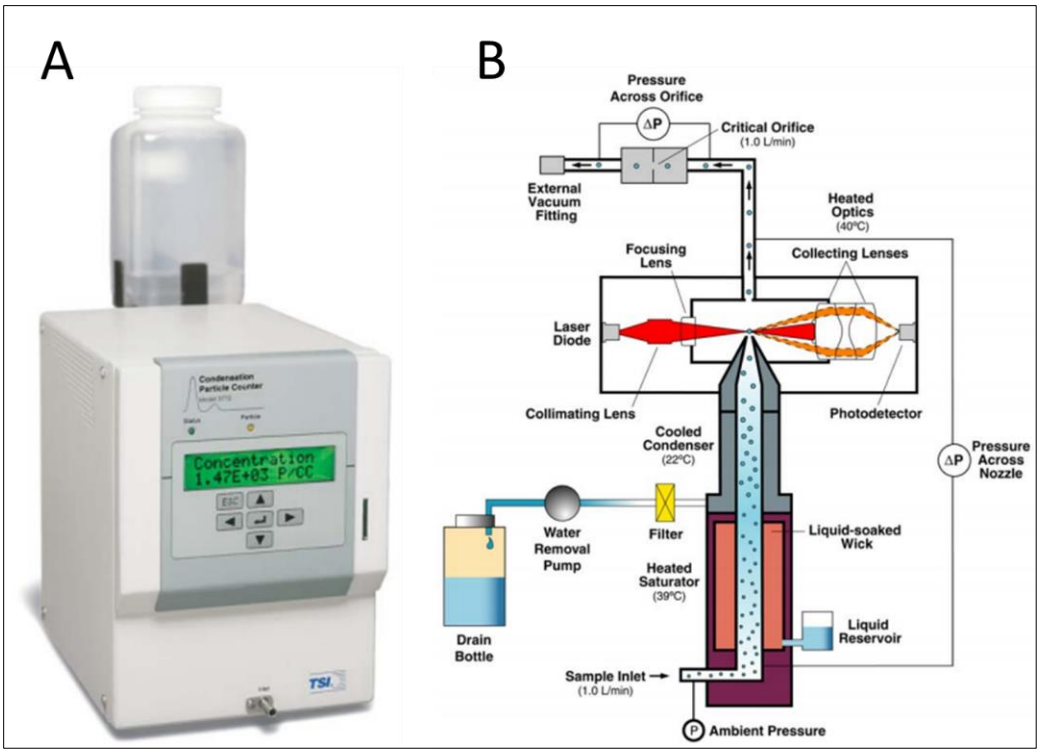

Figure 3-9: Condensation Particle Counter Model 3772 with butanol bottle (A) and flow schematic of the CPC (B). Adapted from TSI (2007).

As with the Electrostatic Classifier, the output of the CPC may also be viewed and manipulated using the Aerosol Instrument Manager® Software (TSI, 2010a). **Figure 3-10** shows an example of the output provided by the CPC when used in isolation i.e. when not connected to the Electrostatic Classifier in an SMPS configuration. The graph in **Figure 3-10** displays the particle concentration as number of particles per cm^3 of air (y-axis) against sampling time (x-axis). Note that the CPC alone cannot provide information regarding different dose metrics and may only provide information regarding particle concentration vs. time.

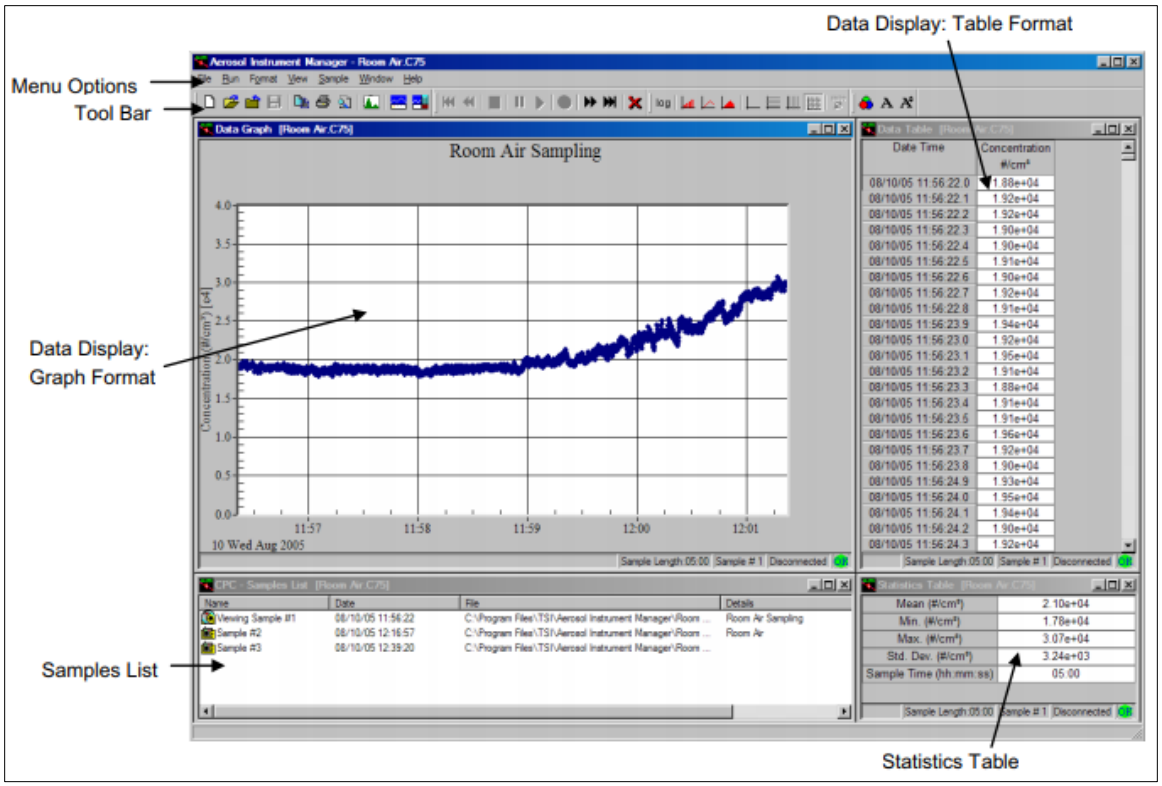

Figure 3-10: Output display of the Condensation Particle Counter Model 3772 using the Aerosol Instrument Manager® Software. Obtained from TSI (2010a).

Aerodynamic Particle Sizer (APS) Model 3321

The APS **(Figure 3-11A)** sizes particles from 0.5 to 20 µm via a sophisticated time-of-flight technique (TSI, 2004). The aerosol sample enters the APS through the inlet located on top of the APS and is accelerated when it flows through an accelerating orifice **(Figure 3-11B)**. The aerodynamic size of a particle determines its rate of acceleration i.e. larger particles accelerate more slowly, compared to smaller particles. Particles exit the nozzle and cross through two partially overlapping laser beams. As particles cross these beams, light is scattered, collected and focused onto an avalanche photodetector (APD). The APD then converts the light pulses into electrical pulses. The configuration of the detection area improves particle detection and minimises Mie-scattering oscillations, which refers to the elastic scattering of light from particles with diameters larger than the wavelength of incident light (Lockwood, 2015). Peak-to-peak time-of-flight is then measured for aerodynamic sizing (TSI, 2004).

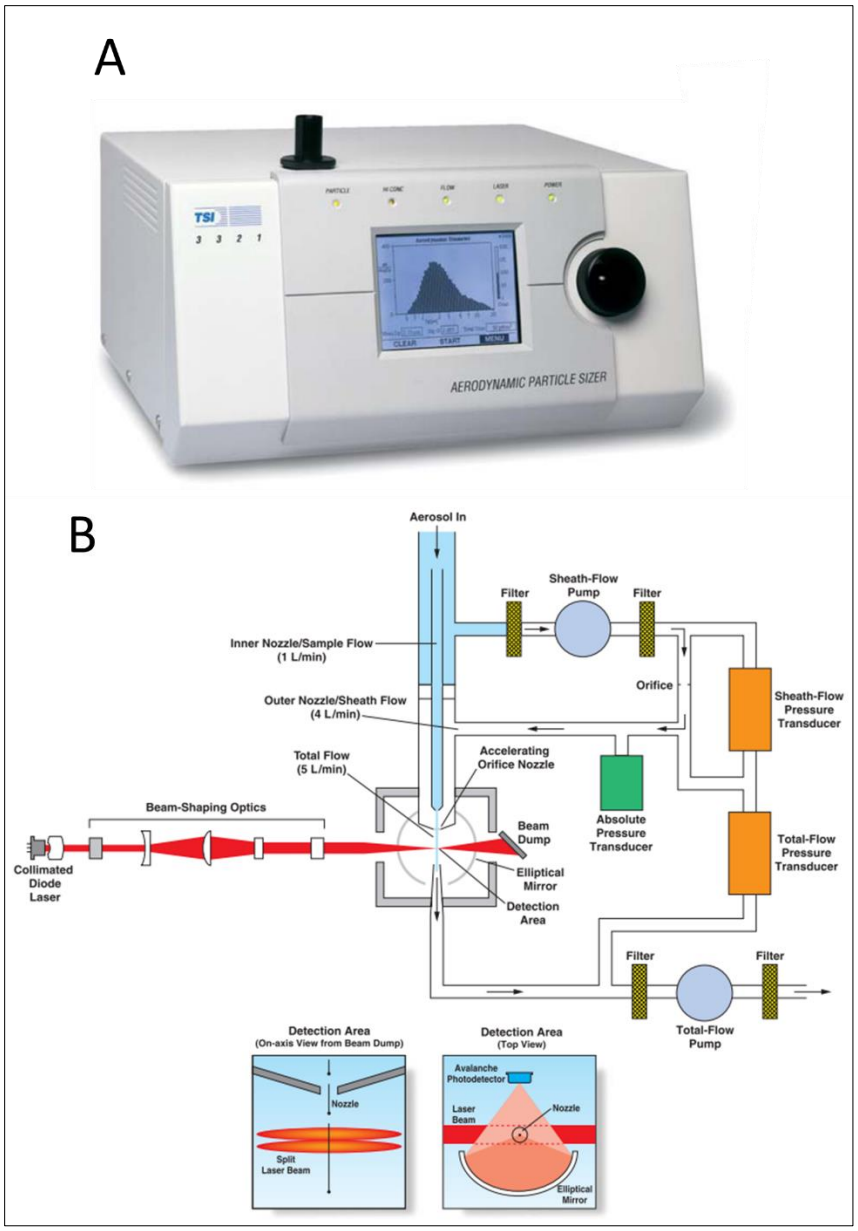

Figure 3-11: Aerodynamic Particle Sizer Model 3321 (A) and flow schematic of the APS (B). Adapted from TSI (2004).

The APS also relies on the use of the Aerosol Instrument Manager® Software (TSI, 2006) for viewing and manipulation of the output, which is illustrated in **Figure 3-12**. The output (i.e. particle number, mass and aerodynamic diameter etc. in graph and tabular format) is similar to that of the Electrostatic Classifier in an SMPS configuration **(Figure 3-8)**.

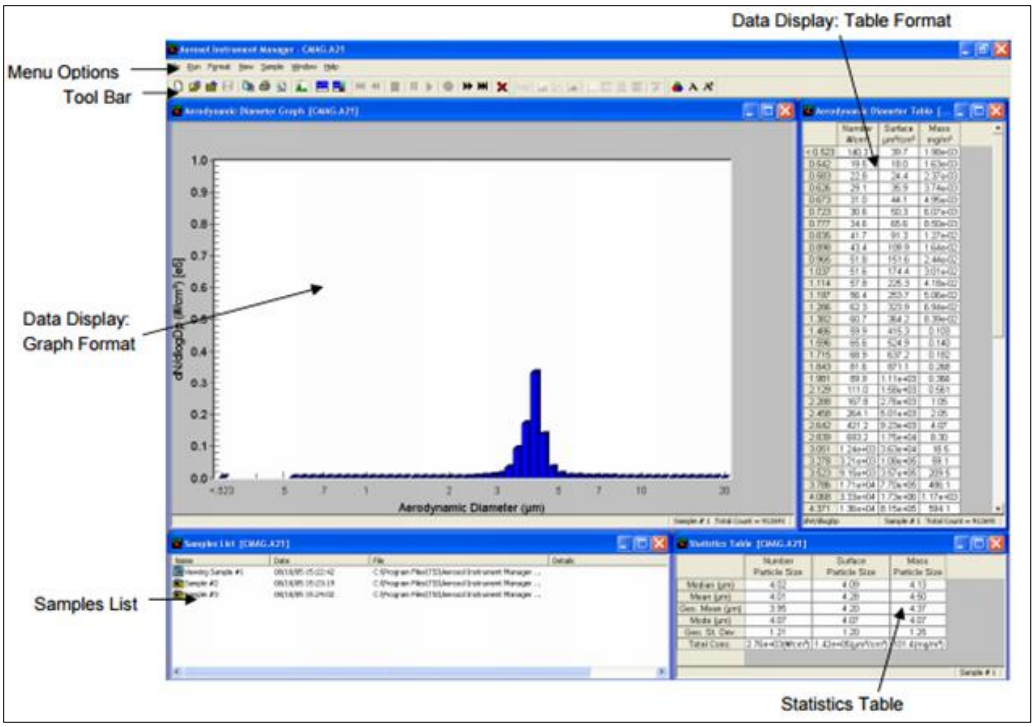

Figure 3-12: Output display of the Aerodynamic Particle Sizer Model 3321 using the Aerosol Instrument Manager® Software. Obtained from TSI (2006).

Small scale powder disperser (SSPD) Model 3433

A big advantage of the instruments mentioned above, is the possibility of sampling airborne particles as well as powders. Powders are placed onto a turntable located inside the SSPD **(Figure 3-13A)**, which is connected to the Electrostatic Classifier and/or APS. Particles are aspirated from the turntable into the Electrostatic Classifier and/or APS via a venturi aspirator **(Figure 3-13B)**, which contains a tube that first narrows cross-sectionally and then expands. A vacuum called the venturi effect is created within the narrow section of the tube (TSI, 2012).

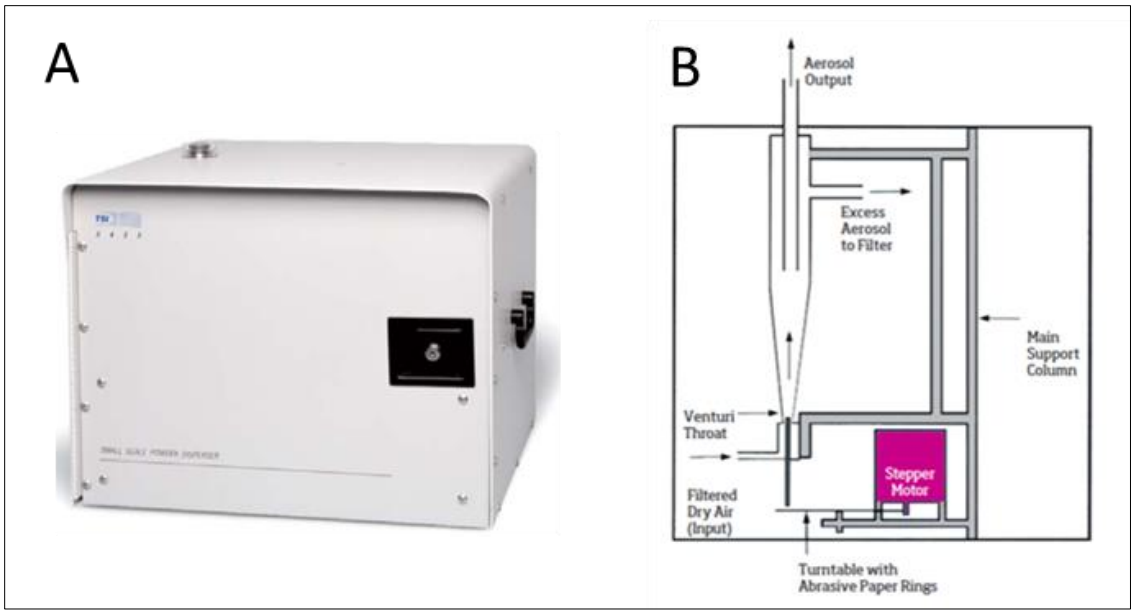

Figure 3-13: Small-Scale Powder Disperser (SSPD) Model 3433 (A) and flow schematic of the SSPD (B). Obtained from TSI (2012).

Data merging

All the instruments mentioned above may be connected in the configuration shown in **Figure 3-14** to allow for the sizing of particles in the range from 2 nm (SMPS) to 20 µm (APS).

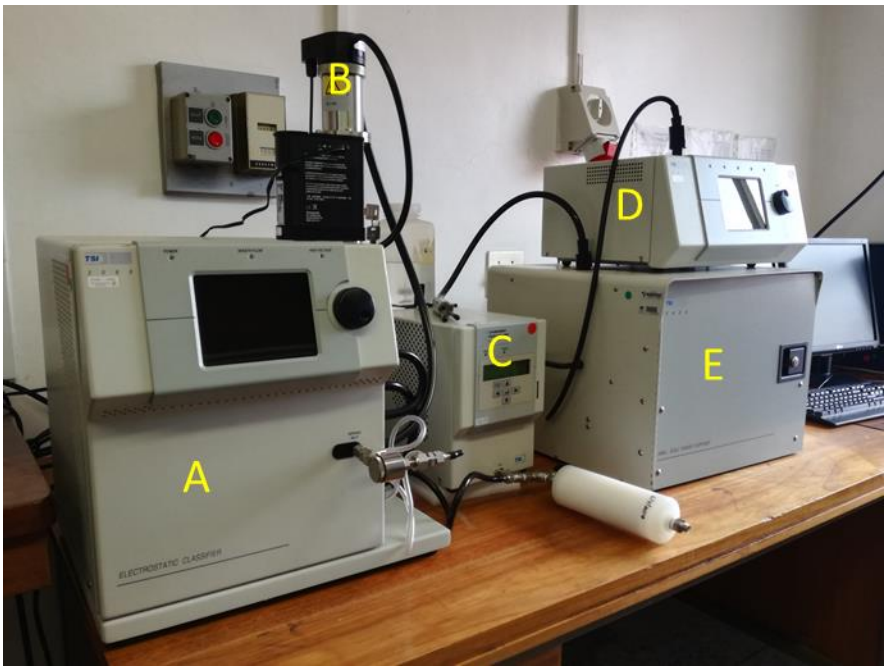

Figure 3-14: Electrostatic Classifier (A), DMA (B), CPC (C), APS (D) and SSPD (E) available at the National Institute for Occupational Health, South Africa.

The merging and fitting of SMPS and APS data require the use of Data Merge® Software (TSI, 2014), of which the output is illustrated in **Figure 3-15**.

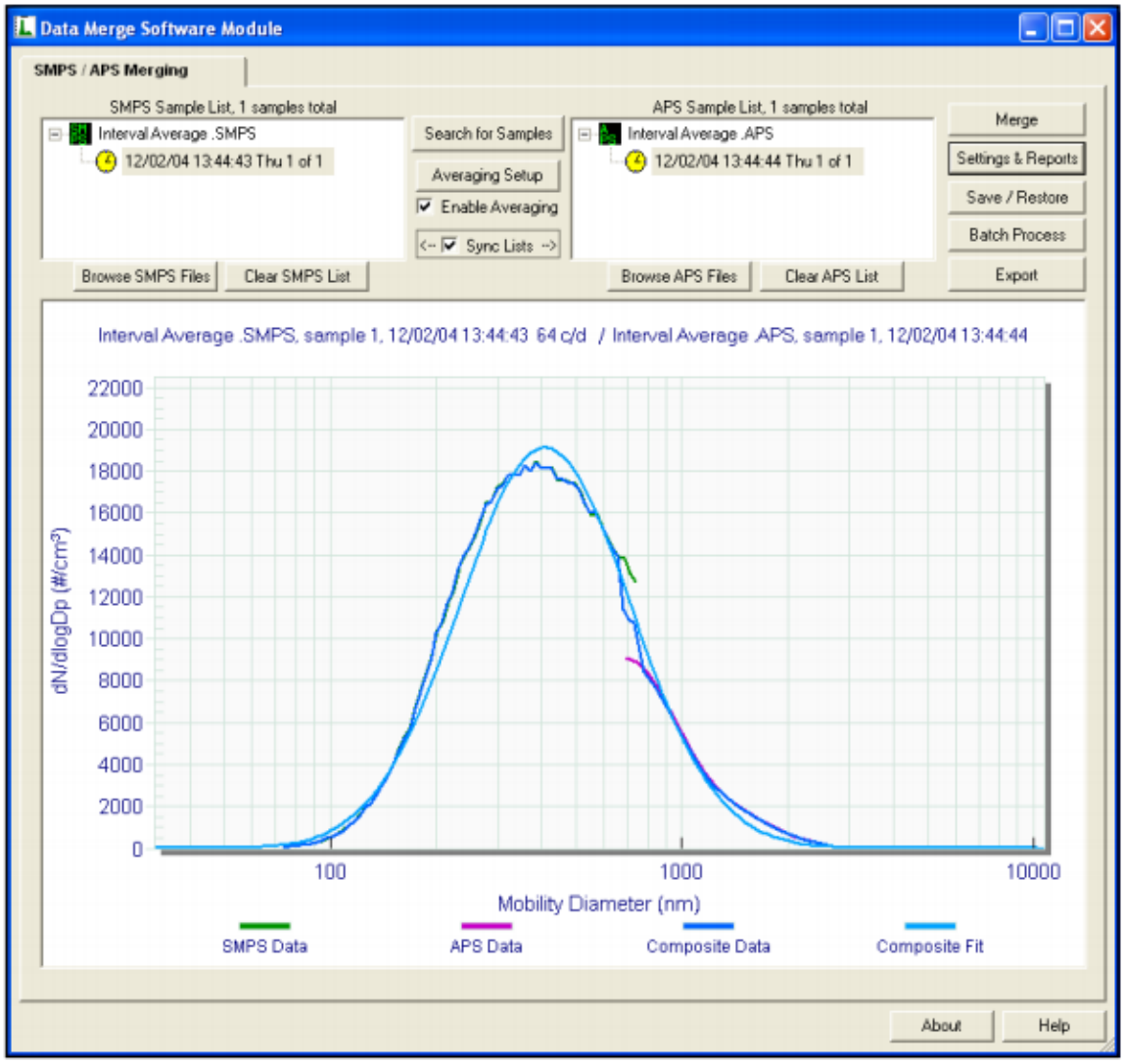

Figure 3-15: Output display of the merging and fitting of SMPS and APS data using the Data Merge® Software. Obtained from TSI (2014).

3.1.3.3. Specific surface area

Brunauer-Emmett-Teller (BET) analysis was performed at the Department of Chemistry, Wits University, South Africa, to determine the specific surface area and porosity of the sieved tailings bulk dust samples. Briefly, dust samples weighing 1 g were degassed in Nitrogen (N_2) at 150 °C for 4 h prior to analysis using a Micromeritics Flow Prep 060, sample degas system at -196 °C. The specific surface area, pore size and volume of the samples were determined using a Micromeritics Tristar Surface Area and Porosity Analyser (continuous flow technique).

3.1.3.4. Shape and surface elemental composition

The ETEC Autoscan (Serial No. 33; EG&G Ortec Model EDDS-II signal processor) Scanning Electron Microscopy with Energy Dispersive X-ray spectroscopy (SEM-EDX) was used to analyse the shape and the elemental composition of the sieved tailings bulk dust samples. The dust particles were mounted on carbon-coated stubs prior to analysis. The elemental composition was analysed using an electron beam accelerated potential of 20 keV down to 5 keV. The voltage used was able to excite spectra to a depth of the order of 0.1 - 0.01 μm on the surfaces of the dust particles. The "point and shoot" method, available from the NORAN analytical software version 3, of ten particles per sample was used to identify elements.

3.1.3.5. Mineral composition

The mineral composition of the sieved tailings bulk dust samples was analysed with X-ray diffraction (XRD) using a PANalytical Empyrean diffractometer with PIXcel detector and fixed slits with Fe filtered Co-Kα radiation. The material was prepared for analysis using a back-loading preparation method or a zero background holder depending on sample quantity. Data were evaluated using X'Pert Highscore plus software. The relative phase amounts (weight%) were estimated using the Rietveld refinement technique.

The method relies on the following equation:

$$Wp = Sp(ZMV)p / \sum_{i-1}^{n} Si(ZMV)i \qquad \text{Equation 3-1}$$

where,

W is the relative weight fraction of phase *p* in a mixture of n phases;

S is the Rietveld scale factor;

Z is the number of formula units per cell;

M is the atomic mass of the formula unit and;

V is the unit cell volume in nm^3 (Young et al., 1993).

3.1.3.6. Elemental composition

Inductively-coupled plasma atomic emission spectroscopy (ICP-AES) was performed at Elliot Lake Research Field Station, Laurentian University, Canada to determine the elemental composition (64 elements in total) of the sieved tailings bulk dust samples. This facility in Canada was chosen based on the fact that they could detect trace quantities of U in samples. A plasma source was used to dissociate the sample into its component atoms or ions by exciting them to a higher energy level. When the atoms or ions return to their ground state they emit photons of a characteristic wavelength depending on the element present and this light is recorded by an optical spectrometer.

Briefly, samples weighing 0.2 g were digested with an acid mixture of 9 ml hydrofluoric acid (HF) and 1 ml HCl in a Vulcan Digestion system at 100 ^{o}C with a ramp time of 30 min and this temperature was held for 280 min. The block was then cooled to 50 ^{o}C. The above step was repeated at 110 ^{o}C with a ramp time of 30 min and this temperature was held for 210 min. The block was then cooled to 50 ^{o}C. The first step was repeated, this time with an acid mixture of 7.5 ml nitric acid (HNO_3) and 7.5 ml HCl heated to 110 ^{o}C with a ramp time of 30 min and this temperature was held for 240 min. The block was again cooled to 50 ^{o}C. The first step was repeated again with an acid mixture of 0.5 ml HF, 2 ml HCl and 10 ml HNO_3 heated to 110 ^{o}C with a ramp time of 30 min and this temperature was held for 60 min. The total volume was reduced to 7 ml. The samples were then diluted with deionised water to 50 ml, stirred and left to stand overnight before ICP-AES analysis.

The elemental composition in mg/kg was calculated as follows:

$$\boldsymbol{x}\ \mu g/L \times \frac{50\ ml}{1000} = \boldsymbol{y}\ \mu g/50\ ml\ \asymp \boldsymbol{y}\ \mu g/0.2\ g \qquad \text{Equation 3-2}$$

$$\boldsymbol{y}\ \mu g/0.2\ g\ \times\ 0.2\ = \boldsymbol{z}\ \mu g/g\ \asymp\ \boldsymbol{z}\ mg/kg \qquad \text{Equation 3-3}$$

where $\boldsymbol{x}$ is equal to the measured amount of element as determined by ICP-AES, $50\ ml$ is the final volume of the sample prior to analysis, $\boldsymbol{y}$ is the measured amount of element in the original 0.2 g of dust and $\boldsymbol{z}$ is the measured amount of element in mg/kg. The elements detected and their corresponding detection limits are shown in **Table 3-3**.

Table 3-3: Elements detected by ICP-AES and their corresponding detection limits.

Element	Detection limit (mg/kg)	Element	Detection limit (mg/kg)	Element	Detection limit (mg/kg)	Element	Detection limit (mg/kg)	Element	Detection limit (mg/kg)	Element	Detection limit (mg/kg)	Element	Detection limit (mg/kg)	Element	Detection limit (mg/kg)
Al	1	Cd	0.05	Eu	0.02	In	0.02	Mo	3	Pr	0.02	Sn	0.7	Tm	0.03
As	0.2	Ce	0.04	Fe	1	Ir	0.02	Na	1	Pt	0.05	Sr	0.02	U	0.06
Au	0.1	Co	0.03	Ga	0.02	K	6	Nb	0.3	Rb	0.03	Ta	2	V	0.2
B	0.2	Cr	0.4	Gd	0.05	La	0.03	Nd	0.02	Rh	0.03	Tb	0.01	W	0.2
Ba	0.2	Cs	0.03	Ge	0.05	Li	0.02	Ni	0.2	Sb	0.07	Te	0.01	Y	0.02
Be	0.05	Cu	0.05	Hf	0.6	Lu	0.03	P	1	Sc	0.2	Th	0.7	Yb	0.02
Bi	0.3	Dy	0.02	Hg	1	Mg	0.1	Pb	0.06	Se	0.6	Ti	1	Zn	0.06
Ca	5	Er	0.03	Ho	0.02	Mn	0.02	Pd	0.05	Sm	0.03	Tl	0.06	Zr	0.06

ICP-AES data analysis

The following equation was used to calculate the factor by which the concentration of the element in question in the tailings dust was higher/lower than the limit concentration of the element as determined by national or international agencies:

$$Factor = \frac{Concentration\ of\ element\ in\ tailings\ bulk\ dust\ sample\ (mg/kg)}{Limit\ concentration\ of\ element\ specified\ by\ agency\ (mg/kg)} \qquad \text{Equation 3-4}$$

Hierarchical cluster analysis based on the Ward's method on all the identified elements was conducted using Statistica 64 version 13.2 (StatSoft Inc. Tulsa, OK 74104, USA), to assess whether the tailings dust from each TSF exhibit their own elemental profile and whether the dusts may be distinguished from the other dusts based on this profile. For example, whether the dusts from the DRD TSF contain significantly higher As and Cd levels compared to the dusts from the CGR TSF.

Random forest analysis (Statistica 64 version 13.2) was conducted next to determine which elements carried more weight in determining the unique elemental profiles of the dusts from each TSF.

3.1.3.7. Surface activity under acellular conditions

Electron spin resonance (ESR) spectroscopy with spin-trapping was used to measure short-lived •OH radicals generated by particles, hereafter referred to as 'surface activity'. ESR has been

shown to be a highly sensitive method, compared to other methods such as the dithiothreitol (DTT) assay and the antioxidant (e.g. ascorbic acid) depletion assay (Janssen et al., 2014, Boogaard et al., 2012). The •OH radicals were measured since it is the most dangerous of all the radicals (Fubini and Fenoglio, 2007). The production of •OH was measured in the absence and presence of H_2O_2. The addition of H_2O_2 facilitates ROS formation via the Fenton type reaction (equation 3-5).

$$H_2O_2 + M^{n+} \rightarrow M^{(n+1)+} + \bullet OH + {}^{-}OH \qquad \text{Equation 3-5}$$

where M is a transition metal cation, e.g. Fe, Cr, Cu, V, Mn etc. (Prousek, 1995, Harrington et al., 2012), which can donate one electron.

The reaction mixtures for ESR measurements contained the following:

- The spin trap 5,5-Dimethyl-1-Pyrroline-N-Oxide (DMPO, Sigma, St. Louis, MO; purified using activated charcoal) at a final concentration of 100 mM for the measurement of the •OH spin adduct DMPO-OH **(Figure 3-16);**
- H_2O_2 either omitted or at a final concentration of 10 mM;
- Particles at a final concentration of 10 µg/ml;
- Deionised water, purified with Chelex (Sigma, St. Louis, MO) at a concentration of 2 g/*l*, to make up the reaction mixture to a final volume of 1 ml.

The reaction mixture was directly transferred to an X band 9.8 GHz, Bruker EMX, Resonant cavity: TM 110; Sample cell holder: 4-bore AquaX ESR instrument (Bruker Instruments, Inc., Billerica, MA). The reaction was monitored at ambient temperature under the following settings: MW Power: 25 mW; Receiver Gain: 5.64 E 5; Time Constant: 40.96 msec; Conversion Time: 40.96 msec; Resolution X: 1024; Scans: 2; Sweep time: 41.94 sec; Sweep width: 100 G; Modulation Frequency: 100 kHz; Modulation amplitude: 3 G.

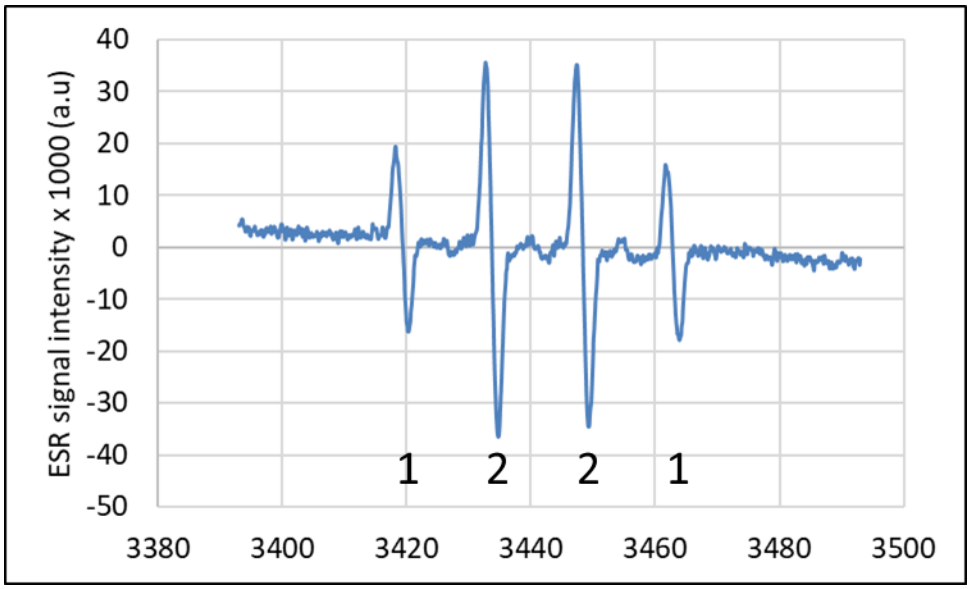

Figure 3-16: Typical ESR signal of the DMPO-OH spin adduct.

As a standard, 4-OH-Tempol (Sigma, St. Louis, MO) was used to calibrate the instrument. A calibration equation of y = 47361x + 4458 (R^2 = 0.99) was achieved between 0 µM and 3 µM 4-OH-Tempol. Consequently, 4-OH-Tempol at a concentration of 2 µM was analysed daily to confirm instrument calibration. The signal intensity from the splitting constants of the 1:2:2:1 spectrum **(Figure 3-16)**, which is characteristic of •OH (Halliwell and Gutteridge, 2015), was used to measure the relative amount of radicals as arbitrary units (a.u.).

3.1.3.8. Crystalline silica positive control, Min-U-Sil 5

Min-U-Sil 5 (alpha quartz), which was generously provided by US Silica Inc. (Berkeley Springs, WV, USA), was also characterised using the techniques mentioned in the previous sections. Min-U-Sil 5 served as the positive control in this study for the following two reasons:

1. Previous studies have shown that tailings dust are mainly composed of crystalline silica (de Andrade Lima et al., 2008).
2. Min-U-Sil 5 has been shown to induce effects *in vitro*, for example, oxidative stress in the cell lines used in this study namely the BEAS-2B (Antognelli et al., 2009) and U937 (Journeay et al., 2009) **(Section 3.1.4.1)**. This is to ensure that the cells are able to generate the response measured and to provide a benchmark for comparison.

3.1.4.Toxicity assessment of tailings dust

3.1.4.1. Cell lines

BEAS-2B cell stocks were purchased from American Type Culture Collection (ATCC: Manassas, VA, USA). The non-tumorigenic BEAS-2B cell line was established by immortalising normal human bronchial epithelial cells through infection with an adenovirus 12 and simian virus 40 (Ad 12-SV40) hybrid (Reddel et al., 1989). The BEAS-2B epithelial cell line was chosen for this study since epithelial cells are the first line of defence against inhaled foreign objects and is often selected as appropriate cell models for the cytotoxicity assessment of coarse and fine PM (Schins et al., 2002, Jimenez et al., 2000, Veranth et al., 2004, Veranth et al., 2006).

A second cell line, i.e., the macrophage-like monocytic U937 cell line, also purchased from ATCC (Manassas, VA, USA), was included in this study as it has been shown previously that particle-induced initiation mechanisms vary among different cell types (Bruch et al., 2004). In addition, macrophages play important roles in allergic responses (e.g. asthma), inflammation (Verstraelen et al., 2008) and particle clearance. The U937 cell line was originally established from a 37-year-old Caucasian male with histiocytic lymphoma (Sundström and Nilsson, 1976).

Primary cells vs. cell lines

It is well known that primary cells represent the *in vivo* condition better than cell lines. However, the acquisition of primary cells requires frequent use of invasive procedures on human and animal models. In addition, primary cells may undergo only a limited number of replications before reaching senescence, and is therefore not suitable for extended incubations. Lastly, using primary cells runs the risk of inter-individual variation as these cells are more variable across human donors (Smith, 2003, Volckens et al., 2009). Consequently, cell lines were chosen for this study to ensure a continuous supply of cells and consistent cellular responses.

3.1.4.2. Culture conditions

The BEAS-2B cell line, which is adherent, were cultured in Roswell Park Memorial Institute (RPMI) 1640 medium containing phenol red and supplemented with 10% heat-inactivated foetal bovine serum (FBS) and 1% penicillin/streptomycin, hereafter referred to as culture medium. Cells were incubated at 37 ^{o}C with 5% CO_2 in a humidified atmosphere. The cells were sub-

cultured at approximately 80 – 90% confluence twice a week in 75 cm^2 culture flasks as follows: the cells were washed with Dulbecco's phosphate buffered saline (DPBS) followed by the addition of 3 ml 1× trypsin/ethylene diamine tetra acetic acid (EDTA) for 5 min at 37 ^oC to detach the cells from the flask surface. The trypsin/EDTA was inactivated with the addition of 5 ml culture medium and the detached cells were transferred to a 50 ml Falcon tube. The cells were then centrifuged for 5 min at 200 × *g* (1000 rpm) after which the supernatant was discarded and the cell pellet was resuspended in 5 ml culture medium. Thereafter, cells were counted using the trypan blue dye exclusion assay (discussed below), seeded at 2×10^5 cells/cm^2 and put in the incubator until the next sub-culture.

The U937 cell line, which is non-adherent, was also cultured in the same culture medium described above. Cells were incubated at 37 ^oC with 5% CO_2 in a humidified atmosphere. The cells were sub-cultured every second day in 75 cm^2 culture flasks as follows: the cells were transferred from the culture flask to a 50 ml Falcon tube and centrifuged for 5 min at 200 × *g* (1000 rpm). The supernatant was discarded and the cell pellet resuspended in 10 ml culture medium. Thereafter, cells were counted using the trypan blue dye exclusion assay, seeded at 5×10^5 cells/ml and transferred back to the incubator until the next sub-culture.

Trypan Blue Dye Exclusion Assay

The trypan blue dye exclusion assay was used to determine cell viability and concentration at which the cells should be seeded. This assay is able to distinguish between viable and dead cells based on the principle that viable cells possess an intact cell membrane and therefore cannot take up the dye while dead cells readily take up the dye through their damaged cell membranes (Strober, 2001). The cells were sub-cultured as described earlier and resuspended in culture medium. Thereafter, a 10 µl of the cell suspension was added to 10 µl trypan blue and 10 µl of this mixture was pipetted into one of the chambers of a plastic Countess™ slide (Waltham, MA USA). The slide was then inserted into the Countess Cell Counter™ to determine the cell viability and concentration of the cell suspension.

Mycoplasma testing

The MycoAlert® Mycoplasma Detection Kit (Lonza, Walkersville, MD, USA) was used for routine testing of cells for mycoplasma. If mycoplasma was detected, the cells and reagent aliquots were discarded immediately and a new stock of cells and reagents were thawed.

3.1.4.3. Particle exposure conditions

A direct submerged exposure method was used where sieved tailings bulk dust samples or Min-U-Sil 5 were weighed and resuspended in cell culture medium without phenol red, hereafter referred to as dispersion medium. Phenol red is known to influence the read-out of toxicity assays, particularly those that are dependent on a colour product formation (Quent et al., 2010) or fluorescence (Ettinger and Wittmann, 2014). Stock solutions of resuspended particles were prepared, which were then serially diluted to the desired concentrations. To prevent particle agglomeration and ensure uniform dispersion, suspensions were vortexed before treatment.

Another parameter that influences the efficacy of toxicity assays is the pH of the medium in which the assay reaction occurs. For example, an altered pH is known to affect the cell's ability to reduce tetrazolium salts as well as lead to the spontaneous reduction of tetrazolium salts (Riss et al., 2016). For this reason, the pH of the dispersion medium was measured before and directly after addition of the particles (100 µg/cm^2) as well as after 24 h using a Cyberscan pH6500 pH/ion meter (Thermo Scientific, NY, USA) at 37 ^{o}C to determine whether the particles have the ability to alter pH.

3.1.4.4. Conventional toxicity assays

Cell-based studies with the crystalline silica positive control, Min-U-Sil 5

Cell cultures

BEAS-2B cells were seeded in appropriate 96-well plates at 5 × 10^4 cells/cm^2. The cells were allowed to reach exponential (log) phase 24 h after seeding and were then treated for 24 h with Min-U-Sil 5 at 25, 50 and 100 µg/cm² in an incubator (37 °C, 5% CO_2). Untreated cells received dispersion medium only. Cell toxicity was assessed with three conventional toxicity assays as per the manufacturers' instructions (see below). All experiments were performed in triplicate on three separate days (n = 9).

3'-(1-[(phenylamino)-carbonyl]-3,4-tetrazolium) bis(4-methoxy-6-nitro) benzenesulfonic acid hydrate (XTT) assay

The XTT toxicity assay (Sigma Aldrich, St. Louis, MO) estimates cell number based on the mitochondrial activity in living cells. The mitochondrial dehydrogenases of viable cells produce NADH, which reduce (cleave) the tetrazolium ring of XTT via the trans-membrane electron transport yielding an orange, water-soluble, formazan derivative. The assay reaction occurs outside the cell at the plasma membrane; NADH on the inside of the cell membrane is oxidised by co-enzyme Q located within the plasma membrane; co-enzyme Q in turn reduces N-methyl dibenzopyrazine methyl sulphate (PMS), an electron acceptor located outside on the cell surface; PMS forms a reactive intermediate, which reduces XTT to formazan chromophore (Berridge et al., 2005).

Cells were treated with Min-U-Sil 5 as described above. After treatment, reconstituted XTT stock reagent (1 mg/ml tetrazolium salt with 1% PMS) was added to the cells and was incubated for 2 h in an incubator. The absorbance was recorded at 450 nm on an ELx 800 spectrophotometric plate reader (BioTek instruments) and KC4 software (version 3.4) to quantify formazan product, which is proportional to the activity of mitochondrial dehydrogenase in viable cells. Viability was calculated as a percentage of the untreated, control cells (equation 3-6).

$$Viability\ (\%) = \frac{Absorbance\ of\ treated\ cells}{Absorbance\ of\ untreated\ cells} \times 100 \qquad \text{Equation 3-6}$$

Adenosine Triphosphate (ATP) assay

The CellTiter Glo luminescent ATP cell viability assay (Promega Southampton, UK) determines the number of viable, metabolically active cells based on the ATP content. The assay relies on the luciferase reaction to quantify the amount of ATP present. Cells are first lysed to release the ATP content. The Ultra-GLo recombinant luciferase then converts beetle luciferin to oxyluciferin (luminophore) + adenosine monophosphate (AMP) + pyrophosphate (PPi) + carbon dioxide (CO_2) + light in the presence of ATP, molecular oxygen and Mg^{2+}.

Cells were treated with Min-U-Sil 5 as described above. After treatment, CellTiter-Glo Reagent (containing beetle luciferin, luciferase and a cell lysis reagent that is proprietary to Promega) was

added to the cells. The plate containing the cells was shaken for 2 min to induce cell lysis and was incubated for another 10 min at room temperature to stabilise the luminescent signal. Luminescence was recorded using the FLx 800 fluorometric plate reader (BioTek instruments, Winooski, VT, USA) and KC4 software (version 3.4) to quantify the luminophore, oxyluciferin product, which is proportional to the amount of ATP present in viable cells. Viability was calculated as a percentage of the untreated, control cells (equation 3-7).

$$Viability\ (\%) = \frac{Luminescence\ of\ treated\ cells}{Luminescence\ of\ untreated\ cells} \times 100 \qquad \text{Equation 3-7}$$

Lactate dehydrogenase (LDH) assay

The CytoTox-ONE Homogeneous membrane integrity assay (Promega), a rapid, fluorescence-based measure of LDH, is a marker for damaged cell membranes. LDH enzymatically reduces resazurin into resorufin in the presence of lactate, oxidized nicotinamide adenine dinucleotide (NAD+) and diaphorase. The assay reaction occurs outside the cells in the supernatant; LDH is released through damaged cell membranes and enters the supernatant upon which it reacts with resazurin.

Cells were treated with Min-U-Sil 5 as described above. After treatment, CytoTox-ONE Reagent containing resazurin substrate was added to the cells and was incubated for 10 min at room temperature. Fluorescence was recorded at 560/590 nm using the FLx 800 fluorometric plate reader and KC4 software (version 3.4) to quantify the amount of resorufin product, which is proportional to the amount of LDH released by dead/damaged cells. Cytotoxicity was calculated as a percentage of the Maximum LDH Release, which is untreated cells lysed with 9% Triton X-100 to release all cytoplasmic LDH (equation 3-8).

$$Cytotoxicity\ (\%) = \frac{Fluorescence\ of\ treated\ cells}{Fluorescence\ of\ Maximum\ LDH\ Release\ cells} \times 100 \qquad \text{Equation 3-8}$$

xCELLigence real-time cell analyser (RTCA) single plate (SP) instrument

The toxicity of the BEAS-2B cells when treated with Min-U-Sil 5 was also assessed using the xCELLigence RTCA instrument (ACEA Biosciences, San Diego, California, USA), the principle of which is discussed later in **Section 3.1.4.5**.

A total of 50 µl of dispersion medium was added to each well of an E-Plate 96 and the plate was left to equilibrate for 30 min at room temperature in a sterile environment. The plate was then placed in the RTCA station and read to establish a baseline. Thereafter, the cells were sub-cultured as previously described and 100 µl of cell suspension was added to each well of the plate to obtain a final concentration of 5×10^4 cells/cm^2. The plate was left to equilibrate for 30 min at room temperature in a sterile environment after which the plate was then placed in the RTCA station at 37 °C with 5% CO_2 in a humidified atmosphere. Cells were allowed to proliferate for 24 h to reach 50% confluence prior treatment. The cells were then treated with Min-U-Sil 5 at 25, 50 and 100 µg/cm². Untreated cells received dispersion medium only. Scans were acquired every 5 min for 24 h, and then every 15 min for the remainder of the experiment.

Cell-free interference studies

Cell-free interference studies are essential with particles as they are known to absorb light, adsorb molecules on their surfaces and also contribute to catalytic reactions (Oostingh et al., 2011, Kroll et al., 2012, Monteiro-Riviere et al., 2009, Holder et al., 2012). Min-U-Sil 5 as well as three dust samples (≤ 20 µm fraction) were selected to test interference in the XTT, ATP and LDH assays in the absence of cells. The dust samples were selected based on their colour: CGR 07 (light brown), CGR 18 (dark brown) and DRD 06 (white), to represent various particle types during interference testing. The particles were suspended in dispersion medium.

The study design implemented to assess the interference of tailings particles and Min-U-Sil 5 with the relevant assay systems used is shown in **Figure 3-17**. These included the investigation of, (1) particle interference at the wavelengths of the optical read-out (absorbance, luminescence, fluorescence) and (2) particle interference with the assay components i.e. substrate and/or product. For interference of particles with the optical read-out, the tailings dusts and Min-U-Sil 5 were suspended in dispersion medium only and the absorbance/luminescence/fluorescence was

recorded at the wavelength used for each assay to determine whether particles interfere with the signal. For interference of particles with assay components, dusts were incubated with assay substrate and/or product and the absorbance/luminescence/fluorescence was recorded to determine whether particles interfere with these components via absorption at the optical read-out, surface adsorption or surface catalytic activity.

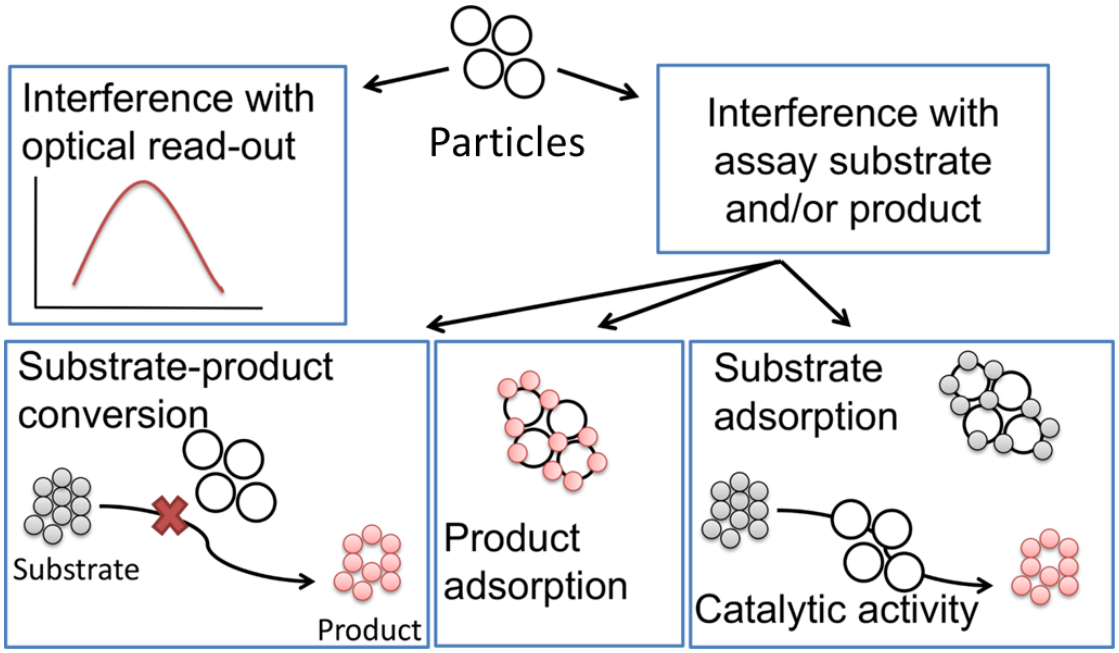

Figure 3-17: Schematic diagram of the study design for interference experiments.

All interference experiments were conducted in the absence of cells. Min-U-Sil 5 and tailings dust concentrations used were 80, 160, 320 µg/ml (corresponding to 25, 50 and 100 µg/cm²). All cell-free interference results are presented in µg/cm² dosages for easy comparison with cell-based studies, in which dusts were dosed at µg particles per cm² of cells occupying the surface of the well.

For the XTT assay, experiments were performed in sterile transparent 96-well plates (Costar Corning Inc., Corning, NY). For CytoTox One (LDH) and CellTiter Glo (ATP) assays, experiments were performed in sterile, opaque-walled 96-well plates (Costar Corning Inc.) to minimise luminescence or fluorescence interference between wells. All experiments were repeated three times in triplicate (n = 9).

XTT assay

Reaction of particles in dispersion medium only

Particles were suspended in dispersion medium only and the absorbance was recorded at 450 nm to determine if particles absorb light at the same wavelength as the formazan chromophore product

Reaction of particles in the conversion of XTT substrate to formazan product in the presence of 0.1 mM NADH co-factor

Reconstituted XTT stock reagent (substrate) was added to wells containing particles in dispersion medium with 0.1 mM NADH as co-factor (Roche Diagnostics, Germany). Control wells contained XTT substrate, dispersion medium and 0.1 mM NADH but without particles. NADH was used as reductant as it has been shown to be the most effective for XTT (Berridge et al., 2005, Berridge et al., 1996). After a 2 h incubation period at 37 °C to allow formazan product formation, absorbance was recorded at 450 nm.

Reaction of particles with formazan chromophore product

Formazan was produced from XTT substrate in the presence of 0.1 mM NADH. The plate was allowed to incubate for 4 h to ensure that product formation reached saturation (plateau). Particles were added to the wells containing formazan and the absorbance was recorded. Control wells received dispersion medium only.

Reaction of particles with XTT substrate

XTT substrate only was added to wells containing particles in dispersion medium. Control wells contained XTT substrate and dispersion medium but without particles. Absorbance was recorded after a 2 h incubation period.

ATP assay

Reaction of particles in dispersion medium only

Particles were suspended in dispersion medium only and the luminescence was recorded to determine if particles emit light at the same wavelength as the oxyluciferin product.

Reaction of particles in the conversion of luciferin substrate to oxyluciferin luminophore product in the presence of 1.5 µM ATP co-factor

CellTiter-Glo Reagent containing the substrate luciferin, was added to wells containing particles in dispersion medium with 1.5 µM ATP as co-factor (Sigma Aldrich). Control wells contained luciferin, dispersion medium and 1.5 µM ATP but without particles. The reaction mixture was mixed for 2 min on an orbital shaker and allowed to incubate for 10 min at room temperature to stabilise the luminescent signal. After incubation the luminescence was recorded.

Reaction of particles with oxyluciferin product

Oxyluciferin was produced from luciferin substrate in the presence of 1.5 µM ATP. The reaction mixture was mixed for 2 min and allowed to incubate for 10 min to allow saturated product formation. Particles were added to the wells containing oxyluciferin luminophore and the luminescence was recorded. Control wells received dispersion medium only.

Reaction of particles with luciferin substrate

Luciferin was added to wells containing particles in dispersion medium. Control wells contained the substrate luciferin only and dispersion medium but without particles. Luminescence was recorded after a 2 min mix and 10 min incubation.

LDH assay

Reaction of particles in dispersion medium only

Particles were suspended in dispersion medium only and the fluorescence was recorded at 560/590 nm to determine if particles fluoresce at the same wavelength as the resorufin fluorophore product.

Reaction of particles in the conversion of resazurin substrate to resorufin product in the presence of 0.1 mM NADH co-factor

CytoTox-ONE Reagent containing resazurin substrate was added to wells containing particles in dispersion medium with 0.1 mM NADH as co-factor. Control wells contained resazurin, dispersion medium and 0.1 mM NADH but without particles. NADH has been used previously

as a reductant to produce resorufin product via diaphorase (Han et al., 2011). After a 10 min incubation at room temperature fluorescence was recorded at 560/590 nm.

Reaction of particles with resorufin product

Resorufin was produced from resazurin substrate in the presence of 0.1 mM NADH. The plate was allowed to incubate at room temperature for 10 min to allow saturated product formation. Particles were added to wells containing resorufin and the fluorescence was recorded. Control wells received dispersion medium only.

Reaction of particles with resazurin substrate

The substrate resazurin only was added to wells containing particles in dispersion medium. Control wells contained resazurin and dispersion medium but without particles. Fluorescence was recorded after a 10 min incubation period.

3.1.4.5. Label-free toxicity analysis

Real time measurements of cell viability and cytotoxicity based on cellular adherence were obtained using the xCELLigence RTCA and RTCA software (version 1.2.1). The xCELLigence RTCA is based on the principle that cells are seeded in an E-plate containing micro-electrodes integrated on the bottom of the wells. Cells act as insulators on the electrode surface leading to an increase in impedance. Viable cells are spread and attached strongly resulting in greater impedance of the electrodes. This electrode impedance is defined by a unitless parameter known as the cell index (CI). The xCELLigence RTCA monitors cellular events such as cell viability, proliferation, degree of cell adhesion, cell number and morphology in real time by measuring the electrical impedance across the micro-electrodes. Low CI values, compared to untreated cells, indicate cytotoxicity while high CI values indicate cell adhesion and proliferation.

The CI value is calculated as follows:

$$CI = max_{i=1} N \left[R_{cell}(f_i) / R_b(f_i) - 1\right] \quad \text{Equation 3-9}$$

where $R_{cell}(f_i)$ is frequency-dependent electrode impedance at any time, $R_b(f_i)$ is background impedance measured at the initial time without cells, and N is the number of the frequency points at which the impedance is measured.

The normalized CI (NCI) value is calculated as follows:

$$NCI_i = CI_i(t) / CI_i(t\ of\ dose) \quad \text{Equation 3-10}$$

where $CI_i(t)$ is CI at any time and $CI_i(t\ of\ dose)$ is CI at the time of particle dosing.

Verification of the xCELLigence RTCA was achieved using the resistor plate provided, with the RTCA station outside the incubator and then again when the RTCA station was placed inside the incubator.

xCELLigence optimisation

Prior to conducting experiments on the xCELLigence RTCA, it was important to first optimise the seeding densities of BEAS-2B and U937 cells since the manufacturer (ACEA Biosciences Inc.) recommended that the CI reaches a value of at least 1 during the exponential growth phase prior treatment.

BEAS-2B cells

Various concentrations of BEAS-2B cells at 5×10^3, 1×10^4, 2.5×10^4, 5×10^4 or 1×10^5 cells/well) were seeded in an E-Plate 96 using the method described earlier in **Section 3.1.4.4 (xCELLigence RTCA)**. The plate was placed in the RTCA station in an incubator and the proliferation of BEAS-2B cells was monitored over a period of 3 days. The seeding densities at 2.5×10^4, 5×10^4 or 1×10^5 cells/well reached plateau in less than 24 h after seeding while the seeding density at 5×10^3 cells/well was too low and never reached a CI value of 1. The density at 1×10^4 cells/well reached 1 during the exponential phase and was therefore selected for all subsequent toxicity studies.

U937 cells

Fibronectin, collagen and poly-L-lysine coating

The xCELLigence RTCA relies on the adherence of cells to the surface of the well in order to create an impedance. It is therefore more suitable for adherent cell lines as opposed to suspension cell lines. U937 cells are non-adherent, therefore, the plate had to first be coated with an extracellular matrix (ECM) protein, e.g. fibronectin, collagen or poly-L-lysine, in order to successfully perform toxicity tests on the xCELLigence RTCA. Working solutions of the ECM protein was prepared by dissolving fibronectin in DPBS, collagen in 0.02 N acetic acid and poly-L-lysine in sterile distilled water (dH_2O) to final concentrations of 1, 2.5, 5 and 10 $\mu g/cm^2$. A volume of 25 µl of each ECM protein working solution was added to the wells of an E-plate and allowed to incubate for 1 h (for fibronectin and collagen) or 5 min (for poly-L-lysine) at room temperature. The remaining solution was then aspirated from each well, and the plate was rinsed once with 100 µl DPBS (for fibronectin and collagen) or 100 µl dH_2O (for poly-L-lysine). The coated plate was allowed to air-dry overnight in a sterile environment prior to seeding.

U937 differentiation

The U937 cell line is a monocytic cell line and therefore required differentiation into mature macrophages prior to toxicity testing as the focus of this study was on macrophage (and not monocyte) response to tailings dust. Briefly, the U937 cells were removed from tissue culture flasks as described earlier in **Section 3.1.4.1 (Culture conditions)**, differentiated with 32 nM phorbol-12-myristate-13 acetate (PMA; Sigma) per ml of cell suspension and seeded at concentrations of 1×10^4, 2.5×10^4 or 5×10^4 cells/well either in uncoated or coated wells (fibronectin, collagen or poly-L-lysine at different concentrations) of the E-plate. The plate was then placed in the RTCA station in an incubator and the cells were allowed to differentiate for 3 days.

The most optimal conditions for U937 cells appeared to be at a cell density of 2.5×10^4 cells/well in fibronectin-coated plates at 5 $\mu g/cm^2$ and was therefore selected for all subsequent toxicity studies.

Assessing the toxicity of sieved tailings bulk dust samples and the crystalline silica positive control, Min-U-Sil 5, with the xCELLigence RTCA

Cytotoxic experiments were performed with both cell lines seeded at optimised densities of 1×10^4 cells/well (5×10^4/cm²) for BEAS-2Bs and 2.5×10^4 cells/well (1.25×10^5/cm²) for differentiated U937s in dispersion medium. For U937 cells, the wells of the plate were first coated with fibronectin prior to the addition of cells. The BEAS-2B cells were left to adhere and proliferate for 24 h prior to treatment while the U937 cells were allowed to differentiate for 3 days (72 h). During this time, CI readings were taken every 15 min. For treatment, the medium was replaced with fresh dispersion medium containing sieved tailings bulk dust samples or Min-U-Sil 5 at concentrations of 25, 50 and 100 µg/cm^2. These concentrations were based on the fact that lung cells are typically exposed to 10 – 100 µg/cm^2 of ambient particles (Veranth et al., 2004, Veranth et al., 2006). Control cells received dispersion medium only. CI readings were taken at 5 min intervals for the first 2 h and then at 15 min intervals for the remainder of the experiment. Experiments were performed in two independent runs with cells at different passages (i.e. two biological replicates) with three technical replicates per run (i.e. n = 6).

Assessing the toxicity of sieved tailings bulk dust samples and the crystalline silica positive control, Min-U-Sil 5, with the LDH assay

The LDH assay was used to determine if the decrease in CI value was in fact due to cytotoxicity via disruption of cellular membranes. The principle of the LDH assay is discussed in detail earlier in **Section 3.1.4.4 (LDH assay)**. The cells were sub-cultured as described earlier and were then seeded in a sterile opaque 96-well plate at 5×10^4/cm² (for BEAS-2B) and 1.25×10^5/cm² (for differentiated U937) in 100 µl dispersion medium. For U937 cells, the wells of the plate were first coated with fibronectin prior to the addition of cells. BEAS-2B cells and U937 cells were incubated for 24 h and 3 days, respectively, to allow the cells to adhere and proliferate before treatment. Wells containing medium only were used as blanks. The medium was then replaced with fresh dispersion medium containing sieved tailings bulk dust samples or Min-U-Sil 5 at final concentrations of 25, 50 and 100 µg/cm^2 for a treatment period of 24 h. Control cells received dispersion medium only. Thereafter, a 100 µl CytoTox-ONE™ reagent was added to each well and the plate was incubated at room temperature for 10 min. Fluorescence was recorded at 560/590 nm using the FLx 800 fluorometric plate reader and KC4 software (version

3.4) to quantify the amount of resorufin product, which is proportional to the amount of LDH released by dead/damaged cells. Cytotoxicity was calculated as a percentage of the Maximum LDH Release, which is untreated cells lysed with 9% Triton X-100 to release all cytoplasmic LDH. Experiments were performed in two independent runs with cells at different passages (i.e. two biological replicates) with three technical replicates per run (i.e. n = 6).

3.1.5.Cellular uptake studies of tailings dust

The CytoViva® Hyperspectral Imaging (HSI) system (Auburn, AL, USA) is a dark field imaging system that is dependent on the scattering of light by particles, which in turn is dependent on certain optical properties of particles such as particle size and particle refractive index (Mercer et al., 2017). The HSI system differs from the traditional light microscope in that a direct light stop is inserted after the condenser to form a hollow cone of light. In contrast, the light microscope allows all the light from the light source to enter the objective lens **(Figure 3-18)**.

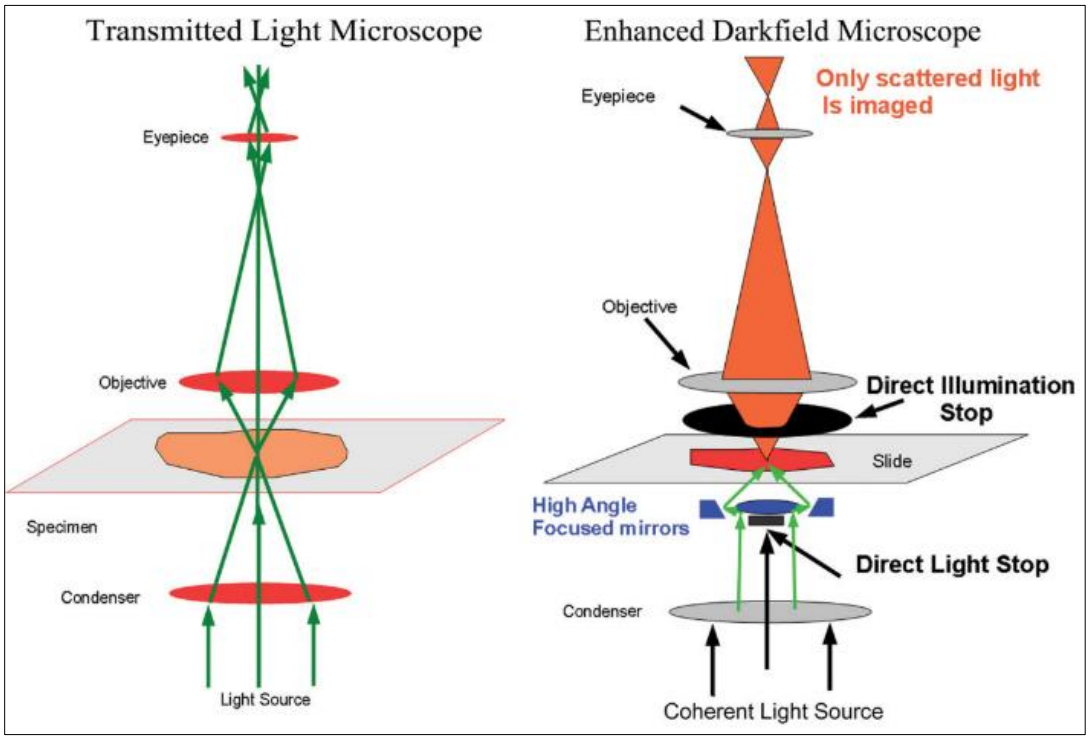

Figure 3-18: Principles of the traditional light microscope (left) and enhanced darkfield microscope (right). Obtained from Mercer et al. (2017).

The CytoViva® HSI system was used to visualise the uptake and interaction of particles with the cells. In order to successfully identify particles from cells, it is important that the refractive index of the particles in question is much higher than the refractive index of the cells (Mercer et al., 2017).

The microscope slides were prepared as follows: The cells were seeded on 8-well EZ-slides at 5 × 10^4/cm² (for BEAS-2B) and 1.25 × 10^5/cm² (for differentiated U937) in 500 µl dispersion medium. For U937 cells, the slides were first coated with fibronectin prior to the addition of cells. BEAS-2B cells and U937 cells were incubated for 24 h and 3 days, respectively, to allow the cells to adhere and proliferate before treatment. The medium was then replaced with fresh dispersion medium containing sieved tailings bulk dust samples or Min-U-Sil 5 at final concentrations of 10 and 50 µg/cm^2 for treatment periods of 1, 12 and 24 h. Control cells received dispersion medium only. Thereafter, the slides were washed 3 times with dispersion medium and a further 3 times with DPBS. The cells were then fixed in a solution of 4% formalin diluted with 0.1 M Tris/HCl pH 7.4 for 15 min at 4 ^oC. The slides were washed once with DPBS and air dried. A coverslip was glued to the slides using 40 µl Kaiser's gelatine and left to air-dry overnight. Dark-field images were captured at 60× magnification using the CytoViva 150 Unit integrated onto the Olympus BX43 microscope (Auburn, AL, USA). Images were acquired using a Dagexcel X16 camera and the DAGE Exponent software (Auburn, AL, USA). HSI was performed at 60× magnification using the HSI System 1.1 and ENVI software (Auburn, AL, USA).

In addition to the HSI scans of the particle-treated cells, scans were also performed of the particles alone. For this analysis, particles were suspended in dispersion medium only, placed on a microscope slide and allowed to air-dry. A coverslip was placed on the slide prior to the acquisition of an HSI scan at 60× magnification. Spectral libraries, which are indicative of the refractive index of the particles in the visible near-infrared range (400 – 1000 nm) were compiled by collecting approximately 20 spectra of randomly selected particles. The image classification algorithm, Spectral Angle Mapper (SAM), was performed using the ENVI software to map the spectral libraries of the particles only onto the scans of the particle-treated cells in order to

determine if the particles entered the cells. Scale bars were inserted using Image J software (Schindelin et al., 2015, Schneider et al., 2012).

3.1.6.Statistical analysis

For all the tests mentioned in the previous sections, significant differences were calculated using the non-parametric Kruskal-Wallis test followed by the non-parametric Mann-Whitney U test. A $P \leq 0.05$ was considered significant. Linear regression and non-parametric Univariate Spearman correlation analyses were performed to assess the correlation between the surface activity and *in vitro* toxicity of the tailings particles with their physicochemical properties. All tests were performed with Statistica 64 version 13.2. The accuracy of each analytical test method was assessed by using spiked samples of the known positive particle control, Min-U-Sil 5, which has been extensively characterised by previous research groups. Reproducibility and variation of each analytical test method was assessed by analysing triplicate samples of Min-U-Sil 5 every time the test method was performed.

3.2. EXPOSURE ASSESSMENT

The exposure assessment section of this thesis has been published in Andraos et al. (2018a) and Andraos et al. (2018b).

3.2.1.Meteorological data

It is well known that exposure to ambient particles is highly influenced by meteorological parameters such as wind direction, wind speed and rainfall. For this reason, it was decided to obtain the historical meteorological data from the nearest weather stations at each TSF as this would guide the decision in identifying the most appropriate times and sampling sites for data and filter collection. **Figure 3-19** shows the locations of the different weather stations i.e. at Roodepoort, the Johannesburg Botanical Gardens, Boksburg, Brakpan, Springs and Klerksdorp, in relation to the TSFs.

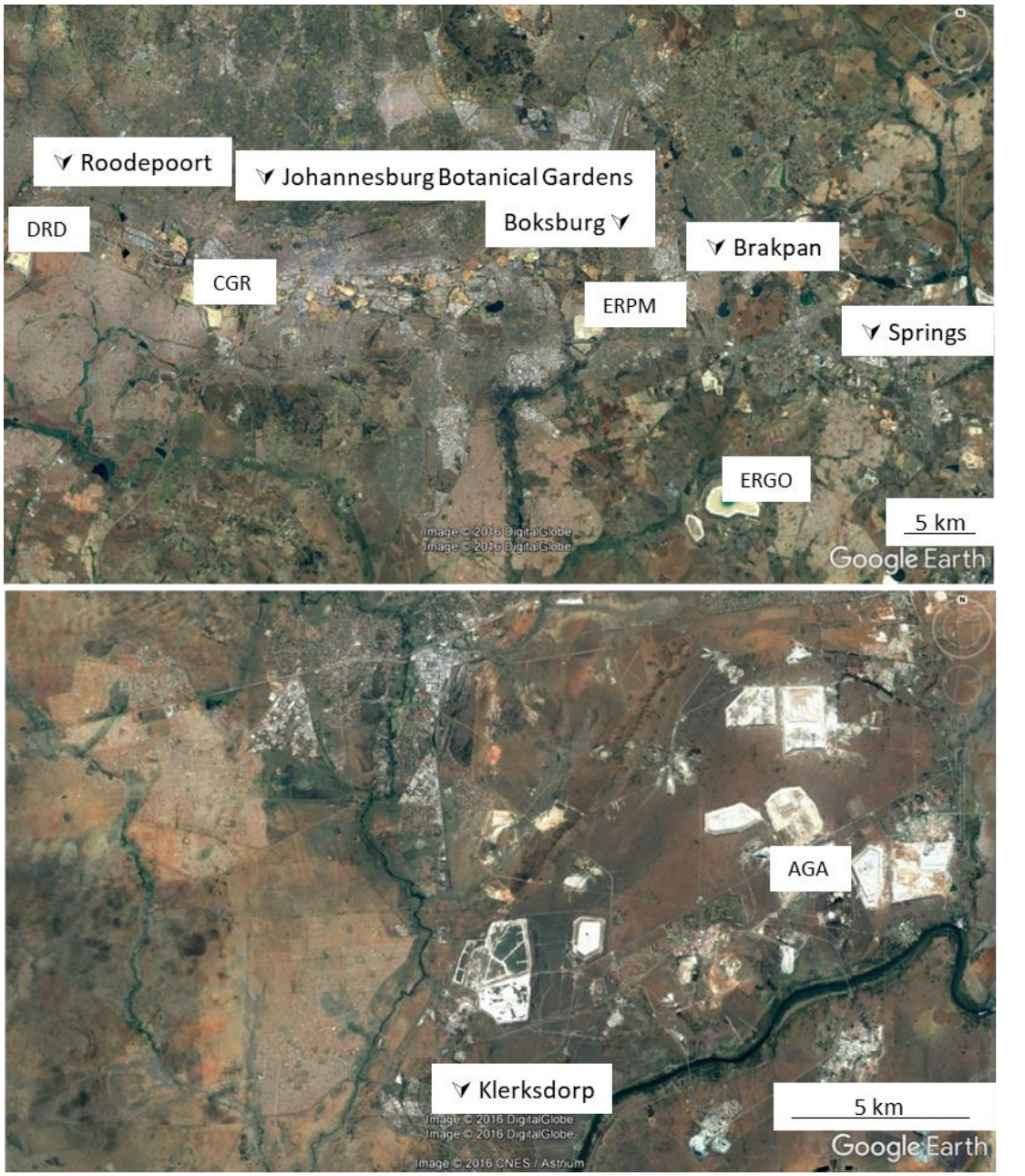

Figure 3-19: Locations of the weather stations used for meteorological data analysis.

3.2.1.1. Rain data

The average monthly rainfall data from the weather stations at Roodepoort for the period from 1986 to 2016, (for DRD sampling sites), the Johannesburg botanical gardens from 1985 to 2016 (for CGR sampling sites), Boksburg from 1903 to 2005 (for ERPM sampling sites), Brakpan from 1986 to 2007 (for ERGO sampling sites) and Klerksdorp from 1993 to 2016 (for AGA TSF sampling sites) were obtained from the South African Weather Service (SAWS). **Table 3-4**

shows that the wet and dry seasons spanned between the periods of October – April and May – September, respectively. Based on these results, it was decided to conduct sampling during August and September representing the dry season and during October representing the wet season.

Table 3-4: Average monthly rainfall data at Roodepoort, Johannesburg botanical gardens, Boksburg, Brakpan and Klerksdorp. Adapted from Andraos et al. (2018b).

Month	Roodepoort (average rainfall, mm)	Johannesburg botanical gardens (average rainfall, mm)	Boksburg (average rainfall, mm)	Brakpan (average rainfall, mm)	Klerksdorp (average rainfall, mm)
Jan	16.2 (131.7)	14.1 (130.7)	12.7 (121.3)	7.8 (100.5)	12.3 (80.2)
Feb	13.4 (117.3)	10.9 (103.2)	9.3 (93.9)	6.5 (98.8)	9.6 (57.7)
Mar	11.9 (109.4)	9.9 (88.8)	9.1 (85.9)	7.1 (100.8)	10.4 (59.9)
Apr	8.3 (46.3)	5.1 (31.7)	5.5 (40.2)	3.1 (29.9)	6.5 (34)
May	3.2 (15)	3.2 (16.2)	2.8 (18.1)	0.5 (7.4)	4.1 (15.7)
Jun	2.4 (9.1)	1.4 (7.2)	1.3 (5.8)	0.9 (9)	1.4 (4.7)
Jul	0.9 (1.6)	0.6 (2)	1.1 (6.4)	0.1 (0.2)	0.5 (0.9)
Aug	2.5 (7)	1.8 (6.7)	1.4 (7.5)	0.9 (5.5)	1.9 (6.4)
Sep	4.6 (22.5)	2.6 (12.8)	3 (22.7)	2.2 (20.1)	2.7 (10.2)
Oct	11.5 (70.1)	9 (63)	7.9 (64.8)	6.3 (58.5)	8.5 (43.4)
Nov	14.4 (108.7)	11.4 (82.8)	11.5 (106.5)	8.3 (93.7)	9.2 (54.1)
Dec	17.2 (129.6)	13.6 (112.8)	12.2 (109.8)	9.8 (115.7)	13.8 (104.1)

3.2.1.2. Wind data

Wind blowing in the direction from the TSF to the surrounding community increases the possibility of higher dust exposures, compared to wind blowing in the opposite direction. Therefore, average monthly wind direction and speed data from weather stations at the Johannesburg botanical gardens, Springs and Klerksdorp were obtained from the SAWS. The wind data from the Johannesburg botanical gardens were used to represent wind data at the sampling sites of the DRD and CGR TSFs, the wind data from the Springs weather station were used to represent wind data at the sampling sites of ERPM and ERGO TSFs (historical data for Boksburg and Brakpan weather stations were not available from SAWS, hence the use of the Springs weather station) and the wind data from the Klerksdorp weather station were used to represent wind data at the sampling sites of the AGA TSF (Andraos et al., 2018b).

Wind data are represented as wind rose plots of hourly wind data from midnight to midnight over a 22 (1994 – 2016), 15 (1998 – 2013) and 23 (1993 – 2016) year period for the Johannesburg botanical gardens, Springs and Klerksdorp weather stations, respectively, during August-September in the dry season **(Figure 3-20)** and during October in the wet season **(Figure 3-21)**. A total of 16 cardinal wind directions is plotted i.e. north (N), north-northeast (NNE), northeast (NE), east-northeast (ENE), east (E), east-southeast (ESE), southeast (SE), south-southeast (SSE), south (S), south-southwest (SSW), southwest (SW), west-southwest (WSW), west (W), west-northwest (WNW), northwest (NW) and north-northwest (NNW). The length of the spokes indicates the percentage frequency of winds i.e. a longer spoke represents higher frequency of winds. Each colour within a spoke represents the wind speed in m/s as indicated in each figure.

For the weather station at the Johannesburg botanical gardens in the dry season, the majority of the winds blew from NNW and N in August and from NNW, N and NNE in September **(Figure 3-20)**. Wind speeds at each of these months reached 3.5 to 5.6 m/s. For the Springs weather station, the majority of the winds blew from WNW, NW and NNW in August and September and reached highs of 5.6 to 8.7 m/s. For the Klerksdorp weather station, the winds were very consistent from a NNW direction in August and September and reaching highs of 5.6 to 8.7 m/s.

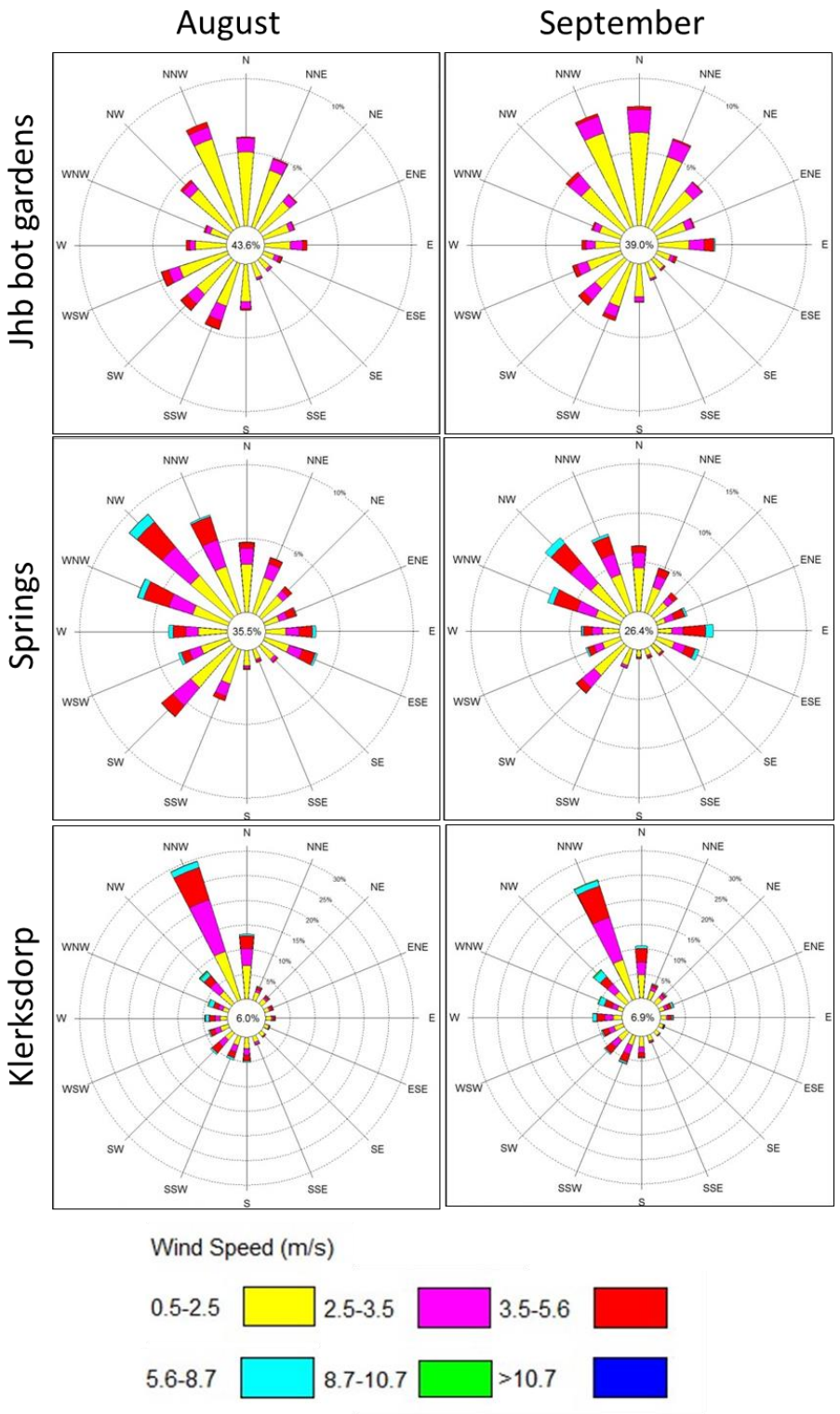

Figure 3-20: Wind rose plot of average wind data from the weather stations at the Johannesburg botanical gardens, Springs and Klerksdorp during August and September (dry season).

During October, the majority of the winds at the Johannesburg botanical gardens came from NNW, N and NNE directions while the weather stations in Springs and Klerksdorp showed the majority of the winds from a NW and NNW directions, respectively **(Figure 3-21)**.

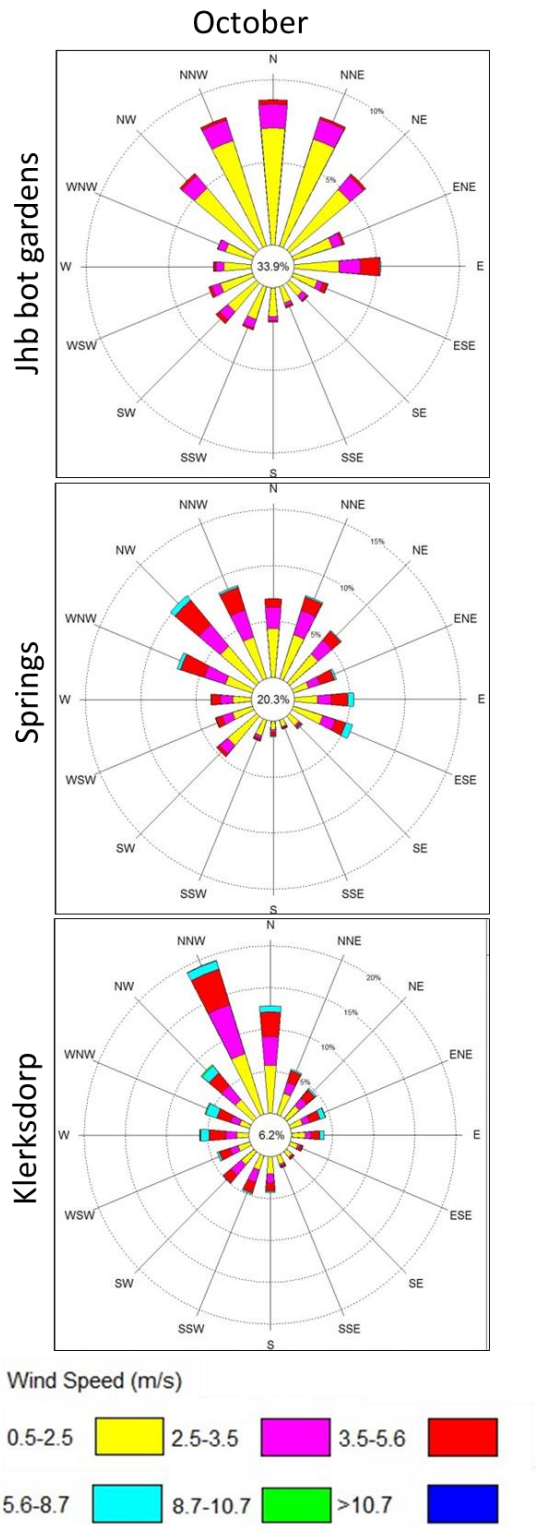

Figure 3-21: Wind rose plot of average wind data from the weather stations at the Johannesburg botanical gardens, Springs and Klerksdorp during October (wet season).

3.2.2.Continuous real-time ambient PM_{10} levels and ambient PM_{10} collected on filters at DRD, CGR and ERPM

3.2.2.1. Sampling sites

In order to determine whether PM_{10} fractions may reach the environment of the surrounding communities and whether the fractions do indeed contain crystalline silica, it was decided to record continuous real-time ambient PM_{10} data and collect ambient PM_{10} on filters at residential sites surrounding the DRD, CGR and ERPM TSFs. The current buffer zone guidelines states that the nearest residential areas should at least be 500 - 1000 m from the foot of the TSF (GDARD, 2009b). However, for DRD, CGR and ERPM, residential developments are located within this buffer zone. The aim of the PM_{10} data collection was to record the PM_{10} levels in a worst-case scenario setting by locating the PM_{10} monitor within a radius of at least 500 m from these TSFs in the backyards of private residences to record the most representative PM_{10} levels experienced by communities. ERGO and AGA were not included in the PM_{10} sampling campaign as the nearest residential areas from these TSFs were located outside of the 500 m radius (i.e. the nearest residences were located at least 1 - 3 km from ERGO and AGA) (Andraos et al., 2018a). Therefore, PM_{10} data were collected at residential sites within a 500 m radius at the DRD, CGR and ERPM TSFs **(Figure 3-22)**. Sampling of continuous real-time ambient PM_{10} data and PM_{10} filter samples at DRD occurred between 1 October 2012 and 31 October 2012; sampling at CGR occurred between 19 September 2011 and 24 October 2011 and sampling at ERPM occurred between 28 September 2010 and 31 October 2010 (Andraos et al., 2018a). The sampling sites at these TSFs were selected as they were downwind from the average prevailing winds.

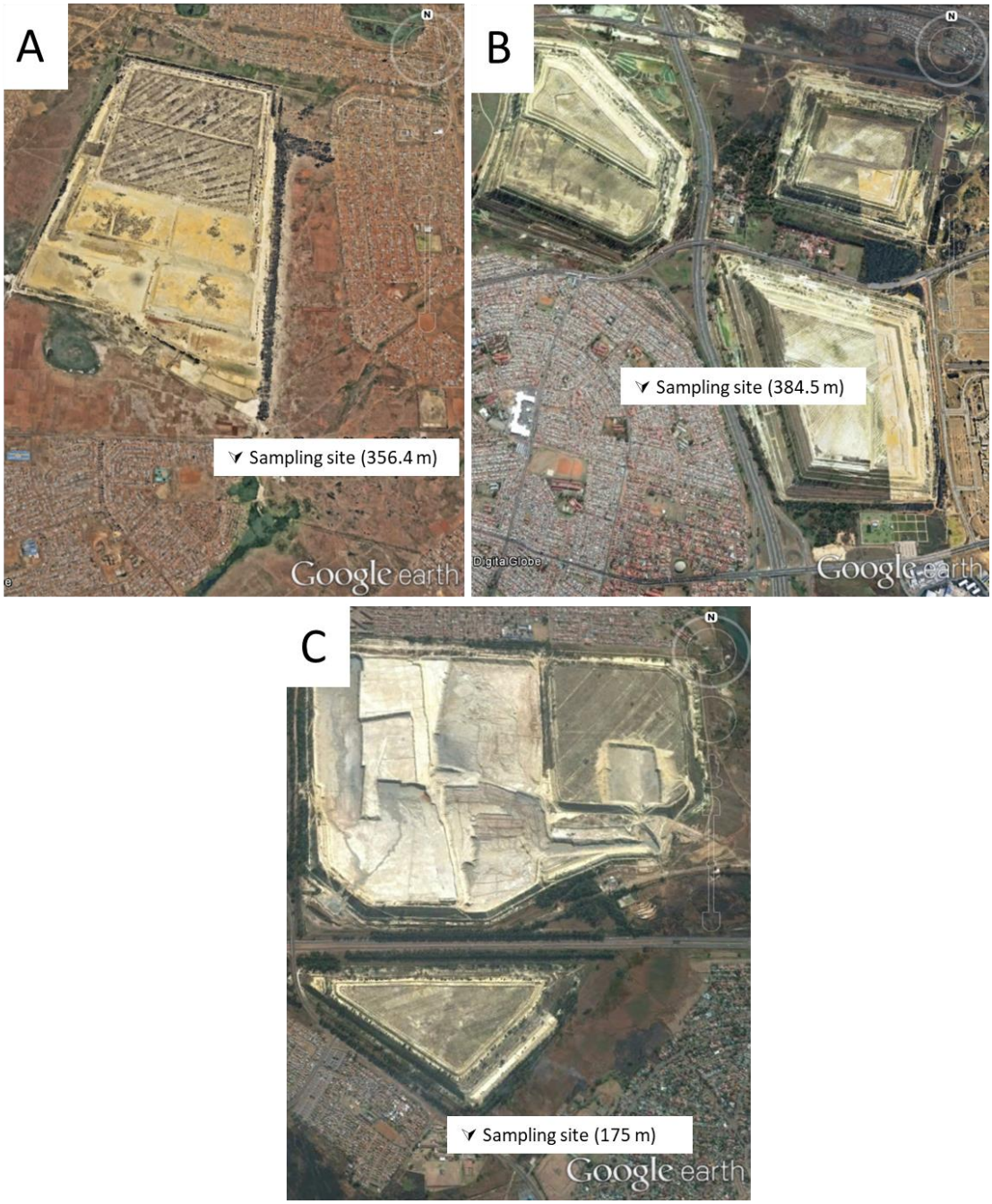

Figure 3-22: Ambient PM_{10} sampling locations. (A) DRD; (B) CGR and (C) ERPM. The distances shown in brackets are the distance between the sampling site of the PM_{10} dust monitor and the nearest point of the TSF.

3.2.2.2. Collection of continuous real-time ambient PM_{10} measurements from DRD, CGR and ERPM

As stated in Andraos et al. (2018a), "continuous real-time ambient PM_{10} levels at 1 min intervals were recorded at a controlled flow rate of 1.2 *l*/min using the GRIMM Environmental Dust Monitor (GRIMM Aerosol Technik GmbH & Co. KG, Ainring, Germany). Routine flow rate measurements were performed to ensure that the correct flow rate was achieved. The GRIMM Environmental Dust Monitor was fitted on a standard mobile trailer and the dust sensor of the monitor was therefore approximately 3 m from the ground. The GRIMM Environmental Dust Monitor was placed in the backyards of private urban residences during sampling. Hourly weather parameters such as wind speed, wind direction and rainfall were recorded using climate sensors, which were attached to the GRIMM Environmental Dust Monitor at the same height as the dust sensor. Therefore, for each day, 22 data points representing 22 h of weather data were captured from 2 am to 11 pm. Using this weather data, it was possible to determine whether emissions from the TSFs could have contributed to dust events recorded by the dust sensor in addition to other general and unavoidable dust sources such as domestic burning, vehicle emissions and regional industrial pollutants that cannot be ruled out". Wind speeds below 3 m/s were interpreted with caution as it has been suggested that only wind speeds above approximately 3 m/s are capable of lifting dust particles (SLR, 2014).

3.2.2.3. Collection of PM_{10} on filters from DRD, CGR and ERPM

The PM_{10} samples on filters were collected on standard 47 mm mixed cellulose ester (MCE) membrane filters at a calibrated flow rate of 3 *l*/min using the MicroVol 1100 low volume sampler (Ecotech Environmental Monitoring Solutions, Melbourne, Australia). The MicroVol was set up to collect PM_{10} for 24 h periods from midnight to midnight in conjunction with the GRIMM Environmental Dust Monitor. No rain was experienced on the days when filter sampling took place. A total of 22 environmental filters were collected from all three TSFs **(Table 3-5)** (Andraos et al., 2018b). Initially, it was decided to collect at least 12 filters per site, which was possible at the DRD TSF. However, the number of filters used was reduced to 6 for the CGR and ERPM sites as the variability in dust concentration in relation to meteoroidal events were comparable.

Table 3-5: Ambient PM_{10} collected on filters from DRD, CGR and ERPM

TSF	Number of filter samples collected
DRD	12
CGR	6
ERPM	4
Total	**22**

The mass of PM_{10} collected on the filters were determined via gravimetric analysis and the concentration of PM_{10} per cubic meter of air (µg/m³) was calculated based on the sampling time and flow rate of the MicroVol 1100 according to equations 3-11 and 3-12.

$$\text{Volume of sampler } (m^3) = \frac{\text{Average flow rate of sampler} \times \text{Sample time (min)}}{1000} \quad \text{Equation 3-11}$$

$$\text{Concentration } PM_{10}\ (\mu g/m^3) = \frac{\text{Dust mass of } PM_{10} \text{ on filter } (\mu g)}{\text{Volume } (m^3)} \quad \text{Equation 3-12}$$

3.2.2.4. Quantification of crystalline silica from ambient PM_{10}

The quantification of crystalline silica in µg per filter was conducted using direct-on-filter X-ray diffraction (MDHS method 101: Methods for the Determination of Hazardous Substances, Crystalline silica in respirable airborne dusts, direct-on-filter analyses by infrared spectroscopy and X-ray diffraction). The concentration of crystalline silica per cubic meter of air (µg/m³) was then calculated based on equations 3-11 and 3-12 (Andraos et al., 2018b).

In addition to calculating the concentrations of PM_{10} and crystalline silica, the percentage of silica by mass of PM_{10} was also calculated using equation 3-13 (Bhagia, 2009, Andraos et al., 2018b).

$$\text{Silica percentage} = \frac{\text{Silica } (\mu g/m^3)}{PM_{10}\ (\mu g/m^3)} \times 100 \quad \text{Equation 3-13}$$

3.2.3. PM_4 collected on personal filters at DRD, CGR, ERPM, ERGO and AGA

It was necessary to determine if the airborne dust from TSFs could reach the breathing zones of those living in surrounding communities and whether the fractions do indeed contain crystalline silica. Therefore, PM_4 samples were collected on personal filters during the wet (October) and

dry (August – September) seasons at sampling sites close to and further away from DRD, CGR, ERPM, ERGO and AGA and subsequently analysed for RCS, as discussed below.

3.2.3.1. Sampling sites

Adolescent learners spending the majority of their day at their respective schools were recruited. Ethical approval (Number: 235/2011) was obtained from the Research Ethics Committee of the Faculty of Health Sciences of the University of Pretoria, Gauteng Department of Education (Number: D2012/79) and the North-West Department of Education (Number: 23-04-2012). Personal PM_4 sampling was conducted in the period from 8 – 31 October 2012 as well as in the period from 26 August 2013 to 10 September 2013. Schools at the ERPM, ERGO and AGA TSFs were chosen such that certain schools were located within a radius of ≤ 2 km and others ≥ 5 km from the TSF **(Figure 3-23, Table 3-6)**. Due to the high density of nearby TSFs in the Soweto and Riverlea region, it was not possible to identify schools further than 5 km from the DRD and CGR TSFs without being affected by other confounding TSFs. Therefore, certain schools were selected based on the direction of the prevailing winds during the period of sampling. For example, for the DRD TSF, a school located NE from the TSF was selected **(Figure 3-23, Table 3-6)** since the frequency of winds from a SW direction in September was low, as recorded by the weather station at the Johannesburg botanical gardens **(Figure 3-20)**. Consequently, one of the schools selected was located SSE from the TSF based on the high frequency of winds from the NNW direction. Similarly, for the CGR TSF a school NE from the TSF and two schools S and SW from the TSF were selected **(Figure 3-23)** based on the wind frequency data in September **(Figure 3-20)**.

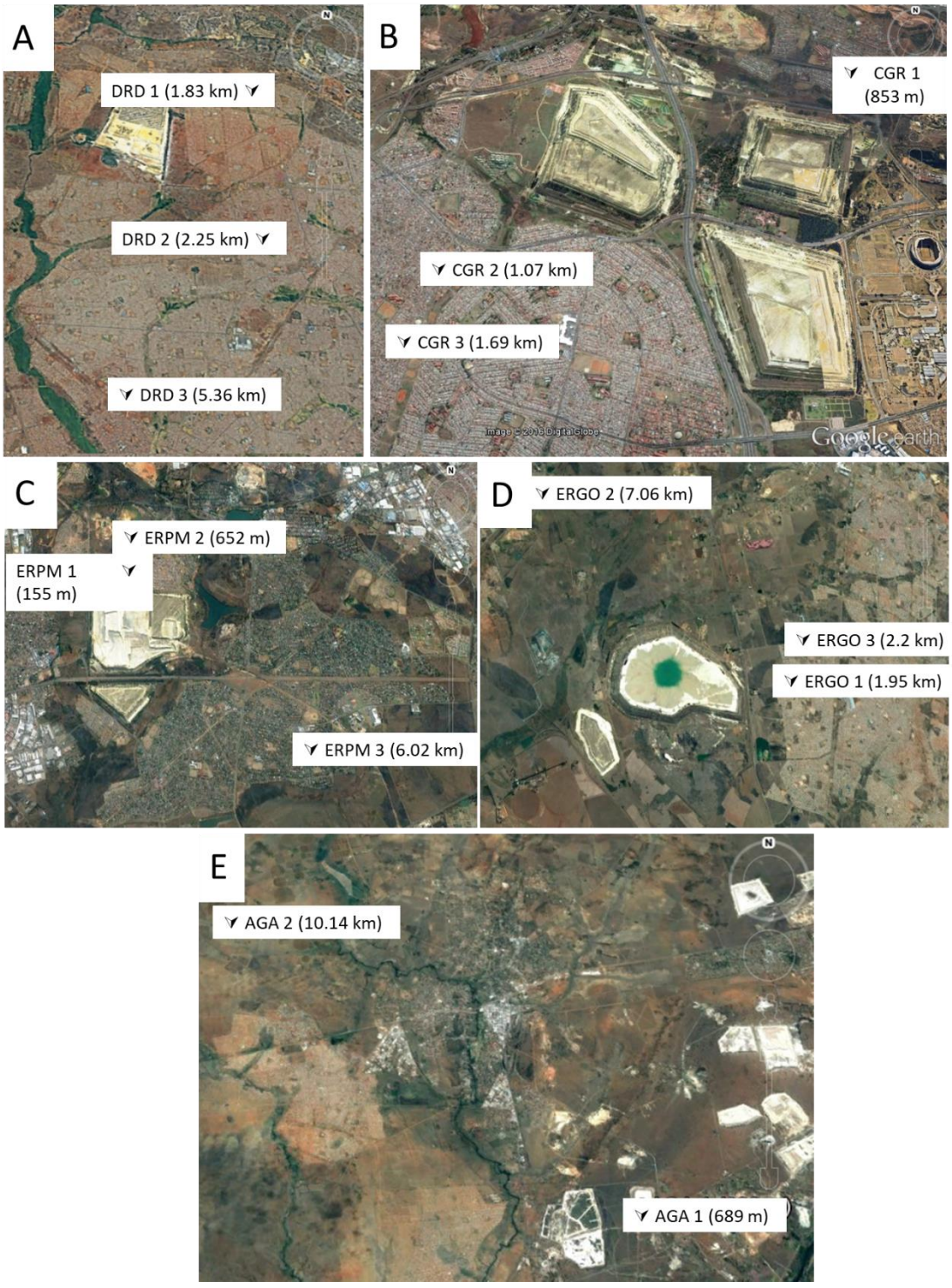

Figure 3-23: Personal PM_4 filter sampling locations. (A) DRD; (B) CGR; (C) ERPM; (D) ERGO and (E) AGA. The distances shown in brackets are the distance between the sampling site and the nearest point of the TSF.

Table 3-6: Personal PM_4 filter sampling locations including names of schools.

TSF	Sampling site	School
DRD	DRD 1	Siyabonga Secondary
	DRD 2	PJ Simelane Secondary
CGR	CGR 1	Riverlea Primary
	CGR 2	Noordgesig Secondary
	CGR 3	Job Radebe Secondary
ERPM	ERPM 1	Lakeside Primary
	ERPM 2	Oosrand Secondary
	ERPM 3	Windmill Park Secondary
ERGO	ERGO 1	Geluksdal Secondary
	ERGO 2	Windmill Park Primary
AGA	AGA 1	Vaal Reefs Technical High
	AGA 2	Nkang Mahalale Secondary

3.2.3.2. Collection of PM_4 on personal filters from DRD, CGR, ERPM, ERGO and AGA

Sampling was conducted continuously from 8:00 in the mornings when the learners arrived at school until 2:00 in the afternoons before leaving the school premises. One Gilian personal air sampler operating at an average flow rate of 2.2 *l*/min and fitted with a 25 mm mixed cellulosed ester (MCE) filter was attached to each learner. The samplers were attached to custom-made waist belts designed specifically for the learners and the tubing leading from the pumps were clipped onto clothing close to the collar bone of the learner to record PM_4 levels within the breathing zone. The flow rates of the samplers were calibrated externally using bubble flow meters prior to sampling. In addition, pre-flow and post-flow rate measurements for each sampler were recorded before and after each sampling session for each pump. Filters were excluded from further analysis if post-flow rate measurements were different than the specified 2.2 *l*/min or when a faulty pump was encountered (Andraos et al., 2018a). The number of filters collected and average sampling times at each site is indicated in **Table 3-7**. No rain was experienced on any of the days when sampling took place. Hourly weather parameters were recorded using a Vantage Pro2 weather station (Davis Instruments, California, USA), which was located outside on the premises of each school during sampling (Andraos et al., 2018a).

Table 3-7: Number and sampling times of PM_4 collected on personal filters during the wet and dry seasons.

TSF	Sampling site	Number of samples collected in the wet season (average sampling time in min ± SD)	Number of samples collected in the dry season (average sampling time in min ± SD)
DRD	1	0	19 (295.5 ± 7.1)
	2	10 (232.7 ± 12.7)	10 (245.7 ± 5.8)
	3	10 (324.2 ± 6.3)	0
CGR	1	0	10 (268.6 ± 4.3)
	2	10 (260.9 ± 2.6)	17 (276 ± 1.5)
	3	10 (232.2 ± 20.7)	19 (241.4 ± 86.3)
ERPM	1	10 (332.2 ± 3.5)	9 (363 ± 4.1)
	2	9 (313.9 ± 18.5)	10 (304.3 ± 3.7)
	3	10 (240.0 ± 2.1)	9 (342.4 ± 18.6)
ERGO	1	0 (316.8 ± 8.0)	7 (317.9 ± 3.9)
	2	10 (244.4 ± 7.9)	10 (316.3 ± 3.9)
	3	10 (300.5 ± 2.2)	0
AGA	1	6 (260.4 ± 6.1)	10 (280.5 ± 48.4)
	2	10 (363.3 ± 40.5)	10 (347 ± 41.8)
Total		**105**	**140**

3.2.3.3. Quantification of PM_4 particles and RCS collected on personal filters

The method of quantification of PM_4 particles and RCS on personal filters was similar to that of ambient PM_{10} discussed earlier in **Section 3.2.2** using equations 3-11, 3-12 and 3-13.

3.2.3.4. Data analysis of PM_4 collected on personal filters

Comparison of sampling sites

In order to allow comparisons between personal PM_4 levels within and between different sampling sites and to account for different sampling times, the concentrations of PM_4 and RCS was converted to 8 h TWA according to equations 3-14 and 3-15 (OSHA, 2016). A TWA of 8 h was chosen in order to benchmark our values to other occupationally-based studies as ambient personal PM_4 limits were not available. Our results were also compared to the current South African OEL of respirable PNOC of 3 mg/m^3 (DMR, 2006, Andraos et al., 2018a) and the suggested OEL limit of 1 mg/m^3 (Cherrie et al., 2013).

$$8\text{ h TWA} = PM_4\ (\mu g/m^3) \times \frac{\text{Sample time (min)}}{480} \qquad \text{Equation 3-14}$$

$$8\text{ h TWA} = \text{RCS}\ (\mu g/m^3) \times \frac{\text{Sample time (min)}}{480} \quad \text{Equation 3-15}$$

where 480 is the number of minutes in 8 h.

Statistical analysis

Significant differences of PM_4 levels between two groups were calculated using the Mann Whitney U test. Significant differences of PM_4 levels between more than two groups were calculated using the Kruskal-Wallis test followed by Mann-Whitney U. A $P \leq 0.05$ was considered significant. Significant differences of RCS levels between groups could not be calculated due to the high number of non-detects observed.

3.3. RISK CHARACTERISATION

Risk characterisation for both cancer-related and non-cancer-related endpoints was conducted from the personal PM_4 RCS levels collected during the dry season as it is more representative of the actual silica levels inhaled by individuals, as compared to ambient PM_{10} sampling (Andraos et al., 2018b).

3.3.1. Non-cancer risk characterisation

Non-cancer risks are estimated on the basis that there is a level of exposure below which adverse health effects are unlikely to occur, and thereby require the use of indices such as the oral reference dose (R*f*D), inhalation reference concentration (R*f*C) or acceptable daily intake (ADI), which are estimates of the daily exposure to the human population including sensitive subgroups 'that are likely to be without an appreciable risk of deleterious effects during a lifetime' (Williams and Paustenbach, 2002). Since our risk characterisation is conducted on personal filters, an R*f*C of 3 µg/m³ as recommended by OEHHA for RCS was chosen. Risks through inhalational exposure can be estimated by comparing the known R*f*C with the actual exposure concentration (EC) (Kolluru, 1996).

The EC in µg/m³ was calculated using the following equation:

$$\text{EC} = \frac{(\text{CA} \times \text{ET} \times \text{EF} \times \text{ED})}{\text{AT}} \quad \text{Equation 3-16}$$

where CA is the concentration of RCS in air in µg/m³, ET is the exposure time in hours/day, EF is the exposure frequency in days/year, ED is the exposure duration in years and AT is the averaging time calculated as exposure duration in years × 365 days/year × 24 hours/day) (US EPA 2009). For our dataset, 95th upper percentiles were calculated using the statistical software, ProUCL 5.1.00, which was developed by the US EPA (EPA, 2002) and is based on the non-parametric Kaplan-Meier method, which is known to tolerate a high number of non-detects (Annan et al., 2009). For the purposes of this study, CA represented the 95th upper percentile of the actual RCS concentrations on the filters collected for each sampling site (i.e. not 8 h TWA concentrations). ET and ED were set as 24 hours/day and 70 years, respectively (ATSDR, 2005, EPA, 2011). For the calculation of the EF, two scenarios were anticipated:

3.3.1.1. Scenario 1:

A maximum EF of 365 days a year was selected to represent a worst case scenario where exposure was assumed for the whole year.

3.3.1.2. Scenario 2:

An EF was calculated based on meteorological data known to govern the atmospheric dispersion of dust i.e. wind speed, wind direction and rainfall. This approach was first used in a recent publicly available, qualitative air quality risk assessment conducted by SLR Global Environmental Solutions Consulting in Ireland as per requested by the Hammond Lane Metal Company, which was finally approved by the US EPA (SLR, 2014):

The historical wind data shown in **Figure 3-20** and **Figure 3-21** were used to calculate the average number of days per month in which the wind blew in the direction from the TSF to the respective sampling site, possibly leading to higher exposure. Only wind speeds above 2.5 m/s were considered in the calculation of the EF (SLR, 2014).

Rainfall as little as 0.2 mm per day is sufficient to suppress dust emissions (SLR, 2014), which in turn drastically decreases the possibility of dust exposures to surrounding communities. Therefore, the rain data in **Table 3-4** were used to calculate the average number of rain days per

month. To calculate the number of dry days, the number of wet days was subtracted from the total number of days per month. The EF was calculated by adding the number of dry days in a year to the number of windy days in a year when wind blew in the direction from the TSFs to the sampling sites and is shown in **Table 3-8** (Andraos et al., 2018b).

Table 3-8: Exposure frequencies (EF; days per year) per sampling site. The EF was calculated based on average wind and rain data from weather stations located close to each sampling site. Adapted from Andraos et al. (2018b).

TSF Site	Days	Jan	Feb	Mar	Apr	May	June	July	Aug	Sep	Oct	Nov	Dec	Total
DRD 1	Wind days	0.3	0.2	0.3	0.4	0.8	1.1	1.0	1.4	1.1	0.7	0.7	0.5	267
	Dry days	30.7	27.8	30.7	29.6	30.2	28.9	30.0	29.6	28.9	30.3	29.3	30.5	
DRD 2	NA[a]	NA[a]	NA[a]	NA[a]	NA[a]	NA[a]	NA[a]	NA[a]	NA[a]	NA[a]	NA[a]	NA[a]	NA[a]	NA[a]
CGR 1	NA[a]	NA[a]	NA[a]	NA[a]	NA[a]	NA[a]	NA[a]	NA[a]	NA[a]	NA[a]	NA[a]	NA[a]	NA[a]	NA[a]
CGR 2	Wind days	1.7	1.6	1.0	0.7	0.5	0.6	0.8	1.0	1.4	1.8	1.5	1.4	295
	Dry days	16.9	17.1	21.1	24.9	27.8	28.6	30.4	29.2	27.4	22	18.6	17.4	
CGR 3	Wind days	1.7	1.6	1.0	0.7	0.5	0.6	0.8	1.0	1.4	1.8	1.5	1.4	295
	Dry days	16.9	17.1	21.1	24.9	27.8	28.6	30.4	29.2	27.4	22	18.6	17.4	
ERPM 1	Wind days	0.2	0.1	0.2	0.3	0.2	0.2	0.4	0.5	0.2	0.4	0.3	0.4	291
	Dry days	18.3	18.7	21.9	24.5	28.2	28.7	29.9	29.6	27	23.1	18.5	18.8	
ERPM 2	Wind days	0.2	0.1	0.2	0.3	0.2	0.2	0.4	0.5	0.2	0.4	0.3	0.4	291
	Dry days	18.3	18.7	21.9	24.5	28.2	28.7	29.9	29.6	27	23.1	18.5	18.8	
ERPM 3	NA[a]	NA[a]	NA[a]	NA[a]	NA[a]	NA[a]	NA[a]	NA[a]	NA[a]	NA[a]	NA[a]	NA[a]	NA[a]	NA[a]
ERGO 1	Wind days	1.1	0.8	1.2	1.6	1.8	1.4	1.5	2.0	2.4	2.4	2.3	2.1	332
	Dry days	23.2	21.5	23.9	26.9	30.5	29.1	30.9	30.1	27.8	24.7	21.7	21.2	
ERGO 2	Wind days	1.3	1.2	1.2	0.7	0.6	0.6	0.9	0.8	1.0	1.0	1.0	1.03	323
	Dry days	23.2	21.5	23.9	26.9	30.5	29.1	30.9	30.1	27.8	24.7	21.7	21.2	
AGA 1	Wind days	6.0	5.0	4.7	5.0	5.0	5.3	5.3	6.0	6.8	7.3	7.2	7.0	290
	Dry days	18.7	18.4	20.6	23.5	26.9	28.6	30.5	29.1	27.3	22.5	20.8	17.2	
AGA 2	NA[a]	NA[a]	NA[a]	NA[a]	NA[a]	NA[a]	NA[a]	NA[a]	NA[a]	NA[a]	NA[a]	NA[a]	NA[a]	NA[a]

[a] Sampling sites where the RCS concentrations of all filters collected were below the detection limit (BDL) were excluded from EF calculation and risk characterisation.

The risk, expressed as an HQ, was then calculated as follows:

$$\mathrm{HQ} = \frac{\mathrm{EC}}{\mathrm{R}f\mathrm{C}} \qquad \text{Equation 3-17}$$

where an HQ value of less than 1 would indicate no possible risk to developing a non-cancer adverse health effect and an HQ higher than 1 would indicate a possible risk (Kolluru, 1996).

3.3.2.Cancer risk characterisation

The objective of the cancer risk characterisation is to estimate the excess cumulative lifetime risk arising from exposure to RCS from the TSFs. The excess or incremental lifetime risk is defined as the 'additional risk (over background) from exposure over an individual's lifetime' (Kolluru, 1996). Generally, the risk of cancer is estimated using cancer potency values, which are typically expressed as a cancer slope factor (CSF). A CSF is defined as an 'upper bound, approximating a 95% confidence limit, on the increased cancer risk from a lifetime exposure to an agent' (Williams and Paustenbach, 2002). It is the slope of the straight line in a dose-response curve extrapolated from the POD that indicates the incremental probability of an individual developing cancer as a result of exposure over a lifetime (Kolluru, 1996). Risk is calculated as follows:

$$\text{Risk} = \text{LADD} \times \text{CSF} \qquad \text{Equation 3-18}$$

where risk is a unitless probability of an individual developing cancer, LADD is the lifetime average daily dose in $mg.kg^{-1}.d^{-1}$, and CSF is expressed as $(mg/kg/d)^{-1}$ (Williams and Paustenbach, 2002).

For cancers resulting from inhalational exposures, inhalational unit risks (IURs), which is also known as unit risk estimates (Rice et al., 2001) and expressed as $(\mu g/m^3)^{-1}$, can be calculated from the CSFs by normalising the CSF data to a known lifetime inhaled concentration of the carcinogen, which is usually set at 1 $\mu g/m^3$ (Goldsmith et al., 1995). Consequently, incremental cancer risks resulting from chronic and sub-chronic exposures can be calculated using equation 3-19 (EPA, 2009):

$$\text{Risk} = \text{IUR} \times \text{EC} \qquad \text{Equation 3-19}$$

EC is the exposure concentration in $\mu g/m^3$, as calculated from equation 3-16 using ET, EF, ED and AT. The ET and ED were set as 24 hours/day and 70 years, respectively. For EF, the two scenarios anticipated in the non-cancer risk calculations were also used for cancer risk calculations. An IUR (or inhalation cancer potency slope as in Goldsmith et al. (1995)) of 6.75×10^{-5} $\mu g/m^3$ was used as this risk estimate was calculated from a cohort mortality study of South

African gold miners who were exposed to gold mining dust composed of mainly quartz (Hnizdo and Sluis-Cremer, 1991, Goldsmith et al., 1995, Rice et al., 2001). Firstly, the Global 86 computer model was used to fit linearized multistage models to experimental data from the South African gold mine study of Hnizdo and Sluis-Cremer (1991) to compute the CSF (or cancer potency slope, CPS, as in Goldsmith et al. (1995)). Thereafter, the IUR was calculated by normalising the CSF data for a lifetime exposure to 1 µg/m^3 of ambient silica dust using equation 3-20 (Goldsmith et al., 1995). Other IUR values were calculated from either animal studies (Collins and Marty, 1995) or from human exposures to dust composed of mainly cristobalite (Goldsmith et al., 1995, Rice et al., 2001), and were therefore not considered further in the calculations of this study (Andraos et al., 2018b).

$$IUR = \frac{CSF \times 20\ m^3\ air.day^{-1} \times 10^{-3} mg.\mu g}{70\ kg\ average\ adult\ weight}$$ Equation 3-20

4. RESULTS

The results chapter has been divided into three sections namely *hazard identification* **(Section 4.1)**, *exposure assessment* **(Section 4.2)** and *risk characterisation* **(Section 4.3)**. With regards to *hazard identification*, S**ection 4.1.1** addresses the physicochemical characteristics and surface activity of the tailings dusts while **Sections 4.1.2** to **4.1.4** address their *in vitro* toxic potential and cellular uptake. The *exposure assessment* section is divided into the assessment of PM_{10} levels **(Sections 4.2.1** and **4.2.2)** and PM_4 levels **(Section 4.2.3)** in surrounding communities. Finally, the *risk* to cancer and non-cancer endpoints of RCS exposure is calculated.

4.1. HAZARD IDENTIFICATION

Hazard identification involves the comprehensive analysis of the physicochemical properties of a particle, its toxic potential and correlation between these two aspects to determine its hazardous potential. This is described in more detail below.

4.1.1.Physicochemical analysis of tailings bulk dust

4.1.1.1. Size distribution of the tailings dusts

Size distribution based on mass

As mentioned earlier in **Section 3.1.3.1**, the bulk tailings dust samples were first sieved to enrich the fraction with smaller particles of respirable size having a higher potential of becoming airborne and reaching surrounding communities. Indeed, **Table 4-1** shows that the sieved fractions of the majority of dusts contained small particles with MMADs around 9 µm (for CGR, ERGO and AGA) while the DRD site showed the smallest size range (8.7 ± 1.3 µm) and the ERPM site the largest (12.3 ± 2.2). All dusts had narrow size distributions, as indicated by the small GSDs **(Table 4-1)**. These results show that the sieved dust samples contained particle sizes in the thoracic as well as the respirable range.

Table 4-1: Median mass aerodynamic diameter (MMAD) and geometric standard deviation (GSD) of the respirable fraction of the bulk dusts from each TSF.

TSF	MMAD (GSD) (µm ± SD)*
DRD	8.7 ± 1.3 (2.0 ± 0.2)
CGR	9.3 ± 0.8 (1.9 ± 0.2)
ERPM	12.3 ± 2.2 (1.4 ± 0.1)
ERGO	9.4 ± 0.7 (1.6 ± 0.1)
AGA	9.5 ± 0.7 (1.3 ± 0.02)
* Determined with the Electrostatic Classifier Model 3080 and APS Model 3321	

Size distribution based on particle number

The MMAD and GSD provide information regarding the size distribution in terms of *mass;* however, it does not give any indication as to the fraction of small particles present, particularly those in the nano-range. **Figure 4-1** shows the merged size distributions from 1 nm to 100 µm vs. particle number for each of the sieved tailings bulk dust samples. The size distribution patterns followed mostly a uni-modal shape with certain dust samples exhibiting a bi-modal shape. The curves of most of the dust samples peaked around 100 nm indicating that a large number of particles exhibited a count mode aerodynamic diameter (CMAD) ≤ 100 nm, with the CMAD indicating the diameter of a particle in which 50% of the particle *count* (rather than *mass*) is greater than the specified cut-point and the other 50% is smaller. The CMAD is obtained from the median of a distribution of diameters whereas the MMAD is obtained from the median of the mass distribution (Jameson and Walters, 2016).

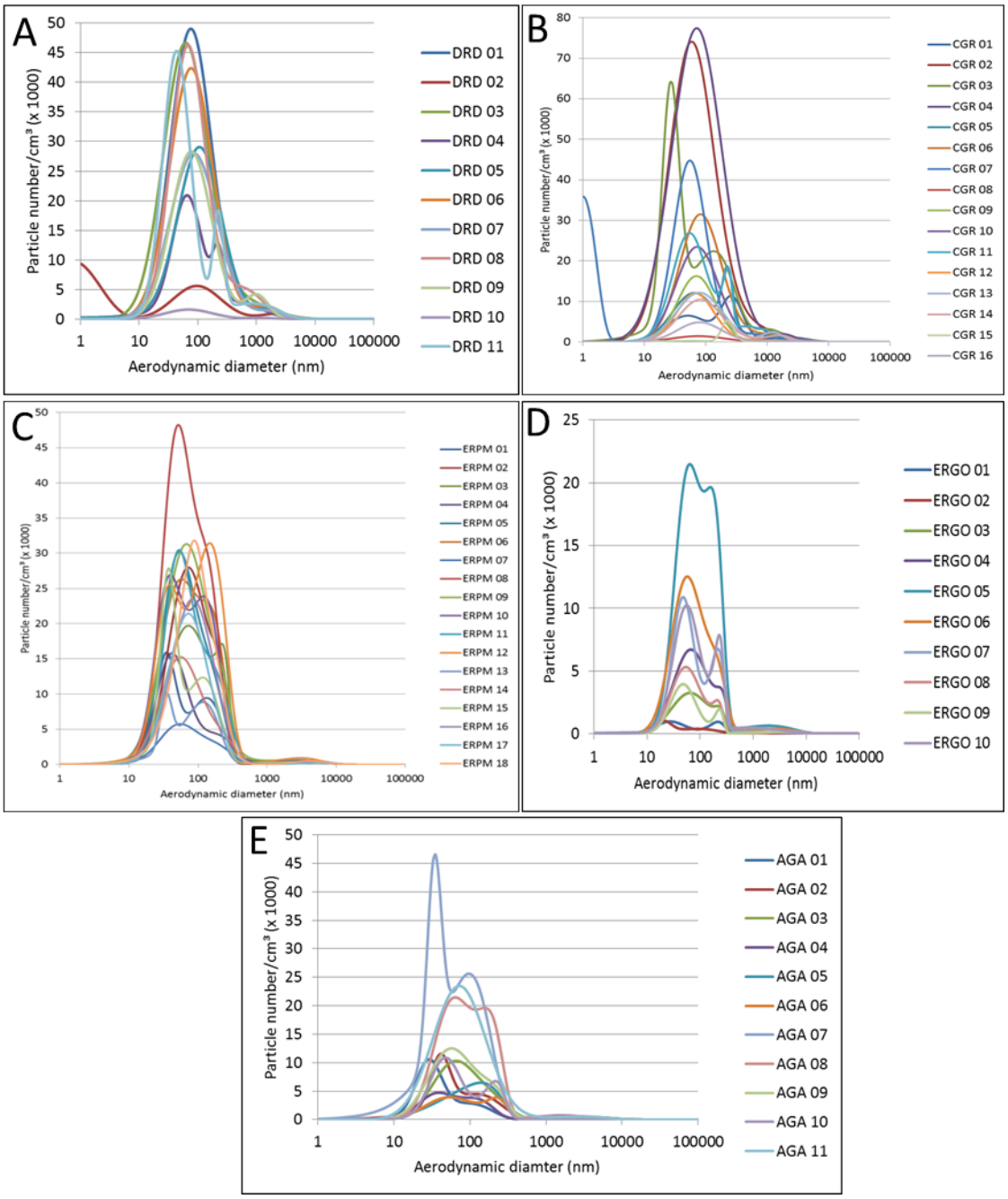

Figure 4-1: The merged size distribution vs. particle number of the respirable fraction of the bulk dusts from each TSF. (A) DRD; (B) CGR; (C) ERPM; (D) ERGO and (E) AGA. Adapted from Andraos et al. (2018b).

As it is known that particles with aerodynamic diameters from 1 - 5 µm and < 0.5 µm are in the respirable range and can easily penetrate the alveolar regions of the respiratory system, it was

decided to calculate the percentage of particles within these ranges. **Table 4-2** shows the percentages of particles 1 - 5 µm and < 0.5 µm based on the merged size distribution data in **Figure 4-1**. It is evident that the percentage number of particles < 0.5 µm for each of the TSFs represented the majority of all the particles present ranging from 86.3% (DRD) to as high as 96.0% (AGA) whereas the larger particles between 1 and 5 µm represented a much smaller percentage (1.6 – 3.5%).

It is clear from **Figure 4-1** and **Table 4-2** that the majority of the particles present in the samples were < 0.5 µm, although this fraction of particles did not contribute to the mass **(Table 4-1)**. Therefore, for a fixed mass of dust, the percentage number of NPs is much higher than the percentage number of micron-particles.

Table 4-2: Percentages of particles between 1 and 5 µm and < 0.5 µm of the ≤ 20 µm fraction of the bulk dusts from each TSF.

TSF	Percentage of particles 1 - 5 µm ± SD	Percentage of particles < 0.5 µm ± SD
DRD	3.2 ± 1.1	86.3 ± 24.8
CGR	3.5 ± 1.9	89.3 ± 19.2
ERPM	1.6 ± 1.0	93.0 ± 20.2
ERGO	2.4 ± 1.2	89.8 ± 23.1
AGA	2.3 ± 1.9	96.0 ± 2.8

4.1.1.2. Specific surface area and porosity of the tailings dusts

The specific surface area of the tailings dusts, as determined with the BET nitrogen adsorption technique, ranged from 1.0 m^2/g (DRD and AGA) to 52.6 m^2/g (one sample from ERGO), showing large variation between TSFs **(Figure 4-2)**.

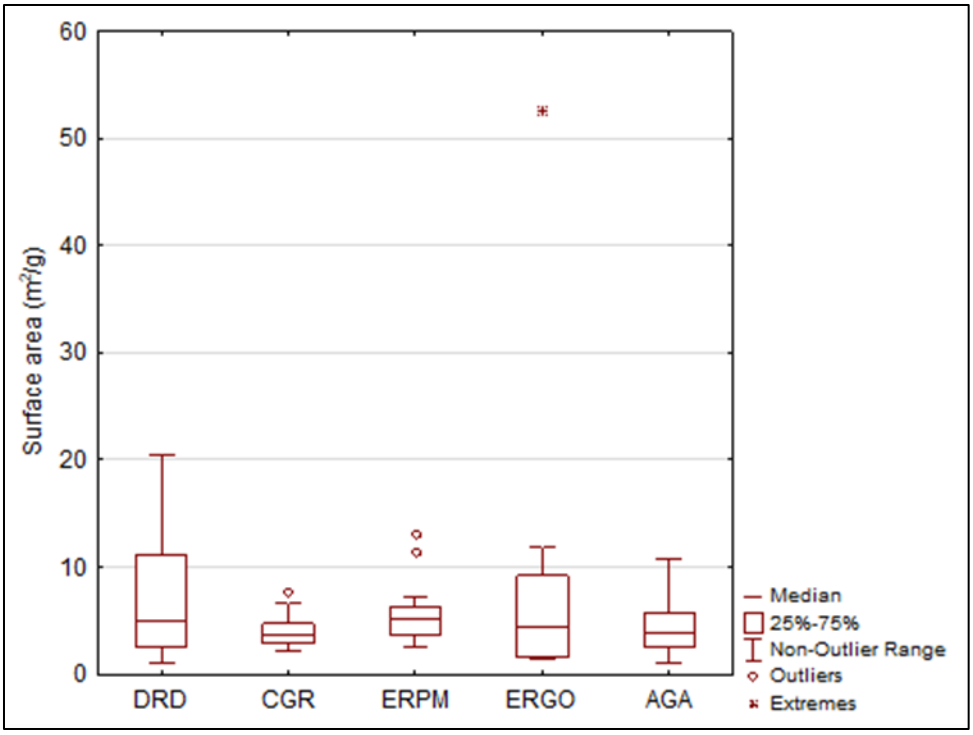

Figure 4-2: Specific surface area of the respirable fraction of the bulk dusts from each TSF.

Specific surface area is dependent not only on size but also on the particle micromorphology i.e. surface texture and porosity. The pore volume ranged from a very low 0.005 cm^3/g (DRD) to a high of 0.06 cm^3/g (ERGO; **Table 4-3**). The pore diameter ranged from 4.5 nm (ERGO) to 25.4 nm (AGA).

Table 4-3: Pore volume and pore diameter of the respirable fraction of the bulk dusts from each TSF.

TSF	Pore volume (PV) and pore diameter (Pd)	Median	Range
DRD	PV (cm^3/g)	0.012	0.005 - 0.051
	Pd (nm)	9.6	7.2 - 19.8
CGR	PV (cm^3/g)	0.011	0.006 - 0.016
	Pd (nm)	11.4	7.3 - 14.4
ERPM	PV (cm^3/g)	0.013	0.007 - 0.026
	Pd (nm)	9.65	7.6 - 16.8
ERGO	PV (cm^3/g)	0.012	0.006 - 0.060
	Pd (nm)	10.5	4.5 - 16.8
AGA	PV (cm^3/g)	0.011	0.006 - 0.036
	Pd (nm)	13.1	7.7 - 25.4

4.1.1.3. Micromorphology of the tailings dusts

SEM analysis revealed that the tailings dust exhibited a complex micromorphology with irregular shapes and sharp edges of which a representative few are shown in **Figure 4-3**.

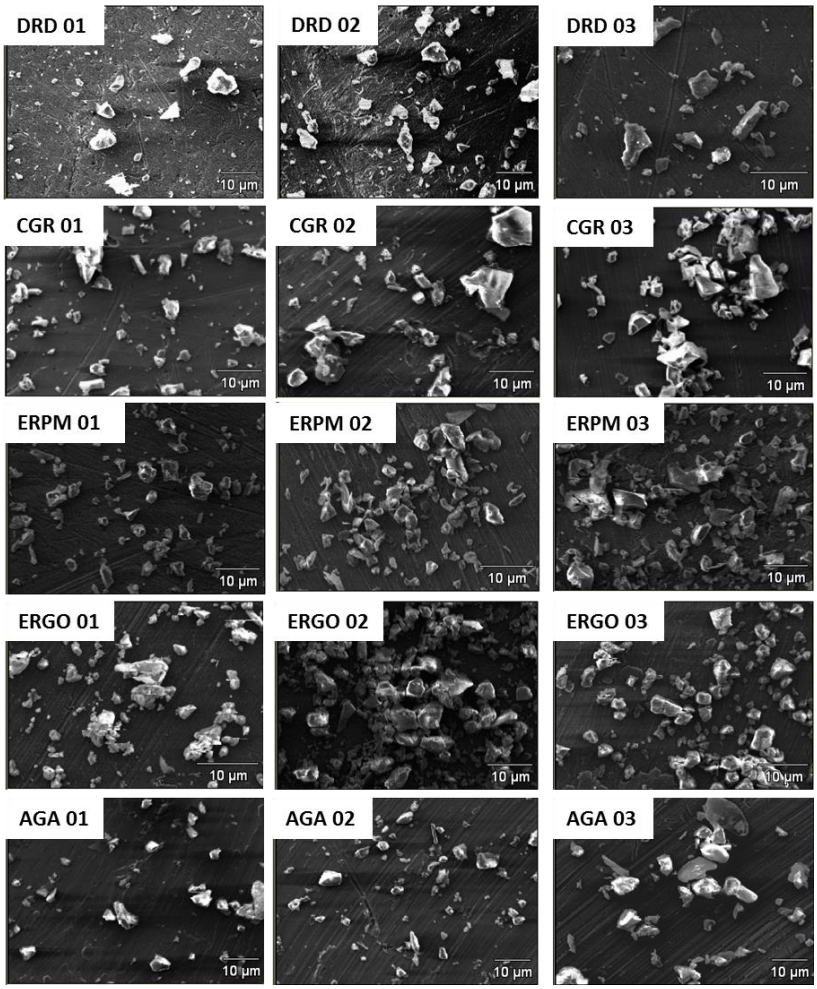

Figure 4-3: SEM images from a representative set of the respirable fraction of the bulk dusts from each TSF.

It is known that high surface areas as well as porous natures and irregular shapes of particles allow for the adsorption of different trace metal ions (Kocyigit et al., 2004). Hence, EDX analysis, a surface analytical technique, was conducted to identify the elements present on the tailings particles' surfaces. EDX analysis showed the major elemental components to be O (median: 48.68 - 51.92%) and Si (median: 22.25 - 42.68%), followed by Al (median: 3.87 - 16.23%), Fe (median: 0.24 - 9.87%) and C (median: 0.72 - 2.80%). Regarding the Fe content ERGO showed a very high maximum of 67.79% followed by CGR (47.87%). The silica % of the tailings dusts was calculated to be 42%.

Other elements in trace quantities such as titanium (Ti), phosphorus (P), Ca, molybdenum (Mo), Cr, chlorine (Cl), Mn, bromine (Br), Zn and indium (In) were also identified in certain tailings samples **(Table 4-4)**. Regarding Zn, very high concentrations were identified for ERGO (73.92%) and AGA (71.75%); however, these values were identified in only one sample and should therefore be interpreted with caution.

Table 4-4: EDX spectroscopic surface elemental analysis of the respirable fraction of the bulk dusts from each TSF.

Element	TSF	Median (weight%[#])	Range	
			Min (weight%[#])	Max (weight%[#])
O	DRD	48.68	4.45	56.52
	CGR	49.30	19.04	100.00
	ERPM	51.92	45.22	53.45
	ERGO	49.14	23.90	53.30
	AGA	51.20	25.53	56.52
Si	DRD	42.68	40.70	44.01
	CGR	22.25	0.35	43.58
	ERPM	28.12	15.42	44.77
	ERGO	25.56	14.06	40.63
	AGA	32.41	8.60	38.29
Al	DRD	3.87	2.07	7.91
	CGR	11.65	1.60	51.22
	ERPM	14.59	1.19	31.16
	ERGO	14.03	4.94	16.05
	AGA	16.23	4.59	41.61
Fe	DRD	0.24	0.23	0.25
	CGR	6.37	0.34	47.87
	ERPM	0.69	0.20	6.62
	ERGO	9.87	0.25	67.79
	AGA	2.74	2.10	3.37
C	DRD	1.18	0.18	17.15
	CGR	0.72	0.29	17.30
	ERPM	0.76	0.18	5.58
	ERGO	0.92	0.61	2.32
	AGA	2.80	0.66	17.15
Mg	DRD*	0.13	0.13	0.13
	CGR	10.12	0.85	13.45
	ERPM	0.24	0.09	6.30

Element	TSF	Median (weight%[#])	Range	
			Min (weight%[#])	Max (weight%[#])
	ERGO	0.72	0.08	6.91
	AGA	0.71	0.34	1.07
S	DRD	BDL	BDL	BDL
	CGR	0.54	0.23	1.23
	ERPM	0.39	0.17	3.10
	ERGO	0.29	0.28	0.60
	AGA	BDL	BDL	BDL
K	DRD*	0.17	0.17	0.17
	CGR	1.03	0.51	9.47
	ERPM	3.37	0.11	13.83
	ERGO	0.60	0.23	4.05
	AGA	2.14	1.74	2.48
Na	DRD*	0.18	0.18	0.18
	CGR	0.64	0.31	1.86
	ERPM	0.68	0.66	0.70
	ERGO*	0.57	0.57	0.57
	AGA	BDL	BDL	BDL
Ti	DRD	BDL	BDL	BDL
	CGR	BDL	BDL	BDL
	ERPM	0.07	0.06	0.57
	ERGO	0.21	0.09	0.33
	AGA*	0.56	0.56	0.56
P	DRD	BDL	BDL	BDL
	CGR*	0.45	0.45	0.45
	ERPM	BDL	BDL	BDL
	ERGO	BDL	BDL	BDL
	AGA	0.73	0.54	0.91
Ca	DRD	BDL	BDL	BDL
	CGR	0.26	0.25	0.27
	ERPM*	0.37	0.37	0.37
	ERGO*	0.84	0.84	0.84
	AGA*	0.54	0.54	0.54
Mo	DRD*	0.58	0.58	0.58
	CGR	3.22	2.25	40.70
	ERPM	BDL	BDL	BDL
	ERGO	BDL	BDL	BDL
	AGA	BDL	BDL	BDL
Cr	DRD	BDL	BDL	BDL
	CGR	BDL	BDL	BDL

Element	TSF	Median (weight%[#])	Range	
			Min (weight%[#])	Max (weight%[#])
	ERPM	0.09	0.11	0.13
	ERGO	BDL	BDL	BDL
	AGA	BDL	BDL	BDL
Cl	DRD	BDL	BDL	BDL
	CGR*	0.28	0.28	0.28
	ERPM	BDL	BDL	BDL
	ERGO*	0.17	0.17	0.17
	AGA*	0.23	0.23	0.23
Mn	DRD	BDL	BDL	BDL
	CGR	BDL	BDL	BDL
	ERPM	BDL	BDL	BDL
	ERGO	BDL	BDL	BDL
	AGA*	0.64	0.64	0.64
Br	DRD	BDL	BDL	BDL
	CGR*	6.77	6.77	6.77
	ERPM	BDL	BDL	BDL
	ERGO	BDL	BDL	BDL
	AGA	BDL	BDL	BDL
Zn	DRD	BDL	BDL	BDL
	CGR	BDL	BDL	BDL
	ERPM	BDL	BDL	BDL
	ERGO*	73.92	73.92	73.92
	AGA*	71.75	71.75	71.75
In	DRD	BDL	BDL	BDL
	CGR*	21.01	21.01	21.01
	ERPM	BDL	BDL	BDL
	ERGO	BDL	BDL	BDL
	AGA*	19.06	19.06	19.06

Each value represents the average of the total number of particles analysed per TSF i.e.:
110 particles for DRD (10 particles × 11 samples)
160 particles for CGR
180 particles for ERPM
100 particles for ERGO
110 particles for AGA
* Average of 10 particles for one sample only
BDL = Below Detection Limit

4.1.1.4. Mineral nature of the tailings dusts

Mineralogical analysis was performed with semi-quantitative XRD, the results of which roughly corresponded with the EDX results showing the most abundant mineral to be silica, in particular quartz **(Table 4-5)**. However, the percentage silica calculated with EDX and XRD was not identical (i.e. 42% vs 78%) likely due to the fact that, with EDX, not all elements analysed produce the same peak height at the same concentration. Using XRD, the DRD dusts had a higher quartz content (median: 87.71%), compared to the dusts from the other TSFs. Only trace amounts of tridymite and crystobalite were identified in all the dusts. Other minerals that were identified included, pyrophilite, kaolinite, muscovite and chloritoid, all of which contained Al, therefore corresponding to the high Al content detected by EDX **(Table 4-4)**. Two minerals containing Fe, namely hematite and chloritoid, were identified by XRD, possibly explaining the Fe content identified by EDX although these two minerals alone cannot explain the very high levels of surface Fe identified in CGR and ERGO samples using EDX **(Table 4-4)**.

Table 4-5: Mineral composition of the respirable fraction of the bulk dusts from each TSF.

Mineral	TSF	Median (weight%)	Range	
			Min (weight%)	Max (weight%)
Quartz (SiO_2; crystal system: Hexagonal)	DRD	87.71	79.14	91.78
	CGR	79.09	66.29	82.54
	ERPM	74.80	57.81	78.27
	ERGO	75.65	52.78	78.29
	AGA	74.61	62.86	78.20
Tridymite (SiO_2; crystal system: Triclinic)	DRD	0.27	0.09	0.65
	CGR	0.24	0.05	0.60
	ERPM	0.27	0.03	1.50
	ERGO	0.29	0.03	1.73
	AGA	0.28	0.06	0.99
Cristobalite (SiO_2; crystal system: Tetragonal)	DRD	BDL	BDL	BDL
	CGR	0.09	0.05	0.14
	ERPM	0.12	0.04	0.22
	ERGO	0.10	0.04	2.38
	AGA	BDL	BDL	BDL
Pyrophyllite Phyllosilicates ($Al_2Si_4O_{10}(OH)_2$)	DRD	2.97	1.66	5.20
	CGR	0.75	0.02	4.41
	ERPM	0.16	0.01	1.69
	ERGO	0.16	0.02	10.82

Mineral	TSF	Median (weight%)	Range	
			Min (weight%)	Max (weight%)
	AGA	3.67	1.85	6.28
Kaolinite ($Al_2Si_2O_5(OH)_4$)	DRD	1.16	0.12	5.66
	CGR	1.19	0.03	2.65
	ERPM	0.86	0.28	2.49
	ERGO	1.43	0.35	11.58
	AGA	2.31	1.46	5.25
Muscovite Phyllosilicates ($KAl_2(AlSi_3O_{10})(F,OH)_2$ *or* $(KF)_2(Al_2O_3)_3(SiO_2)_6(H_2O)$)	DRD	1.32	0.26	2.21
	CGR	9.24	3.28	13.39
	ERPM	12.61	8.65	25.89
	ERGO	10.55	6.56	16.63
	AGA	9.00	6.25	13.68
Hematite (Fe_2O_3)	DRD	0.26	0.05	1.05
	CGR	0.21	0.06	0.51
	ERPM	0.11	0.05	0.47
	ERGO	0.27	0.07	0.68
	AGA	0.76	0.34	1.05
Gypsum ($CaSO_4 \cdot 2H_2O$)	DRD	2.20	1.25	4.80
	CGR	2.43	1.50	5.93
	ERPM	2.37	1.52	19.89
	ERGO	2.37	0.17	4.53
	AGA	3.82	1.69	7.90
Calcite ($CaCO_3$)	DRD	0.53	0.18	1.18
	CGR	0.53	0.04	1.11
	ERPM	0.20	0.07	1.45
	ERGO	0.30	0.21	0.93
	AGA	0.54	0.36	1.15
Chloritoid Phyllosilicates ($(Fe,Mg,Mn)_2Al_4Si_2O_{10}(OH)_4$)	DRD	1.93	0.95	2.44
	CGR	3.78	2.18	7.48
	ERPM	2.22	0.50	4.11
	ERGO	1.82	0.53	4.17
	AGA	0.52	0.21	0.94
Chlorite Phyllosilicates (ClO_2^-)	DRD	1.05	0.20	3.22
	CGR	1.53	0.40	5.55
	ERPM	5.03	0.58	7.97
	ERGO	4.37	1.25	7.04
	AGA	3.67	0.93	6.81
Bassanite ($2CaSO_4 \bullet (H_2O)$)	DRD	0.56	0.14	1.91
	CGR	1.73	0.03	3.42
	ERPM	0.62	0.20	1.61

Mineral	TSF	Median (weight%)	Range	
			Min (weight%)	Max (weight%)
	ERGO	1.30	0.42	3.04
	AGA	0.46	0.30	0.88
BDL = Below Detection Limit				

4.1.1.5. Elemental composition of the tailings dusts

The next step was to assess the elemental composition of the sieved tailings bulk dust using ICP-AES. **Table 4-6** shows the concentrations of a select few of the elements identified including those that are known to be redox-active transition elements i.e. Fe, Cu, Cr, Mn, Ni and V (Baskin and Salem, 1997, Nico et al., 2009, Boogaard et al., 2012). Maximum levels of As were high for all sites with DRD showing the highest level (415 mg/kg). The level of Au ranged from 1.38 mg/kg (ERGO) to 15.40 mg/kg (ERPM). The ERGO and CGR dusts showed the highest median levels of the transition elements Fe and Cu while the ERGO dusts also showed the highest maximum of Fe (67 500 mg/kg) which coincided with the high surface Fe content identified in **Table 4-4**. The ERGO dusts also appeared to have the highest median (70.95 mg/kg) and maximum (199 mg/kg) levels of the transition element V, compared to the other dusts. The dusts from the AGA site exhibited the highest levels of most elements identified compared to the other TSFs i.e. AGA contained higher Cd, Co, Mn, Ni, Pb, U and Zn levels and also showed the highest maximum values of Cu (126 mg/kg) and Cr (1710 mg/kg).

Table 4-6: Elemental composition of the respirable fraction of the bulk dusts from each TSF.

Element*	TSF	Median (mg/kg)	Range	
			Min (mg/kg)	Max (mg/kg)
As	DRD	143	14.20	415
	CGR	130	39.40	209
	ERPM	141	59.90	394
	ERGO	180	14.50	212
	AGA	116	93	193
Au	DRD	0.34	0.17	1.56
	CGR	0.37	0.13	5.19
	ERPM	0.54	0.05	15.40
	ERGO	0.79	0.30	1.38
	AGA	0.31	0.05	3.96
Cd	DRD	0.20	0.07	0.53
	CGR	0.17	0.10	0.31
	ERPM	1.01	0.11	2.54
	ERGO	0.22	0.03	1.16
	AGA	2.70	1.97	4.54
Co	DRD	4.38	1.85	11.90
	CGR	20.10	3.64	41.70
	ERPM	10.34	4.11	35.20
	ERGO	18.30	8.04	63
	AGA	27.70	2.68	55.60
Cu	DRD	20.90	9.41	74.50
	CGR	47.45	18.10	116
	ERPM	23.80	10.50	79.20
	ERGO	39.70	23.10	98.50
	AGA	41	12.10	126
Cr	DRD	170	120	261
	CGR	227.5	112	723
	ERPM	493.5	172	718
	ERGO	408	142	725
	AGA	250	155	1710
Fe	DRD	28 600	6 580	59 100
	CGR	35 000	22 900	46 900
	ERPM	30 800	15 700	45 800
	ERGO	34 050	20 500	67 500
	AGA	27 000	15 200	38 600
Mn	DRD	180	142	640

Element*	TSF	Median (mg/kg)	Range	
			Min (mg/kg)	Max (mg/kg)
	CGR	294.5	143	414
	ERPM	196.5	116	543
	ERGO	204	97.8	2960
	AGA	389	106	5270
Ni	DRD	15.60	9.02	55.60
	CGR	79.80	27.80	133
	ERPM	62.70	26.30	180
	ERGO	98.35	51.70	199
	AGA	123	36.70	756
Pb	DRD	22.90	11.20	50.70
	CGR	24.90	4.65	34.70
	ERPM	10.95	6.29	52.80
	ERGO	13.80	7.97	22.40
	AGA	29.15	9	52.70
U	DRD	3.51	3.03	13.90
	CGR	14.60	3.75	22.60
	ERPM	7.14	3	26.30
	ERGO	6.77	1.86	13.80
	AGA	42.30	6.65	298
V	DRD	33.2	17.7	98.6
	CGR	45.45	20.5	96
	ERPM	66.95	32.6	100
	ERGO	70.95	54.5	199
	AGA	40.1	25.2	61.8
Zn	DRD	31.90	14.80	82.60
	CGR	61.45	29.90	182
	ERPM	33.50	21.80	80.80
	ERGO	48.20	30.50	65.90
	AGA	71.55	14.10	217
* Only selected elements are shown in this table, therefore not all 64 elements identified by ICP-AES				

Although the elemental levels recorded in **Table 4-6** can be compared among the different TSFs, it does not indicate whether these levels could potentially lead to adverse health effects once inhaled. Therefore, in order to determine whether these levels are of any biological importance we sought to compare the determined concentrations to those published limits that have been set by various national and international institutions for the protection of environmental and human health (ATSDR, 2016, CCME, 2016, DIV, 2000). According to the Canadian Council of

Ministers of the Environment (CCME) these guidelines refer to "numerical limits or narrative statements recommended to support and maintain designated uses of the soil environment. Ideally, soil at the guideline levels will provide a healthy functioning ecosystem capable of sustaining the current and possible future uses of the site by ecological receptors and humans." (CCME, 2016). The derivation of these soil guidelines typically follow a risk assessment approach during which a literature survey is conducted to establish the "safe" exposure level of the element or contaminant at or below which no appreciable human health risk is expected. Each institution will have its own particular set of guidelines used for establishing these "safe" exposure levels although all follow the same principle. The guidelines followed by the CCME are as follows: Firstly, the potential toxic effects of the contaminant are established. Then the reference dose believed to be associated with a defined level of incidence of that effect in the population is calculated. Thereafter, the level of exposure via all possible sources and exposure routes (i.e., inhalation, ingestion, and skin absorption) are calculated. Typical exposure pathways taken into account include: ingestion of soil/dust, dermal uptake of contaminants in contact with the skin, inhalation of soil particles into the lungs, contamination of groundwater used as potable water, contamination of indoor air via volatilization into basements, off-site migration of soil/dust, and contamination of produce, milk, and meat from on site. It is important to note that the guidelines particularly for human health are always based on a chronic (i.e. 70 year lifetime) exposure scenario. Lastly, the safe level of exposure to the substance is calculated, taking into account certain factors such as estimated daily intake of soil contaminant, background concentration of contaminant in soil, individual body weight, relative absorption factor for gut lung and skin as well as soil ingestion/inhalation/dermal contact rate etc. (CCME, 2016). Therefore, caution should be taken when soil concentrations above these safe levels for a contaminant in question are encountered.

Table 4-7 shows these published limits for most of the elements shown in **Table 4-6** as well as for additional elements for which soil limits have been set.

In **Table 4-7**, concentrations of the selected elements in the dust samples were divided by the published soil limits:

- elemental concentrations in the tailings dusts that are lower than the published limit are indicated in blue and light pink;
- elemental concentrations in the tailings dusts that are 1 to 10 times higher than the published limit are indicated in bright red;
- elemental concentrations in the tailings dusts that are more than 10 times the published limit are indicated in different hues of darker red; the highest value is indicated in black.

Table 4-7: Heat map of selected elements of the respirable fraction of the bulk dusts from each TSF indicating their concentrations relative to known published soil limits as shown in the second row of the heat map.

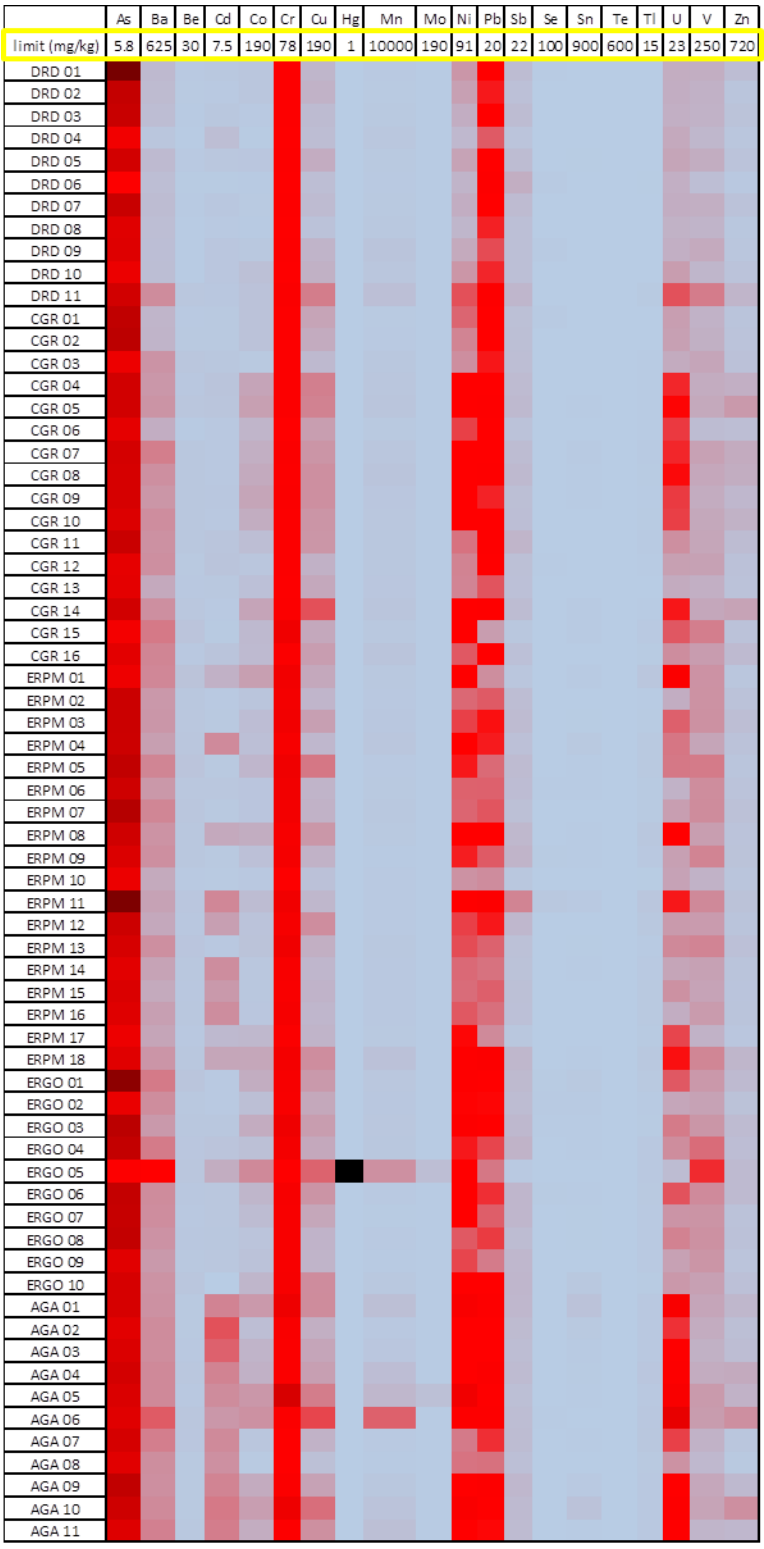

It is apparent that the levels of As and Cr for the dusts from all five TSFs were above the set limits and even reached a maximum level of 71.6 times higher than the set limit for As (DRD 01). For Pb, certain dusts in each TSF also reached levels higher than the set limits (DRD 01, 03, 05 – 07, 11, CGR 01, 02, 04 – 08, 10 – 12, 14, 16, ERPM 08, 11, 18, ERGO 01 – 03, 10, AGA 01 – 06, 09 – 11). Refer back to **Figure 3-3** for the locations of where these dust samples were located. The dusts from the DRD TSF did not exceed the limit set for Ni, unlike that of the dusts from CGR (CGR 04, 05, 07 – 10, 14 and 15), ERPM (ERPM 01, 04, 08, 11, 17 and 18), ERGO (ERGO 01 – 03, 05 – 07 and 10) and AGA (AGA 01 – 06, 09 – 11). Even though the levels of Cd, Co, Cu and Zn in the AGA dusts were higher than that of the other sites **(Table 4-6)**, none of these levels from the AGA dusts exceeded the current published limits and therefore, from a health point of view, does not carry the potential to cause adverse health effects. However, the levels of Cr, Ni and U in the AGA dusts exceeded the published limits to a higher degree than dusts from the other TSFs and even reached factors of 21.9, 8.3 and 13 times higher than the limits for Cr, Ni and U, respectively **(Table 4-7)**.

Although almost all the dusts tested showed Hg values below the detection limit, one dust sample, ERGO 05, stood out from the rest in that it contained an exceptionally high Hg concentration, which was well above that of the published limit. This sample could be considered an outlier, however, note that this sample also contained very high levels of Ba and V concentrations, which were almost as high as that of the set limits.

Hierarchical clustering analysis was performed on all 64 elements identified with ICP-AES to determine whether the elemental profiles of the dusts from each TSF could be distinguished from the dusts of the other TSFs. This would give an indication as to whether dusts from each TSF could be identified based on only their characteristic elemental profile, which would be dependent on the composition of the ore from which the gold was extracted. **Figure 4-4** shows the dendrogram in which the linkage distance (x-axis) represents the degree of similarity between the different dusts. For example, the smaller the linkage distance the higher the degree of similarity. **Figure 4-4** shows that all the dusts from the DRD TSF clustered together with a linkage distance of approximately 13 (A in figure) indicating that these dusts exhibited a similar elemental profile, which was different from that of other TSFs. Similarly, all dusts from the

AGA TSF (except for AGA 01) clustered together with a linkage distance of approximately 15 (B in figure), which is explained by the fact that this TSF is the only TSF located in the North-West province, approximately 300 km southwest of Gauteng. Dusts from the CGR, ERPM and ERGO TSFs appeared to cluster together in four separate clusters with linkage distances of around 15 (C-F in figure), which could be due to these TSFs being located in the same geographical area.

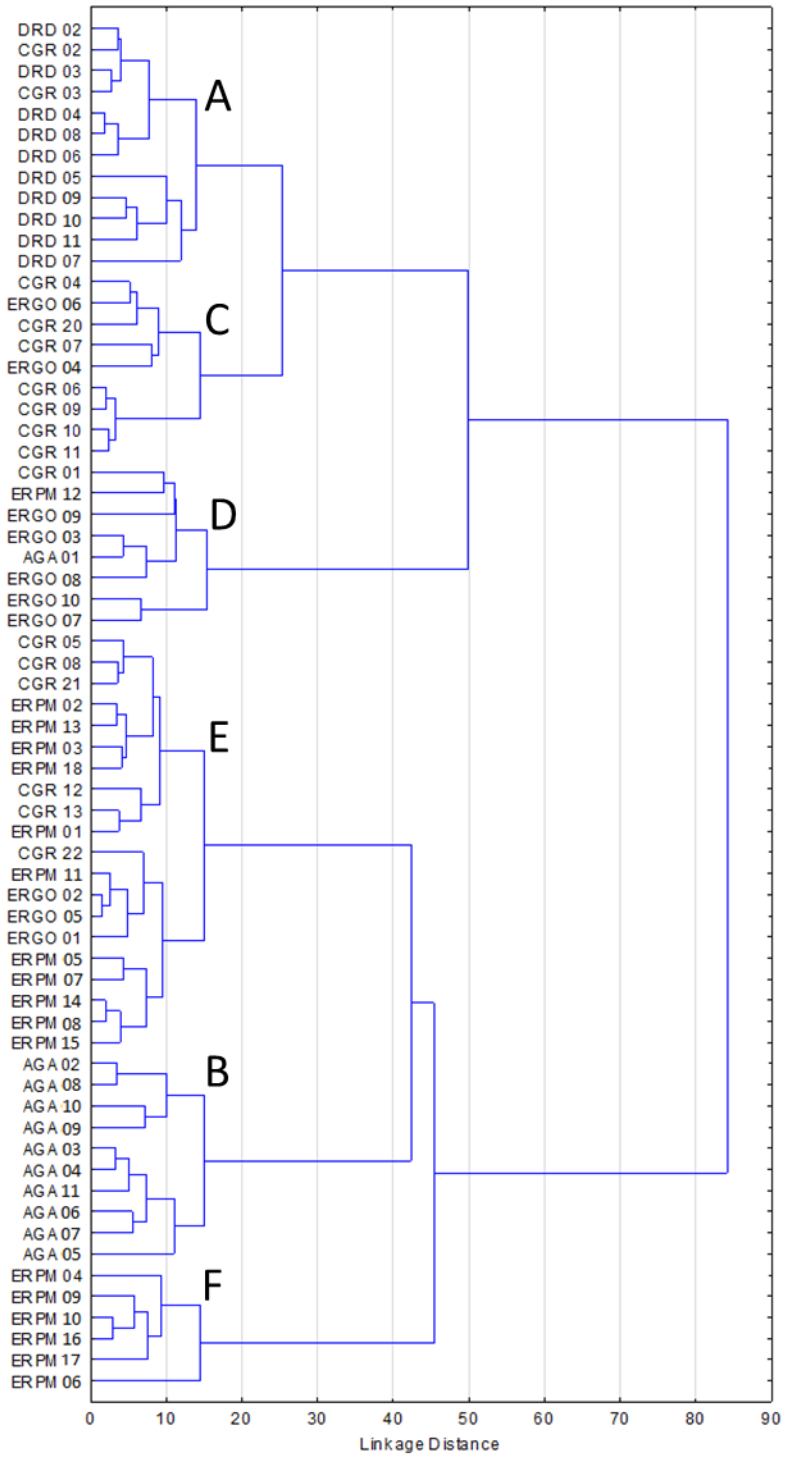

Figure 4-4: Dendrogram of the respirable fraction of the bulk dusts from each TSF based on the 64 elements identified with ICP-AES. Each letter in the dendrogram indicates clusters with linkage distances of at least 15.

Based on the clusters observed in **Figure 4-4**, a variable importance plot (obtained from Random Forest analysis; **Table 4-8**) was constructed using the 64 elements identified to determine which elements were responsible for the differential clustering of the dusts shown in **Figure 4-4**. The first ten most important elements with the highest variable rank (i.e. responsible for the differential clustering) included Sc > Ga > B > Ni > Ti > Ge > Nb > Cd > Tb > P while the ten least important elements included Gd > Au > Tm > Na > Er > Mn > Eu > Sb > Ce > Se.

Table 4-8: Variable importance plot of the 64 elements from the respirable fraction of the bulk dusts from each TSF.

Element	Variable Rank	Importance	Element	Variable Rank	Importance	Element	Variable Rank	Importance
Sc	100	1	Ba	59	0.593782	Lu	42	0.417261
Ga	93	0.932184	Hf	58	0.57671	Zn	41	0.408986
B	92	0.921812	Sr	56	0.558853	Pb	40	0.403085
Ni	90	0.904437	Sm	56	0.558737	Li	39	0.390405
Ti	76	0.761224	V	55	0.545351	La	39	0.386595
Ge	73	0.731205	Bi	54	0.53655	As	37	0.374357
Nb	70	0.69717	Mg	53	0.531648	Pr	36	0.363171
Cd	69	0.69053	Nd	52	0.524676	Be	35	0.347502
Tb	69	0.686863	Cu	49	0.492505	Pt	35	0.345503
P	67	0.670214	Th	48	0.482021	Gd	32	0.319322
Co	67	0.670063	Zr	48	0.477351	Au	32	0.31501
Ho	65	0.654233	Ca	46	0.461195	Tm	31	0.311409
Dy	65	0.649091	Rb	44	0.441334	Na	31	0.311252
K	62	0.619904	Fe	44	0.441238	Er	30	0.301499
Y	61	0.613238	Cs	43	0.434083	Mn	28	0.283839
Tl	61	0.612362	Al	43	0.43397	Eu	27	0.27476
U	60	0.602754	Yb	43	0.43164	Sb	25	0.250233
Cr	60	0.601504	W	43	0.425142	Ce	24	0.239642
Pd	59	0.594202	Sn	42	0.417573	Se	12	0.124127

Although the variable importance plot indicates the elements that predict clustering, it cannot show which dusts contained higher or lower elemental concentrations with respect to other dusts. Hence, another heat map was constructed for this purpose **(Figure 4-5)**. It is apparent that dusts from the ERPM TSF contained the highest concentrations of most of the elements, while dusts

from the AGA TSF contained the highest concentrations of Cd and Ni (as also reflected in **Table 4-6**). Dusts from both DRD and CGR TSFs contained relatively high concentrations of Ge, while having low concentrations of the other elements.

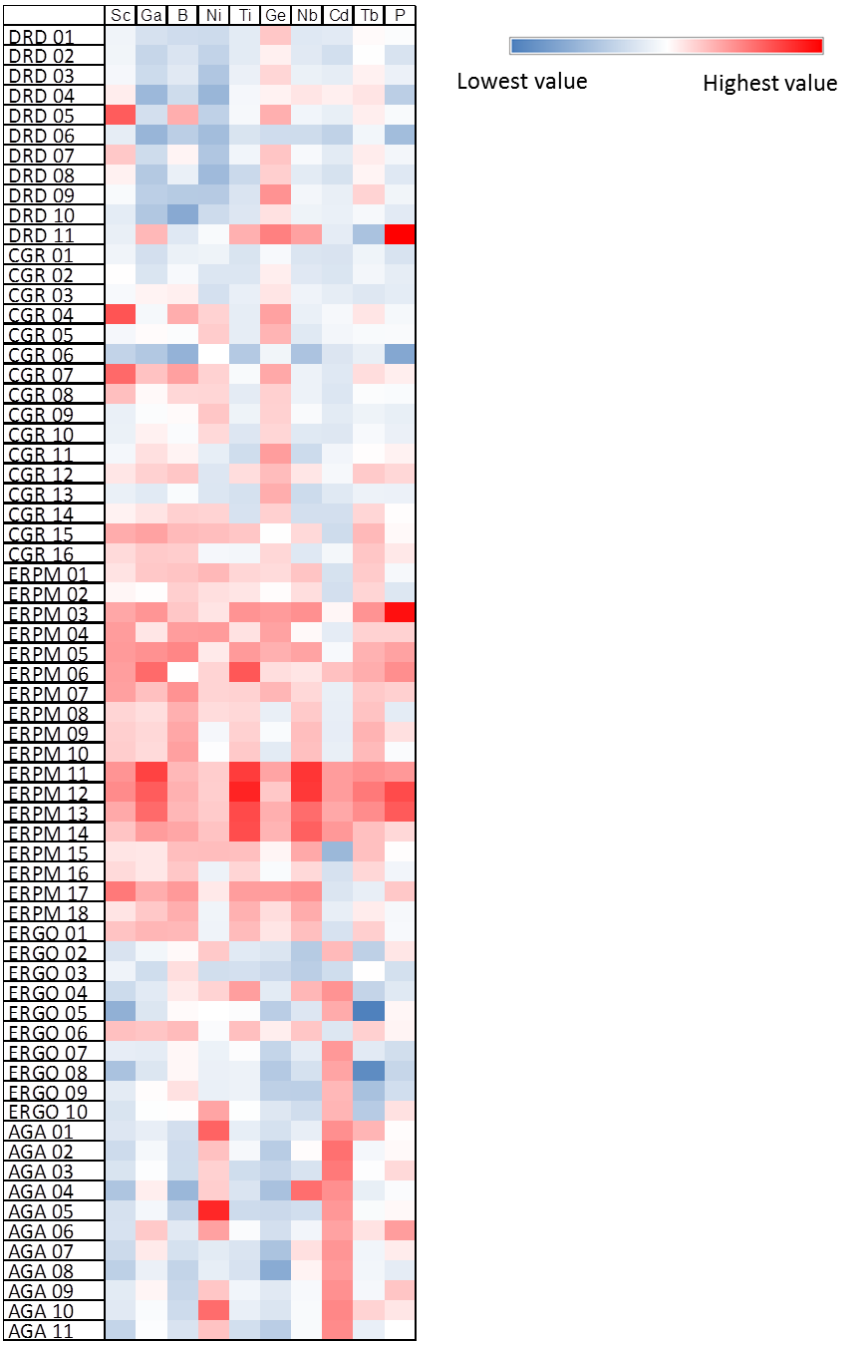

Figure 4-5: Heat map of the ten most important elements that predict clustering.

4.1.1.6. Physicochemical analysis of the crystalline silica positive control, Min-U-Sil 5

The physicochemical properties of Min-U-Sil 5 were also assessed and are presented in **Table 4-9**. Min-U-Sil 5 exhibited a specific surface area of 5.8 m^2/g, thereby correlating with previous studies (Santarelli et al., 2004), and showed mesoporous characteristics based on its porosity **(Table 4-9)**. The surface of Min-U-Sil 5 was, as expected, mainly composed of Si and O and contained 98.7% quartz as well as several trace elements at very low concentrations.

Table 4-9: Physicochemical properties of the crystalline silica positive control, Min-U-Sil 5.

Characteristic	Min-U-Sil 5
Size (MMAD)	1.861 µm
Specific surface area (m^2/g)	5.8
Porosity	Pore volume: 0.015 cm^3/g Pore diameter: 10.5 nm
Elemental analysis (EDX, weight%)	Si (46.13); O (53.17); Al (0.70)
Mineralogical analysis (XRD, weight%)	Quartz (98.7); Kaolinite (0.1); Chloritoid (0.2); Tridymite (0.5); ClinochloreIIb (0.4)
Elemental analysis (ICP-AES) (mg/kg)	Al (1520), Ca (1030), Fe (222), Ti (90.2), P (36.9), K (30.8), B (25.8), Zr (18.9), Ba (7.91), Sr (4.78), Ce (2.58), Mn (2.07), La (1.53), Y (1.33), Sc (1.22), Cu (1.21), Cr (1.02), Nd (0.992), Ni (0.564), Zn (0.531), Ga (0.515), Pb (0.486), Pr (0.271), V (0.271), Ge (0.212), As (0.209), Gd (0.187), Sm (0.187), Dy (0.182), U (0.144), Yb (0.128), Rb (0.123), Er (0.108), Co (0.0509), Ho (0.0243), Tb (0.0118)

According to the size distribution analysis, Min-U-Sil 5 showed an MMAD of 1.861 µm in the micron-range, correlating well with the value provided by the supplier (USSilica, 2010). The size distribution, which appeared to follow a bi-modal shape, is illustrated in **Figure 4-6**, and shows the presence of NPs.

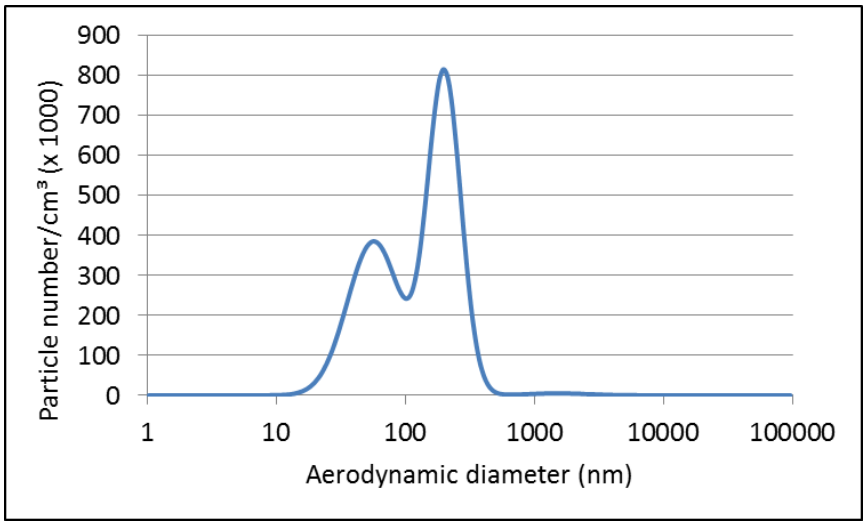

Figure 4-6: The merged size distribution vs. particle number of the crystalline silica positive control, Min-U-Sil 5.

The size and shape of Min-U-Sil 5 particles are illustrated in **Figure 4-7**.

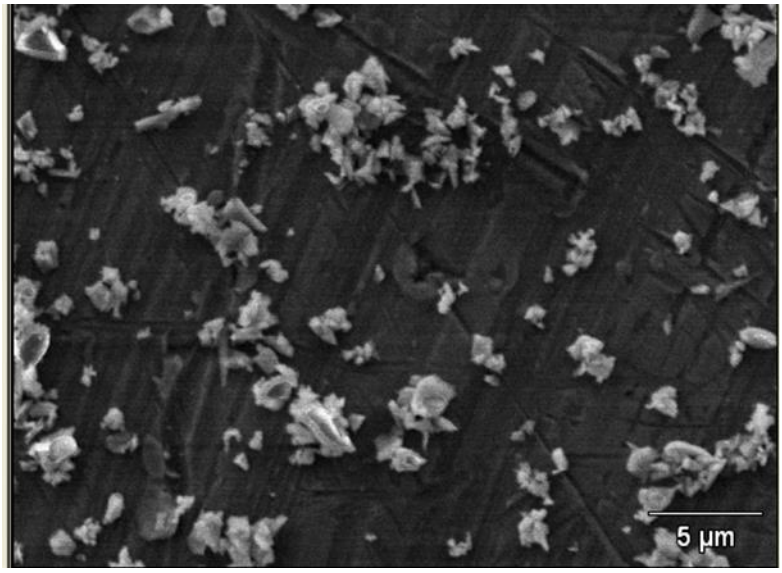

Figure 4-7: SEM image of the crystalline silica positive control, Min-U-Sil 5.

4.1.1.7. Surface activity of the tailings dusts and the crystalline silica positive control, Min-U-Sil 5

Both the tailings dust samples and Min-U-Sil 5 exhibited surface characteristics that could promote their surface activity. Therefore, as reported in the literature (Borm et al., 2007, Ayres et al., 2008), the ability of particles to induce ROS formation in the absence of cells has been used in the present study as a screening method to assess the potential of the tailings particles to display biological reactivity. In **Figure 4-8**, representative ESR signals obtained of the baseline control only **(Figure 4-8A)** as well as of one representative tailings dust **(Figure 4-8B** and **C)** and Min-U-Sil 5 **(Figure 4-8D** and **E)** in the absence and presence of H_2O_2 are shown. As expected, the control did not show any detectable signal. The dust sample and Min-U-Sil 5 showed a detectable signal in the absence of H_2O_2, which increased considerably when H_2O_2 was added therefore indicating that H_2O_2 is needed for the Fenton reaction to occur. The ESR signal obtained was typical of that of the DMPO–OH adduct exhibiting 1:2:2:1 splitting constants.

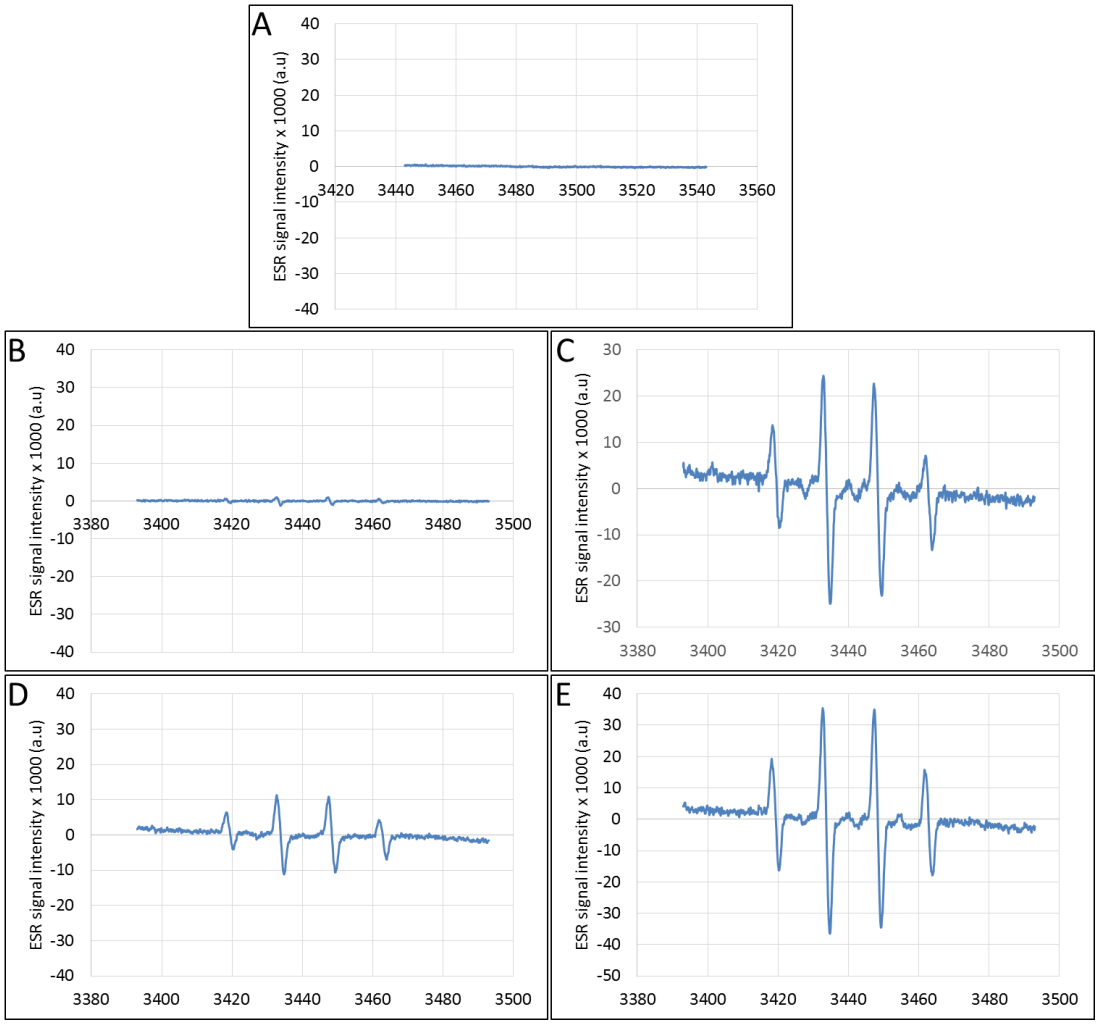

Figure 4-8: Representative ESR signals. (A) Baseline control consisting of 100 mM DMPO and 10 mM H_2O_2; (B) Representative tailings dust sample in the presence of 100 mM DMPO only and (C) in the presence of 100 mM DMPO and 10 mM H_2O_2; (D) Crystalline silica positive control, Min-U-Sil 5, in the presence of 100 mM DMPO only and (E) in the presence of 100 mM DMPO and 10 mM H_2O_2.

The results in **Figure 4-9** show that, for all tailings dust samples, lower signal intensities were observed in the absence of H_2O_2 **(Figure 4-9A)** compared to in its presence **(Figure 4-9B)**. In the presence of H_2O_2, the positive control Min-U-Sil 5 showed an expected high ESR signal intensity, significantly so when compared to dusts from ERPM and AGA **(Figure 4-9B)**. When the ESR intensities were compared among the different TSFs, the ERGO dusts showed the highest intensity, significantly so when compared to the dusts from ERPM and AGA. The CGR

dusts also showed a relatively high ESR signal intensity, which was significantly higher than that of the AGA TSF.

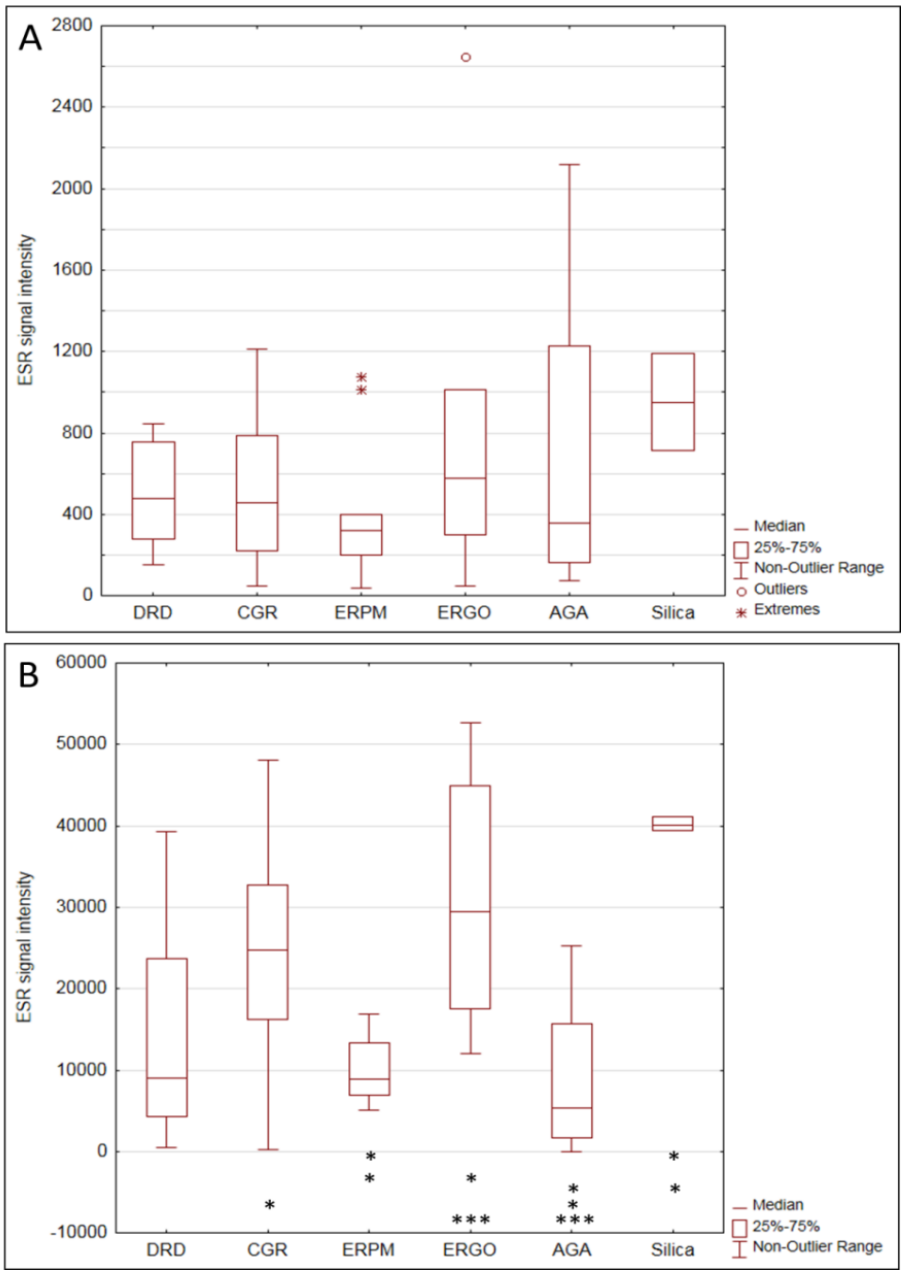

Figure 4-9: ESR signal intensities of the respirable fraction of the bulk dusts from each TSF and the crystalline silica positive control, Min-U-Sil 5. (A) Dusts and Min-U-Sil 5 without H_2O_2 added and (B) with H_2O_2 added. For (A), no significant differences were observed. For (B), *$P \leq 0.05$; ***$P \leq 0.001$.

4.1.2. Toxicity assessment of tailings dust

Initially, toxicity assessment using conventional assay systems was intended for this study as the second step in the hazard identification of tailings dust. However, preliminary studies showed an unexpected interference of particles with several components of these assays leading to false results. The following sections discuss in detail the mechanisms of interference observed.

4.1.2.1. Conventional toxicity assays and interference

Preliminary cell-based studies with the crystalline silica positive control, Min-U-Sil 5

Due to the occurrence of false-positive and -negative results in assays, it is common practice to cross-check the data from one assay system with alternative assays to ensure reliability of results (Kong et al., 2011). The toxicity of Min-U-Sil 5 on BEAS-2B cells was therefore determined using the XTT, ATP and LDH assay systems, each of which measures a different toxicity endpoint **(Figure 4-10)**.

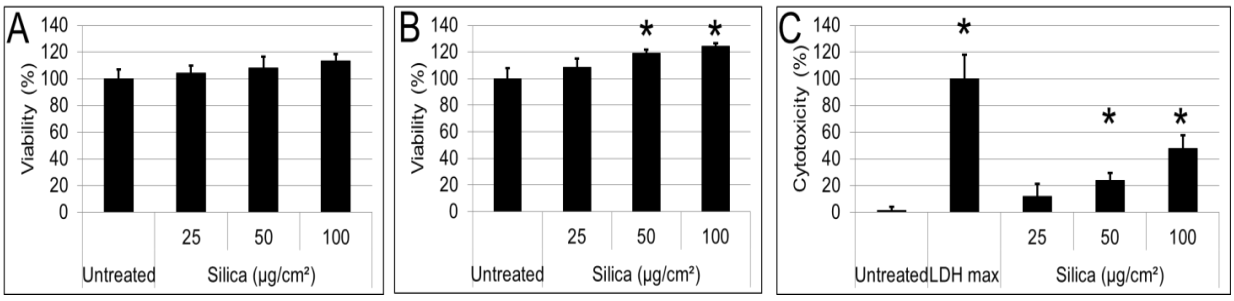

Figure 4-10: Toxicity assessment of BEAS-2B cells treated with the crystalline silica positive control, Min-U-Sil 5, using conventional toxicity assays. (A) XTT toxicity assay; (B) CellTiter Glo assay (ATP) and (C) CytoTox One assay (LDH). Data presented as average values ± SD.

Briefly, BEAS-2B cells were treated with 25, 50 and 100 µg/cm² Min-U-Sil 5 for 24 h and the toxicity was then assayed using the three kits. For the XTT toxicity assay, absorbance was measured at 450 nm. The CellTiter Glo assay (ATP) is based on luminescence. For the CytoTox One assay (LDH), fluorescence was measured at 560/590 nm. For the XTT toxicity assay and CellTiter Glo assay (ATP), average viability is represented as a percentage of the untreated

control cells. For the CytoTox One assay (LDH), average cytotoxicity is represented as a percentage of the maximum LDH release cells.

Discrepancies in results between the three assays were observed **(Figure 4-10)**. The XTT and ATP assays showed an unexpected concentration-dependent increase in viability higher than that of the untreated cells **(Figure 4-10A** and **B)**, which was significant at 50 and 100 µg/cm² with the ATP assay. Only the LDH assay showed an expected, concentration-dependent increase in toxicity **(Figure 4-10C)**.

Our next step was to investigate the toxicity of Min-U-Sil 5, using a system known to be unaffected by particle interference given that it does not rely on an optical read-out system or dyes to generate results *i.e.* the xCELLigence RTCA. **Figure 4-11A** shows the growth curve, indicated by CI, of untreated control BEAS-2B cells as well as 100 µg/cm² Min-U-Sil 5 in dispersion medium, which, in the absence of cells did not produce an increase in CI value and remained zero over time. In the absence of interference, the true, expected toxicity of Min-U-Sil 5 may be obtained. In **Figure 4-11B**, the cells were treated with Min-U-Sil 5 approximately 24 h after seeding and the CI was normalized at a time point just before treatment. Significant differences from the untreated control cells were determined by using the slope of the curves, which describes the changing rate of the CI within the time period from the point of treatment to the point of confluence. By increasing the concentration of Min-U-Sil 5, it was possible to produce a concomitant, significant dose-dependent increase in toxicity.

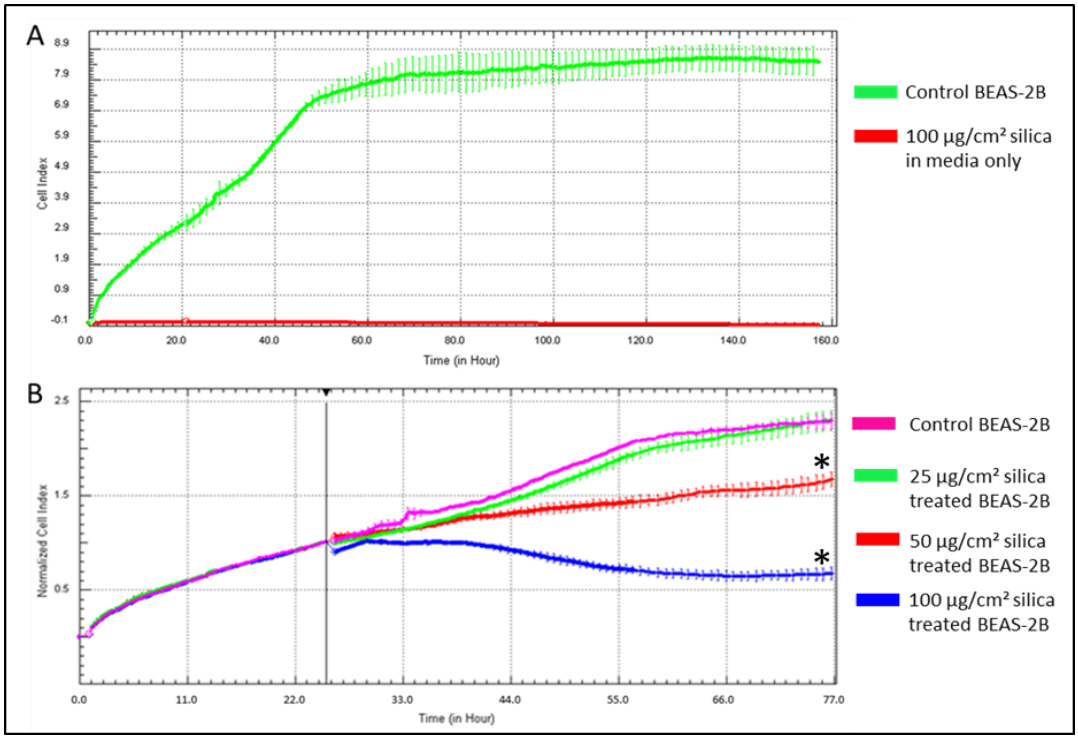

Figure 4-11: Representative cell indices of BEAS-2B cells treated with the crystalline silica positive control, Min-U-Sil 5, as recorded with the xCELLigence RTCA. (A) Cell index of untreated BEAS-2B cells and of Min-U-Sil 5 in medium only showing lack of interference; (B) Normalised cell index showing concentration-dependent toxicity of Min-U-Sil 5. *$P \leq 0.05$ compared to control.

Relationship of the optically-based assays (XTT, ATP and LDH) with the xCELLigence RTCA

The next step was to see whether a parallel relationship existed between the results of the XTT, ATP and LDH assays and those of the xCELLigence RTCA. For BEAS-2B cells treated with Min-U-Sil 5, the results of the three assays and the xCELLigence RTCA were normalized to a response relative to the untreated control cells. The response was calculated at 24 h after exposure to Min-U-Sil 5. This time point was chosen based on the xCELLigence data showing a pronounced dose-dependent toxicity effect at this time interval **(Figure 4-11)**, which facilitated comparison between the different Min-U-Sil 5 treatment concentrations. Only the LDH assay correlated well with the xCELLigence RTCA **(Figure 4-12)**. The response at each Min-U-Sil 5 concentration was similar for both the LDH assay and the xCELLigence RTCA showing a

concentration-dependent increase in toxicity. The XTT and ATP assays did not show any correlation with the xCELLigence RTCA (results not shown).

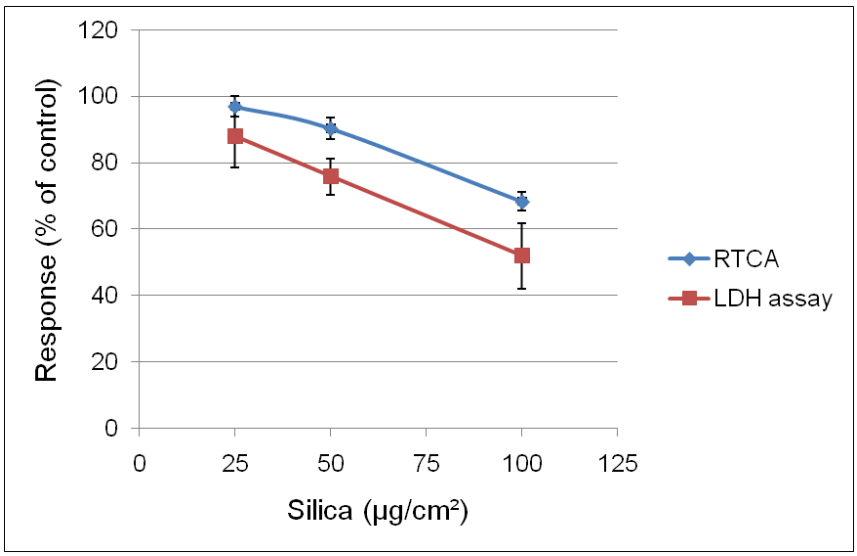

Figure 4-12: The percentage of response of BEAS-2B cells exposed to Min-U-Sil 5 for 24 h using the xCELLigence RTCA and LDH assay. Data presented as average values ± SD.

Cell-free interference studies with the crystalline silica positive control, Min-U-Sil 5

Interference studies were conducted in a cell-free environment to determine if the discrepancies seen among the XTT, ATP and LDH assays in the presence of cells exposed to Min-U-Sil 5 were as a result of interference from the particles.

Interference with the optical read-out of the final product of the XTT, ATP and LDH assays was first assessed. Thereafter, the ability of particles to interfere directly with the assay components, including substrates and products as well as their ability to catalyse the conversion of substrate to product was investigated.

XTT assay

Min-U-Sil 5 was first suspended in dispersion medium only and the absorbance was recorded at 450 nm to determine if the particles interfered with the absorbance at the wavelength at which the final product, formazan chromophore, is read **(Figure 4-13A)**.

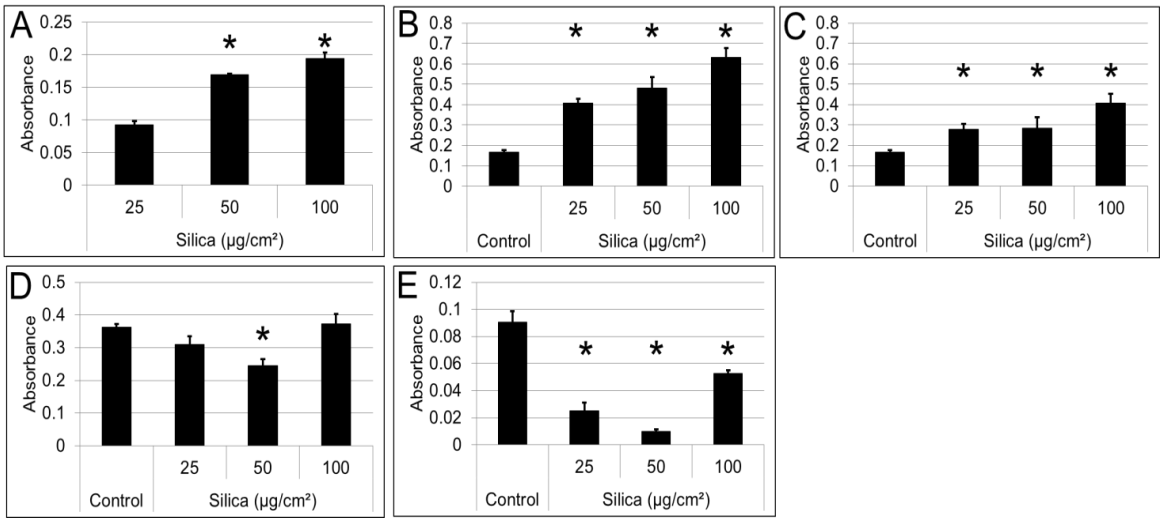

Figure 4-13: Reaction of the crystalline silica positive control, Min-U-Sil 5, with the XTT assay. (A) Min-U-Sil 5 in dispersion medium only; (B) Min-U-Sil 5 in XTT substrate and NADH co-factor; (C) Subtraction of (A) from (B); (D) Min-U-Sil 5 in formazan product; (E) Min-U-Sil 5 in XTT substrate. Data presented as average absorbance values at 450 nm ± SD; *$P \leq 0.05$, compared to 25 µg/cm² (for A), or to control (for B-E).

Min-U-Sil 5 showed a significant increase in absorbance at 450 nm with an increase in silica concentration. Although non-plasmonic in nature (*i.e.* does not exhibit a characteristic absorbance maximum), crystalline silica is optically dense meaning that it absorbs light at all wavelengths in the ultraviolet - visible (UV-vis) spectrum **(Figure 4-14)**.

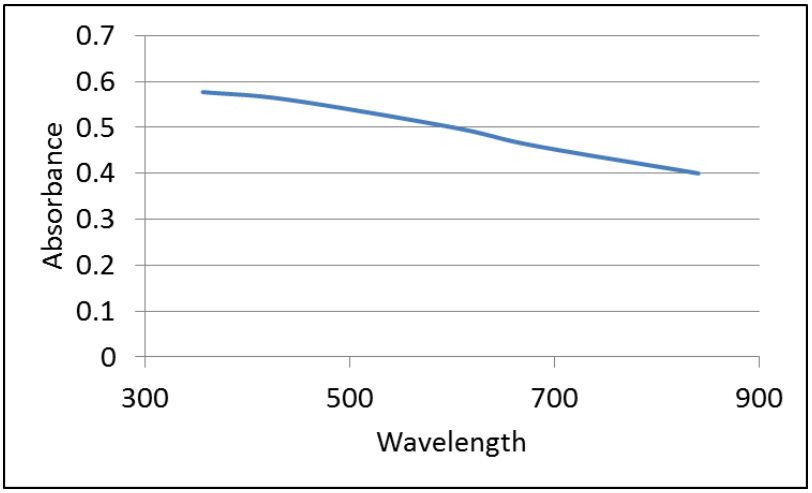

Figure 4-14: UV-vis absorption spectra of the crystalline silica positive control, Min-U-Sil 5.

The next step was to determine whether Min-U-Sil 5 has the ability to interfere with XTT assay components. First, Min-U-Sil 5 was incubated with XTT substrate and NADH co-factor. NADH reduces the tetrazolium ring of XTT to produce the formazan product, thereby simulating a typical cell-based XTT assay. **Figure 4-13B** shows an increase in absorbance with increasing Min-U-Sil 5 concentration at 450 nm. From these results it can be said that such interference by Min-U-Sil 5 with XTT components was significant enough to alter the results of a cell-based study shown in **Figure 4-10A**, which may be falsely interpreted as an overestimation of cell viability.

To further confirm the mechanisms of interference, it was argued that if there was no interference between Min-U-Sil 5 and the assay components, the absorbance at different concentrations of Min-U-Sil 5 in **Figure 4-13B** would have been the combined absorbance of the control and the absorbance of silica at different concentrations shown in **Figure 4-13A**. The absorbance of different concentrations of Min-U-Sil 5 at 450 nm in the presence of XTT substrate and NADH **(Figure 4-13B)** was indeed additive between the control value and the absorbance of Min-U-Sil 5 in dispersion medium shown in **Figure 4-13A**. However, an additional increase in absorbance was noted, which may be attributed to the catalytic ability of Min-U-Sil 5, converting XTT substrate to formazan in the presence of NADH. Indeed, when the absorbance of Min-U-Sil 5 in dispersion medium only **(Figure 4-13A)** was subtracted from the

absorbance of Min-U-Sil 5 in XTT substrate and NADH **(Figure 4-13B)**, a concentration-dependent increase in absorbance was still observed **(Figure 4-13C)**, confirming this catalytic activity.

When Min-U-Sil 5 was incubated with formazan alone the already converted product **(Figure 4-13D)** and XTT substrate alone **(Figure 4-13E)**, a decrease in absorbance was observed, which was more pronounced at 25 and 50 µg/cm² compared to 100 µg/cm². Therefore, in the absence of co-factor, Min-U-Sil 5 was able to adsorb XTT components at low concentrations. Note that **Figure 4-13D** and E show the results after subtraction of the absorbance values of particles in dispersion medium.

ATP assay

The interference of particles with the ATP assay system was next investigated. Firstly, interference with luminescence of Min-U-Sil 5 was assessed. Although luminescence values were detected, the relative luminescence units were approximately 1% of what is generally obtained in the presence of ATP assay components. Subtracting the optical interference from the data did not cause any significant change in the luminescence recorded (results not shown).

Min-U-Sil 5 showed a slight concentration-dependent increase in luminescence, which reached significance at 100 µg/cm², when incubated with luciferin and ATP **(Figure 4-15A)**. This increase in luminescence mirrors what is seen in the cell-based study **(Figure 4-10B)**, which may falsely be interpreted as an overestimation of cell viability.

When Min-U-Sil 5 was incubated with oxyluciferin alone or luciferin alone, no change in luminescence was seen with the former **(Figure 4-15B)** and a substantial decrease was seen with the latter at 25 and 50 µg/cm² **(Figure 4-15C)**. These results suggest that Min-U-Sil 5 has catalytic properties in the presence of co-factor and adsorptive properties with the substrate in the absence of co-factor; similar to what was observed with Min-U-Sil 5 and the XTT assay components in the presence and absence of a co-factor.

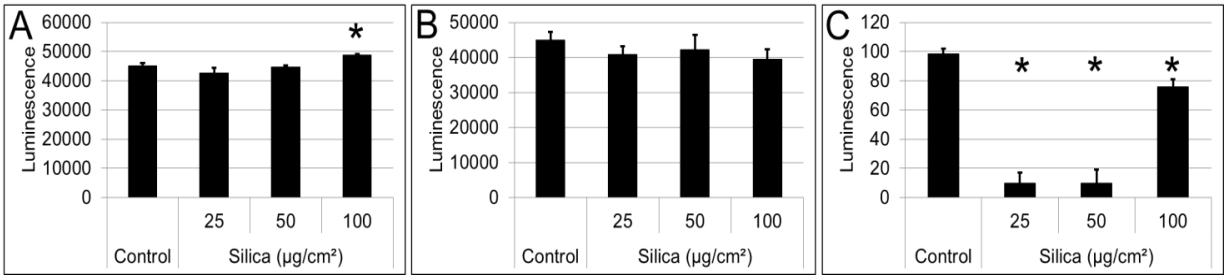

Figure 4-15: Reaction of the crystalline silica positive control, Min-U-Sil 5, with the ATP assay. (A) Min-U-Sil 5 in luciferin substrate and ATP co-factor; (B) Min-U-Sil 5 in oxyluciferin product; (C) Min-U-Sil 5 in luciferin substrate. Data presented as average luminescence values ± SD; *$P \leq 0.05$, compared to control.

LDH assay

The interference of Min-U-Sil 5 with the LDH assay system was investigated next. None of the particles showed any significant fluorescence values at 560 nm excitation, 590 nm emission, the wavelengths used to detect the resorufin product in the LDH assay (results not shown). Furthermore, none of the crystalline Min-U-Sil 5 particles showed interference with the LDH assay components in the presence or absence of NADH co-factor **(Figure 4-16)**. The lack of interference therefore shows that the results obtained with the LDH assay represent the true toxicity of Min-U-Sil 5, which is confirmed with the correlation of the LDH assay results with those of the xCELLigence RTCA **(Figure 4-12)**. The lack of interference of Min-U-Sil 5 particles with the LDH assay varied from those obtained with the XTT assay. In particular, the XTT assay showed catalytic activity in the presence of NADH. Both XTT and LDH assays depend on NADH as co-factor; however, the XTT assay requires an incubation period of 2 h whereas the LDH assay requires a 10 min incubation period. As no interference was observed with the LDH assay in the presence of NADH, it could be speculated that Min-U-Sil 5 interacted with NADH and that this interaction was time-dependent.

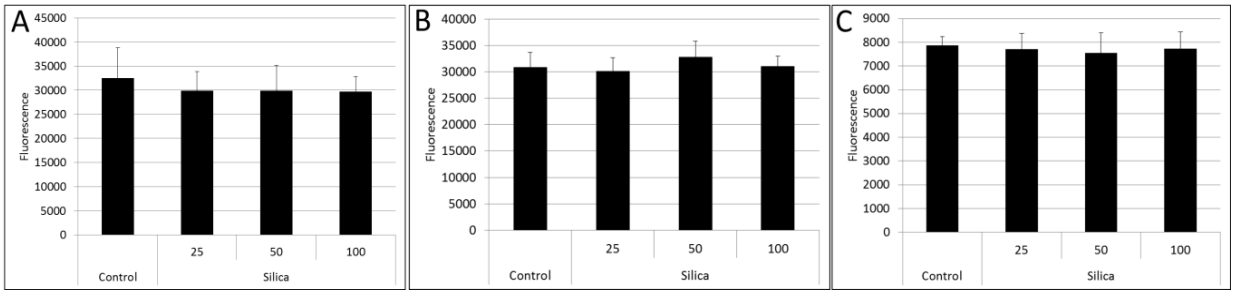

Figure 4-16: Reaction of the crystalline silica positive control, Min-U-Sil 5, with the LDH assay. (A) Min-U-Sil 5 in resazurin substrate and NADH co-factor; (B) Min-U-Sil 5 in resorufin product; (C) Min-U-Sil 5 in resazurin substrate. Data presented as average luminescence values. None of the values were significantly different from one another.

Cell-free interference studies with the respirable fraction of the dusts from the TSFs

XTT assay

Three randomly selected tailings dust samples, i.e. CGR 07, CGR 18 and DRD 06, were also investigated for their potential interference with the XTT assay system. The physicochemical properties of these dust samples are shown in **Table 4-10**. These three dust samples varied in their characteristics from particle size to colour to present a well-rounded selection of properties for interference assessment. As mentioned earlier, the dust samples did not alter the pH of the dispersion medium, as shown in **Table 4-10**. Similar results of the remaining dust samples showing unaltered pH values were obtained for all the samples including Min-U-Sil 5 and are therefore not shown.

Table 4-10: Particle characteristics of CGR 07, CGR 18 and DRD 06 tailings dust samples.

Characteristic	CGR 07	CGR 18	DRD 06
Size (nm)[a]	52.3 ± 1.97	66.2 ± 1.70	84.6 ± 2.00
Quartz content (%)	77.88	75.19	89.26
Specific surface area[b] (m^2/g)	3.5	6.8	4
pH at 37 °C[c,d]	7.75	7.765	7.5
Colour	Light brown	Dark brown	White

[a] Geometric mean diameter ± Geometric Standard Deviation determined with the Electrostatic Classifier Model 3080 and the APS Model 3321
[b] Determined with BET
[c] In dispersion medium
[d] pH of dispersion medium = 7.535

As with Min-U-Sil 5, these particles are optically dense and absorb light at all wavelengths in the UV-vis spectrum **(Figure 4-17)**.

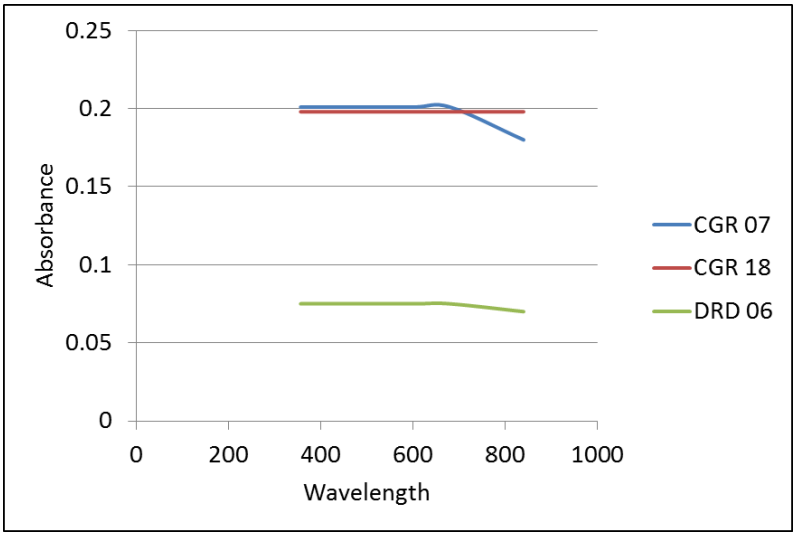

Figure 4-17: UV-vis absorption spectra of CGR 07, CGR 18 and DRD 06 tailings dust samples.

Therefore, due to their optically dense properties, these dust samples, when suspended in dispersion medium alone, have shown an increase in absorbance at 450 nm with increasing particle concentrations **(Figure 4-18A)**. These particles also showed interference when incubated with XTT substrate and NADH **(Figure 4-18B)**. But in contrast to Min-U-Sil 5, when the absorbance of the dust particles in dispersion medium alone **(Figure 4-17A)** was subtracted from the absorbance of particles in XTT substrate with NADH **(Figure 4-17B)**, a decrease in

absorbance was observed with all particles, compared to the control, indicating adsorption of assay components **(Figure 4-17C)**.

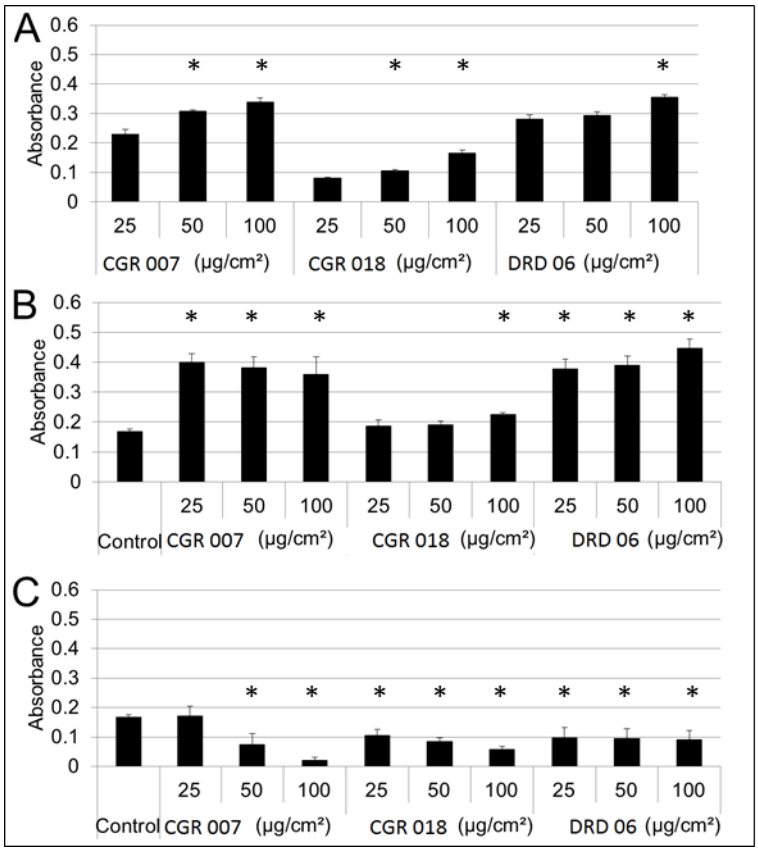

Figure 4-18: Reaction of the respirable fraction of tailings dusts with the XTT assay. (A) CGR 07, CGR 18, and DRD 06 in dispersion medium only; (B) CGR 07, CGR 18, and DRD 06 in XTT substrate and NADH co-factor; (C) Subtraction of (A) from (B). Data presented as average absorbance values at 450 nm ± SD; *$P \leq 0.05$, compared to 25 µg/cm² (for A), or to control (for B-E).

ATP assay

These particles did not show any interference with the luciferin substrate and ATP co-factor **(Figure 4-19A)** or final product of the ATP assay **(Figure 4-19B)**. However, DRD 06 did show a significant increase with the substrate only at 50 and 100 µg/cm³ **(Figure 4-19C)**, indicating possible catalytic activity.

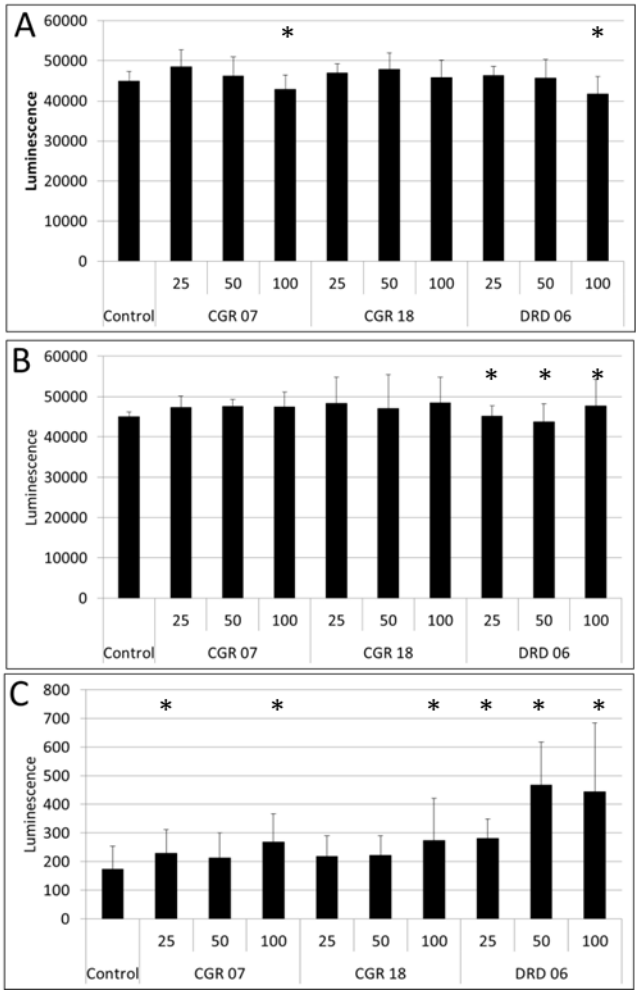

Figure 4-19: Reaction of the respirable fraction of tailings dusts with the ATP assay. (A) CGR 07, CGR 18, and DRD 06 in luciferin substrate and ATP co-factor; (B) CGR 07, CGR 18, and DRD 06 in oxyluciferin product; (C) CGR 07, CGR 18, and DRD 06 in luciferin substrate. Data presented as average luminescence values ± SD; *$P \leq 0.05$, compared to control.

LDH assay

With regards to the LDH assay, none of the particles showed any significant interference **(Figure 4-20)**, which corresponded to the lack of interference observed with Min-U-Sil 5 and the LDH assay.

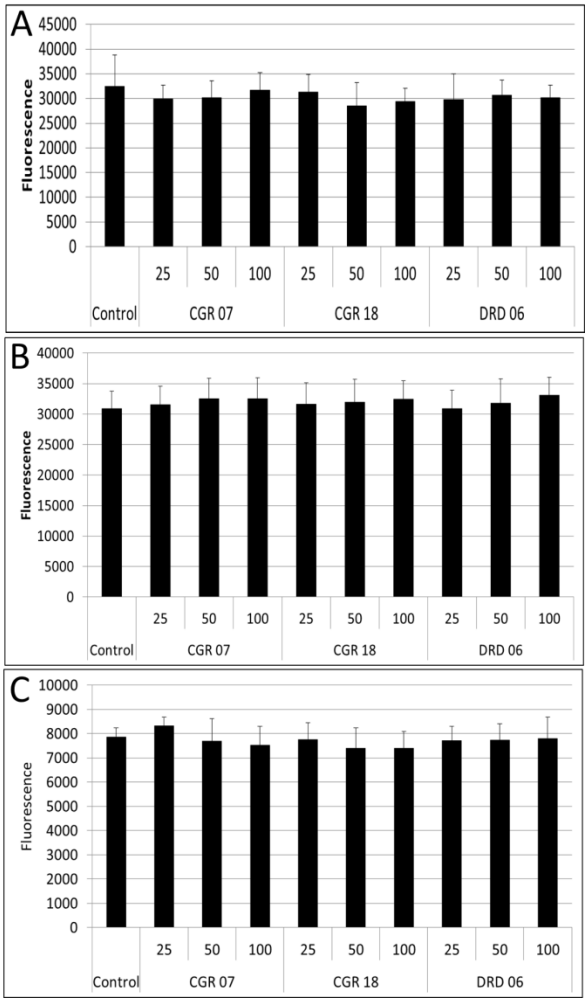

Figure 4-20: Reaction of the respirable fraction of tailings dusts with the LDH assay. (A) CGR 07, CGR 18, and DRD 06 in resazurin substrate and NADH co-factor; (B) CGR 07, CGR 18, and DRD 06 in resorufin product; (C) CGR 07, CGR 18, and DRD 06 in resazurin substrate. Data presented as average fluorescence values at 560/590 nm. None of the values were significantly different from one another.

4.1.2.2. Label-free toxicity analysis

Based on the results above, it was decided to further assess toxicity of all the tailings dusts using the label-free xCELLigence RTCA. Representative results for both BEAS-2B and U937 cells treated with dust samples are shown in **Figure 4-21**. However, Atienzar et al. (2011) have found that a decrease in the CI value obtained from the xCELLigence RTCA system does not always indicate cell death; in some cases, it may just indicate morphological changes, which may cause

detachment of viable cells from the surface of the well. For this reason, it is important to use the xCELLigence RTCA system in combination with other toxicity assays in order to confirm the results obtained from the xCELLigence RTCA system. The LDH assay seemed to be the most suitable for this purpose as it showed no interference with the particles tested and was therefore used to confirm the results from the xCELLigence RTCA system (presented in the next section). For the BEAS-2B cells in **Figure 4-21A**, a considerable increase in CI values were noted for the ERGO 14 dust samples at 25 and 50 µg/cm² from time point 54 h (i.e. approximately 30 h after initial addition of the dust), probably indicating recovery of cells.

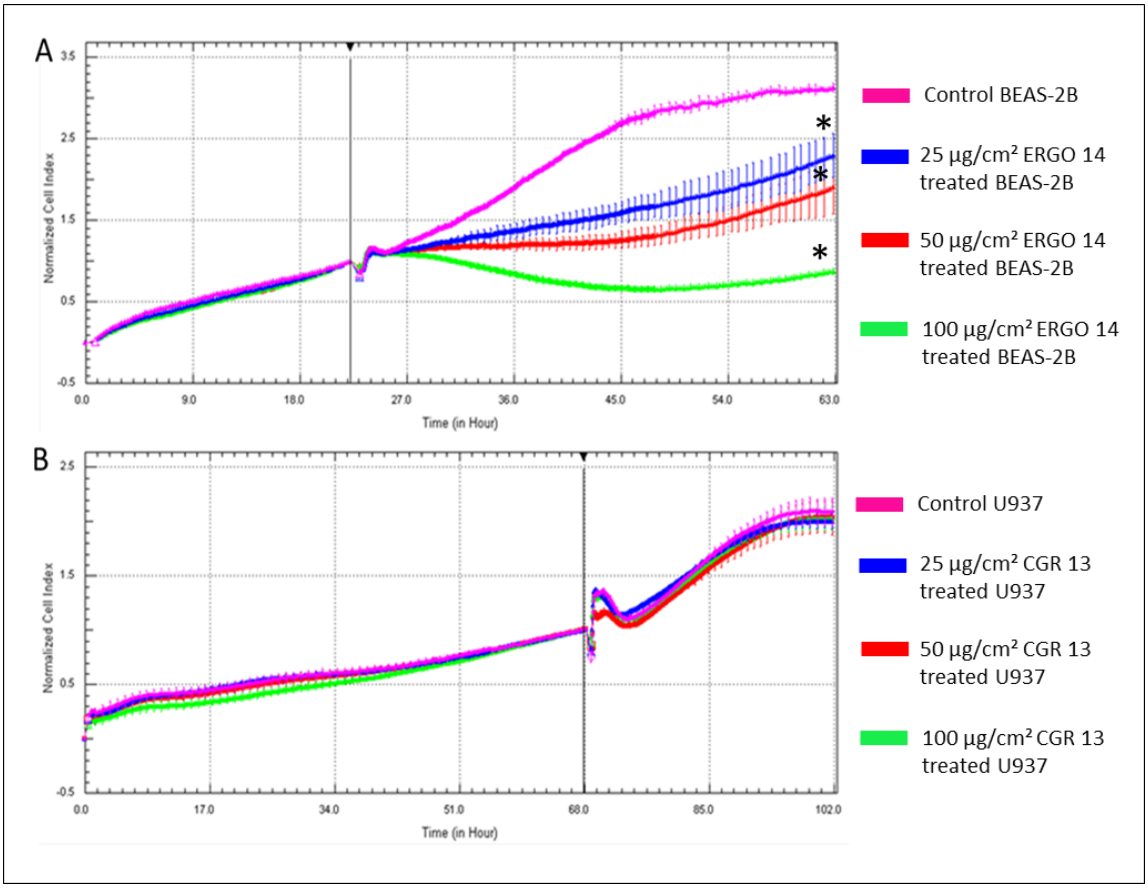

Figure 4-21: Representative cell indices of BEAS-2B and U937 cells treated with the respirable fraction of tailings dusts, as recorded with the xCELLigence RTCA. (A) BEAS-2B cells treated with tailings dust samples; (B) U937 cells treated with tailings dust samples. *$P \leq 0.05$ compared to control.

Toxicity assessment of various tailings dust concentrations and confirmation thereof

Ten randomly selected dust samples plus Min-U-Sil 5 was analysed and it was shown that, for each dust sample, a concentration-dependent toxicity in the BEAS-2B cell line was observed with the xCELLigence RTCA **(Figure 4-22A)** with a corresponding concentration-dependent increase in LDH release at 24 h after initial treatment **(Figure 4-22B)**, indicating cytotoxicity via membrane-damage. Even though cytotoxicity was observed for certain dust samples with the U937 cell line, the cytotoxicity was found not to be concentration-dependent, except for Min-U-Sil 5, which was expected **(Figure 4-23A)**. These results corresponded with the LDH assay showing a lack of a concentration-dependent increase in LDH release in the U937 cell line for the dust samples except for Min-U-Sil 5 **(Figure 4-23B)**.

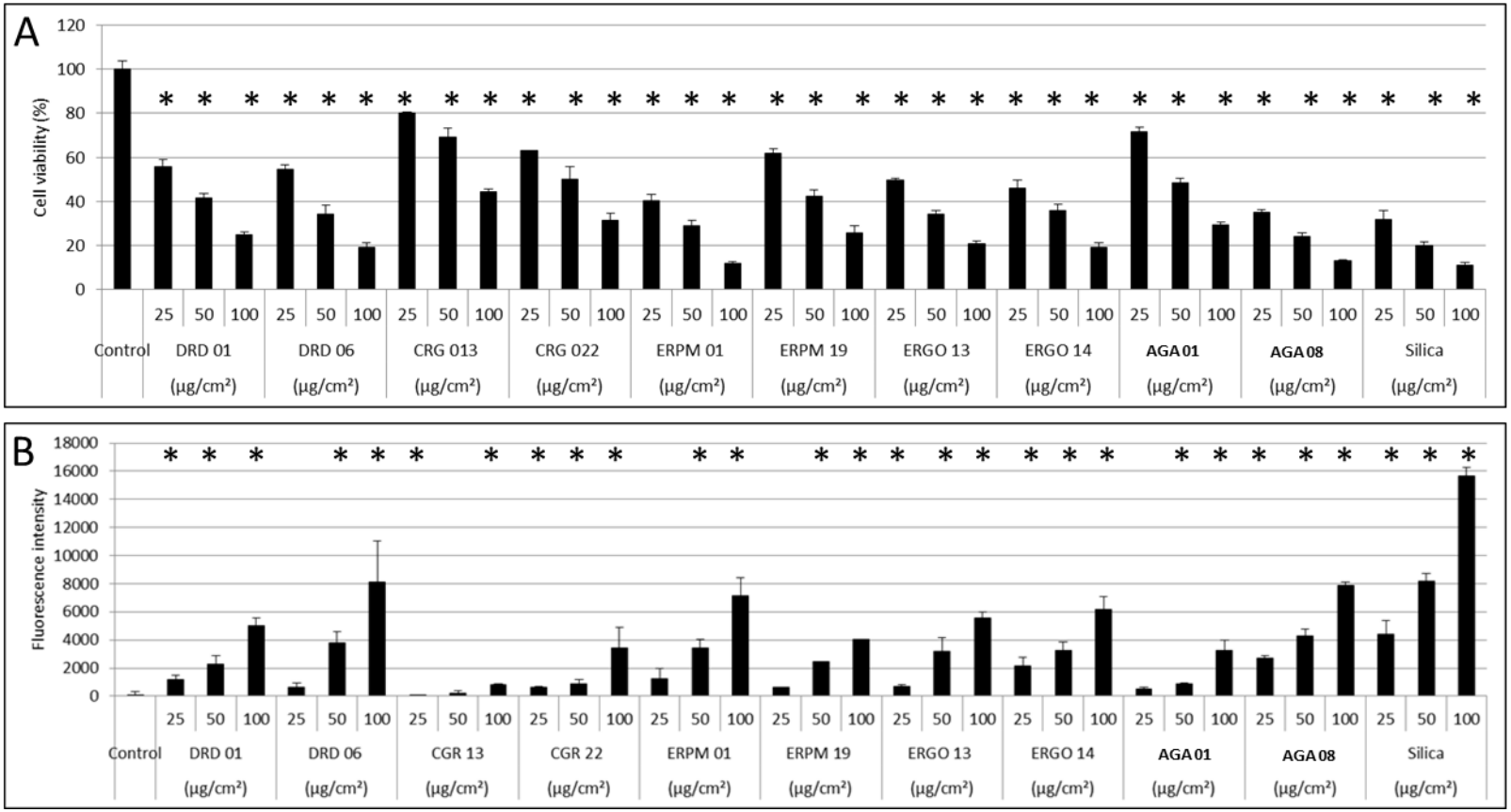

Figure 4-22: Toxicity assessment of BEAS-2B cells treated with tailings dust samples and crystalline silica positive control, Min-U-Sil 5, after 24 h using the xCELLigence RTCA (A) and the LDH assay (B). *$P \leq 0.05$ compared to control.

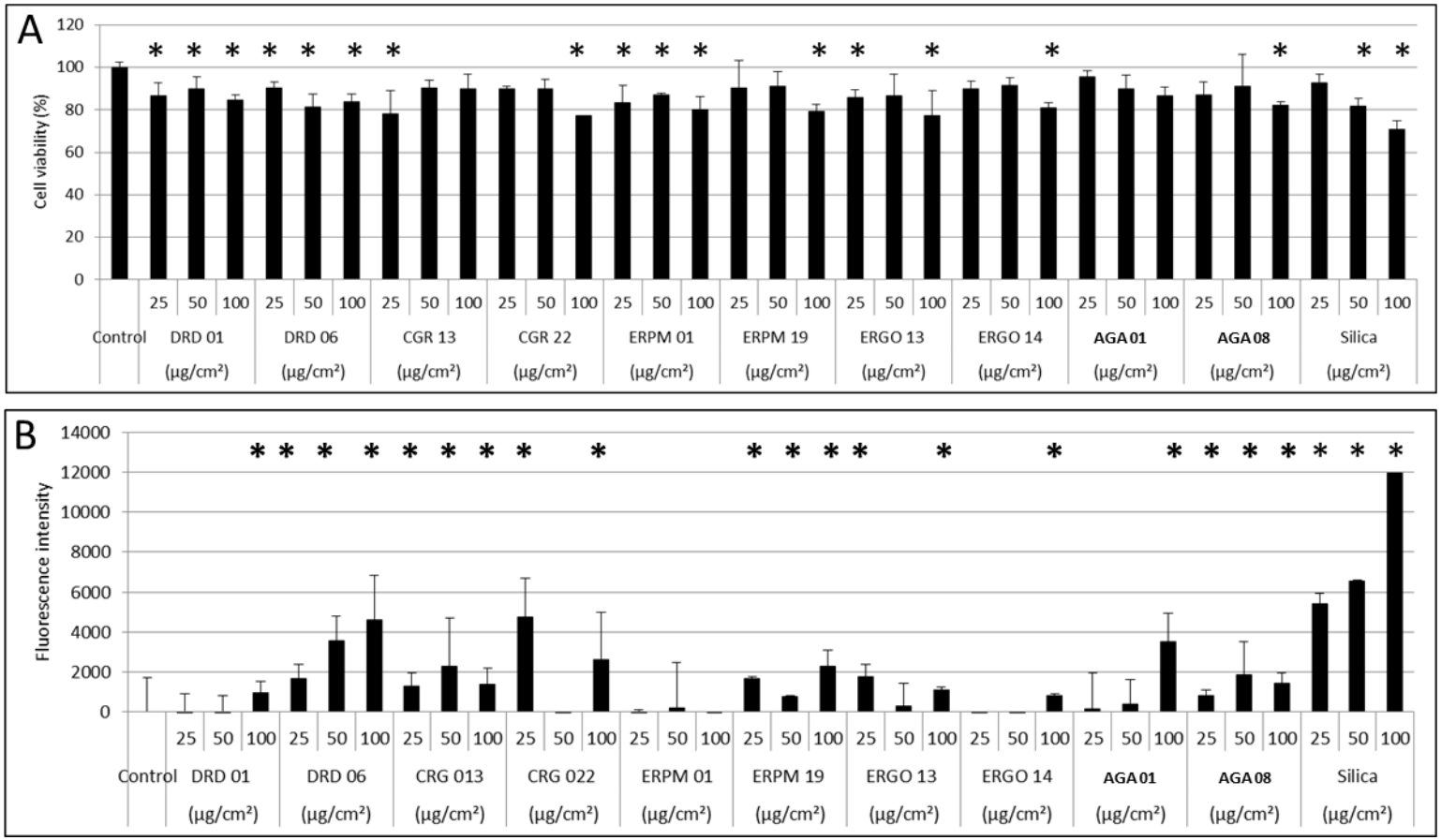

Figure 4-23: Toxicity assessment of U937 cells treated with tailings dust samples and crystalline silica positive control, Min-U-Sil 5, after 24 h using the xCELLigence RTCA (A) and the LDH assay (B). *$P \leq 0.05$ compared to control.

Toxicity assessment at various time points

The next step was to determine the degree of cytotoxicity of all the tailings bulk dust samples collected from the 5 TSFs at different time points using the xCELLigence RTCA.

Comparison among tailings dusts

For BEAS-2B cells, few significant differences were observed between the dust samples among the different TSFs although it appeared that the dusts from the ERGO TSF was significantly more toxic compared to the other dusts at certain time points, for example with ERPM at 3 h, with ERPM and AGA at 6 h and 12 h, with AGA at 24 h and with DRD and CGR at 48 h **(Figure 4-24)**. For U937 cells on the other hand, dusts from the DRD TSF showed a significantly higher toxicity, for example with ERPM and AGA at 1 h, with CGR, ERPM and AGA at 3 h, with ERPM at 6 h, with ERPM and AGA at 12 h, and with CGR, ERPM and AGA at 24 h **(Figure 4-25)** while dusts from the ERPM TSF appeared to be the least toxic.

Comparison of dust-treated cells with untreated control cells

For BEAS-2B cells, **Figure 4-24** shows that a significant increase in toxicity of the dusts of all TSFs was observed compared to the untreated control cells, as early as 1 h after initial exposure ($P = 0.027$). The toxicity continued to increase up to 48 h after initial exposure, with highly significant differences between control, untreated cells and the tailings dust-treated cells combined at each time point ($P = 0.000$). For U937 cells, on the other hand, a high variability in toxicity of dust samples were observed at 1 h after exposure, which is evident from the stretched box plots and non-significant difference between the control untreated cells and tailings dust-treated cells **(Figure 4-25)**. Thereafter, the cells appeared to have stabilised and no significant increase in toxicity was observed at 3 and 6 h. Only at 12 and 24 h, were significant increases in toxicities noted between control untreated cells and tailings dusts combined (12 h: $P = 0.000$; 24 h: $P = 0.001$). Based on these fewer significant differences with control untreated cells, the U937 cells appeared to be less sensitive to the dust particles when compared to BEAS-2B cells. The lower sensitivity of U937 cells to the tailings dusts compared to the BEAS-2B cells is also supported by the fact that U937 cells did not show dose-dependent toxicities as discussed earlier **(Figure 4-23)**. At 48 h, both BEAS-2B and U937 cells have appeared to have recovered from the

toxicity (more so for U937 cells than BEAS-2B cells), and showed higher viabilities compared to 24 h, similar to what was illustrated in **Figure 4-21A**.

Toxicity of Min-U-Sil 5

When BEAS-2B cells were treated with Min-U-Sil 5, a gradual increase in toxicity was observed and at 24 and 48 h, Min-U-Sil 5 showed the highest significant toxicity, compared to the dusts from the TSFs **(Figure 4-24)**. A more complex pattern was observed when U937 cells were treated with Min-U-Sil 5 with a high significant toxicity observed at 1 h after treatment and then again only at 12 and 24 h **(Figure 4-25)**.

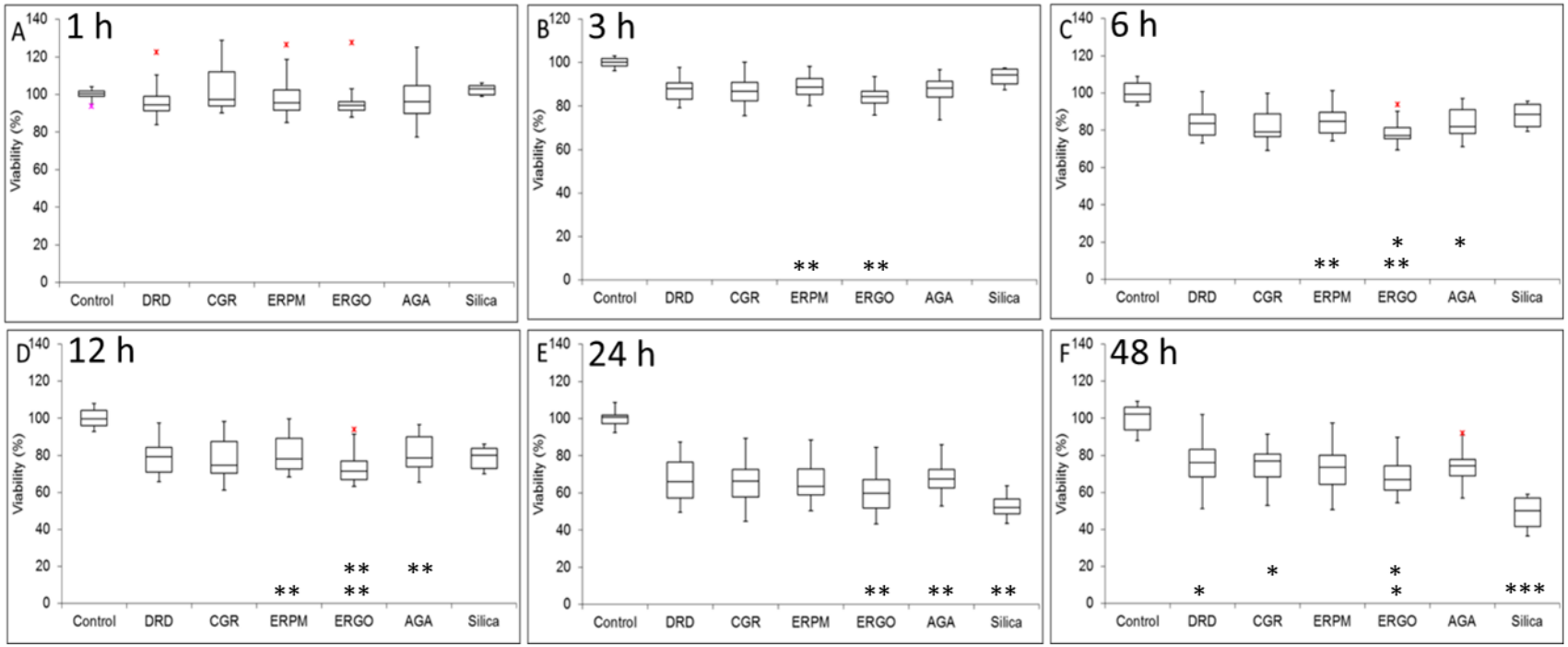

Figure 4-24: Toxicity assessment of BEAS-2B cells treated with tailings dust samples and the crystalline silica positive control, Min-U-Sil 5, at a concentration of 50 µg/m³ at various time points using the xCELLigence RTCA. Comparison between tailings dusts (combined) with control: 1 h: *P* = 0.027; 3 h: *P* = 0.000; 6 h: *P* = 0.000; 12 h: *P* = 0.000; 24 h: *P* = 0.000; 48 h: *P* = 0.000. Comparisons among the different TSF groups are indicated within the figures: **P* ≤ 0.05; ***P* ≤ 0.01; ****P* ≤ 0.001. In figures E and F, the viability of cells treated with Min-U-Sil 5 was significantly lower than those treated with the tailings dusts.

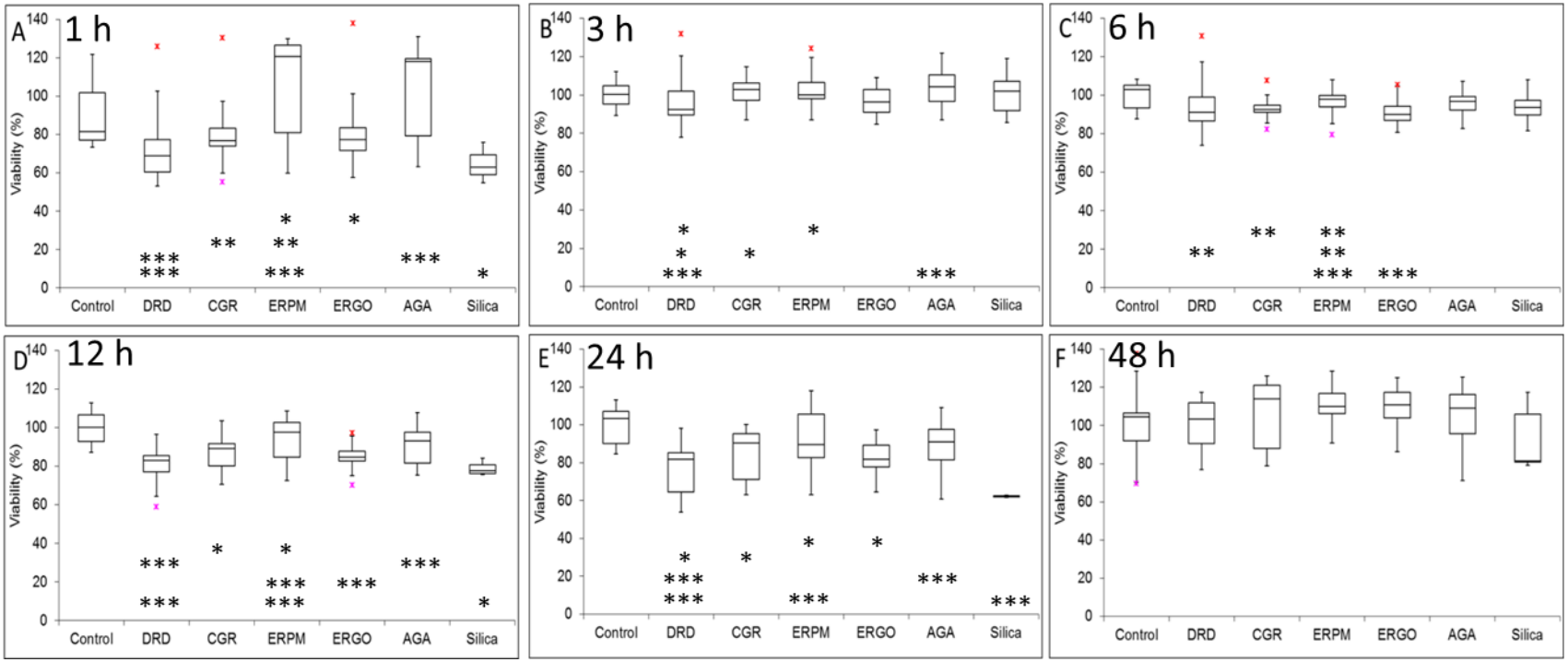

Figure 4-25: Toxicity assessment of U937 cells treated with tailings dust samples and the crystalline silica positive control, Min-U-Sil 5, at a concentration of 50 µg/m³ at various time points using the xCELLigence RTCA. Comparison between tailings dusts (combined) with control: 1 h: No significant difference; 3 h: No significant difference; 6 h: No significant difference; 12 h: *P* = 0.000; 24 h: *P* = 0.001; 48 h: No significant difference. Comparisons among the different TSF groups are indicated within the figures: **P* ≤ 0.05; ***P* ≤ 0.01; ****P* ≤ 0.001. In figures A, D and E, the viability of cells treated with Min-U-Sil 5 was significantly lower than those treated with the tailings dusts.

4.1.3.Correlation analysis

The previous sections have shown that, indeed, the tailings dusts exhibited the potential to produce ROS **(Section 4.1.1.7)** as well as toxicity *in vitro* **(Section 4.1.2.2)**. The next step was to determine whether a correlation existed between these two characteristics and the particles' physicochemical properties i.e. size, specific surface area, quartz content or elemental composition.

Univariate Spearman's correlation was carried out for each TSF separately using various combinations of surface activities and toxicities with physicochemical properties. Univariate Spearman's correlation was chosen as it has been the most popular choice for previous studies attempting to correlate biological endpoints of particles with their physicochemical properties (Boogaard et al., 2012, Steenhof et al., 2011, Veranth et al., 2006, Janssen et al., 2014). Although not all correlations are shown below, it was decided to focus on the most important finding, i.e. that a combination of physicochemical properties, rather than just one property, is often needed to elicit a biological response. This was noted with four particles from four TSFs i.e. ERGO, DRD, ERPM and AGA:

ERGO

None of the correlations in **Figure 4-26** are significant, however, one specific dust sample was shown to be an extreme outlier in all the correlations shown in **Figure 4-26A – G**. The main reason for keeping this outlier is to draw attention to the significance of the high elemental levels of certain dust samples in relation to surface activity. For this specific dust sample, its high surface activity could have been attributed to a combination of its high concentrations of redox-active transition elements Fe, Cu, V and Mn as shown in the top right corner of **Figure 4-26A, B, D** and **E**, respectively, as well as its large specific surface area (52.6 m^2/g, **Figure 4-26G**). Note that this is the particle that exhibited the highest concentrations of Hg and Ba shown earlier in **Table 4-7**.

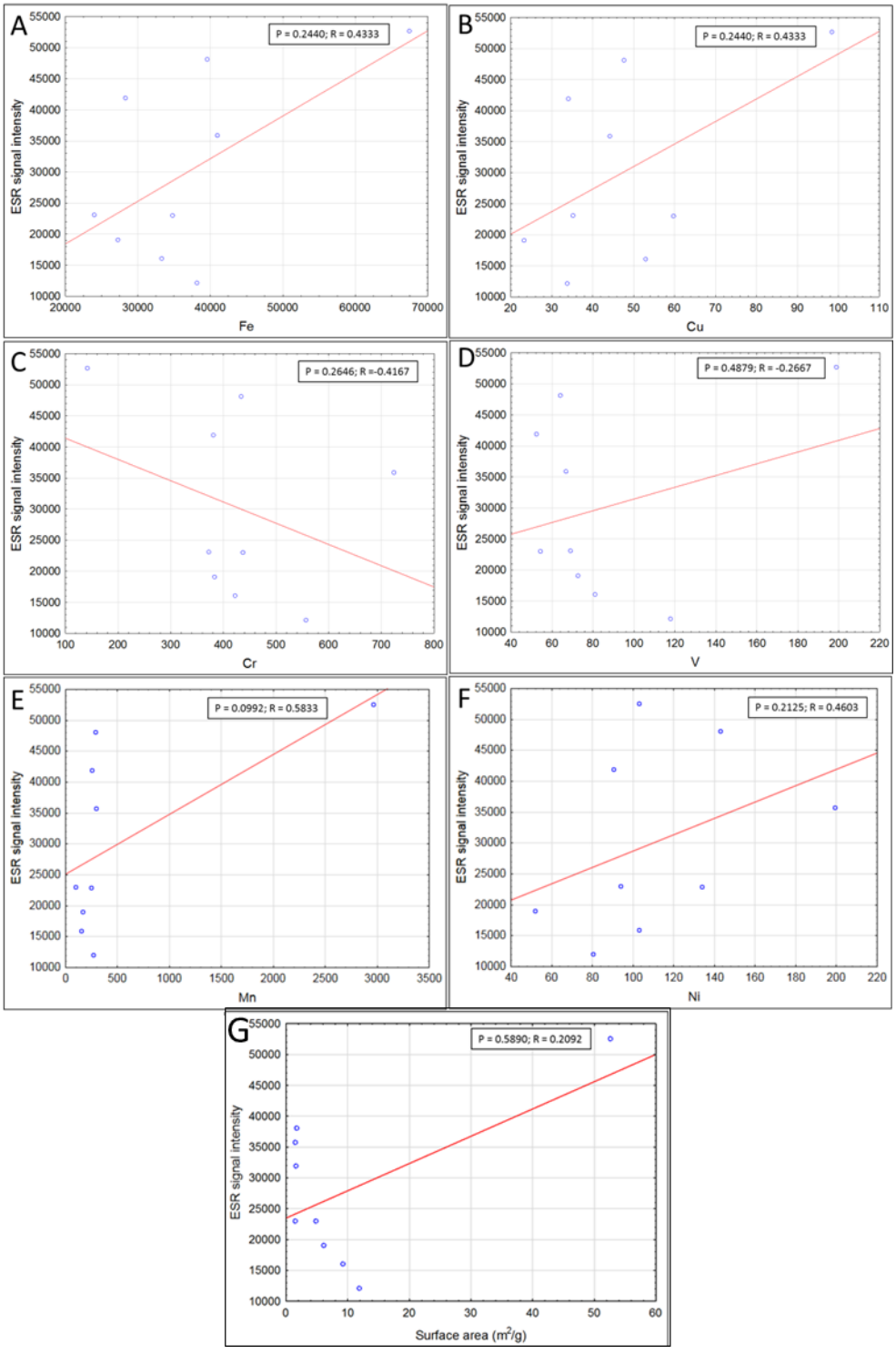

Figure 4-26: Correlation analysis of the surface activity of the tailings dusts from the ERGO TSF with redox active elements and specific surface area. (A) Fe; (B) Cu; (C) Cr; (D) V; (E) Mn; (F) Ni and (G) specific surface area.

DRD

One particular dust sample from the DRD TSF, another extreme outlier identified from correlation analysis, showed higher toxicity, relative to the other dust samples, which could be attributed to a combination of its unique properties i.e. it exhibited the highest levels of several redox-active elements studied i.e. Fe, Cu, Cr, V, Ni and Mn (bottom right corner, **Figure 4-27A-F**) as well as U **(Figure 4-27G)** and also had the largest specific surface area **(Figure 4-27H)**. As expected, when this outlier was omitted from the correlation analysis all significant results became non-significant. Once again, the main reason for keeping the outlier is to draw attention to the significance of the high elemental levels (and surface area) of dust in relation to toxicity.

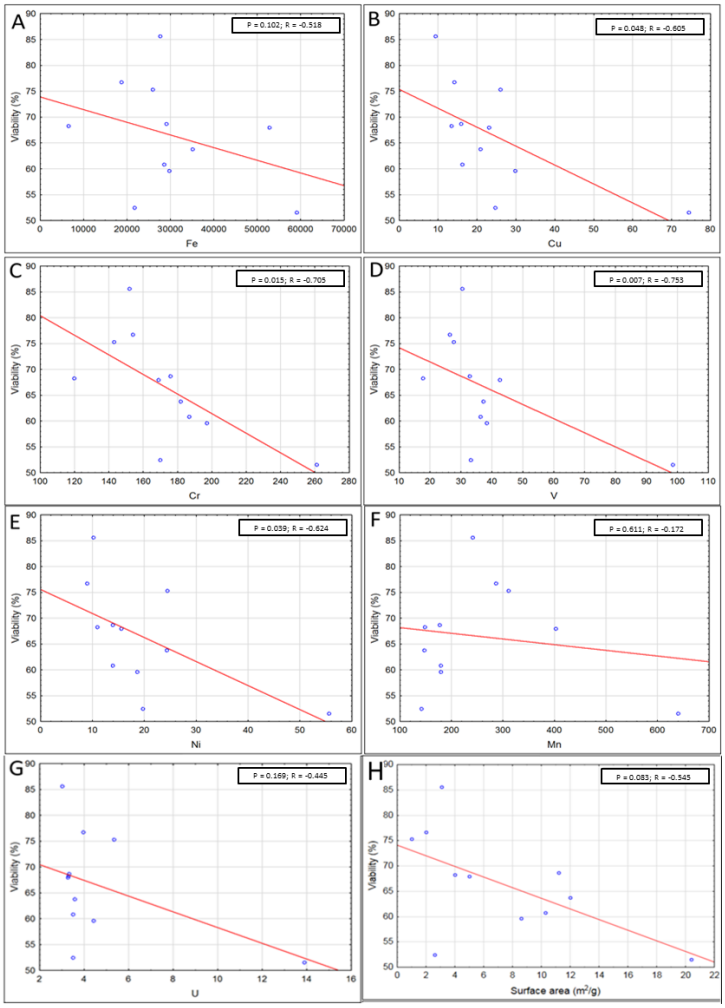

Figure 4-27: Correlation analysis of the *in vitro* toxicity potential of the tailings dusts collected from the DRD TSF with redox active elements and specific surface area. (A) Fe; (B) Cu; (C) Cr; (D) V; (E) Ni; (F) Mn; (G) U and (H) specific surface area.

ERPM

In **Figure 4-28A**, the ERPM sample exhibiting the highest U level (extreme outlier, bottom right corner) was the same dust sample that showed the highest ESR intensity and toxicity in **Figure 4-28B**. It could be speculated that either the high U concentration or high surface activity, or a combination thereof, could have led to increased toxicity. Note that, when this outlier was omitted from the correlation analysis all significant results became non-significant. Here again, the main reason for keeping the outlier is to draw attention to the significance of the high elemental levels (and surface activity) of dust in relation to toxicity.

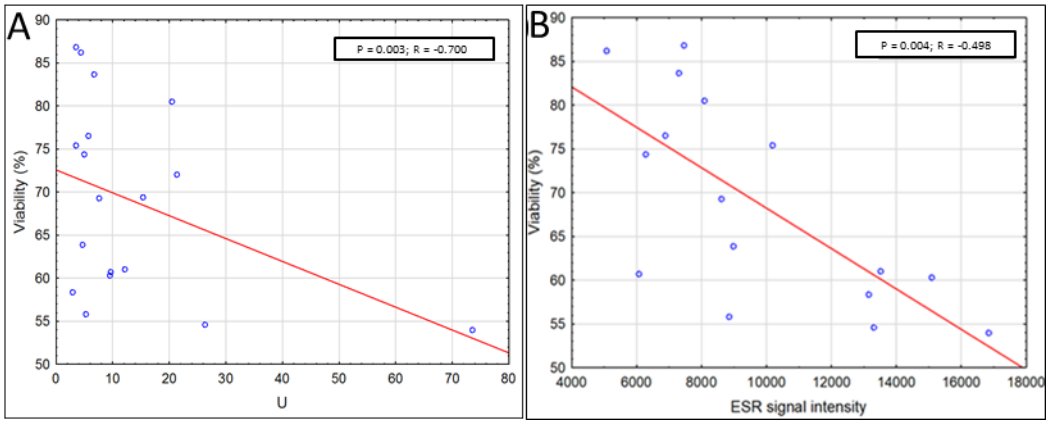

Figure 4-28: Correlation analysis of the *in vitro* toxicity potential of tailings dusts from the ERPM TSF with U content (A) and surface activity (B).

AGA

One AGA dust sample showed the highest levels of Cu, Mn and U (extreme outlier, bottom right corner, **Figure 4-29A-C**) as well as the largest specific surface area **(Figure 4-29D)**, which could have contributed to its high toxicity, relative to the other dust samples.

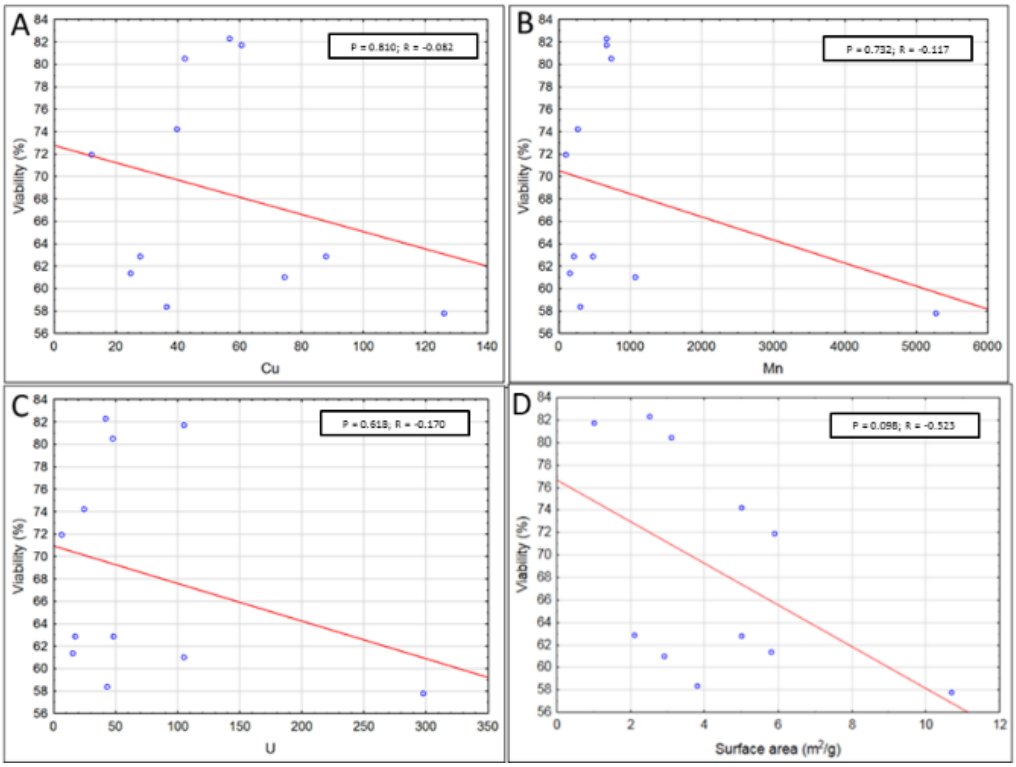

Figure 4-29: Correlation analysis of the *in vitro* toxicity potential of tailings dusts from the AGA TSF with Cu (A), Mn (B), U (C) and specific surface area (D).

4.1.4.Cellular uptake studies of tailings dust

4.1.4.1. Hyperspectral imaging (HSI), collection of particle spectral libraries and spectral angle mapper (SAM)

The CytoViva® HSI system was used to assess the uptake of the tailings dusts and Min-U-Sil 5 particles into the BEAS-2B and U937 cells. The first step was to collect spectral profiles of the dust particles in the absence of cells as this would be used to confirm whether the particles have been internalised by the cell or adsorbed to the surface of the cell by matching the particles' spectral profiles to the HSI scans of the particle-treated cells. Spectral profiles were collected from randomly selected particles from each dust sample. **Figure 4-30** represents the spectral profiles of the ten representative dust samples previously selected **(Figure 4-22)** as well as of Min-U-Sil 5. Each coloured line represents the spectrum from a single pixel of a particle. Generally, more than one pixel (or spectrum) is collected per dust sample and these collections of representative spectra form a known 'spectral library'. **Figure 4-30** shows that the spectral profiles of the dust samples differed from one another in that certain dust samples showed

homogeneous profiles (AGA 08, **Figure 4-30J**) while others showed heterogeneous profiles (ERPM 19, **Figure 4-30F**) indicating that dust particles within the same sample appeared to have different characteristics (e.g. colour, intensities, shape etc.) thereby affecting their profile signatures. Compared to the tailings dust samples, the homogeneity of Min-U-Sil 5 was reflected in its spectral profile **(Figure 4-30K)**.

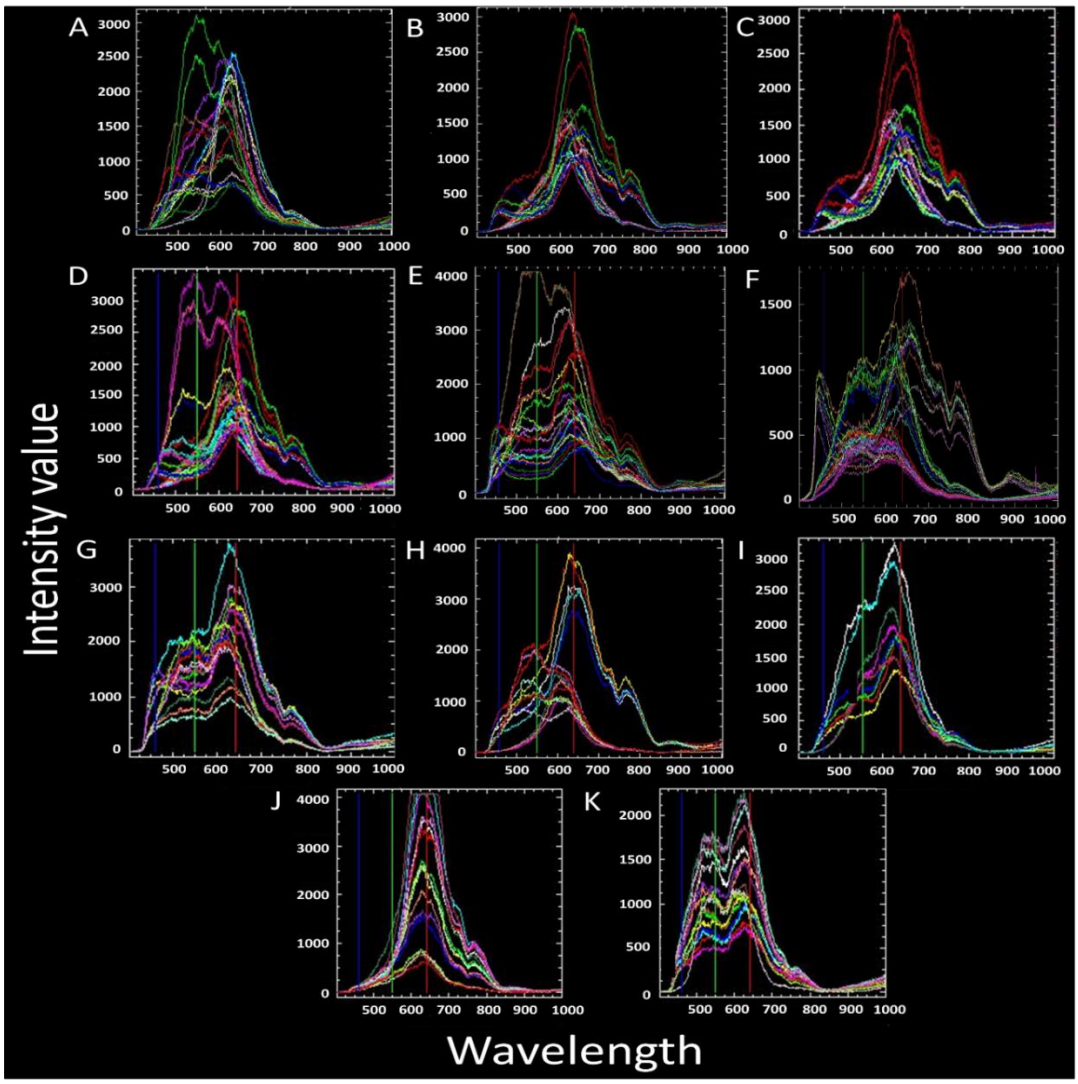

Figure 4-30: Spectral profiles of tailings dust particles and the crystalline silica positive control, Min-U-Sil 5. (A) DRD 01; (B) DRD 06; (C) CGR 013; (D) CGR 022; (E) ERPM 01; (F) ERPM 19; (G) ERGO 13; (H) ERGO 14; (I) AGA 01; (J) AGA 08; (K) Min-U-Sil 5.

SAM was used to assess the uptake of particles into BEAS-2B cells using the unique 'spectral library' of each dust sample. **Figure 4-31** shows a representative image of the SAM analysis in which the spectral library of CGR 013 **(Figure 4-30D)** was used to identify particles in BEAS-2B cells treated with CGR 013 particles. Each colour pixel in **Figure 4-31** represents a spectral profile of the same colour in **Figure 4-30D**, which was recognised by the SAM analysis tool as being a unique profile of the CGR 013 dust particles.

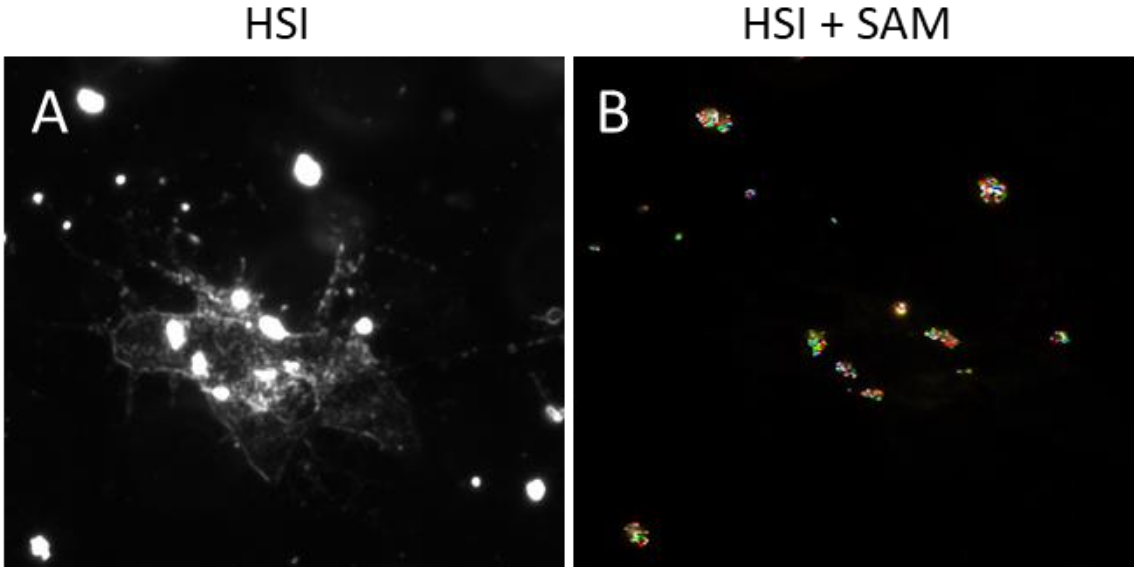

Figure 4-31: Representative images of the spectral angle mapper (SAM) analysis tool. (A) BEAS-2B cells were treated with CGR 013 tailings dust particles and analysed using HSI; (B) The tailings dust particles were identified using SAM where each pixel in the figure matches up with the spectral profile of the same colour in Figure 4-30D.

4.1.4.2. Particle uptake into BEAS-2B cells

The uptake of Min-U-Sil 5 into BEAS-2B cells is illustrated in **Figure 4-32**.The left panel shows HSI scans only while the right panel shows the SAM analysis of the corresponding HSI scan. **Figure 4-32A** shows the HSI image of untreated control BEAS-2B cells, while **Figure 4-32B** shows that the SAM analysis confirmed the lack of any Min-U-Sil 5 particles present in the control samples. After 1 h incubation of 50 µg/cm² Min-U-Sil 5 particles with BEAS-2B cells some uptake of particles (both singularly dispersed and aggregated) was noted using the SAM analysis tool as represented by the red pixels in **Figure 4-32D**. A higher degree of uptake was noted after 12 h of incubation with Min-U-Sil 5 particles **(Figure 4-32F)**, compared with the

cells after 1 h incubation, while after 24 h of incubation, a very high degree of accumulation of particles within cells was noted **(Figure 4-32H)**. In addition, the morphology of the cells after 24 h of incubation was markedly different than that of the untreated, control cells in that the cells were more rounded and exhibited less cellular adhesions with neighbouring cells. These results agree with those obtained with the xCELLigence RTCA **(Figure 4-24)**, which showed a gradual decrease in viability from 1 h **(Figure 4-24A)** to 12 h **(Figure 4-24D)** to 24 h **(Figure 4-24E)**. When BEAS-2B cells were treated with a lower concentration (10 µg/cm²) of Min-U-Sil 5 **(Figure 4-32J)**, internalisation of particles was noted after 24 h, however, compared to the higher concentration of Min-U-Sil 5 particles at 24 h **(Figure 4-32H)**, less toxicity was seen as the morphological appearance of the cells were more comparable to that of the control cells than the cells in **Figure 4-32H**.

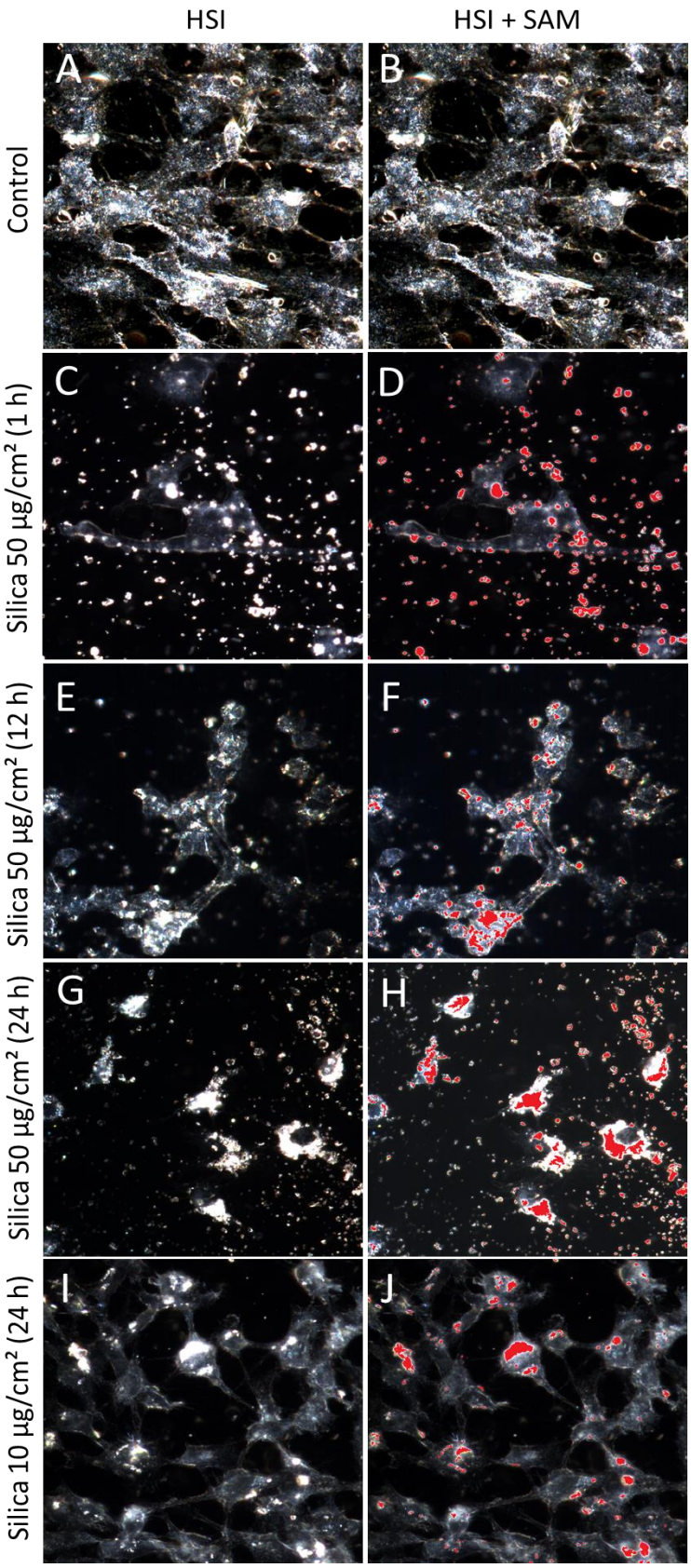

Figure 4-32: Representative images of the uptake of the crystalline silica positive control, Min-U-Sil 5, in BEAS-2B cells. The left panel shows HSI scans only while the right panel shows the SAM analysis of the corresponding HSI scan. (A and B) Control, untreated BEAS-2B cells; (C and D) BEAS-2B cells treated with 50 µg/cm² silica for 1 h; (E and F) BEAS-2B cells treated with 50 µg/cm² silica for 12 h; (G and H) BEAS-2B cells treated with 50 µg/cm² silica for 24 h; (I and J) BEAS-2B cells treated with 10 µg/cm² silica for 24 h).

We next investigated the uptake of a randomly selected tailings dust sample, which did not show any significant toxicity using the xCELLigence RTCA to determine whether toxicity is related to the interaction and uptake into BEAS-2B cells. **Figure 4-33** shows that, although the concentration of the dust sample administered to the BEAS-2B cells was the same as that for Min-U-Sil 5 (50 µg/cm²) fewer particles were observed of which most interacted or were taken up by the cells after 1 h incubation **(Figure 4-33A** and **B).** However, after 12 h **(Figure 4-33C** and **D)** and 24 h **(Figure 4-33E** and **F)**, the degree of uptake and accumulation of particles in the cells did not appear to increase dramatically, as was observed with the Min-U-Sil 5 particles **(Figure 4-32E – H)**. In addition, the morphology of the cells from 1 h to 12 h to 24 h appeared to remain unchanged with several adhesions present between neighbouring cells. After 24 h incubation, large particle aggregates were visible which did not appear to interact with the cells.

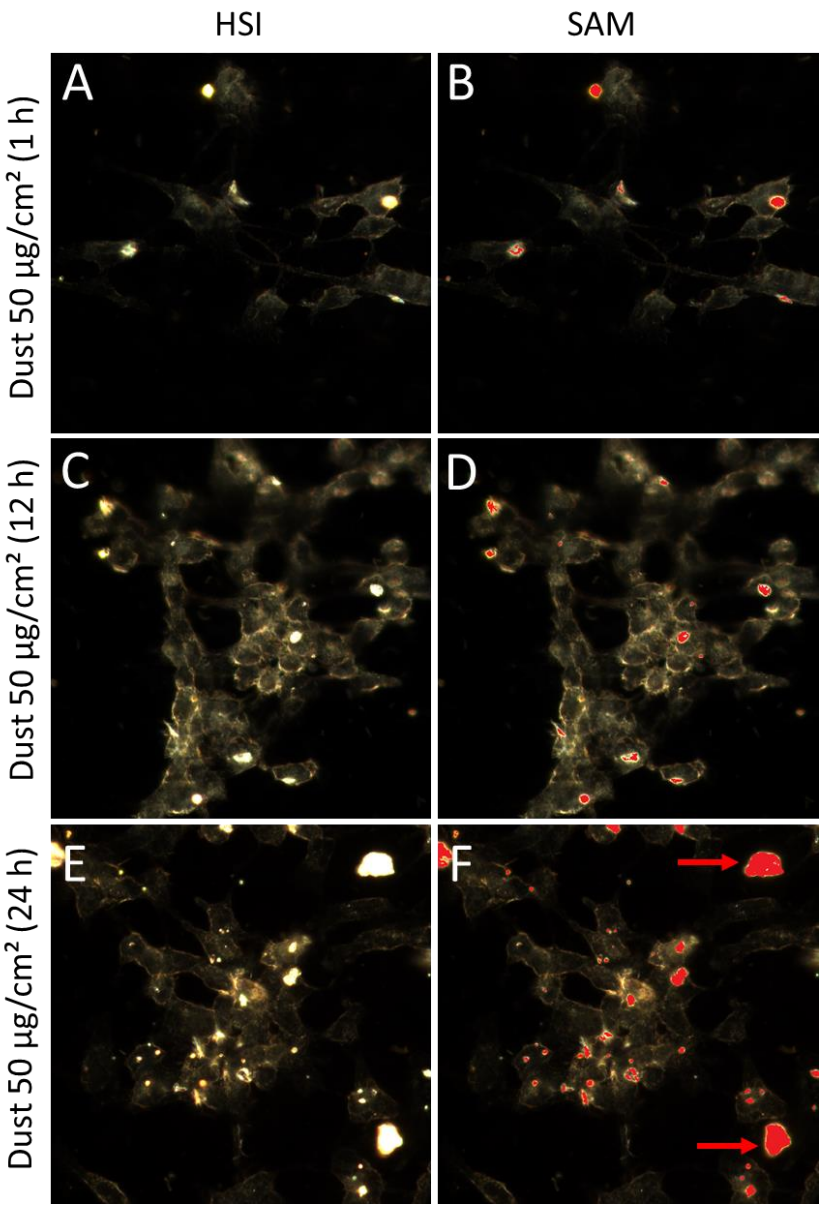

Figure 4-33: Representative images of the uptake of a randomly selected, non-toxic, tailings dust sample in BEAS-2B cells. The left panel shows HSI scans only while the right panel shows the SAM analysis of the corresponding HSI scan. (A and B) BEAS-2B cells treated with 50 µg/cm² dust for 1 h; (C and D) BEAS-2B cells treated with 50 µg/cm² dust for 12 h; (E and F) BEAS-2B cells treated with 50 µg/cm² dust for 24 h. Red arrows indicate aggregated particles outside cells.

4.1.4.3. Particle uptake into U937 cells

Similar to the BEAS-2B cells the U937 cells showed a gradual uptake of 50 µg/cm² Min-U-Sil 5 from 1 to 24 h **(Figure 4-34D, F** and **H)**, which led to a gradual increase in cellular toxicity. Interestingly, even though gradual uptake was also noted with a non-toxic tailings dust particle from 1 h to 24 h for U937 cells **(Figure 4-35B, D** and **F)**, the uptake did not appear to affect viability as readily as with Min-U-Sil 5 particles as several viable cells were still observed.

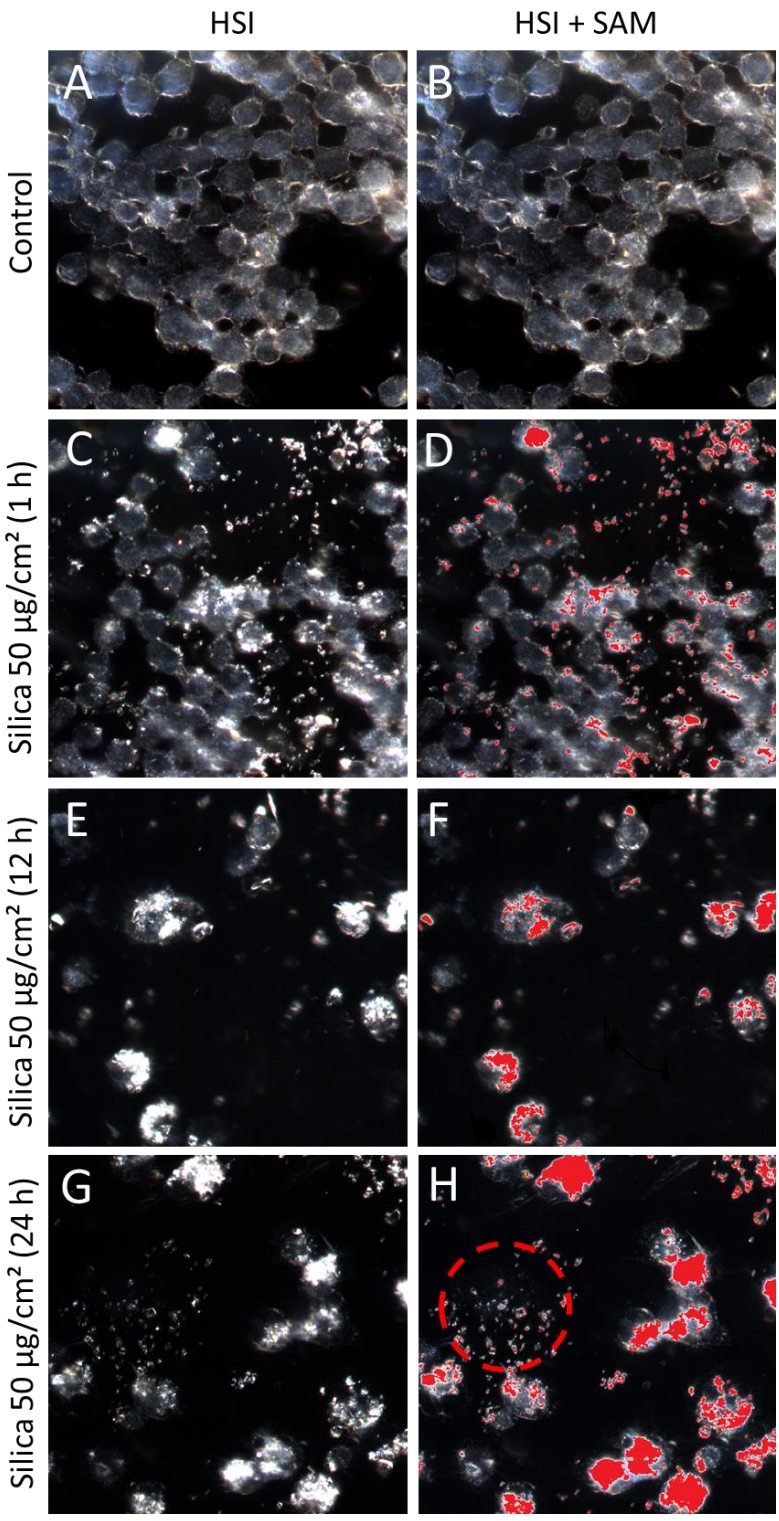

Figure 4-34: Representative images of the uptake of crystalline silica positive control, Min-U-Sil 5, in U937 cells. The left panel shows HSI scans only while the right panel shows the SAM analysis of the corresponding HSI scan. (A and B) Control, untreated U937 cells; (C and D) U937 cells treated with 50 µg/cm² silica for 1 h; (E and F) U937 cells treated with 50 µg/cm² silica for 12 h; (G and H) U937 cells treated with 50 µg/cm² silica for 24 h. The dashed circle indicates a burst U937 cell after internalising several silica particles.

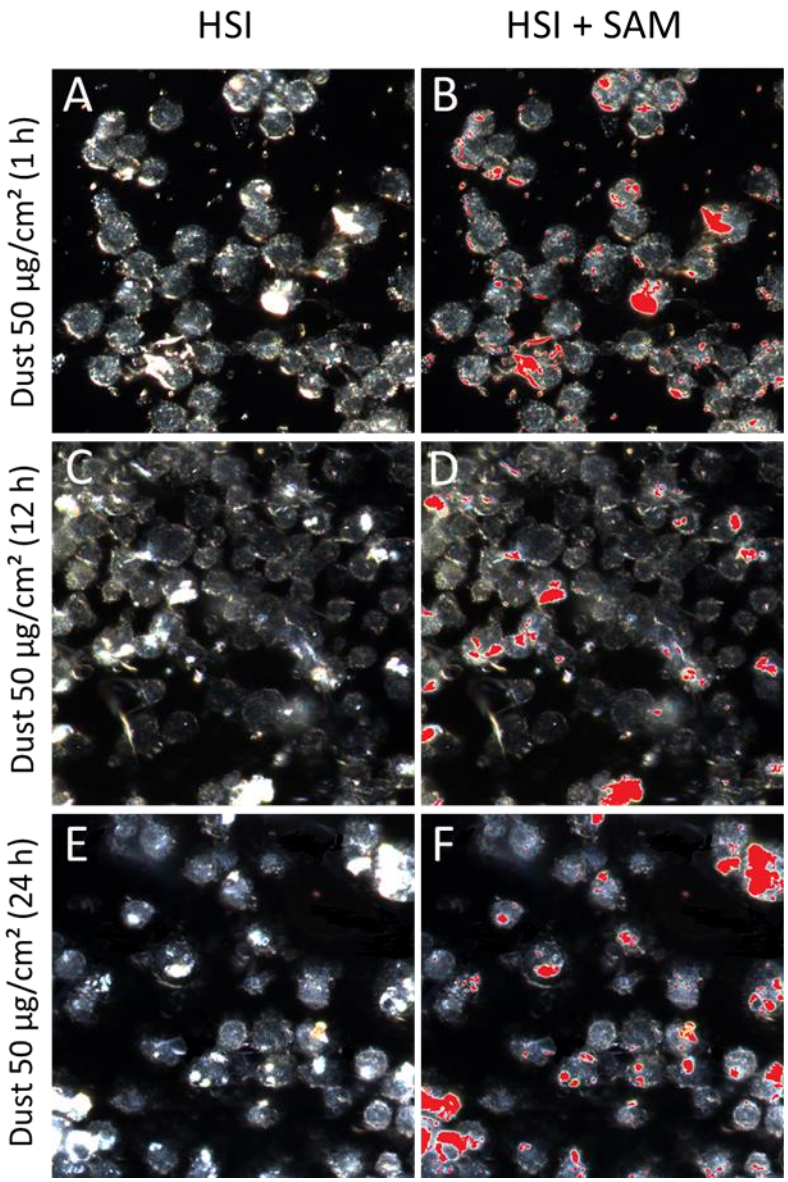

Figure 4-35: Representative images of the uptake of a randomly selected, non-toxic, tailings dust sample (CGR 013) in U937 cells. The left panel shows HSI scans only while the right panel shows the SAM analysis of the corresponding HSI scan. (A and B) U937 cells treated with 50 µg/cm² dust for 1 h; (C and D) U937 cells treated with 50 µg/cm² dust for 12 h; (E and F) U937 cells treated with 50 µg/cm² dust for 24 h.

4.2. EXPOSURE ASSESSMENT

Even though hazard identification can reveal important information regarding the toxicity potential of tailings dust, it does not necessarily imply risk to surrounding communities if communities are not exposed to the tailings dust. Therefore, exposure assessment was conducted by collecting PM_{10} and PM_4 data from residential areas in surrounding communities. All the results from the exposure assessment section have been published in Andraos et al. (2018a) and Andraos et al. (2018b).

4.2.1.Continuous real-time ambient PM_{10} levels collected at DRD, CGR and ERPM

Continuous real-time ambient PM_{10} levels were recorded using the GRIMM Environmental Dust Monitor. The GRIMM Monitor collects particle size ranges from 0.25 µm to > 32 µm. For the purposes of this study, the 'coarse' fraction between 1 and 10 µm was considered to be the PM_{10} fraction, similar to the approach taken by Ojelede et al. (2012). **Figure 4-36A** shows that at the DRD TSF, the 24 h National Ambient PM_{10} Standard of 75 $\mu g/m^3$ was exceeded, up to four times. Using the weather data collected by the climate sensors of the GRIMM Environmental Dust Monitor **(Figure 4-36B)**, it was possible to determine whether TSF emissions could have contributed to these dust exceedances, hereafter referred to as dust events, in addition to other unavoidable dust sources such as domestic burning, vehicle emissions and regional industrial pollutants. For example, the first dust event reaching peaks of 707 and 509 $\mu g/m^3$ occurred on 7 and 8 October 2012 **(Figure 4-36A)**. According to the wind direction, speed and frequency data recorded on these days **(Figure 4-36B)**, approximately 40% of winds higher than 3 m/s came from the northerly direction. As the dust monitor was located south of the TSF (refer back to **Figure 3-22A**), it is possible that TSF emissions could have contributed to this dust event. TSF emissions could also have contributed to the second dust event on 17 October 2012, which reached a peak of 331 $\mu g/m^3$ **(Figure 4-36A)** as northerly winds above 3 m/s were recorded **(Figure 4-36B)**. However, winds from the south may have also resulted in other dust sources south of the dust monitor to contribute to the dust event. The third dust event reaching a peak of 171 $\mu g/m^3$, occurred on 19 October 2012 **(Figure 4-36A)**, and could also have been the result of dust emissions from the TSF as a large percentage of high winds from the NW and NNW directions were recorded **(Figure 4-36B)**. It should be noted that the peak of this dust event is evidently lower than the first two dust events **(Figure 4-36A)**, and could be explained by the

precipitation recorded (approximately 55.4 mm) during sampling of the third dust event which, expectedly, lowered ambient dust pollution. Similarly, the fourth dust event recorded on 25 October, and reaching 117 µg/m³ **(Figure 4-36A)**, was possibly due to the contribution of TSF emissions based on the wind direction data recorded **(Figure 4-36B)**, however, high precipitation (approximately 100.1 mm) prevented this dust event from reaching a high peak (Andraos et al., 2018a).

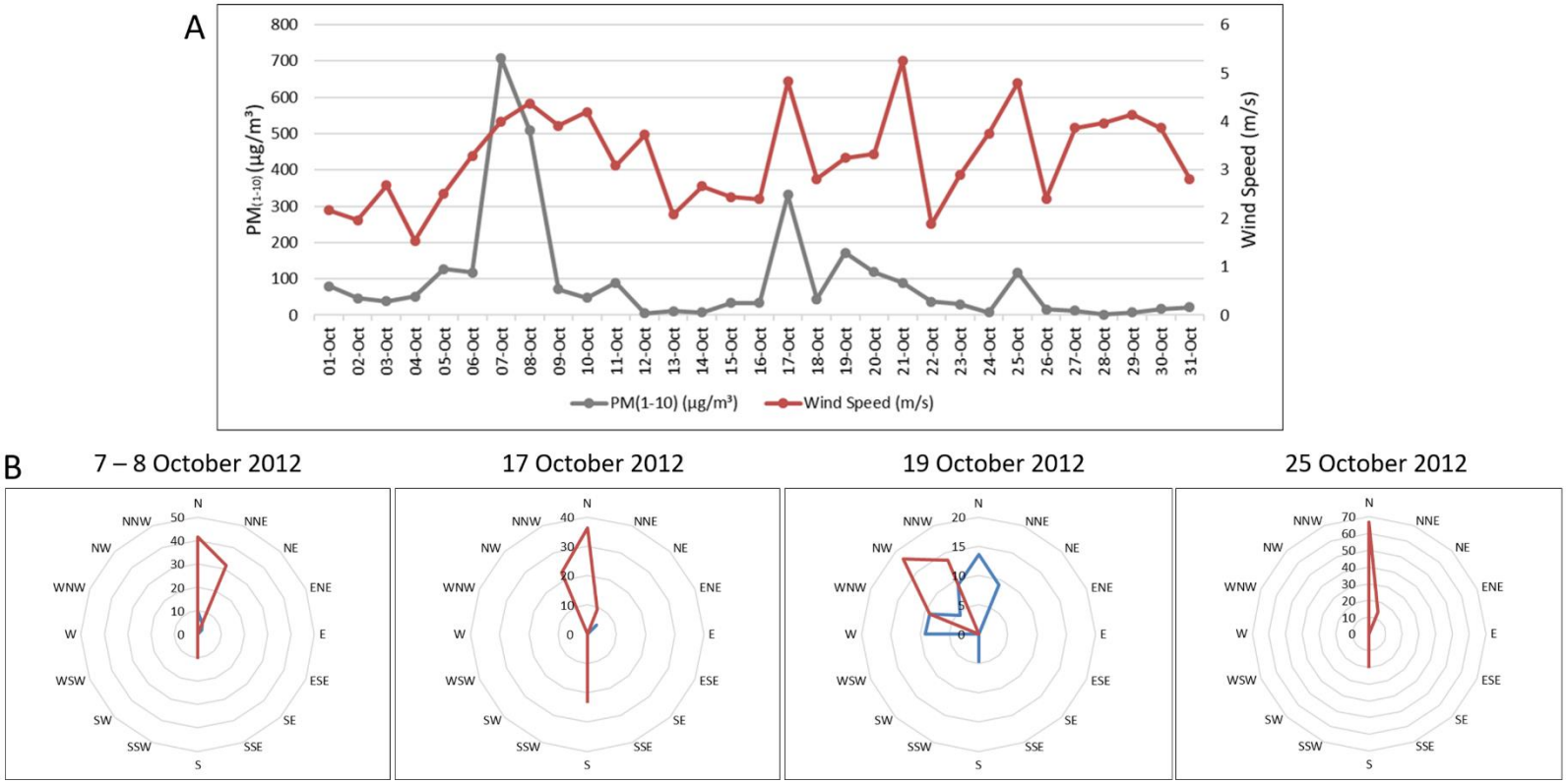

Figure 4-36: Dust events recorded at DRD. (A) Daily averages of mass concentrations of $PM_{(1-10)}$ as well as daily average wind speeds recorded between 1 October 2012 and 31 October 2012 at DRD; (B) Wind parameters, i.e. wind direction, speed and frequency, on the days when high dust events were recorded as indicated in (A). Red indicates wind speeds higher than 3 m/s while blue indicates wind speeds lower than 3 m/s. The length of the spokes indicates the frequency in percentage with which the wind blew from a particular direction during the time period from 2 am to 11 pm. Obtained from Andraos et al. (2018a).

For the CGR TSF the ambient PM_{10} Standard was exceeded three times during the sampling period **(Figure 4-37A)**. The first dust event peaking at 165 µg/m³ occurred on 23 September 2011 **(Figure 4-37A)**. The majority of the winds on this day were less than 3 m/s with a small percentage of high winds coming from the southerly direction **(Figure 4-37B)**. The dust monitor was located southwest from the TSF **(Figure 3-22B)**, therefore the source of this dust event excluded emissions from the TSF. The second dust event, which peaked at 225 µg/m³ on 30 September 2011 **(Figure 4-37B)**, may have possibly been the result of TSF emissions as the majority of high winds came from a NNE direction **(Figure 4-37B)**. The source of the major dust event on 19 October 2011, peaking at 352 µg/m³ **(Figure 4-37B)**, could not have been caused by TSF emissions as the majority of high winds came from a NW direction **(Figure 4-37B)** (Andraos et al., 2018a).

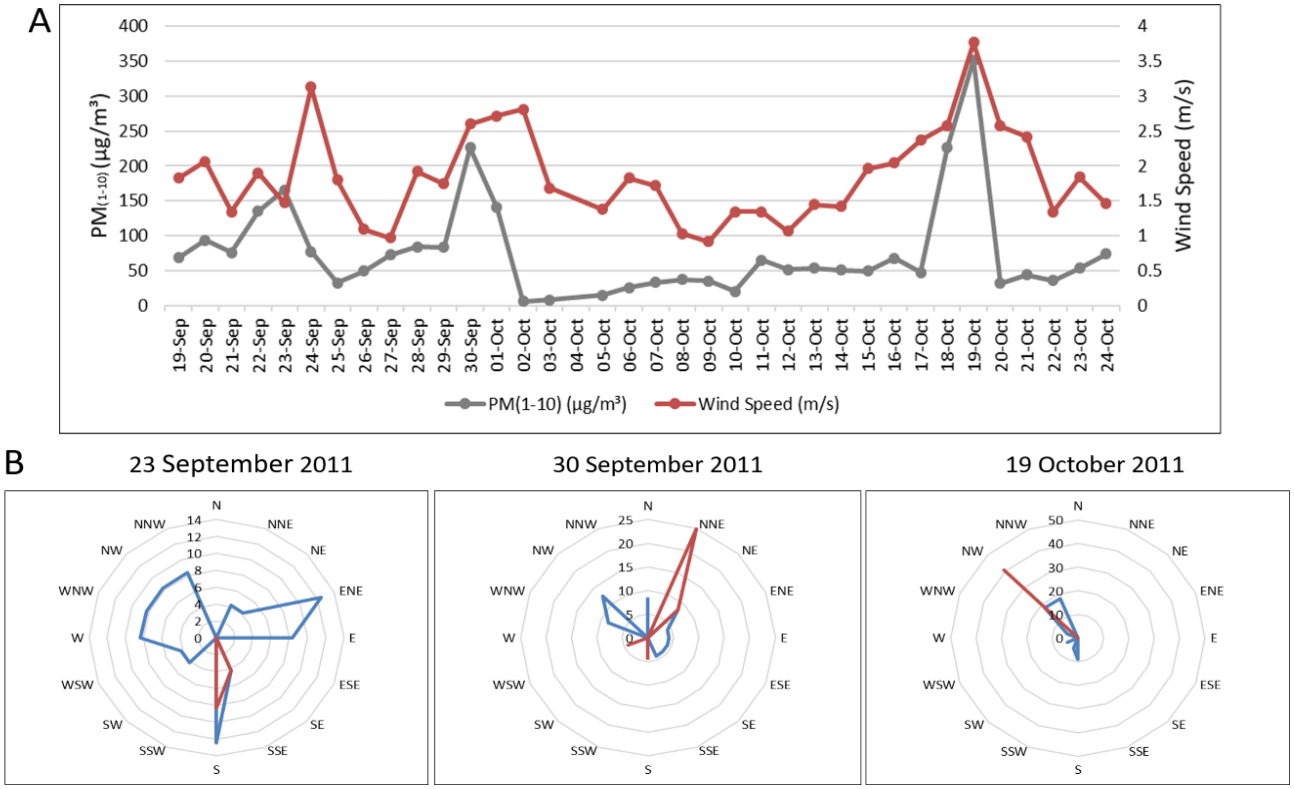

Figure 4-37: Dust events recorded at CGR. (A) Daily averages of mass concentrations of $PM_{(1-10)}$ as well as daily average wind speeds recorded between 19 September 2011 and 24 October 2011 at the CGR TSF; (B) Wind parameters, i.e. wind direction, speed and frequency, on the days when high dust events were recorded as indicated in (A). Red indicates wind speeds higher than 3 m/s while blue indicates wind speeds lower than 3 m/s. The length of the spokes indicates the frequency in percentage with which the wind blew from a particular direction during the time period from 2 am to 11 pm.

Obtained from Andraos et al. (2018a).

For the ERPM TSF, four major dust events exceeding the ambient PM_{10} Standard during the sampling period were recorded on 10, 13, 24 and 27 October 2010 **(Figure 4-38A)**. Wind data showed, however, that emissions from the TSF could not have contributed to these high dust events as northerly winds were not recorded (**Figure 4-38**B). Therefore, deposition of TSF emissions to the south of the TSF where the monitor was located **(Figure 3-22C)** was unlikely (Andraos et al., 2018a). It should be mentioned that even though the contribution of tailings dusts to these dust storm events were unlikely, it is possible that previously deposited tailings dust from the ERPM TSF could have been re-aerosolised by local winds.

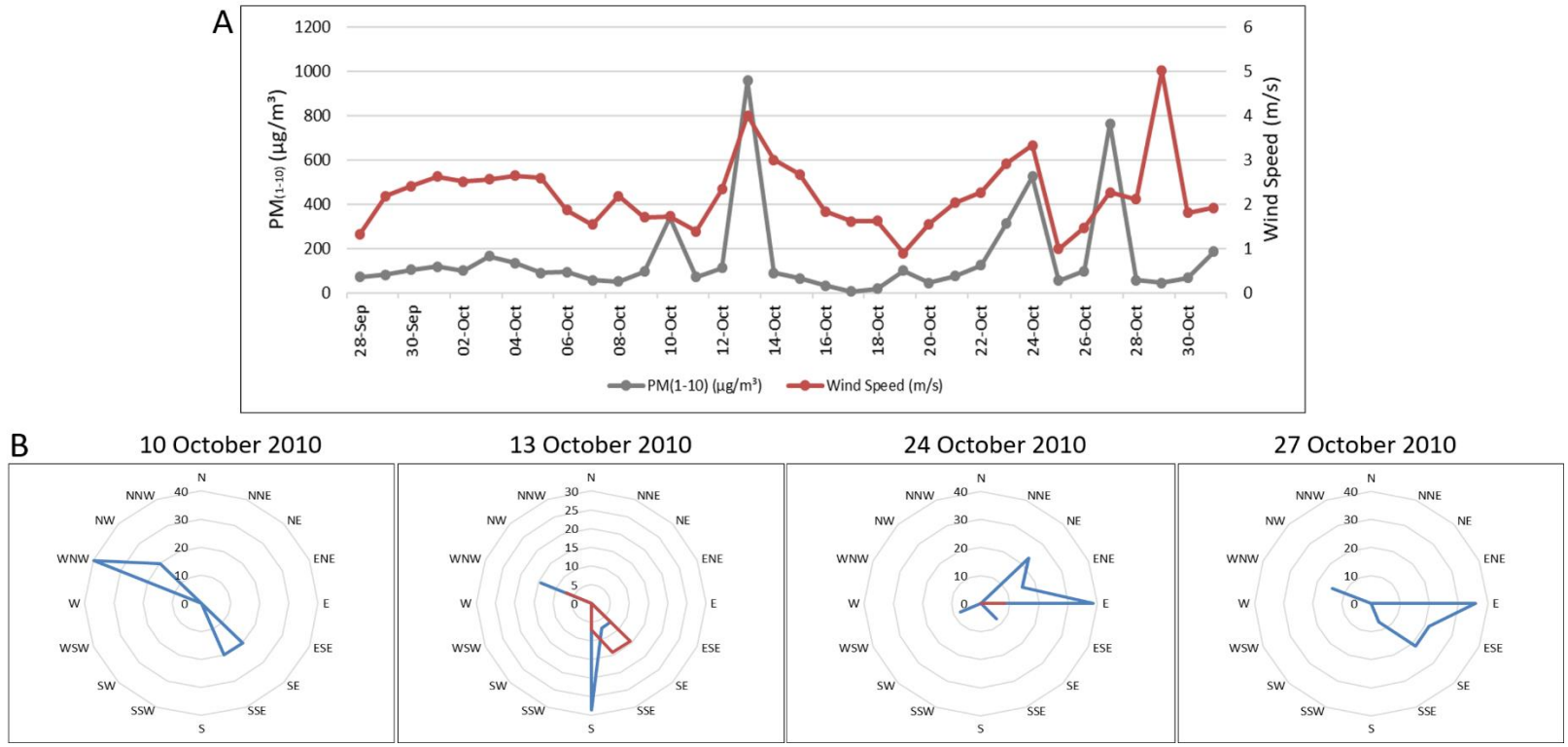

Figure 4-38: Dust events recorded at ERPM. (A) Daily averages of mass concentrations of $PM_{(1-10)}$ as well as daily average wind speeds recorded between 28 September 2010 and 31 October 2010 at the ERPM TSF; (B) Wind parameters, i.e. wind direction, speed and frequency, on the days when high dust events were recorded as indicated in (A). Red indicates wind speeds higher than 3 m/s while blue indicates wind speeds lower than 3 m/s. The length of the spokes indicates the frequency in percentage with which the wind blew from a particular direction during the time period from 2 am to 11 pm. Obtained from Andraos et al. (2018a).

4.2.2.Ambient PM_{10} collected at DRD, CGR and ERPM

PM_{10} were collected on filters in conjunction with the continuous real-time ambient PM_{10} readings. The 24 h PM_{10} levels calculated from the filters collected at the DRD sampling site reached a minimum and maximum of 245.80 and 331.80 µg/m³, respectively, while that at the CGR and ERPM sites reached minimums and maximums of 131.30 to 213.70 µg/m³ and 119.90 to 250.50 µg/m³, respectively **(Table 4-11)**.

Table 4-11: PM_{10} levels, crystalline silica levels and silica percentages calculated from the PM_{10} dust collected on filters at DRD, CGR and ERPM.

Concentration	TSF	n*	Median	Range	
				Min	Max
PM_{10} (µg/m³)	DRD	12	300.05	245.80	331.80
	CGR	6	173.05	131.30	213.70
	ERPM	4	142.50	119.90	250.50
Silica (µg/m³)	DRD	11	6.95	4.63	90.28
	CGR	1	6.02	6.02	6.02
	ERPM	3	6.02	5.09	74.54
Silica percentage	DRD	11	2.93	1.53	28.71
	CGR	1	2.99	2.99	2.99
	ERPM	3	2.40	2.09	62.17

The median values of the crystalline silica levels from PM_{10} were around 6 µg/m³ for all three sampling sites; however, very high maximums of 90.28 µg/m³ and 74.54 µg/m³ were recorded at the DRD and ERPM sites **(Table 4-11)** also signifying extreme dust events. As mentioned earlier **(Section 2.6.3, Silica)**, South Africa has not as yet set an interim limit for non-occupational crystalline silica, therefore international PM_{10} silica limits were used in this study as points of reference. Accordingly, the ambient PM_{10} crystalline silica levels presented in **Table 4-11** have exceeded the current international interim limit of 5 µg/m³ (EPA, 1996). With regards to the silica percentage of dust collected on the filters, maximums of 62.17% and 28.71% at the ERPM and DRD sites were observed while that at the CGR site was much lower (2.99%). These low silica percentages (apart from the 62.17% observed at ERPM) could indicate that the PM_{10} collected at these sites could not solely have originated from TSFs since the silica percentage in the bulk tailings dust was recorded to be much higher (~ 70 – 80%, **Table 4-5**).

The high PM_{10} levels in surrounding communities of DRD, CGR and ERPM justified the additional monitoring of respirable PM_4 levels in the surrounding communities of all five TSFs, as discussed below.

4.2.3. PM_4 collected on personal filters at DRD, CGR, ERPM, ERGO and AGA

4.2.3.1. October 2012 vs. August/September 2013

Since dust exposure is highly dependent on environmental parameters, it was decided to compare the PM_4 levels (8 h TWA) from learners sampled during October 2012 with those sampled during August/September 2013. As expected, **Figure 4-39** shows a significantly higher level of 8 h TWA PM_4 during August/September 2013 compared to October 2012 ($P < 0.001$), which is indeed a result of the lower precipitation levels, higher wind speeds and lower humidity levels as compared to October 2012 **(Table 4-12)**. For this reason, the period of October 2012 and August/September 2013 will hereafter be referred to as the wet and dry seasons, respectively (Andraos et al., 2018a). It is clear from these results that the dust levels recorded during the wet and dry seasons differ remarkably and should be taken into account when future sampling campaigns are planned. The PM_4 levels, stratified by TSF from each season, were further analysed, as discussed below.

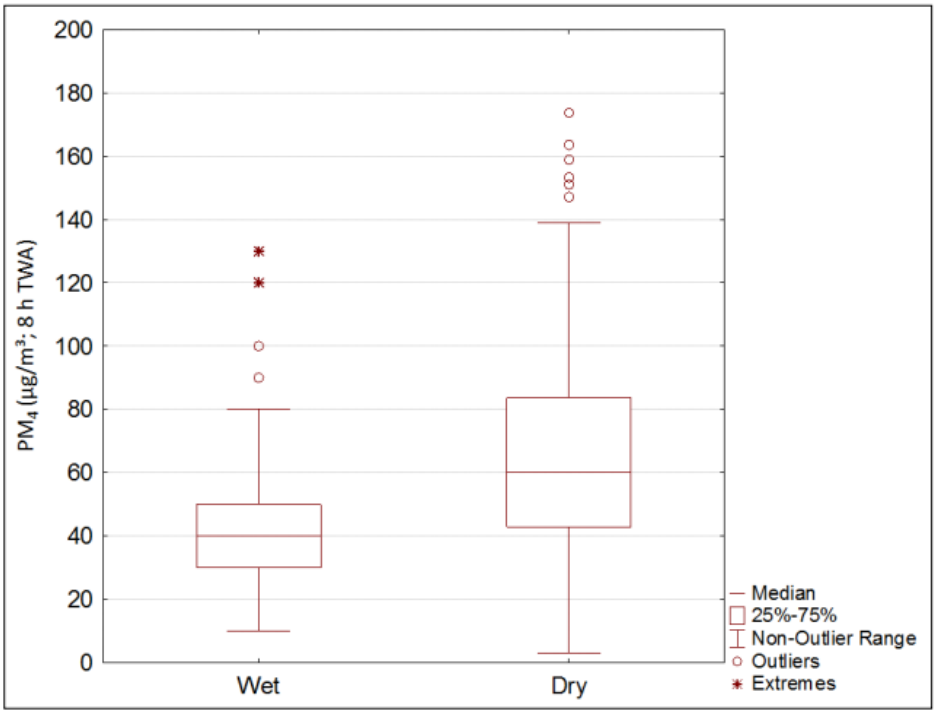

Figure 4-39: Personal PM_4 levels during the wet and dry seasons. PM_4 levels are represented as the TWA for an 8 h period at all the sites combined. The PM_4 levels recorded in the dry season were significantly higher than those recorded during the wet season ($P < 0.001$). Obtained from Andraos et al. (2018a).

Table 4-12: Weather parameters during the wet and dry seasons. Obtained from Andraos et al. (2018a).

Weather parameters	Wet season (October 2012)	Dry season (August/September 2013)
Average precipitation (mm)	1.88 ± 7.73	0.008 ± 0.06
Total precipitation (mm)	116.26	1.52
Minimum precipitation (mm)	0.25	0.25
Maximum precipitation (mm)	52.6	0.51
Number of rain days	11	4
Temperature (°C)	24.17 ± 4.78	23.54 ± 3.97
Wind speed (m/s)	1.49 ± 1.27	2.0 ± 1.44
Relative humidity (%)	45.95 ± 11.66	25.51 ± 6.80

4.2.3.2. PM_4 levels at the TSF sampling sites – Wet season

Figure 4-40 shows the 8 h TWA PM_4 levels calculated from the personal filters obtained from learners at their respective schools during the wet season. The sampling sites that showed the highest levels of PM_4 were DRD 2 **(Figure 4-40A)**, CGR 2 **(Figure 4-40B)**, ERPM 2 **(Figure 4-40C)** and AGA 2 **(Figure 4-40E)** with maximums of 100, 80, 90 and 80 µg/m^3, respectively. For DRD **(Figure 4-40A)** and CGR **(Figure 4-40B)** sampling sites closer to the TSFs showed significantly higher PM_4 levels compared to the sampling sites further away (Andraos et al., 2018a).

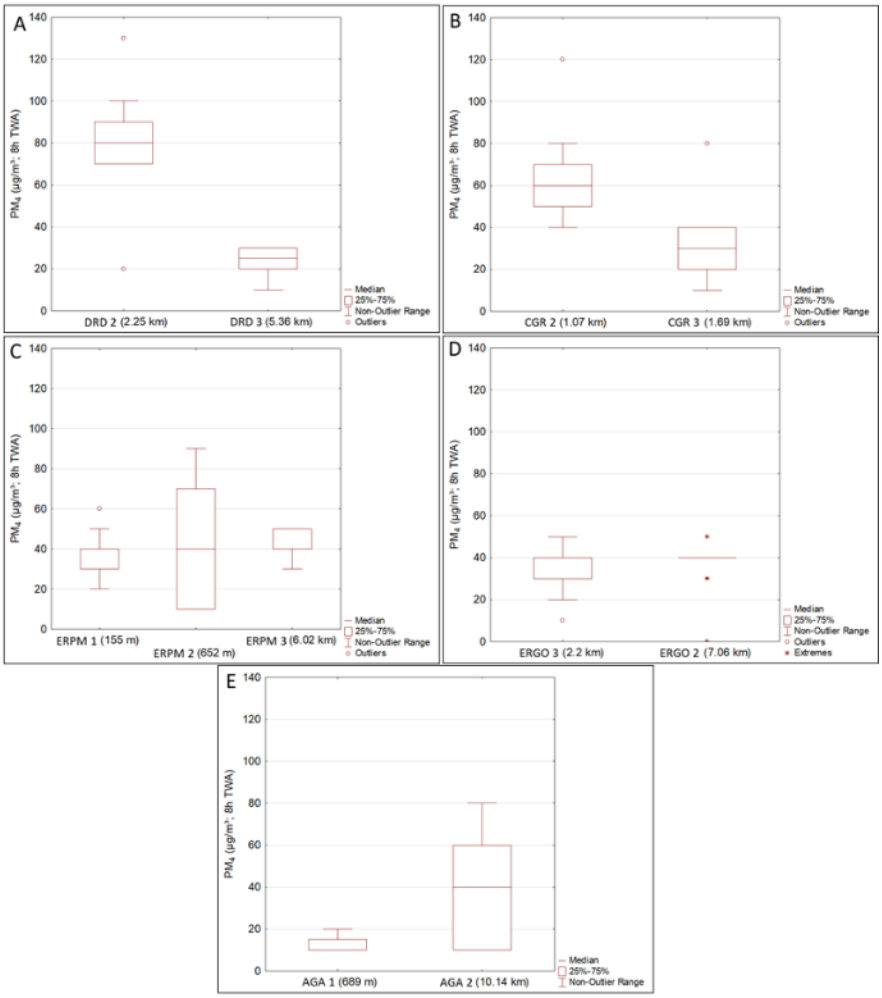

Figure 4-40: Personal PM_4 levels during the wet season stratified per TSF. PM_4 levels are represented as the TWA for an 8 h period. (A) DRD; (B) CGR; (C) ERPM; (D) ERGO and (E) AGA. For A, DRD 2 was significantly higher than DRD 3 (P = 0.010); For B, CGR 2 was significantly higher than CGR 3 (P = 0.003); For E, AGA 2 was significantly higher than AGA 1 (P = 0.005). Obtained from Andraos et al. (2018a).

4.2.3.3. PM_4 levels at the TSF sampling sites – Dry season

Figure 4-41 shows the PM_4 levels at the respective sampling sites during the dry season. For DRD, the site closer to the TSF experienced higher levels of PM_4 compared to the site further from the TSF, similar to what was observed during the wet season **(Figure 4-40A)**. For ERPM **(Figure 4-41C)**, the PM_4 levels recorded at the two sites close to the TSFs (ERPM 1 and 2) were higher than the site that was more than 6 km away (ERPM 3; Andraos et al., 2018a).

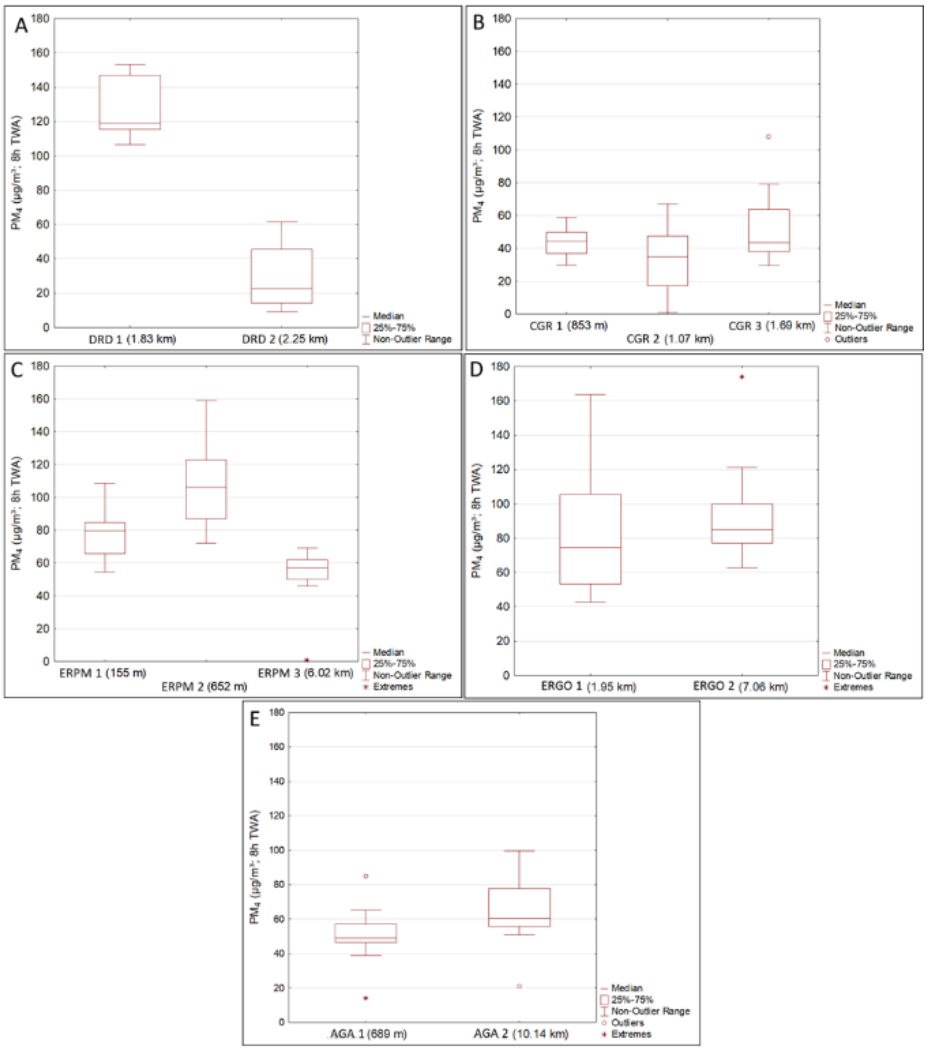

Figure 4-41: Personal PM_4 levels during the dry season stratified per TSF. PM_4 levels are represented as the TWA for an 8 h period. (A) DRD; (B) CGR; (C) ERPM; (D) ERGO and (E) AGA. For A, DRD 2 was significantly lower than DRD 1 ($P < 0.001$) and for C, ERPM 3 was significantly lower than ERPM 2 ($P < 0.001$). Obtained from Andraos et al. (2018a).

There is currently no non-occupational PM_4 limit and it was not possible to compare the PM_4 values obtained in this study to current ambient PM_{10} or $PM_{2.5}$ standards as these standards are based on 24 h time-scales and different particulate size ranges. However, in order to put this study into perspective, it was decided to compare these results to the current South African OEL of respirable PNOC of 3 mg/m^3 (DMR, 2006) and the suggested OEL limit of 1 mg/m^3 (Cherrie et al., 2013). The results show that the PM_4 levels recorded were well below the South African OEL and suggested OEL limit of 1 mg/m^3.

4.2.3.4. Analysis of wind data recorded during PM_4 sampling

Weather data recorded by the Vantage Pro2 monitor were analysed in conjunction with the PM_4 levels in order to determine whether any of the PM_4 levels close to the TSFs could have been the result of dust emitted from the TSFs.

Figure 4-42 shows the wind speeds and directions recorded at DRD 1 on 30 August 2013, at DRD 2 on 8 October 2012 and at DRD 3 on 17 October 2012. The median personal PM_4 levels at these sites are also shown for ease of reference. Note that on these three days, no rain was experienced during the sampling period. It is clear that none of the predominant wind speeds blew in the direction from the TSF to the schools. Even though the wind direction was not from the direction of the TSF, one needs to be mindful of the fact that the TSF could have perhaps contributed via previously deposited tailings dust being re-aerosolised by the movement of many schoolchildren. Indeed, the degree of resuspension of indoor dust by human activity has been shown to play a role in indoor dust concentrations (Thatcher, 1995, Diapouli et al., 2013). The majority of the winds at DRD 1 were above 3 m/s correlating well with the high median PM_4 level of 120 µg/m³, which may also have been the result of other contributing dust sources in addition to perhaps re-aerosolised tailings dusts.

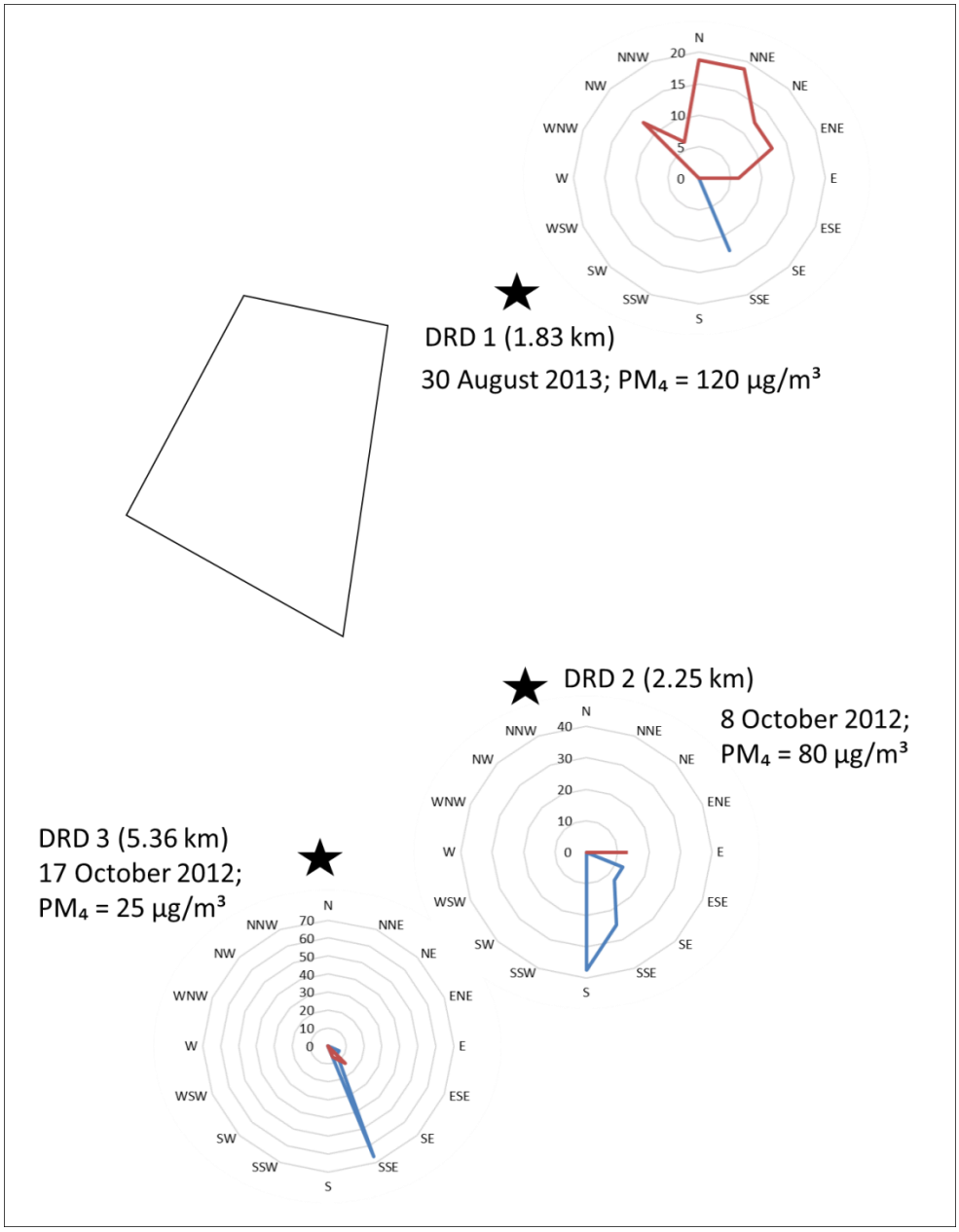

Figure 4-42: Wind parameters recorded at DRD 1 on 30 August 2013, at DRD 2 on 8 October 2012 and at DRD 3 on 17 October 2012. The median PM_4 levels recorded at the respective sampling site and day are also illustrated for ease of reference. Red indicates wind speeds > 3 m/s while blue indicates wind speeds < 3 m/s. The length of the spokes indicates the frequency in percentage with which the wind blew from a particular direction during the sampling period. Note that weather data were not recorded at TSF 1B during August/September 2013 due to faulty sensors on the Vantage Pro2 monitor. Obtained from Andraos et al. (2018a).

Figure 4-43 shows the wind data recorded at CGR 1 on 2 September 2013 and at CGR 3 on 3 September 2013. At CGR 3, approximately 11% of the winds above and below 3 m/s came from the east, thereby suggesting that emissions from the southern deposition pond of the TSF could have contributed to the PM levels at CGR 3 located to the west. Unlike CGR 3, CGR 1 did not appear to be affected by emissions from the TSF based on the wind direction data.

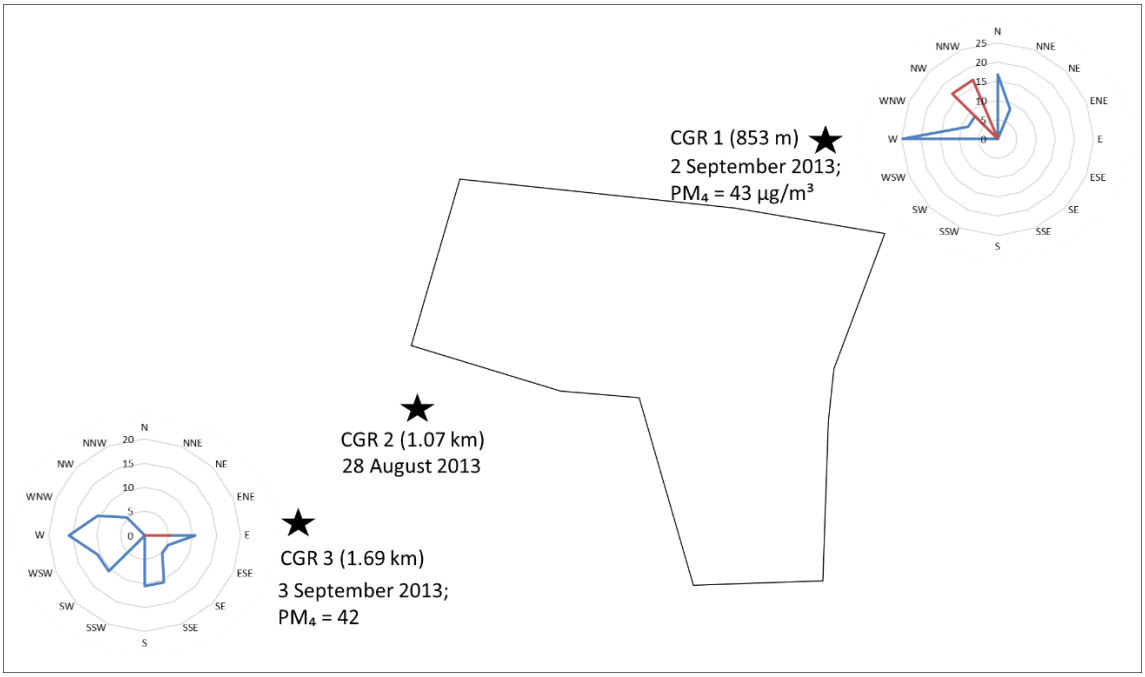

Figure 4-43: Wind parameters recorded at CGR 1 on 2 September 2013 and at CGR 3 on 3 September 2013. The median PM_4 levels recorded at the respective sampling site and day are also illustrated for ease of reference. Red indicates wind speeds > 3 m/s while blue indicates wind speeds < 3 m/s. The length of the spokes indicates the frequency in percentage with which the wind blew from a particular direction during the sampling period. Obtained from Andraos et al. (2018a).

Figure 4-44 shows the wind data recorded at ERPM 1 on 15 October 2012, ERPM 2 on 29 August 2013 and ERPM 3 on 11 October 2012. For ERPM 1, more than 60% of the winds were blowing in the direction from the TSF to the school and even though these winds were < 3 m/s it is possible that TSF emissions could have contributed to the PM_4 levels as this school was merely 155 m from the TSF. For ERPM 2, winds from almost all directions were recorded with

the majority of winds coming from the northerly direction. A small percentage of wind also blew in the direction from the TSF to the school, therefore numerous dust sources including the TSF could have contributed to the PM_4 levels recorded. ERPM 3 was more than 6 km from the TSF and, although approximately 10% of strong wind blew from the TSF to the school, it is unlikely that TSF emissions could have contributed to the PM_4 levels recorded at this school (Andraos et al., 2018a).

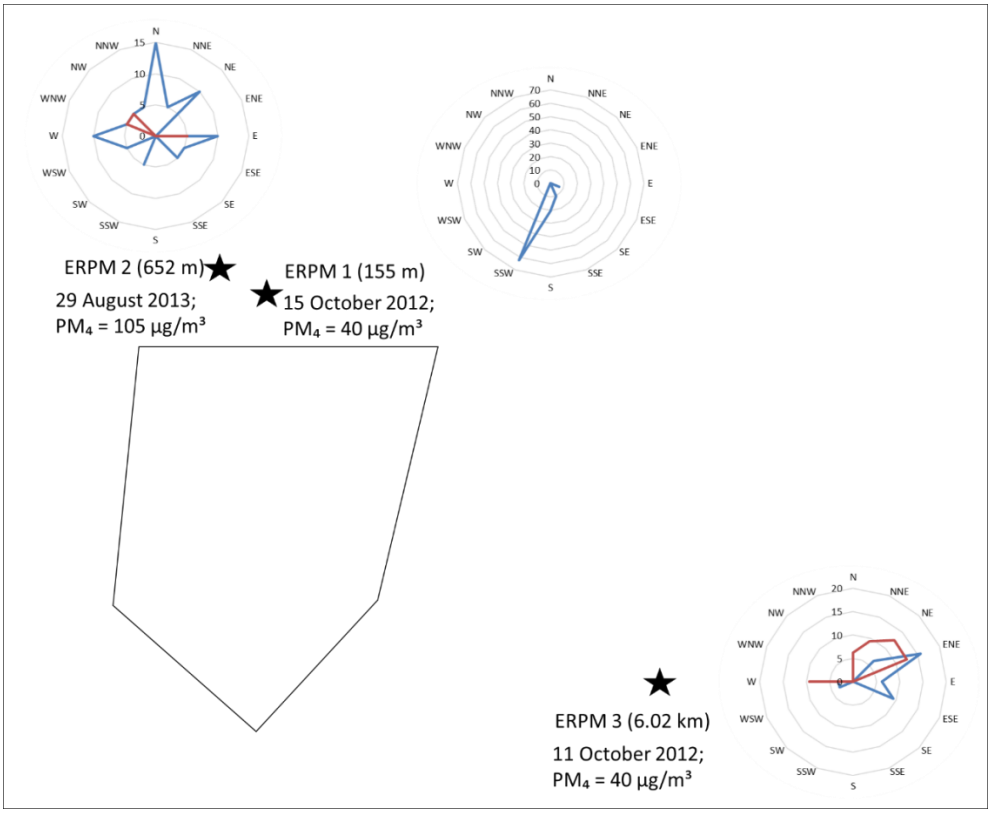

Figure 4-44: Wind parameters recorded at ERPM 1 on 15 October 2012, ERPM 2 on 29 August 2013, and ERPM 3 on 11 October 2012. The median PM_4 levels recorded at the respective sampling site and day are also illustrated for ease of reference. Red indicates wind speeds > 3 m/s while blue indicates wind speeds < 3 m/s. The length of the spokes indicates the frequency in percentage with which the wind blew from a particular direction during the sampling period. Note that weather data were not recorded at TSF 3A during August/September 2013, TSF 3B during October 2012 and TSF 3C during August/September 2013 due to faulty sensors on the Vantage Pro2 monitor. Obtained from Andraos et al. (2018a).

According to **Figure 4-45** it appeared that neither ERGO 1 nor ERGO 2 were affected by possible emissions from the TSF. Although a small percentage of calm winds came from the ESE direction on 16 October 2012, this could not have affected the PM recorded at ERGO 2 as this site was located more than 7 km from the TSF.

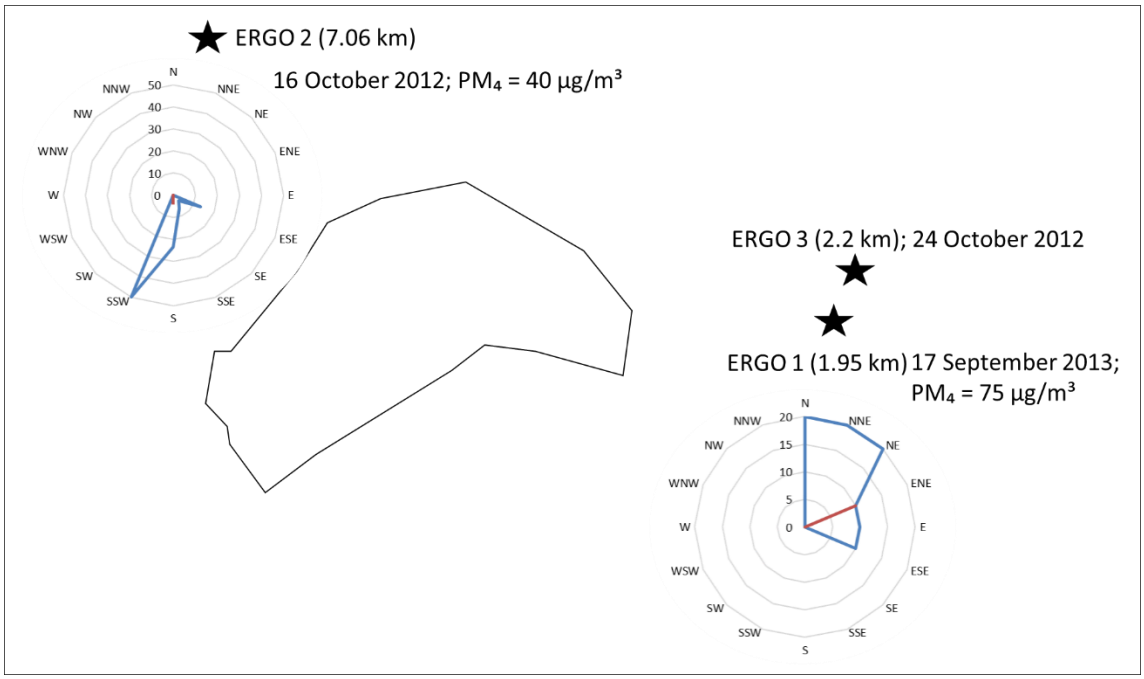

Figure 4-45: Wind parameters recorded at ERGO 1 on 17 September 2013 and at ERGO 2 on 16 October 2012. The median PM_4 levels recorded at the respective sampling site and day are also illustrated for ease of reference. Red indicates wind speeds > 3 m/s while blue indicates wind speeds < 3 m/s. The length of the spokes indicates the frequency in percentage with which the wind blew from a particular direction during the sampling period. Obtained from Andraos et al. (2018a).

Figure 4-46 shows that the emissions from the AGA TSF could have contributed to the PM levels recorded at AGA 1 on 9 September 2013 as wind from all directions were recorded. AGA 2 was located more than 10 km from the TSF and could therefore not have been affected by emissions from the TSF despite winds coming in the direction from the TSF to AGA 2.

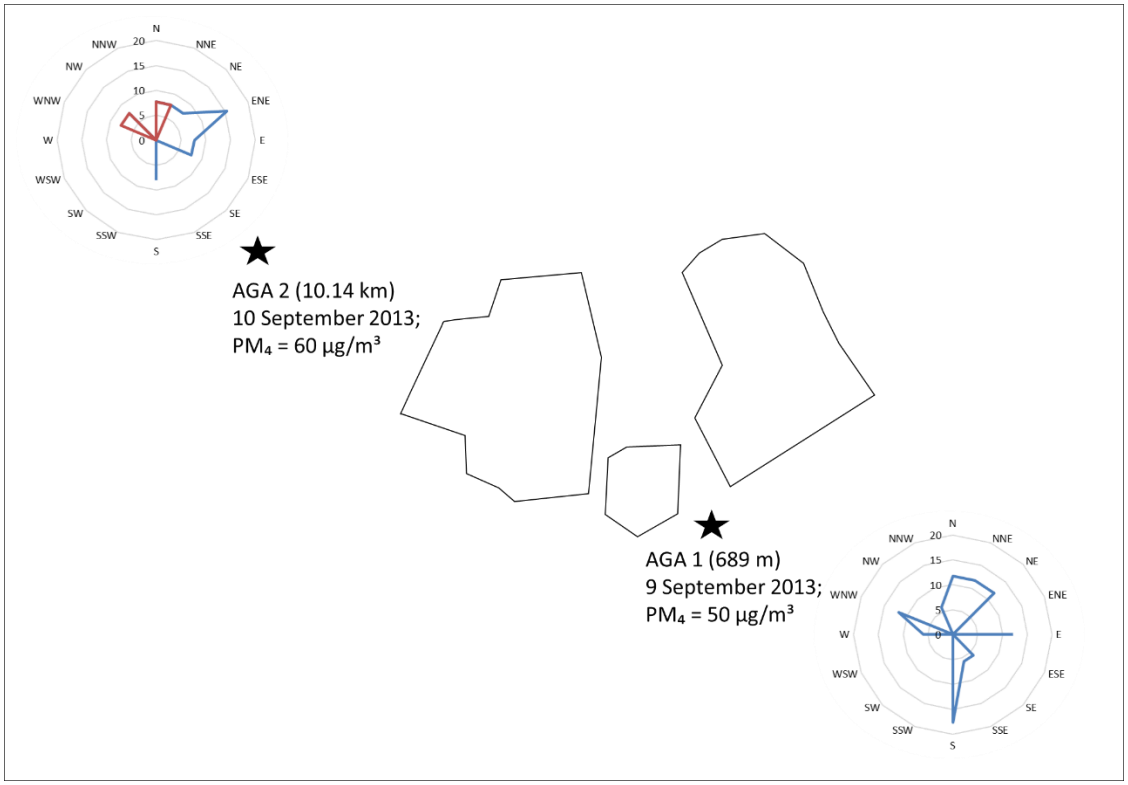

Figure 4-46: Wind parameters recorded at AGA 1 on 9 September 2013 and at AGA 2 on 10 September 2013. The median PM_4 levels recorded at the respective sampling site and day are also illustrated for ease of reference. Red indicates wind speeds > 3 m/s while blue indicates wind speeds < 3 m/s. The length of the spokes indicates the frequency in percentage with which the wind blew from a particular direction during the sampling period. Obtained from Andraos et al. (2018a).

4.2.3.5. RCS levels from PM_4

The RCS levels calculated from almost all of the PM_4 collected on filters during the wet season were below the limit of detection and was therefore not considered further. This was not the case for filters collected during the dry season and were therefore analysed further. The RCS levels from the dry season are shown in **Figure 4-47A**, which varied among the sampling sites. Overall, 78.6% of the filters from all sites combined were below the limit of detection while 19.3% of the filters showed RCS levels between 12 – 28 µg/m³ (for DRD 1, CGR 3, ERPM 1 & 2, ERGO 1 & 2 and AGA 1), therefore exceeding the international RCS interim standard of 3 µg/m^3 (Bridge, 2009, OEHHA, 2005). The highest RCS levels were recorded for three filters from CGR 2, which were 37.2, 37.6 and 50.9 µg/m³, therefore exceeding this limit more than 12, 12 and 16

times, respectively. Since these schools could also be considered an occupational environment for teachers, it was decided to also convert these values to 8-h TWA converted values. The 8-h TWA values **(Figure 4-47B)** showed levels of 8.3 – 17.6 µg/m³ for DRD 1, CGR 3, ERPM 1 & 2, ERGO 1 & 2, and AGA 1, which was below the OELs for RCS set at 25 µg/m³ by ACGIH and 50 µg/m³ by OSHA (OSHA, 2017b). However, the three filters from CGR 2 showed levels of 23.4, 23.8 and 29.1 µg/m³, respectively, with the first two filters almost approaching the ACGIH limit of 25 µg/m³ and the third filter exceeding this limit (Andraos et al., 2018b). When comparing these RCS values to other RCS values recorded at school-based occupational settings, only one other study comparable to ours was found (Fechser et al., 2014). The difference however was in the method of sampling where in the latter work, the recorded 8 h TWA RCS levels were based on area sampling while in the present study it was based, for the first time, on personal sampling. Fechser et al. (2014) recorded 8 h TWA RCS levels at eleven high school ceramics classrooms located in Salt Lake County, Utah, USA, and found that two classrooms and one kiln had silica concentrations above the ACGIH limit of 25 µg/m³ at 43 and 74 µg/m³ in the classrooms and 39 µg/m³ at the kiln.

For RCS percentages in these personal filter samples **(Figure 4-47C)**, 33.8% of the filters showed values between 10.2 and 32.9%, while 3.4% of the filters showed RCS percentages between 38.5 and 72.9% (for DRD 1 and CGR 2). When these RCS percentages were compared to that of Hnizdo and Sluis-Cremer (1993) (30%) and Churchyard et al. (2004) (12 - 16%, at goldmining company in the North-West Province), approximately a third of the filters from the present study coincided with these published values. It is evident that CGR 2 exhibited the highest level of RCS as well as RCS percentages compared to the other sampling sites (Andraos et al., 2018b).

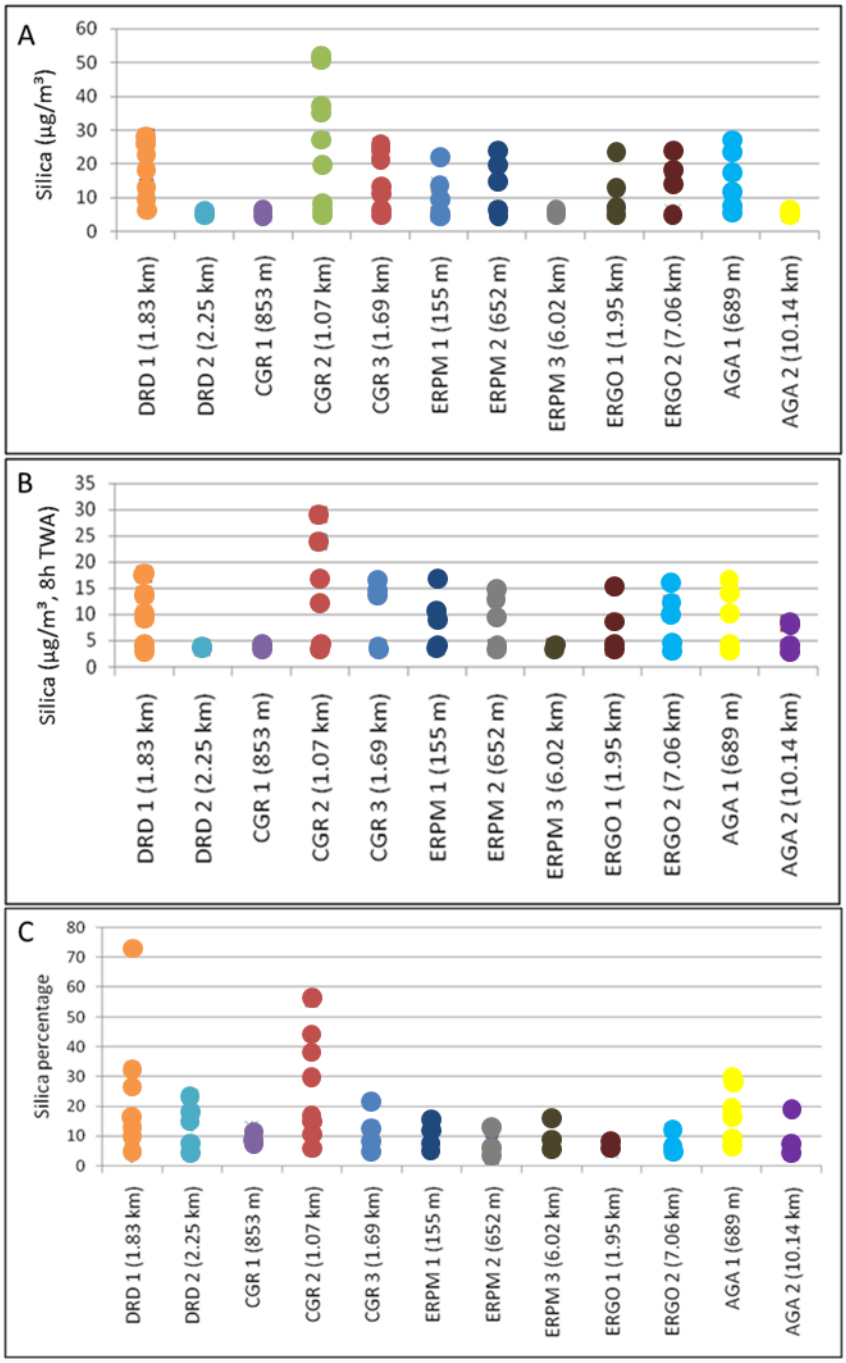

Figure 4-47: RCS levels calculated from PM_4 collected on personal filters. (A) RCS levels; (B) 8 h TWA RCS levels and (C) silica percentages. For illustrative purposes, filters with RCS levels below the detection limit are shown at values half the detection limit. Adapted from Andraos et al. (2018b).

The results from **Figure 4-47B** were further stratified according to the different TSFs **(Figure 4-48)** in order to determine whether sampling sites closer to the TSFs showed higher RCS levels compared to the sampling sites further away. For DRD **(Figure 4-48A)**, ERPM **(Figure 4-48C)** and AGA **(Figure 4-48E)**, sampling sites closer to the TSFs showed higher RCS levels compared to the sampling sites further away, possibly indicating a trend. These results were also reflected with the RCS percentage, which showed higher RCS percentages at sampling sites close to DRD, ERPM and AGA, compared to those further away (results not shown) (Andraos et al., 2018b).

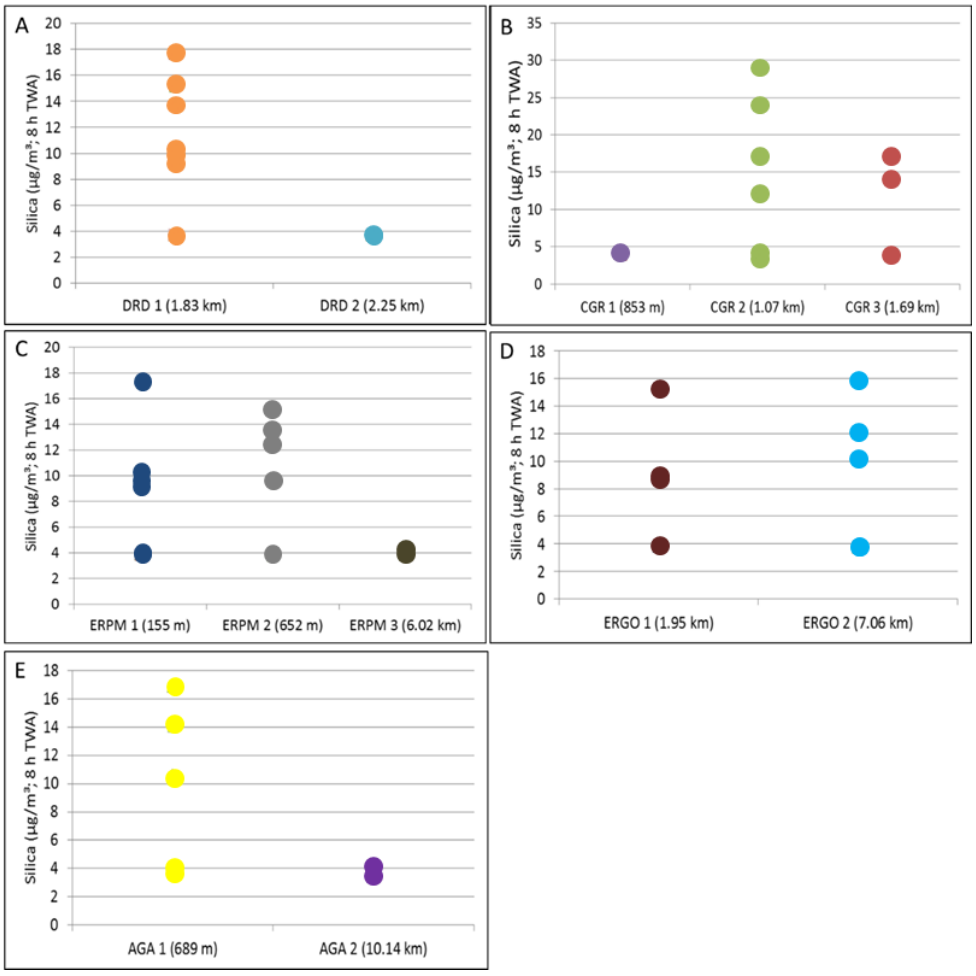

Figure 4-48: RCS levels calculated from PM_4 collected on personal filters stratified by TSF. (A) DRD; (B) CGR; (C) ERPM; (D) ERGO and (E) AGA. For illustrative purposes, filters with RCS levels below the detection limit are shown at values half the detection limit, i.e. below 5 µg/m³ in the figure. Adapted from Andraos et al. (2018b).

4.3. RISK CHARACTERISATION

Due to the high RCS levels recorded during the dry season, it was decided to assess the potential non-cancer and cancer risks according to two possible scenarios: For scenario 1, the worst-case was anticipated i.e. exposure during the whole year (EF = 365 days) whereas for scenario 2, exposure only on dry, windy days was anticipated.

For both scenarios, all HQ values were well above 1 indicating that all areas, irrespective of distance from the TSFs, carry the potential for developing non-cancer adverse health effects **(Table 4-13)**. The greater the HQ value the greater the level of concern (Kolluru, 1996), therefore it appears as if individuals at the CGR 2 sampling site, carry the highest risk of developing non-cancer adverse health effects based on its high HQ (scenario 1 = 11.6; scenario 2 = 9.4), which was a result of its high RCS levels and RCS percentages **(Figure 4-48)** (Andraos et al., 2018b).

Table 4-13: Potential non-cancer and cancer risk from exposure to RCS. Adapted from Andraos et al. (2018b).

Sampling site	Distance from TSF	RCS concentration (µg/m³)[a]	Scenario 1			Scenario 2		
			EF	Non-cancer risk (HQ)	Cancer risk[b] per 1000 individuals	EF[c]	Non-cancer risk (HQ)	Cancer risk[b] per 1000 individuals
DRD 1	1.83 km	23.7	365	7.9	1.61	267	5.8	1.18
DRD 2	2.25 km	NA[d]	NA[d]	NA[d]	NA[d]	NA[d]	NA[d]	NA[d]
CGR 1	853 m	NA[d]	NA[d]	NA[d]	NA[d]	NA[d]	NA[d]	NA[d]
CGR 2	1.07 km	34.9	365	11.6	2.37	295	9.4	1.92
CGR 3	1.69 km	18.7	365	6.2	1.27	295	5.0	1.03
ERPM 1	155 m	17.4	365	5.8	1.18	291	4.6	0.943
ERPM 2	652 m	22.9	365	7.6	1.56	291	6.1	1.24
ERPM 3	6.02 km	NA[d]	NA[d]	NA[d]	NA[d]	NA[d]	NA[d]	NA[d]
ERGO 1	1.95 km	19.5	365	6.5	1.33	332	5.9	1.21
ERGO 2	7.06 km	20.1	365	6.7	1.37	323	5.9	1.21
AGA 1	689 m	24.2	365	8.1	1.65	290	6.4	1.31
AGA 2	10.14 km	NA[d]	NA[d]	NA[d]	NA[d]	NA[d]	NA[d]	NA[d]

[a] 95th percentile from actual RCS concentrations measured (i.e. not 8 h TWA). Calculated using the Kaplan Meier method (ProUCL statistical software)
[b] IUR = 6.75×10^{-5} µg/m³
[c] EF calculated based on meteorological data
[d] Sampling sites where the RCS levels of all filters collected were BDL were excluded from risk characterisation

For the cancer risk characterisation, OSHA, NIOSH and the US EPA states that cancer risk estimates higher than 1 in 10 000 individuals potentially developing cancer in their lifetime are considered to be of regulatory concern (NIOSH, 2017, EPA, 2018). The results in **Table 4-13** show that for scenario 1, risks ranged between 1.18 individuals per 1000 (for ERPM 1) and 2.37 individuals per 1000 (for CGR 2). For scenario 2, almost similar risks were observed ranging from 0.9 individuals per 1000 for ERPM 1 to 1.92 individuals per 1000 for CGR 2, which is much higher than the regulatory cut-off point suggested by Kolluru (1996) and was therefore unacceptably high (Andraos et al., 2018b).

5. DISCUSSION

There are currently no known studies addressing the possible toxic potential of tailings dusts using *in vitro* methodologies or the possible physicochemical properties of tailings dusts governing toxicity. It was therefore of great interest to investigate such a relationship between the different physicochemical properties of dust collected from TSFs in South Africa and their observed *in vitro* toxicity (i.e. *Hazard Identification*). In addition, proper air quality monitoring systems in the vicinities of populations surrounding TSFs (*Exposure Assessment*) and calculation of risk (*Risk Characterisation*) are also currently limited.

5.1. HAZARD IDENTIFICATION

An important finding of this study revealed that tailings particles from South African gold mine TSFs are indeed toxic to cells derived from the human airway respiratory tract, i.e. BEAS-2B and U937, as determined with *in vitro* toxicological methodologies. Moreover, these *in vitro* toxicities could be ascribed to different physicochemical characteristics, as presented in **Table 5-1** below.

Table 5-1: Trends of the biological activities and physicochemical properties of tailings dusts and the crystalline silica positive control, Min-U-Sil 5. The biological activities i.e. surface activity and toxicity was assessed by the levels of •OH and cell viability, respectively. Numbers in the table indicate median values unless otherwise indicated.

Surface activity[a] 					
In presence of H_2O_2	Min-U-Sil 5 silica control (40 080)	ERGO (29 863) CGR (25 445)		DRD (9 680) ERPM (9 431)	AGA (5 408)
***In vitro* toxicity with BEAS-2B cells[b]** 					
24 h	Min-U-Sil 5 silica control (47.0)	ERGO (40.1)	ERPM (36.4)	DRD (34.0) CGR (33.7)	AGA (32.4)
***In vitro* toxicity with U937 cells[b]**					
24 h	Min-U-Sil 5 silica control (38.0)	ERGO (18.3) DRD (18.1)	ERPM (10.5) CGR (9.5)		AGA (8.9)
Elemental composition 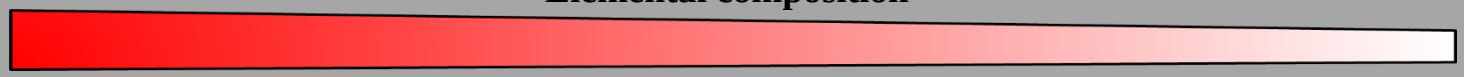					
Surface Fe (%)[c]	ERGO (9.9) (ERGO [e]: 67.8) CGR (6.4)	AGA (2.7)	ERPM (0.7) DRD (0.2)		Min-U-Sil 5 silica control (Not detected)
Fe (mg/kg)[d]	CGR (35 000) ERGO (34 050) (ERGO [e]: 67 500)	ERPM (30 800) DRD (28 600) AGA (27 000)			Min-U-Sil 5 silica control (222)
Cu (mg/kg)[d]	CGR (47.5) AGA (41) (AGA [e]: 126) ERGO (39.7)		ERPM (23.8) DRD (20.9)		Min-U-Sil 5 silica control (1.2)
Cr (mg/kg)[d]	ERPM (493.5) (AGA [e]: 1710) ERGO (408)	AGA (250) CGR (227.5) DRD (170)			Min-U-Sil 5 silica control (1.0)
V (mg/kg)[d]	ERGO (71.0) (ERGO [e]: 199) ERPM (67.0)	CGR (45.5) AGA (40.1) DRD (33.2)			Min-U-Sil 5 silica control (0.3)

Quartz content 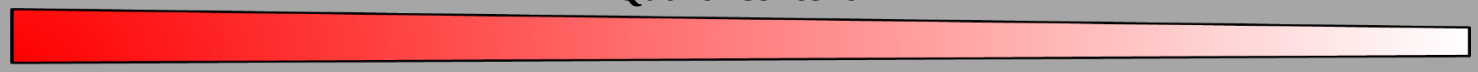				
%[f]	Min-U-Sil 5 silica control (98.7)	DRD (87.7)	CGR (79.1) ERGO (75.7) ERPM (74.8) AGA (74.6)	
Specific surface area 				
m^2/g[g]	Min-U-Sil 5 silica control (5.8) (ERGO [e]: 52.6)	ERPM (5.1) DRD (5.0)	ERGO (4.5)	CGR (3.8) AGA (3.8)
Size 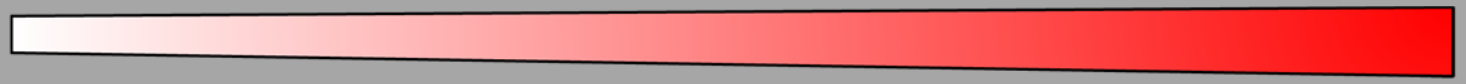				
MMAD and GSD (µm)	Min-U-Sil 5 silica control (1.861 (0.8))	DRD (8.7 (2.0))	CGR (9.3 (1.9)) ERGO (9.4 (1.6)) AGA (9.5 (1.3))	ERPM (12.3 (1.4))
Cellular uptake of particles 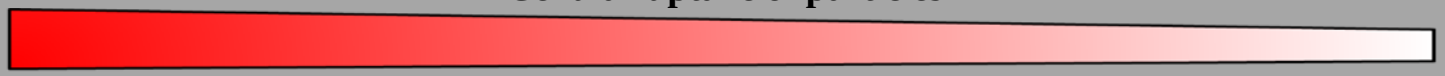				
Uptake with BEAS-2B cells	Min-U-Sil 5 silica control (concentration and time-dependent uptake with large agglomeration formation inside cells)	DRD ERGO ERPM CGR	AGA (majority of particles did not show time- and/or concentration-dependent uptake or agglomeration formation)	
Uptake with U937 cells	Min-U-Sil 5 silica control (concentration and time-dependent uptake with large agglomeration formation inside cells)	DRD ERPM ERGO CGR	AGA (majority of particles did not show time- and/or concentration-dependent uptake or agglomeration formation)	

[a] As represented by ESR signal intensity

[b] Treatment concentration of 50 µg/cm²

[b] Values represent average level of toxicity i.e. 100% minus viability % of particle-treated cells

[b] Only the 24 h time point is considered in this table although other time points have been discussed in **Section 4.1.2.2**.
[c] Surface elemental composition – EDX results
[c] Only surface Fe is considered in this table (refer to **Table 4-4** for other surface elements)
[d] Elemental composition as determined with ICP-MS – Redox active Transition elements

[e] TSFs and values indicated in brackets are those TSFs that have exhibited dust samples with the highest maximum values
[f] Determined with XRD
[g] Determined with BET

5.1.1.Oxidative stress in relation to toxicity of dust

The current unifying hypothesis for ambient PM states that their pathogenicity is exerted through their ability to elicit oxidative stress through ROS production in the lung, and, in the case of UFPs, also in other organs. It is shown that the ability of PM to elicit oxidative stress through their surface activity leads to inflammation via a cascade of events including the activation of various transcription factors and production of cytokines (Kelly and Fussell, 2012). Indeed, several researchers have found associations between particle surface activity and toxicity for which the term "ROS hypothesis" was coined. The ROS hypothesis states that the ability of particles to induce ROS formation in abiotic/cell-free environments can predict a particle's toxicity (Øvrevik et al., 2015, Borm et al., 2007). Therefore, higher surface activities result in higher toxicities. Indeed, our results have shown this to be true for our positive control, Min-U-Sil 5, as well as for the ERGO, DRD, and AGA dusts. For example, Min-U-Sil 5 showed the highest surface activity and *in vitro* toxicity in the BEAS-2B cell line while the ERGO dusts showed the second highest surface activity and second highest toxicity **(Table 5-1)**. Similarly, the DRD dusts showed the third lowest surface activity and third lowest toxicity while the AGA dusts exhibited the lowest in both categories **(Table 5-1)**. Similar toxicity was also observed in the U937 cell line where both Min-U-Sil 5 and the ERGO dusts as well as the AGA dusts showed positive associations between surface activity and toxicity, and is therefore in agreement with the ROS hypothesis. It should be noted that the tailings dusts showed an overall lower toxicity in U937 cells than in BEAS-2B cells, which corresponds to the study of Li et al. (2002) concluding that macrophages in general are less sensitive to foreign particle insults than epithelial cells.

It is not surprising that most of the particles studied showed agreement with the ROS hypothesis since this has been observed previously with other environmental PM. For example, Steenhof et al. (2011) observed a significant positive correlation between the surface activities of PM collected at different sites in the Netherlands and their abilities to induce cytotoxicity.

Overall, high ESR signals of all the tailings dusts in the presence of H_2O_2 indicates that the ability of the dusts to produce ROS was perhaps due to a physicochemical property or a combination thereof. Although no studies could be found addressing free radical production of

gold mine tailings particles *per se*, it was expected to see some surface activity as has been observed with most environmental PM. For example, several studies have shown the ability of a variety of particle types such as urban dust, diesel particulate matter, coal fly ash, kaolinite, and silica (Alaghmand and Blough, 2007) as well as with TSP, $PM_{10–2.5}$ and $PM_{2.5}$ (Shi et al., 2003b) to produce free radicals, generally only in the presence and not in the absence of H_2O_2.

The physicochemical characteristics contributing to the surface activities of the tailings particles may include (1) their surface molecular structure and their amenity to fracture and produce ROS in the presence of H_2O_2 or (2) the presence of transition metal ions either in their structure or as adsorbed contaminants. In addition, size and surface area may contribute to enhancing reactive surfaces. For this reason, characteristics such as elemental composition, size, surface area and quartz content of Min-U-Sil 5 and tailings dusts were determined as these characteristics have previously been shown to be major factors contributing to the oxidative-related pathogenicity of environmental dusts (Kelly and Fussell, 2012).

5.1.2. The effect of physicochemical properties on the surface activity of Min-U-Sil 5 and tailings dusts

In **Table 5-1**, it is shown that a number of physicochemical properties of dusts could be correlated to their surface activities, which may include surface molecular structure and transition elemental composition.

5.1.2.1. Surface molecular structure

This mechanism of increased surface activity in relation to toxicity is applicable in the case of crystalline silica and, indeed, our Min-U-Sil 5 crystalline positive control sample showed both the highest surface activity and *in vitro* toxicity. The toxicity of silica was originally believed to be due to its crystallinity alone, therefore not taking into account the combination of the following **'surface'** features that govern surface reactivity:

(1) dangling bonds i.e. unpaired electrons on both silicon and oxygen atoms, which generate surface radicals;

(2) solid-based radicals formed by the fracturing of silica particles i.e. silyl radical (≡Si•) and siloxy radical (≡SiO•) (Pavan and Fubini, 2016, Rimola et al., 2013);
(3) surface ROS i.e. OH•, $O_2^{\bullet-}$ and peroxy radical (−SiO_2•) generated due to solid-based radicals reacting with atmospheric components;
(4) silanol and siloxane groups, the amount of which determines its hydrophobicity (siloxanes) and hydrophilicity (silanols);
(5) surface charges formed by fracturing i.e. silyl cation (≡Si^+), siloxy anion (≡SiO^-) or geminal silanolate (>$Si(O^-)_2$) (Rimola et al., 2013);
(6) the presence of metal ions and impurities (Pavan and Fubini, 2016, Rimola et al., 2013)

The degree to which each of these surface features contribute to toxicity is still unclear. However, it is postulated that a combination of these different **'surface'** features, rather than just only one, contributes to the pathogenesis of silica, each of which is involved in a different event of the mechanism of toxicity (Pavan and Fubini, 2016). Determining which and to what degree each surface feature is involved or contributes to each step in the toxic mechanism of action of silica is complicated by the variability of the silica surfaces as well as by the complexity of cellular models and have therefore not as yet been elucidated (Pavan and Fubini, 2016). Nevertheless, it is proposed that silanol disorganisation on the silica surface is responsible for triggering the inflammatory reaction, one of the initial steps in silica pathogenicity. It is also proposed that variabilities in the distribution of silanol groups on the silica surface **(Figure 5-1)**, which are mostly reactive due to their H-bonding potential with biological molecules, governs the variability of toxicity between different silicas (Dalstein et al., 2017, Pavan and Fubini, 2016).

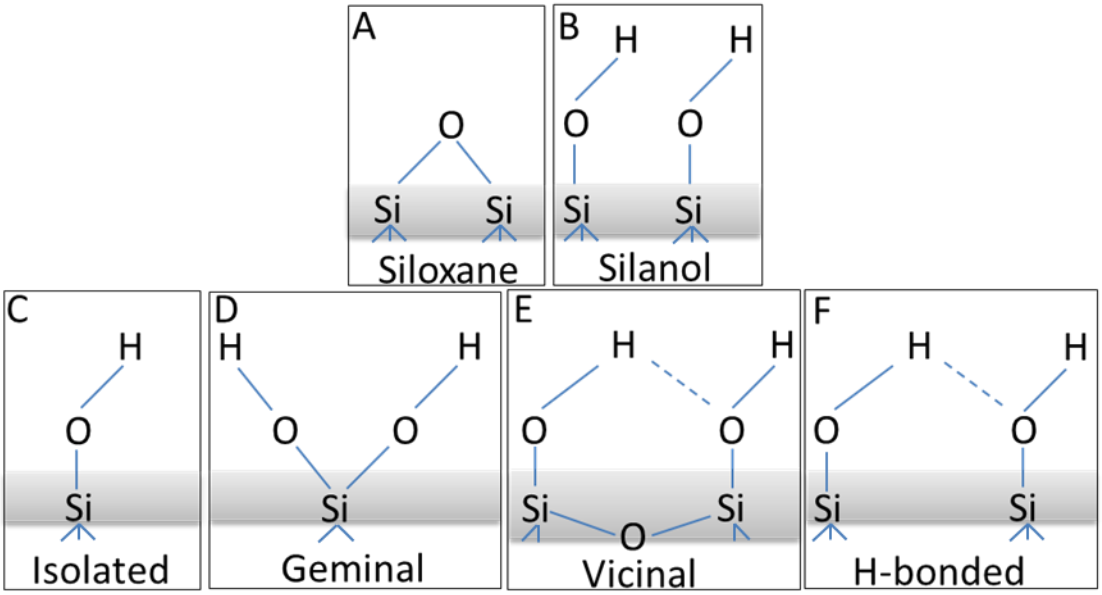

Figure 5-1: Siloxane and silanol groups. (A) Siloxane group; (B) Silanol group; (C) Isolated silanol group; (D) Geminal silanol group; (E) Vicinal silanol group; (F) H-bonded silanol group. Modified from Pavan and Fubini (2016).

It is therefore not surprising that Min-U-Sil 5 showed a high surface activity, which correlated with previous studies showing high ROS generation of Min-U-Sil 5 (Lehman et al., 2016). It is speculated that the toxicity caused by Min-U-Sil 5 in the BEAS-2B and U937 cell lines was due to the initiation of oxidative stress via particle-derived ROS production. This would complement the results of Antognelli et al. (2009), who have also shown high toxicity of Min-U-Sil 5 in the BEAS-2B cell line and have proposed that particle-derived ROS, together with cellular-derived ROS and methylglyoxal-induced ROS, led to an enhanced oxidative stress environment leading to cell toxicity. Due to the high toxicity of Min-U-Sil 5, it was therefore justified to use these silica particles in the present study as a well-characterised positive control as recommended in other in particle toxicity studies (Badding et al., 2014, Sellamuthu et al., 2011, Vuong et al., 2017, Lin et al., 2006, Lehman et al., 2016).

5.1.2.2. Transition elemental composition

The most apparent physicochemical difference between tailings particles and Min-U-Sil 5 is the much higher concentration of various metals in tailings particles compared to that of Min-U-Sil 5 **(Table 5-1)**. Therefore, in the case of tailings dusts, the presence of transition metal ions may be instrumental in producing ROS. For years, it has been suggested that the elemental composition of PM is critical in governing its pathogenic potential. Indeed, several metals bound to PM have been associated with adverse health effects, which are covered in an extensive review by Chen and Lippmann (2009). For example, epidemiological evidence has shown associations between Ni, V, Cu and Pb content of ambient PM and mortality (Lipfert et al., 2006a, Pope III et al., 2007, Schober et al., 2006).

Even though epidemiological evidence suggests a link between PM elemental composition and adverse health effects, it is toxicological studies that provide further mechanistic support to epidemiological evidence thereby strengthening scientific arguments (Kelly and Fussell, 2012). The mechanistic support stems from the notion that particle-bound metals, particularly transition metals such as Fe, may enhance particle surface activity by converting H_2O_2 into highly reactive •OH through the Fenton-reaction, leading to oxidative damage (Dixon and Stockwell, 2014). Downstream consequences involve activation of MAPKs, NLRP3-ASC-caspase 1, tyrosine kinase Src or NF-κB signalling and therefore altered expression of cytokines, chemokines, proinflammatory genes and leukocytes recruitment (Milnerowicz et al., 2015, Samet et al., 1998). The role of transition metals in governing the toxicity of PM by enhancing its surface activity has been well characterised in previous toxicological studies (Boogaard et al., 2012, Steenhof et al., 2011, Jung et al., 2006, Donaldson et al., 1997, Shi et al., 2003b, van Maanen et al., 1999, Godri et al., 2011, Gilmour et al., 1996). For example, Gilmour et al. (1996) showed that the Fe-content from PM_{10} collected from Edinburgh induced DNA damage *in vitro*. Furthermore, Frampton et al. (1999) concluded that transition metal content (Fe, Cu and Zn) is an important determinant of the respiratory health effects of PM_{10} exposure. Residual oil fly ash (ROFA), a transition metal-rich particle, has often been used as a model particle for assessing the adverse effects of transition metals and there is strong evidence that V, Fe and Cu from ROFA particles are able to stimulate pro-inflammatory responses both *in vivo* and *in vitro* (Carter et al., 1997, Dreher et al., 1997, Pritchard et al., 1996).

The *in vitro* toxicological results of the current study could also provide further mechanistic support showing a role of transition elements in the possible toxicity of tailings particles. For example, ERGO dusts, which showed the highest surface activity and toxicity compared to the other tailings dusts, also exhibited the highest levels of the transition element Fe (both total and surface levels as measured with ICP-MS and SEM-EDS, respectively) **(Table 5-1)**. This phenomenon could be specific to certain mining-related particles as Fe was also the main contributor resulting in the high surface activity of coal mine dusts (Vallyathan, 1994, Dalal et al., 1995). From an epidemiological point of view, co-exposure of Fe with silica has been shown to produce mixed dust pneumoconiosis (Nemery, 1990), as mentioned in **Section 2.2.4**, i.e. Fe appears to modify the effect of silica. Therefore, it is proposed that the high Fe content in the silica-containing ERGO dusts could possibly increase its toxicity potential. Not only were the ERGO dusts high in Fe but also in other transition elements known to govern surface activity i.e. Cu, Cr and V **(Table 5-1)**. It is speculated that a combination of these transition elements could contribute to the higher surface activity of the ERGO dusts.

It was noted that the high surface activity of CGR dusts could also have been the result of its high levels of transition elements i.e. Fe and Cu although the surface activity of CGR dusts did not appear to translate to high toxicity in the BEAS-2B or U937 cells, as was found with ERGO dusts **(Table 5-2)**. The concentration of Cu was high in both ERGO and CGR dusts and appears to be a major transition metal governing the surface activities of certain environmental PM. For example, Shi et al. (2003a) and Boogaard et al. (2012) observed the strongest significant positive correlation between surface activity and Cu content of PM fractions from Germany and the Netherlands, respectively. Correspondingly, Shi et al. (2003b) has shown that metal particles coated with Cu^{2+} exhibited a surface activity approximately four to eight times that of particles coated with Fe^{2+}, Fe^{3+}, Ni^{2+}, Zn^{2+}, V^{2+} or V^{5+}.

Even though the elemental composition of the Min-U-Sil 5 particles appeared to be exceptionally low compared to that of the tailings dusts, it should not be disregarded as one of the possible factors contributing to the surface activity of silica. For example, Elias et al. (2002) showed that Min-U-Sil 5 particles exhibited a reduced ability to produce OH• after treatment with the iron chelators ferrozine and desferrioxamine. Therefore, their results suggest that the Fe impurities

present on Min-U-Sil 5 particles, in addition to silanol groups, have the ability to contribute to its surface activity.

5.1.3.The possible effect of the physicochemical properties on the surface activity and the toxicity of tailings dusts

As shown in **Table 5-1**, a number of physicochemical properties were also studied in relation to their toxicity. These have included the quartz content as well as size and surface area.

5.1.3.1. Quartz content

Min-U-Sil 5 is 99% quartz, compared to the tailings dusts and, although this high quartz content could explain the high toxicity of Min-U-Sil 5, it may not be the case as it has been suggested earlier that, unlike surface silanol groups, the crystal structure *per se* is rarely in direct contact with cells and tissues (Pavan and Fubini, 2016, MAK, 2000).

Tailings particles are possibly directly influenced by adsorbed contaminants rather than by surface silanol groups. However, it was still thought necessary to determine if the quartz content of tailings particles could perhaps govern surface activity and toxicity or whether the quartz content of tailings particles is perhaps masked by other properties. The generally high quartz levels of the tailings dusts identified via XRD analysis coincided with other previous studies showing similar levels in various gold mine tailings from the Witwatersrand gold reef (59-83%, Vermeulen (2007); 70-90%, Stanley (1987); 77.7%, Malatse and Ndlovu (2015)) and the Vaal Reef (75.8-88.3%, Von Rahden (1970)). Even though the DRD dusts showed the highest quartz content, compared to the other dusts, it didn't correspond to a high surface activity **(Table 5-1)**. This lack of correlation between quartz and surface activity could be due to the fact that the quartz content is masked by other surface-bound factors possibly in direct contact with cells, as opposed to the quartz crystal structure. Indeed, such lack of association between quartz content and toxicity has also been observed by other investigators (Nij et al., 2002) where it was shown that the binding of trivalent ions such as Al^{3+} or Fe^{3+} could reduce the effects of quartz on cell membranes (Nolan et al. 1981).

5.1.3.2. Size and surface area

Size could also be a possible factor governing toxicity as epidemiological evidence in favour of UFPs leading to adverse health effects have been reported, particularly for respiratory and cardiovascular diseases (Wichmann et al., 2000, Stölzel et al., 2007, Atkinson et al., 2010, Kelly and Fussell, 2012). Toxicological studies have also supported the role of particle size in the pathogenesis of PM and have suggested that the mechanisms by which UFPs induce toxicity is via (1) their large surface areas facilitating adsorption of various organic compounds and metals from the ambient air (Kelly and Fussell, 2012), (2) the direct interaction of their large surface areas with biological systems (Brown et al., 2000), (3) their efficient translocation from the respiratory tract to extra-pulmonary sites e.g. brain and liver (Oberdörster et al., 2004), and lastly (4) their efficient internalisation into cells therefore leading to organelle damage (Kelly and Fussell, 2012).

Compared to the tailings dusts, Min-U-Sil 5 contained the smallest MMAD (1.861 µm), and therefore also the largest surface area (5.8 m^2/g), which corresponded with its high surface activity and high *in vitro* toxicity in both BEAS-2B and U937 cells **(Table 5-1)**. It can therefore be suggested that one of the mechanisms of toxicity for Min-U-Sil 5, apart from its silica functional groups, stems from its large surface area resulting in a higher surface activity as well as toxicity. Compared to Min-U-Sil 5, none of the tailings dusts appeared to lead to toxicity via the same mechanism i.e. small size and large surface area leading to high surface activity and high toxicity. This may be explained by the fact that other characteristics such as elemental composition may play a larger role in producing toxicity of tailings particles. Indeed, ERGO and CGR dusts appeared to exert their surface activity (as well as toxicity in the case of ERGO dusts) possibly via their elemental composition as discussed earlier.

In conclusion, it should be noted that a combination of characteristics, rather than just one, could be governing the toxicity of particles. This is indeed true for Min-U-Sil 5 particles showing numerous characteristics conducive to toxicity i.e. surface functional groups as well as high quartz content, small size and large surface area. The same might be true for tailings particles. For example, **Table 5-1** shows that the DRD dusts exhibited quite a high toxicity in U937 cells, relative to the other dusts, and this could be the due to the fact that the DRD dusts had a high

quartz content, as well as the second lowest MMAD after Min-U-Sil 5 and second largest surface area (together with ERPM). Therefore, a combination of its quartz content, size and surface area could have led to its high toxicity in U937 cells. Similarly, a combination of factors appeared to have resulted in AGA dusts exhibiting the lowest surface activity and toxicity in both BEAS-2B and U937 cells compared to the other tailings dusts i.e. the AGA dusts exhibited the lowest surface area and lowest quartz content as well as lowest Fe and V content. Moreover, the *in vitro* toxicities of four individual dust particles from the ERGO, DRD, ERPM and AGA TSFs could be ascribed to a combination of physicochemical characteristics, which was noted during correlation analysis.

5.1.4.Cell internalisation in relation to toxicity of dusts

As mentioned earlier, smaller particles may easily be internalised by cells thereby causing organelle damage and toxicity. Our results showed that, indeed, smaller particles led to a higher degree of particle uptake when comparing the degree of uptake of the Min-U-Sil 5 particles with that of tailings dusts. For example, Min-U-Sil 5 particles exhibited the smallest MMAD compared to the tailings dusts and also showed the highest concentration- and time-dependent uptake leading to the formation of large agglomerates within both BEAS-2B and U937 cells. Previous studies, for example that of Perkins et al. (2012), have also shown apparent internalisation of crystalline silica particles (2.16 ± 2.00 µm) at 14.71 µg/cm² as well as of amorphous silica particles (3.55 ± 0.45 µm) at 34.1 µg/cm² into BEAS-2B cells after 24 h. Interestingly, the AGA dusts, which showed the lowest toxicity as well as lowest surface area, lowest quartz content and lowest Fe and V content also showed the lowest degree of uptake in both BEAS-2B and U937 cells, when compared to the other tailings dusts **(Table 5-1)**. The low degree of uptake of AGA dusts is therefore yet another possible reason for its low toxicity.

The mechanism of internalisation of UFPs has been suggested to occur via diffusion or adhesive interactions rather than by endocytic processes (Geiser et al., 2005). Consequently, the toxic potential of UFPs is greatly enhanced by their free location and movement within cells as they are not restricted by endocytic vesicles. Their free location within cells thereby was suggested to promote interactions with intracellular proteins and organelles and even nuclear DNA (Geiser et

al., 2005). It is therefore speculated that the internalisation of tailings particles could lead to a higher toxicity based on their mechanism of internalisation.

5.2. EXPOSURE ASSESSMENT

As with *hazard identification* it was important to compare the extent of exposure among the different TSFs (summarised in **Table 5-2**) as it could provide insight into the level of risk potentially experienced by surrounding communities.

Table 5-2: Exposure assessment of the tailings dusts recorded at residential areas and schools surrounding the TSFs.

PM_{10} dust levels	
DRD	Levels exceeded current standard[a] 4 times (707, 331, 171, 117 µg/m^3) during 1 October 2012 and 31 October 2012; Wind data analysis showed that TSF emissions could have contributed to dust events.
CGR	Levels exceeded standard[a] 3 times (165, 225, 352 µg/m^3) during 19 September 2011 and 24 October 2011; wind data analysis showed that TSF emissions could have contributed to dust events
ERPM	Levels exceeded standard[a] 4 times (380, 992, 582, 797 µg/m^3) during 28 September 2010 and 31 October 2010; TSF did not contribute to any of the dust events
PM_{10} silica levels	
DRD	Levels exceeded current standards[b] (range: 4.63 – 90.28 µg/m^3)
CGR	Levels exceeded current standards[b] (6 µg/m^3; one filter)
ERPM	Levels exceeded current standards[b] (range: 5.1 – 74.5 µg/m^3)
PM_4 dust levels[c]; dry season	
ERPM	Wind data analysis showed that TSF emissions could have contributed to higher PM_4 dust levels at schools closer to TSF (range: 55 - 160 µg/m^3) compared to school further away (range: 45 – 70 µg/m^3)
AGA	Wind data analysis showed that TSF emissions could have contributed to PM_4 dust levels at school close to TSF (range: 40 – 65 µg/m^3). However, school further away exhibited higher dust levels (range: 50 – 100 µg/m^3)
CGR	Wind data analysis showed that TSF emissions could have contributed to PM_4 dust levels at one school close to TSF (range: BDL - 70 µg/m^3). However, school further away exhibited similar dust levels (range: 30 – 80 µg/m^3).
ERGO	Wind data analysis showed that TSF emissions could not have contributed to PM_4 levels close to school (range: 40 – 160 µg/m^3). School further away exhibited similar dust levels (range: 60 – 120 µg/m^3)
DRD	Wind data analysis showed that TSF emissions could not have contributed to higher PM_4 dust levels at school closer to TSF (range: 105 – 155 µg/m^3) compared to school further away (range: 10 – 60 µg/m^3)
PM_4 silica levels (RCS); dry season	
CGR	Levels exceeded current standard[d] Silica levels close to TSF: 21 – 52 µg/m^3 Silica levels further away: 10 – 28 µg/m^3

ERPM	Levels exceeded current standard[d] Silica levels close to TSF: 10 – 25 µg/m^3 Silica levels further away: BDL	
AGA	Levels exceeded current standard[d] Silica levels close to TSF: 11 – 28 µg/m^3 Silica levels further away: BDL	
ERGO	Levels exceeded current standard[d] School close to TSF and further away have same silica concentrations (12 – 27 µg/m^3)	
DRD	Levels exceeded current standard[d] Silica levels close to TSF 12 – 28 µg/m^3. Silica levels further away: BDL	
Risk characterisation (based on 90th percentile of RCS; site close to TSF)		
	Non-cancer (HQ[e])	Cancer (in 1000 individuals)
CGR	11.6	2.37
AGA	8.1	1.65
DRD	7.9	1.61
ERPM	7.6	1.56
ERGO	6.5	1.33

[a] 24 h National Ambient PM_{10} Standard of 75 µg/m^3 (DEA, 2009)
[b] Current international interim silica limit of 5 µg/m^3 (EPA, 1996)
[c] No current standard as yet
[d] International PM_4 crystalline silica interim standard of 3 µg/m^3 (OEHHA, 2005, Bridge, 2009)
[e] HQ = Hazard quotient

It can be seen from **Table 5-2** that the continuous real-time ambient PM_{10} levels recorded at the DRD, CGR and ERPM TSFs exceeded the 24 h National Ambient PM_{10} Standard of 75 µg/m^3 four, three and four times, respectively. According to the DEA, this limit should not be exceeded four times within a calendar year (DEA, 2009), which shows the high dust levels experienced within these surrounding communities as this limit was exceeded within a very short period i.e. in as little as approximately one month of sampling. Moreover, it can also be seen that the majority of the crystalline silica levels of the PM_{10} dust calculated from these filters exceeded the current international interim silica limit of 5 µg/m^3 (EPA, 1996). These results suggest that residential areas that are only a few hundred meters from the TSFs are exposed to unacceptably high PM_{10} dust and silica levels (Andraos et al., 2018b).

Analysis of the wind speed and direction recorded during these dust events presented in **Table 5-2** showed that the dust emissions from the DRD and CGR TSFs contributed to the dust events, recorded. Even though the wind analysis suggested that the ERPM TSF could not have contributed to the dust events recorded it should still be borne in mind that re-aerosolisation of previously deposited tailings dust could have been possible. Other unavoidable dust sources such as domestic burning, vehicle emissions and regional industrial pollutants could also have contributed to these dust events and should therefore not be disregarded. From this table, it can be seen that not only were the PM_{10} emissions from the DRD at the surrounding communities high but the PM_{10} silica levels were higher than that of CGR and ERPM. The high PM_{10} exposure near the DRD TSF combined with the higher *in vitro* toxicity of the bulk dusts in the U937 cell line, compared to ERPM and CGR, as discussed earlier, suggests that the dusts from the DRD TSF show high exposure to surrounding communities with high toxicity once inhaled.

The dust emissions from the CGR TSF also contributed to high PM_{10} levels in the residential sites, which was comparable to the PM_{10} levels at the DRD TSF **(Table 5-2)**. However, one important finding of the sampling sites surrounding the CGR TSF is the high RCS levels from the PM_4 recorded, compared to the other sites. Despite these high RCS levels, which clearly exceeded the international PM_4 crystalline silica interim standard of 3 $\mu g/m^3$ (OEHHA, 2005, Bridge, 2009), the CGR bulk dusts did not show high *in vitro* toxicity in both the BEAS-2B and U937 cell lines. It can therefore be concluded that the communities surrounding the CGR TSF may be exposed to high PM_{10} and RCS levels, although this may not necessarily translate into a toxic potential as high as that of DRD dusts.

Unlike the DRD and CGR TSFs, the ERPM TSF did not appear to contribute to the PM_{10} dust levels experienced at the residential site during the recorded dust events **(Table 5-2)**. However, the ERPM TSF did appear to contribute to the higher PM_4 levels at the school close to the TSF, compared to the site further away. Compared to the other tailings dusts, the dusts from the ERPM TSF showed moderate toxicity and it can therefore be concluded that the ERPM dusts showed high PM_4 exposure but a lower toxicity compared to the other tailings dusts. On the contrary, the ERGO dusts showed the highest *in vitro* toxicity due to its high surface activity and elemental composition but did not appear to contribute to the levels of PM_4 and RCS recorded in

its surrounding areas. It can therefore be concluded that, compared to the other TSFs, the ERGO dusts exhibited high hazard but low exposure to surrounding communities. Finally, despite the low *in vitro* toxicity of the AGA dusts compared to the other tailings dusts, the AGA TSF still appeared to contribute to the PM_4 and RCS levels experienced by the school located 689 m from the TSF, based on the analysis of the wind speed and direction recorded on the day of sampling. Therefore, it is suggested that the AGA TSF may have a high exposure but lower toxicity once inhaled.

5.3. RISK CHARACTERISATION

The risk characterisation analysis, based on cancer and non-cancer endpoints, is also presented in **Table 5-2**. Results could show that the CGR dusts exhibited the highest risk, followed by the AGA, DRD, ERPM and lastly ERGO dusts.

The potential risk of cancer and non-cancer endpoints was calculated using the reference interim respirable crystalline silica limit of 3 µg/m^3. As indicated in **Section 2.6.3**, this interim limit was calculated using a typical risk-based approach. For example, an initial benchmark concentration of 9.8 µg/m^3 was calculated by the OEHHA using epidemiological data from white South African miners. The benchmark concentration refers to the dose levels corresponding to specific response levels near the low end of the observable range of the data (EPA, 2012) i.e. health effects at this level of 9.8 µg/m^3 were already expected to be low. In order to derive at a level that is protective to the general population this benchmark concentration was divided further by a factor of 3 to obtain an even lower "safety" level of 3 µg/m^3. It is therefore anticipated that no health effects would or should be recorded at or below this derived safety level. Anything above this safety level carries a potential risk to the general population. The derivation of these "safety" limits are generally derived with the aim of being precautionary, that is, it is better to set a low safety level that is guaranteed to be protective to the general population than to set a higher level at which protection is not guaranteed and at which health effects have already been observed.

To our knowledge, this study is the first to report on cancer and non-cancer risks from RCS levels at sampling sites around TSFs in South Africa. Although the study by Oosthuizen et al. (2015) calculated the non-cancer risks of crystalline silica in a residential area not far from the

DRD TSF and found no possible risks, it should be noted that their risk characterisation was performed on environmental PM_{10} samples (i.e. less representative of actual silica levels possibly deposited in the deeper area of the respiratory system). In addition, the benchmark value used in their study to calculate risks was that of the South African OEL of 100 µg/m³ and not the ambient international interim silica limits (EPA, 1996) as implemented in our study (Andraos et al., 2018b).

A summary of results obtained from the *hazard identification*, *exposure assessment* as well as cancer and non-cancer *risk characterisation* for different TSFs are presented in **Table 5-3** to enable the comparison of the risk they pose to the surrounding communities. Note that these comparisons among the TSFs are purely relative to one another. The DRD and CGR TSFS appear to show high possible health effects relative to the other TSFs.

Table 5-3: Overall risk posed by the different TSFs.

TSF	**Hazard identification (based on *in vitro* toxicity)**	**Exposure assessment**	**Cancer and non-cancer risk characterisation** (note that all TSFs showed high risk, however, the order shown below is based in relation to the other TSFs)	**Comments**
DRD	High (due to toxicity in U937 cells)	High (due to high PM_{10} dust and silica levels)	Median	Possible health effects: High
CGR	Low (showed low toxicity despite having the second highest surface activity and Fe content)	High (due to high RCS levels)	Highest	Possible health effects: High
ERPM	Median	High	Second lowest	Possible health effects: Low
ERGO	High (highest toxicity in both cell lines as well as surface activity)	Low	Lowest	Possible health effects: Low
AGA	Low (lowest toxicity	High	Second highest	Possible

	in both cell lines)			health effects: Median

5.4. Recommendations

Based on the results obtained in this study a few recommendations are proposed:

- **Stricter implementation of rehabilitation strategies is required**

  Several rehabilitation strategies are available as discussed earlier in **Section 2.5.2**. However, despite these different approaches, efficient rehabilitation is complicated by the presence of many ownerless and derelict mines in Gauteng, illegal occupation, poor management of property ownership, insufficient funds and poor communication among provincial and local authorities (GDARD, 2009a, GDARD, 2012) **(Section 2.6.2)**, which need to be addressed first before stricter rehabilitation strategies are implemented.

- **The relevant authorities should consider setting environmental air quality limits for RCS**

  The presence of high levels of RCS in this study suggests that South Africa should consider establishing an environmental RCS exposure limit. Once this limit is set, compliance and monitoring by DEA and GDACE will be crucial to ensure protection of surrounding communities. In addition, strategies should be in place to provide continuous monitoring not only for PM_{10} but also for PM_4 and RCS concentrations once limits have been established.

- **Establishing clear buffer zones is critical in lowering the exposure of communities to dust**

  Kneen et al. (2015) has shown using historical aerial photographs and census data that encroachment of surrounding communities onto land close to TSFs from 1952 to 2011 has increased considerably, despite the current recommended buffer zones of 1000 or 500 m **(Section 2.6.4)**. Our results have revealed that, even if these buffer zones are to be legally enforced, they may still not be protective based on the fact that communities residing as far as 1 and 2 km from the TSFs showed high PM_{10}, PM_4 and RCS levels as well as possible development of non-cancer and cancer adverse health effects. Therefore,

it is recommended that a buffer zone of at least 5 km from these TSFs be established to ensure protection from dust generated from these TSFs. In support of our results, Sutton and Weiersbye (2008) have determined the extent of elemental and mineralogical contamination of surrounding areas by tailings dust using a GIS and an ASTER sensor. They have shown that U-bearing ore that is unique to TSFs was found in a residential area well beyond 3 km of the border of a TSF. Based on their study and our findings, it is concluded that a buffer zone of 5 km should be sufficient to protect surrounding communities from the health hazards posed by these TSFs.

- As the surface activity of Min-U-Sil 5 crystalline silica is probably governed by the variabilities in the distribution of silanol groups it would be worthwhile to identify these active silanol sites using Fourier-transform infrared (FT-IR) spectroscopy and Nuclear Magnetic Resonance (NMR) spectroscopy. Indeed, Pavan and Fubini (2016) have suggested that these analytical methods may become useful tools to predict the toxicity potential of silica dust.

5.5. Limitations of the study

It should be noted that the TSFs studied were not randomly selected and is therefore not representative of all TSFs present in the Gauteng and North-West provinces. Rather, these TSFs were selected due to their lack of proper remediation to adequately prevent dust erosion. In addition, these TSFs were selected due to their large size as larger TSFs are anticipated to have a larger impact on the ambient environment and surrounding populations.

For the PM_4 respirable exposure assessment section of this study, it was impossible to deduce precisely what proportion of the sampling period the learners had spent indoors and what proportion was spent outdoors. In addition, one cannot assume that the respirable indoor dust concentrations were the same as that of outdoors. Therefore, the respirable levels recorded during this study may not be representative of the actual levels during a 24 h period, which was assumed during the risk characterisation calculations.

As stated in Andraos et al. (2018a), “it should be noted that one of the limitations of the exposure assessment study is that each school was analysed once (i.e. one day) per season and may not be representative of what occurs throughout the season. Nevertheless, these results could form the basis for further, more comprehensive investigations”. Furthermore, as stated in Andraos et al. (2018b), “this study did not take into account the synergistic effects from other hazardous elements within the dust or other routes of exposures for silica such as ingestion and skin absorption. Therefore, the results of this study could possibly underestimate the possible risk estimates for surrounding populations, thereby further emphasizing the importance of ambient crystalline silica monitoring and proper dust control measures”.

It has been mentioned earlier that other dust sources such as domestic burning, vehicle emissions and regional industrial pollutants could have contributed to the dust levels recorded during this study (**Sections 4.2.1, 4.2.3.4** and **5.2**). The potential toxicity of these other confounding dust sources has not been assessed in this study, which could very well further underestimate the hazards present in these surrounding communities.

6. CONCLUSION

In conclusion, the results from each objective of this study can be summarised as follows:

- *Hazard Identification* revealed that the tailings dusts from all the TSFs exhibited an inherent *in vitro* toxicity potential, which was possibly governed either by their elemental composition or a combination of other physicochemical properties. For example, the dusts from the ERGO TSF showed the highest surface activity and toxicity, which could have been the result of their high levels of the transition element Fe. In contrast, the toxicity of the dusts from the DRD TSF may have been due to a combination of their quartz content, size and surface area.

- *Exposure Assessment* showed that the ambient PM_{10} levels in surrounding populations exceeded the current South African limit several times during the sampling period. More importantly, wind data analysis showed that the emissions from the DRD and CGR TSFs could have contributed to these dust events. In addition, the RCS levels collected from PM_4 from surrounding communities exceeded the current international interim limits and this study therefore suggests that South Africa should set and monitor its own interim limit.

- *Risk Characterisation* showed the possibility of surrounding communities potentially developing cancer and non-cancer adverse health effects based on the RCS levels recorded in this study, further emphasising the need for proper dust management and continued systematic monitoring.

The results of this study adds to the field of particle toxicology with regards to tailings dusts in that, unlike most studies, it incorporates both *in vitro* toxicity assessment and exposure assessment as well as risk characterisation. Despite the limitations of this study, the results recorded herein could assist future epidemiological studies in finding a possible causal relationship, if any, between tailings dust exposure and the onset of disease.

APPENDIX A: DECLARATION BY STUDENT AND CO-AUTHORS' AGREEMENT FOR PUBLISHED ARTICLES

Declaration: Student's contribution to article(s) and agreement of co-author(s)

I, Charlene Andraos, student number 585802, declare that this Thesis/Dissertation/Research Report is my own work and that I contributed adequately towards research findings published in the article(s) stated below which are included in my Thesis/Dissertation/Research Report.

Signature of Student ..... **Date** 17/1/19

Name of Primary Supervisor...Prof Mary Gulumian.....

Signature of Primary Supervisor ..... **Date** 17 Jan 2019

Agreement by co-authors: By signing this declaration, the co-authors listed below agree to the use of the article(s) by the student as part of his/her Thesis/Dissertation/Research Report. In cases where the student is not the 1st author of a published article, the primary supervisor must explain (under comments) why the student is entitled to use the paper for his/her degree purposes.

Article 1: Title: ... Exceedance of environmental exposure limits to crystalline silica in communities surrounding gold mine tailings storage facilities in South Africa.....

Journal name, year, volume and page numbers: ... Science of The Total Environment, 2018, 619, 504-516.....

Authors	Name	Signature	Date
1st author	Charlene Andraos		17/1/19
2nd author	Dr Wells Utembe		17/1/19
3rd author	Prof Mary Gulumian		17 Jan 2019

Comments by primary supervisor:

.....

.....

Article 2: Title: ... Ambient PM_{10} and respirable dust levels near gold mine tailings storage facilities in South Africa .....

Journal name, year, volume and page numbers: CLEAN–Soil, Air, Water, DOI: 10.1002/clen.201800103.....

Authors	Name	Signature	Date
1st author	Charlene Andraos		17/1/19
2nd author	Mr Kobus Dekker		18/01/2019
3rd author	Prof Mary Gulumian		17 Jan 2019

Comments by primary supervisor:

.....

.....

APPENDIX B: PERMISSION FROM JOURNALS

Copyright Clearance Center RightsLink®

Home | Create Account | Help

Title: Exceedance of environmental exposure limits to crystalline silica in communities surrounding gold mine tailings storage facilities in South Africa

Author: Charlene Andraos,Wells Utembe,Mary Gulumian

Publication: Science of The Total Environment

Publisher: Elsevier

Date: 1 April 2018

LOGIN

If you're a copyright.com user, you can login to RightsLink using your copyright.com credentials.

Already a RightsLink user or want to learn more?

Please note that, as the author of this Elsevier article, you retain the right to include it in a thesis or dissertation, provided it is not published commercially. Permission is not required, but please ensure that you reference the journal as the original source. For more information on this and on your other retained rights, please visit: https://www.elsevier.com/about/our-business/policies/copyright#Author-rights

BACK | CLOSE WINDOW

Title: Ambient PM10 and Respirable Dust Levels Near Gold Mine Tailings Storage Facilities in South Africa

Author: Charlene Andraos, Kobus Dekker, Mary Gulumian

Publication: CLEAN - Soil, Air, Water

Publisher: John Wiley and Sons

Date: Jan 4, 2019

Order Completed

Thank you for your order.

This Agreement between National Institute for Occupational Health -- Charlene Andraos ("You") and John Wiley and Sons ("John Wiley and Sons") consists of your license details and the terms and conditions provided by John Wiley and Sons and Copyright Clearance Center.

Your confirmation email will contain your order number for future reference.

printable details

License Number	4504031019414
License date	Jan 08, 2019
Licensed Content Publisher	John Wiley and Sons
Licensed Content Publication	CLEAN - Soil, Air, Water
Licensed Content Title	Ambient PM10 and Respirable Dust Levels Near Gold Mine Tailings Storage Facilities in South Africa
Licensed Content Author	Charlene Andraos, Kobus Dekker, Mary Gulumian
Licensed Content Date	Jan 4, 2019
Licensed Content Volume	0
Licensed Content Issue	0
Licensed Content Pages	10
Type of use	Dissertation/Thesis
Requestor type	Author of this Wiley article
Format	Print and electronic

Portion	Full article
Will you be translating?	No
Title of your thesis / dissertation	IN VITRO TOXICITY ASSESSMENT OF DUST EMISSIONS FROM FIVE SOUTH AFRICAN GOLD MINE TAILINGS SITES
Expected completion date	Jan 2019
Expected size (number of pages)	294
Requestor Location	National Institute for Occupational Health 25 Hospital Street Constitution Hill Johannesburg Johannesburg, Gauteng 2001 South Africa Attn: Charlene
Publisher Tax ID	EU826007151
Total	0.00 USD

Would you like to purchase the full text of this article? If so, please continue on to the content ordering system located here: Purchase PDF

If you click on the buttons below or close this window, you will not be able to return to the content ordering system.

ORDER MORE CLOSE WINDOW

APPENDIX C: ETHICS CLEARANCE CERTIFICATE

University
of the Witwatersrand,
Johannesburg

Human Research Ethics Committee (Medical)
(formerly Committee for Research on Human Subjects (Medical)

Secretariat: Research Office, Room SH10005, 10th floor, Senate House • Telephone: +27 11 717-1234 • Fax: +27 11 339-5708
Private Bag 3, Wits 2050, South Africa

Ref: W-CJ-120601-1

01/06/2012

TO WHOM IT MAY CONCERN:

Waiver: This certifies that the following research does not require clearance from the Human Research Ethics Committee (Medical).

Investigator: **Charlene Andraos (student no 585802).**

Project title: ***In vitro* toxicological assessment of dust emissions from six South African gold mine tailings sites.**

Reason: This is a laboratory study using commercially available cell cultures including U937 and BEAS-2B. No humans are involved.

UNIVERSITY OF THE WITWATERSRAND
PROF PETER CLEATON-JONES
HREC (MEDICAL)
2012 -06- 01
JOHANNESBURG

Professor Peter Cleaton-Jones
Chair: Human Research Ethics Committee (Medical)

copy: Anisa Keshav, Research Office, Senate House, Wits

APPENDIX D: PLAGIARISM DECLARATION

UNIVERSITY OF THE WITWATERSRAND, JOHANNESBURG

FACULTY OF HEALTH SCIENCES

PLAGIARISM DECLARATION TO BE SIGNED BY ALL HIGHER DEGREE STUDENTS

SENATE PLAGIARISM POLICY: APPENDIX ONE

I CHARLENE ANDRAOS (Student number: 585802) am a student registered for the degree of PHD HAEM9000 in the academic year 2019.

I hereby declare the following:

- I am aware that plagiarism (the use of someone else's work without their permission and/or without acknowledging the original source) is wrong.
- I confirm that the work submitted for assessment for the above degree is my own unaided work except where I have explicitly indicated otherwise.
- I have followed the required conventions in referencing the thoughts and ideas of others.
- I understand that the University of the Witwatersrand may take disciplinary action against me if there is a belief that this is not my own unaided work or that I have failed to acknowledge the source of the ideas or words in my writing.
- I have included as an appendix a report from "Turnitin" (or other approved plagiarism detection) software indicating the level of plagiarism in my research document.

Signature: _____ Date: 15/1/19

SNAPSHOT FROM TURNITIN REPORT

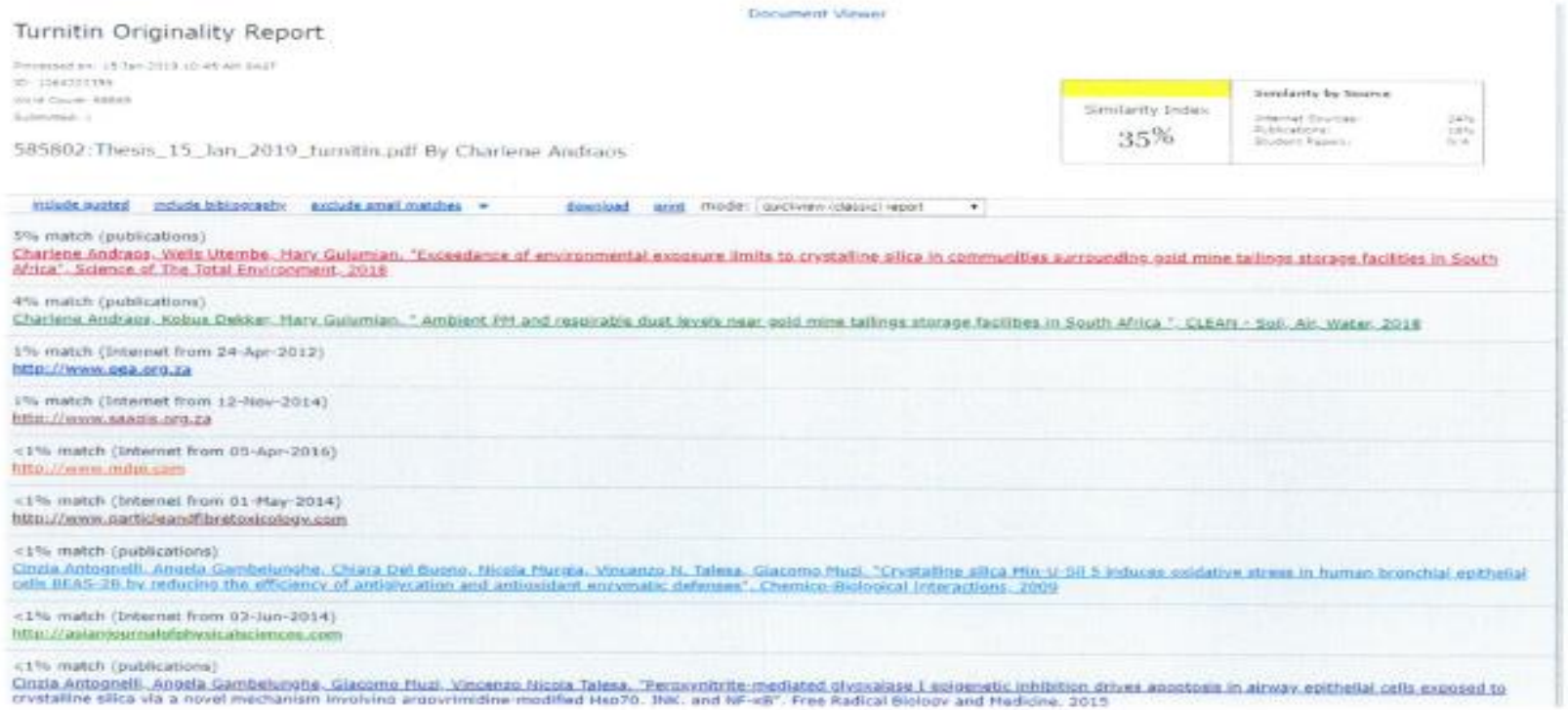

Turnitin Originality Report

585802:Thesis_15_Jan_2019_turnitin.pdf By Charlene Andraos

Similarity Index 35%

5% match (publications)
Charlene Andraos, Wells Utembe, Mary Gulumian, "Exceedance of environmental exposure limits to crystalline silica in communities surrounding gold mine tailings storage facilities in South Africa", Science of The Total Environment, 2018

4% match (publications)
Charlene Andraos, Kobus Dekker, Mary Gulumian, " Ambient PM and respirable dust levels near gold mine tailings storage facilities in South Africa ", CLEAN - Soil, Air, Water, 2018

1% match (Internet from 24-Apr-2012)
http://www.pga.org.za

1% match (Internet from 12-Nov-2014)
http://www.saaps.org.za

<1% match (Internet from 05-Apr-2016)
http://www.mdpi.com

<1% match (Internet from 01-May-2014)
http://www.particleandfibretoxicology.com

<1% match (publications)
Cinzia Antognelli, Angela Gambelunghe, Chiara Dal Bosco, Nicola Muroia, Vincenzo N. Talesa, Giacomo Muzi, "Crystalline silica Min-U-Sil 5 induces oxidative stress in human bronchial epithelial cells BEAS-2B by reducing the efficiency of antioxidant and antioxidant enzymatic defenses", Chemico-Biological Interactions, 2009

<1% match (Internet from 02-Jun-2014)
http://asianjournalofphysicalsciences.com

<1% match (publications)
Cinzia Antognelli, Angela Gambelunghe, Giacomo Muzi, Vincenzo Nicola Talesa, "Peroxynitrite-mediated glyoxalase I epigenetic inhibition drives apoptosis in airway epithelial cells exposed to crystalline silica via a novel mechanism involving argpyrimidine-modified Hsp70, INK, and NF-κB", Free Radical Biology and Medicine, 2015

Acknowledgement by student:

Charlene Andraos — Date: 17/1/19

Acknowledgement by supervisor:

Prof Mary Gulumian — Date: 17 Jan 2019

REFERENCES

Abdel-Hamid, M., El-Desoky, S. and Magdi, S. (1990). Estimation of manganese in blood between exposed workers to different concentrations at industrial units. *Egyptian Journal of Pharmaceutical Sciences,* 31, 143-150.

ACGIH (2005). American Conference of Governmental Industrial Hygienis (ACGIH) TLVs and BEIs: Based on the documentation of the threshold limit values for chemical substances and physical agents and biological exposure indices. *Cincinnati, OH: ACGIH*.

ACS (2016). *American Cancer Society* [Online]. Available: http://www.cancer.org/cancer/cancercauses/othercarcinogens/intheworkplace/arsenic [Accessed April 2016].

Adams, C. R., Ziegler, D. K. and Lin, J. T. (1983). Mercury intoxication simulating amyotrophic lateral sclerosis. *The Journal of the American Medical Association,* 250, 642-643.

Ahlberg, E. and Broo, A. E. (1997). Electrochemical reaction mechanisms at pyrite in acidic perchlorate solutions. *Journal of the Electrochemical Society,* 144, 1281-1286.

Akbar-Khanzadeh, F. (1993). Short-term respiratory function changes in relation to workshift welding fume exposures. *International Archives of Occupational and Environmental Health,* 64, 393-397.

Akugizibwe, P. (2014). *Systematic review of the association and dose-response and relationship between silica exposure or silicosis, and risk of TB disease and TB mortality*. MPH dissertation, University of Cape Town, South Africa.

Alaghmand, M. and Blough, N. V. (2007). Source-dependent variation in hydroxyl radical production by airborne particulate matter. *Environmental Science & Technology,* 41, 2364-2370.

Alessandrini, E. R., Stafoggia, M., Faustini, A., et al. (2016). Association between short-term exposure to $PM_{2.5}$ and PM_{10} and mortality in susceptible subgroups: A multisite case-crossover analysis of individual effect modifiers. *American Journal of Epidemiology,* 184, 744-754.

Andersen, Z. J., Loft, S., Ketzel, M., et al. (2008). Ambient air pollution triggers wheezing symptoms in infants. *Thorax,* 63, 710-716.

Andraos, C., Dekker, K. and Gulumian, M. (2018a). Ambient PM_{10} and respirable dust levels near gold mine tailings storage facilities in South Africa. *CLEAN–Soil, Air, Water*, 1800103.

Andraos, C., Utembe, W. and Gulumian, M. (2018b). Exceedance of environmental exposure limits to crystalline silica in communities surrounding gold mine tailings storage facilities in South Africa. *Science of the Total Environment,* 619, 504-516.

Anglogold (2004). Anglogold Ashanti environmental report, Woodlands Project - Good Progress being made with Phytoremediation Project. Johannesburg.

Anhaeusser, C., Feather, C., Liebenberg, W., et al. (1987). Geology and mineralogy of the principal goldfields in South Africa (Retroactive Coverage). *South African Institute of Mining and Metallurgy, The Extractive Metallurgy of Gold in South Africa.,* 1, 1-67.

Annan, S. Y., Liu, P. and Zhang, Y. (2009). Comparison of the Kaplan-Meier, Maxilllum Likelihood, and ROS Estimators for left-Censored data using simulation studies.

Antognelli, C., Gambelunghe, A., Del Buono, C., et al. (2009). Crystalline silica Min-U-Sil 5 induces oxidative stress in human bronchial epithelial cells BEAS-2B by reducing the

efficiency of antiglycation and antioxidant enzymatic defenses. *Chemico-Biological Interactions,* 182, 13-21.

Anttila, S., Sutinen, S., Paananen, M., et al. (1986). Hard metal lung disease: a clinical, histological, ultrastructural and X-ray microanalytical study. *European Journal of Respiratory Diseases,* 69, 83-94.

Asikhulume (2013). DRDGold Limited Let's Talk Magazine, Issue 26, December 2013.

Askergren, A. and Mellgren, M. (1975). Changes in the nasal mucosa after exposure to copper salt dust A preliminary report. *Scandinavian Journal of Work, Environment & Health,* 1, 45-49.

Atienzar, F., Tilmant, K., Gerets, H., et al. (2011). The use of real-time cell analyzer technology in drug discovery: Defining optimal cell culture conditions and assay reproducibility with different adherent cellular models. *Journal of Biomolecular Screening,* 16, 575-587.

Atkinson, R. W., Fuller, G. W., Anderson, H. R., et al. (2010). Urban ambient particle metrics and health: a time-series analysis. *Epidemiology,* 21, 501-511.

ATSDR (2005). *Agency for Toxic Substances and Disease Registry, Public Health Assessment Guidance Manual* [Online]. Available: http://www.atsdr.cdc.gov/hac/phamanual/appg.html [Accessed February 2016].

ATSDR (2016). Agency for Toxic Substances and Disease Registry (http://www.atsdr.cdc.gov/toxprofiles/index.asp).

Aucamp, P. and Van Schalkwyk, A. (2003). Trace element pollution of soils by abandoned gold mine tailings, near Potchefstroom, South Africa. *Bulletin of Engineering Geology and the Environment,* 62, 123-134.

Ayres, J. G., Borm, P., Cassee, F. R., et al. (2008). Evaluating the toxicity of airborne particulate matter and nanoparticles by measuring oxidative stress potential—a workshop report and consensus statement. *Inhalation Toxicology,* 20, 75-99.

Badding, M. A., Stefaniak, A. B., Fix, N. R., et al. (2014). Cytotoxicity and characterization of particles collected from an indium–tin oxide production facility. *Journal of Toxicology and Environmental Health, Part A,* 77, 1193-1209.

Bagci, C., Bozkurt, A., Cakmak, E., et al. (2004). Blood lead levels of the battery and exhaust workers and their pulmonary function tests. *International Journal of Clinical Practice,* 58, 568-572.

Bailey, M. (1994). The new ICRP model for the respiratory tract. *Radiation Protection Dosimetry,* 53, 107-114.

Bailey, P. and Stanley, G. (1987). The extractive metallurgy of gold in South Africa. *The South African Institute of Mining and Metallurgy,* 1, 379-449.

Baskin, S. and Salem, H. (1997). *Oxidants, antioxidants and free radicals*, CRC Press, p 144, 178.

Bast-Pettersen, R., Ellingsen, D. G., Hetland, S. M., et al. (2004). Neuropsychological function in manganese alloy plant workers. *International Archives of Occupational and Environmental Health,* 77, 277-287.

Beckett, W., Moore, J., Keogh, J., et al. (1986). Acute encephalopathy due to occupational exposure to arsenic. *British Journal of Industrial Medicine,* 43, 66-67.

Beelen, R., Hoek, G., van Den Brandt, P. A., et al. (2008). Long-term effects of traffic-related air pollution on mortality in a Dutch cohort (NLCS-AIR study). *Environmental Health Perspectives,* 116, 196-202.

Bencko, V., Wagner, V., Wagnerova, M., et al. (1982). Immuno-biochemical findings in groups of individuals occupationally and non-occupationally exposed to emissions containing nickel and cobalt. *Journal of Hygiene, Epidemiology, Microbiology, and Immunology,* 27, 387-394.

Bencko, V., Wagner, V., Wagnerova, M., et al. (1986). Human exposure to nickel and cobalt: Biological monitoring and immunobiochemical response. *Environmental Research,* 40, 399-410.

Berge, S. R. and Skyberg, K. (2003). Radiographic evidence of pulmonary fibrosis and possible etiologic factors at a nickel refinery in Norway. *Journal of Environmental Monitoring,* 5, 681-688.

Berridge, M. V., Herst, P. M. and Tan, A. S. (2005). Tetrazolium dyes as tools in cell biology: new insights into their cellular reduction. *Biotechnology Annual Review,* 11, 127-52.

Berridge, M. V., Tan, A. S., McCoy, K. D., et al. (1996). Biochemical and cellular basis of cell proliferation assays that use tetrazolium salts. *Biochemica,* 4, 14-19.

Bhagia, L. (2009). Non-occupational exposure to silica dust in vicinity of slate pencil industry, India. *Environmental Monitoring and Assessment,* 151, 477-482.

Bhagia, L. J. (2012). Non-occupational exposure to silica dust. *Indian Journal of Occupational Environmental Medicine,* 16, 95-100.

Bjerre, B., Berglund, M., Harsbo, K., et al. (1993). Blood lead concentrations of Swedish preschool children in a community with high lead levels from mine waste in soil and dust. *Scandinavian Journal of Work, Environment & Health,* 19, 154-161.

Blanc, P., Hogan, M., Mallin, K., et al. (1985). Cyanide intoxication among silver-reclaiming workers. *The Journal of the American Medical Association,* 253, 367-371.

Blanc, P., Wong, H., Bernstein, M. S., et al. (1991). An experimental human model of metal fume fever. *Annals of Internal Medicine,* 114, 930-936.

Blight, G. (1989). Erosion losses from the surfaces of gold-tailings dams. *Journal of the South African Institute of Mining and Metallurgy,* 89, 23-29.

Blight, G. (2010). *Geotechnical engineering for mine waste storage facilities*, CRC Press Leiden, the Netherlands, p 462.

Blight, G., Robinson, M. and Diering, J. (1981). The flow of slurry from a breached tailings dam. *Journal of the South African Institute of Mining and Metallurgy*, 81, 1-8.

Blond, M. and Netterstrom, B. (2007). Neuromotor function in a cohort of Danish steel workers. *Neurotoxicology*, 28, 336-344.

Bluhm, R. E., Bobbitt, R. G., Welch, L. W., et al. (1992). Elemental mercury vapour toxicity, treatment, and prognosis after acute, intensive exposure in chloralkali plant workers. Part I: History, neuropsychological findings and chelator effects. *Human & Experimental Toxicology,* 11, 201-210.

Böckelmann, I., Pfister, E. A., McGauran, N., et al. (2002). Assessing the suitability of cross-sectional and longitudinal cardiac rhythm tests with regard to identifying effects of occupational chronic lead exposure. *Journal of Occupational and Environmental Medicine,* 44, 59-65.

Bogen, E. and Pasternack, M. (1954). Pleural adhesions, their incidence and significance as shown in autopsies at the Los Angeles General Hospital, 1911-1951. *Chest,* 25, 166-171.

Boice Jr, J. D., Cohen, S. S., Mumma, M. T., et al. (2007a). Mortality among residents of Uravan, Colorado who lived near a uranium mill, 1936–84. *Journal of Radiological Protection,* 27, 299-319.

Boice Jr, J. D., Mumma, M., Schweitzer, S., et al. (2003). Cancer mortality in a Texas county with prior uranium mining and milling activities, 1950–2001. *Journal of Radiological Protection,* 23, 247-262.

Boice Jr, J. D., Mumma, M. T. and Blot, W. J. (2007b). Cancer and noncancer mortality in populations living near uranium and vanadium mining and milling operations in Montrose County, Colorado, 1950-2000. *Radiation Research,* 167, 711-726.

Bolan, N. S., Kirkham, M. B. and Ok, Y.-S. (2017). *Spoil to soil: mine site rehabilitation and revegetation*, CRC Press, Chapter 6.1.

Boogaard, H., Janssen, N. A., Fischer, P. H., et al. (2012). Contrasts in oxidative potential and other particulate matter characteristics collected near major streets and background locations. *Environmental Health Perspectives,* 120, 185-191.

Boojar, M. M. A. and Goodarzi, F. (2002). A longitudinal follow-up of pulmonary function and respiratory symptoms in workers exposed to manganese. *Journal of Occupational and Environmental Medicine,* 44, 282-290.

Borda, M. J., Elsetinow, A. R., Schoonen, M. A., et al. (2001). Pyrite-induced hydrogen peroxide formation as a driving force in the evolution of photosynthetic organisms on an early Earth. *Astrobiology,* 1, 283-288.

Borm, P. J., Kelly, F., Künzli, N., et al. (2007). Oxidant generation by particulate matter: from biologically effective dose to a promising, novel metric. *Occupational and Environmental Medicine,* 64, 73-74.

Bouchard, M., Mergler, D. and Baldwin, M. (2005). Manganese exposure and age: neurobehavioral performance among alloy production workers. *Environmental Toxicology and Pharmacology,* 19, 687-694.

Bradshaw, A. D. and Chadwick, M. J. (1980). *The restoration of land: the ecology and reclamation of derelict and degraded land*, Univ of California Press, p 143.

Bridge, I. (2009). Crystalline Silica: A review of the dose response relationship and environmental risk. *Air Quality and Climate Change,* 43, 17-23.

Brieger, H., Semisch, C., Stasney, J., et al. (1954). Industrial antimony poisoning. *Industrial Medicine and Surgery,* 23, 521-3.

Brook, R. D., Rajagopalan, S., Pope, C. A., et al. (2010). Particulate matter air pollution and cardiovascular disease. *Circulation,* 121, 2331-2378.

Brown, D. M., Stone, V., Findlay, P., et al. (2000). Increased inflammation and intracellular calcium caused by ultrafine carbon black is independent of transition metals or other soluble components. *Occupational and Environmental Medicine,* 57, 685-691.

Brown, J. L. (1988). Zinc fume fever. *The British Journal of Radiology,* 61, 327-329.

Brown, J. S., Gordon, T., Price, O., et al. (2013). Thoracic and respirable particle definitions for human health risk assessment. *Particle and Fibre Toxicology,* 10, 1-12.

Bruch, J., Rehn, S., Rehn, B., et al. (2004). Variation of biological responses to different respirable quartz flours determined by a vector model. *International Journal of Hygiene and Environmental Health,* 207, 203-216.

Bulger, R. E. (1986). Renal damage caused by heavy metals. *Toxicologic Pathology,* 14, 58-65.

Bussières, D., Ayotte, P., Levallois, P., et al. (2004). Exposure of a Cree population living near mine tailings in northern Quebec (Canada) to metals and metalloids. *Archives of Environmental Health: An International Journal,* 59, 732-741.

Carter, J. D., Ghio, A. J., Samet, J. M., et al. (1997). Cytokine production by human airway epithelial cells after exposure to an air pollution particle is metal-dependent. *Toxicology and Applied Pharmacology,* 146, 180-188.

CCME (2016). *Canadian Council of Ministers of the Environment, Canadian Environmental Quality Guidelines* [Online]. Available: http://www.ccme.ca/en/resources/canadian_environmental_quality_guidelines/ [Accessed April 2016 2016].

CEN (1993). European Committee for Standardization (CEN) *Workplace atmospheres-size fraction definitions for measurement of airborne particles (Report No. BS EN 481:1993) London, England: CEN, British Standards Institute*.

Chapman, E. M. (1932). Acute silicosis. *Journal of the American Medical Association,* 98, 1439-1441.

Chen, K. and Rose, C. L. (1952). Nitrite and thiosulfate therapy in cyanide poisoning. *Journal of the American Medical Association,* 149, 113-119.

Chen, L. C. and Lippmann, M. (2009). Effects of metals within ambient air particulate matter (PM) on human health. *Inhalation Toxicology,* 21, 1-31.

Chen, L. H., Knutsen, S. F., Shavlik, D., et al. (2005). The association between fatal coronary heart disease and ambient particulate air pollution: Are females at greater risk? *Environmental Health Perspectives,* 113, 1723-1729.

Chen, R., Wei, L. and Huang, H. (1993). Mortality from lung cancer among copper miners. *British Journal of Industrial Medicine,* 50, 505-509.

Chen, W., Zhuang, Z., Attfield, M., et al. (2001). Exposure to silica and silicosis among tin miners in China: exposure-response analyses and risk assessment. *Occupational and Environmental Medicine,* 58, 31-37.

Cheng, Y., Schwartz, J., Vokonas, P. S., et al. (1998). Electrocardiographic conduction disturbances in association with low-level lead exposure (the Normative Aging Study). *The American Journal of Cardiology,* 82, 594-599.

Cherrie, J., W., Brosseau, L., M., Hay, A., et al. (2013). Low-Toxicity Dusts: Current Exposure Guidelines Are Not Sufficiently Protective. *Annals of Occupational Hygiene,* 57, 685–691.

Chevrel, S., Courant, C., Cottard, F., et al. (2003). Very high resolution remote sensing coupled to GIS-based environmental assessment–East Rand gold field, South Africa. *Report BRGM/RP*.

Chevrel, S., Croukamp, L., Bourguignon, A., et al. A Remote-Sensing and GIS-Based Integrated Approach for Risk-Based Prioritisation of Gold Tailings Facilities—Witwatersrand, South Africa. Proceedings of the Third International Seminar on Mine Closure, 2008. 14-17.

Churchyard, G., Ehrlich, R., Pemba, L., et al. (2004). Silicosis prevalence and exposure-response relations in South African goldminers. *Occupational and Environmental Medicine,* 61, 811-816.

Cohn, C. A., Borda, M. J. and Schoonen, M. A. (2004). RNA decomposition by pyrite-induced radicals and possible role of lipids during the emergence of life. *Earth and Planetary Science Letters,* 225, 271-278.

Cohn, C. A., Laffers, R., Simon, S. R., et al. (2006a). Role of pyrite in formation of hydroxyl radicals in coal: possible implications for human health. *Particle and Fibre Toxicology,* 3, 16.

Cohn, C. A., Mueller, S., Wimmer, E., et al. (2006b). Pyrite-induced hydroxyl radical formation and its effect on nucleic acids. *Geochemical Transactions,* 7, 1-11.

Collins, J. F. and Marty, M. A. (1995). Cancer risk assessment for crystalline silica to implement California's Hot Spots Act. *Scandinavian Journal of Work, Environment & Health,* 21, 99-103.

Collins, J. F., Salmon, A. G., Brown, J. P., et al. (2005). Development of a chronic inhalation reference level for respirable crystalline silica. *Regulatory Toxicology and Pharmacology,* 43, 292-300.

Cook, M., Chappell, W. R., Hoffman, R. E., et al. (1993). Assessment of blood lead levels in children living in a historic mining and smelting community. *American Journal of Epidemiology,* 137, 447-455.

Cooper, D. A., Pendergrass, E. P., Vorwald, A. J., et al. (1968). Pneumoconiosis among workers in an antimony industry. *American Journal of Roentgenology,* 103, 495-508.

Cooper, J. R., Stradling, G. N., Smith, H., et al. (1982). The behaviour of uranium-233 oxide and uranyl-233 nitrate in rats. *International Journal of Radiation Biology and Related Studies in Physics, Chemistry and Medicine,* 41, 421-433.

Craighead, J. (1988). Diseases associated with exposure to silica and nonfibrous silicate minerals. *Archives of Pathology and Laboratory Medicine,* 112, 673-720.

Csavina, J., Field, J., Taylor, M. P., et al. (2012). A review on the importance of metals and metalloids in atmospheric dust and aerosol from mining operations. *Science of the Total Environment,* 433, 58-73.

Dalal, N. S., Newman, J., Pack, D., et al. (1995). Hydroxyl radical generation by coal mine dust: possible implication to coal workers' pneumoconiosis (CWP). *Free Radical Biology and Medicine,* 18, 11-20.

Dalstein, L., Potapova, E. and Tyrode, E. (2017). The elusive silica/water interface: isolated silanols under water as revealed by vibrational sum frequency spectroscopy. *Physical Chemistry Chemical Physics,* 19, 10343-10349.

Damiano, J. S., Oliveira, V. and Welsh, K. (2004). Heterotypic interactions among NACHT domains: implications for regulation of innate immune responses. *Biochemical Journal,* 381, 213-219.

Dankert, B. T. and Hein, K. A. (2010). Evaluating the structural character and tectonic history of the Witwatersrand Basin. *Precambrian Research,* 177, 1-22.

Danse, I. H., Garb, L. G. and Moore, R. H. (1995). Blood lead surveys of communities in proximity to lead-containing mill tailings. *American Industrial Hygiene Association,* 56, 384-393.

Davies, T. L. (1946). Manganese pneumonitis. *British Journal of Industrial Medicine,* 3, 111-135.

de Andrade Lima, L., Bernardez, L. and Barbosa, L. (2008). Characterization and treatment of artisanal gold mine tailings. *Journal of Hazardous Materials,* 150, 747-753.

DEA (2009). National Environmental Management: Air Quality Act, 2004 (ACT NO. 39 OF 2004) National Ambient Air Quality Standards Government Gazette No. 32816.

DEA (2012). National Environmental Management: Air Quality Act, 2004 (ACT NO. 39 OF 2004) National Ambient Air Quality Standard for Particulate Matter with Aerodynamic Diameter less than 2.5 micron meters ($PM_{2.5}$) Government Gazette No. 35463.

Dellinger, B., Lomnicki, S., Khachatryan, L., et al. (2007). Formation and stabilization of persistent free radicals. *Proceedings of the Combustion Institute,* 31, 521-528.

Deng, J.-F., Sinks, T., Elliot, L., et al. (1991). Characterisation of respiratory health and exposures at a sintered permanent magnet manufacturer. *British Journal of Industrial Medicine,* 48, 609-615.

Diapouli, E., Chaloulakou, A. and Koutrakis, P. (2013). Estimating the concentration of indoor particles of outdoor origin: A review. *Journal of the Air & Waste Management Association,* 63, 1113-1129.DIV (2000). *Dutch Intervention Values, Dutch Target and Intervention Values, 2000 (the New Dutch List)* [Online]. Available: http://www.esdat.net/Environmental%20Standards/Dutch/annexS_I2000Dutch%20Environmental%20Standards.pdf [Accessed April 2016].

Dixon, S. J. and Stockwell, B. R. (2014). The role of iron and reactive oxygen species in cell death. *Nature Chemical Biology,* 10, 9-17.

DMR (2006). *Department of Mineral Resources, Republic of South Africa, Occupational Exposure Limits for Airborne Pollutants* [Online]. Available: http://www.dmr.gov.za/publications/finish/33-mine-health-and-safety/343-occupationalhygieneregulations/0.html [Accessed December 2017].

Dockery, D. W., Pope, C. A., Xu, X., et al. (1993). An association between air pollution and mortality in six US cities. *New England Journal of Medicine,* 329, 1753-1759.

Doherty, M., Healy, M., Richardson, S., et al. (2004). Total body iron overload in welder's siderosis. *Occupational and Environmental Medicine,* 61, 82-85.

Doll, R., Andersen, A., Cooper, W., et al. (1990). Report of the international-committee-on-nickel-carcinogenesis-in-man. *Scandinavian Journal of Work Environment & Health,* 16, 1-82.

Dolovich, J., Evans, S. and Nieboer, E. (1984). Occupational asthma from nickel sensitivity: I. Human serum albumin in the antigenic determinant. *British Journal of Industrial Medicine,* 41, 51-55.

Donaldson, K., Brown, D. M., Mitchell, C., et al. (1997). Free radical activity of PM_{10}: iron-mediated generation of hydroxyl radicals. *Environmental Health Perspectives,* 105, 1285-1289.

Donaldson, K., Stone, V., Clouter, A., et al. (2001). Ultrafine particles. *Occupational and Environmental Medicine,* 58, 211-216.

DRDGold (2009). DRD Gold Annual Report 2009, Review of operations.

DRDGold (2014). Integrated Report.

DRDGold (2015). Integrated Report.

DRDGold (2018). Integrated Report.

Dreher, K. L., Jaskot, R. H., Lehmann, J. R., et al. (1997). Soluble transition metals mediate residual oil fly ash induced acute lung injury. *Journal of Toxicology and Environmental Health Part A,* 50, 285-305.

Drinker, K. R. and Drinker, P. (1928). Metal Fume Fever: V. Results of the Inhalation by Animals of Zinc and Magnesium Oxide Fumes. *Journal of Industrial Hygiene,* 10, 56-70.

Dungworth, D., Hahn, F. and Nikula, K. (1989). Noncarcinogenic responses of the respiratory tract to inhaled toxicants. *Concepts in Inhalation Toxicology.* Hemisphere New York, p 273-298.

Dutkiewicz, T., Sokołowska, D. and Kulka, E. (1992). Health risk assessment in children exposed to lead compounds in the vicinity of mine-smelter plant" Orzel Bialy". *Polish Journal of Occupational Medicine and Environmental Health,* 6, 71-78.

Eftim, S. E., Samet, J. M., Janes, H., et al. (2008). Fine particulate matter and mortality: a comparison of the six cities and American Cancer Society cohorts with a medicare cohort. *Epidemiology,* 19, 209-216.

El Ghawabi, S. H., Gaafar, M. A., El-Saharti, A. A., et al. (1975). Chronic cyanide exposure: a clinical, radioisotope, and laboratory study. *British Journal of Industrial Medicine,* 32, 215-219.

Elias, Z., Poirot, O., Daniere, M., et al. (2002). Role of iron and surface free radical activity of silica in the induction of morphological transformation of Syrian hamster embryo cells. *Annals of Occupational Hygiene,* 46, 53-57.

Enstrom, J. E. (2005). Fine particulate air pollution and total mortality among elderly Californians, 1973–2002. *Inhalation Toxicology,* 17, 803-816.

EPA (1996). United States Environmental Protection Agency, Ambient Levels and Non-cancer Health Effects of Inhaled Crystalline and Amorphous Silica: Health Issue Assessment (EPA/600/R-95/115).

EPA (2002). United States Environmental Protection Agency, Calculating upper confidence limits for exposure point concentrations at hazardous waste sites (OSWER9285).

EPA (2003). United States Environmental Protection Agency, Ecological Soil Screening Level for Iron Interim Final OSWER Directive 9285.7-69.

EPA (2009). United States Environmental Protection Agency, Risk Assessment Guidance for Superfund Volume I: Human Health Evaluation Manual (Part F, Supplemental Guidance for Inhalation Risk Assessment).

EPA (2011). United States Environmental Protection Agency, Exposure factors handbook.

EPA (2018). United States Environmental Protection Agency, National Air Toxics Assessment.

EPA (2019). *United States Environmental Protection Agency, Integrated Risk Information System (IRIS) Glossary* [Online]. Available: https://iaspub.epa.gov/sor_internet/registry/termreg/searchandretrieve/glossariesandkeywordlists/search.do?details=&vocabName=IRIS%20Glossary [Accessed June 2019].

Ettinger, A. and Wittmann, T. (2014). Fluorescence live cell imaging. *Methods in Cell Biology,* 123, 77-94.

Fanning, D. (1988). A mortality study of lead workers, 1926–1985. *Archives of Environmental Health: An International Journal,* 43, 247-251.

Feather, C. and Koen, G. (1975). Mineralogy of the Witwatersrand reefs. *Minerals Science and Engineering,* 7, 189-224.

Fechser, M., Alaves, V., Larson, R., et al. (2014). Evaluation of Respirable Crystalline Silica in High School Ceramics Classrooms. *International Journal of Environmental Research and Public Health,* 11, 1250-1260.

Filleul, L., Rondeau, V., Vandentorren, S., et al. (2005). Twenty five year mortality and air pollution: results from the French PAARC survey. *Occupational and Environmental Medicine,* 62, 453-460.

Frampton, M., W. (2007) Does inhalation of ultrafine particles cause pulmonary vascular effects in humans? *Inhalation Toxicology,* 19(Suppl 1), 75-79.Frampton, M. W., Ghio, A. J., Samet, J. M., et al. (1999). Effects of aqueous extracts of PM_{10} filters from the Utah Valley on human airway epithelial cells. *American Journal of Physiology-Lung Cellular and Molecular Physiology,* 277, L960-L967.

Frimmel, H. (2005). Historic Overview of the Witwatersrand Goldfields. *Economic Geology,* 100, 1051-1052.

Fubini, B. (1998). Surface Chemistery and Quartz Hazard. *Annals of Occupational Hygiene,* 42, 521-530.

Fubini, B. and Arean, C. O. (1999). Chemical aspects of the toxicity of inhaled mineral dusts. *Chemical Society Reviews,* 28, 373-381.

Fubini, B. and Fenoglio, I. (2007). Toxic potential of mineral dusts. *Elements,* 3, 407-414.

Funke, J. (1990). The water requirements and pollution potential of South African gold and uranium mines (Report: KV 9/90, ISBN 0 947447 27X). Water Research Commission South Africa.

Gardenhire, D. S. (2015). *Rau's Respiratory Care Pharmacology - Elsevier eBook on VitalSource, 9th Edition,* Elsevier Health Sciences, p 33.

GDACE (2004). Department of Agriculture, Conservation and Environment, Gauteng State of Environment Report. Gauteng Provincial Government.

GDARD (2009a). Gauteng Department of Agriculture and Rural Development, Conceptual Study on Reclamation of Mine Residue Areas for Development Purposes, Final Report November 2009. Gauteng Provincial Government.

GDARD (2009b). Gauteng Department of Agriculture and Rural Development, Gauteng Province Air Quality Management Plan, Final Report August 2009. Gauteng Provincial Government.

GDARD (2011). Gauteng Department of Agriculture and Rural Development, Gauteng State of Environment Report. Gauteng Provincial Government.

GDARD (2012). Gauteng Mine Residue Areas Strategy. Gauteng Provincial Government.

GDARD (2017). Gauteng Department of Agriculture and Rural Development, The Gauteng Pollution Buffer Zones Guideline, Sustainable Use of the Environment, Current Review Facilitated by the Directorate Environmental Policy Planning and Coordination, Final Report March 2017. Gauteng Provincial Government.

Gehling, W., Khachatryan, L. and Dellinger, B. (2014). Hydroxyl radical generation from environmentally persistent free radicals (EPFRs) in $PM_{2.5}$. *Environmental Science & Technology,* 48, 4266-4272.

Gehring, U., Heinrich, J., Krämer, U., et al. (2006). Long-term exposure to ambient air pollution and cardiopulmonary mortality in women. *Epidemiology,* 17, 545-551.

Geiser, M., Rothen-Rutishauser, B., Kapp, N., et al. (2005). Ultrafine particles cross cellular membranes by nonphagocytic mechanisms in lungs and in cultured cells. *Environmental Health Perspectives,* 113, 1555-1560.

Gilmour, P. S., Brown, D. M., Lindsay, T. G., et al. (1996). Adverse health effects of PM_{10} particles: involvement of iron in generation of hydroxyl radical. *Occupational and Environmental Medicine,* 53, 817-822.

Godri, K. J., Harrison, R. M., Evans, T., et al. (2011). Increased oxidative burden associated with traffic component of ambient particulate matter at roadside and urban background schools sites in London. *PLoS One,* 6, e21961.

Goldberg, M. S., Burnett, R. T., Stieb, D. M., et al. (2013). Associations between ambient air pollution and daily mortality among elderly persons in Montreal, Quebec. *Science of the Total Environment,* 463-464, 931-942.

Goldsmith, D. F., Ruble, R. P. and Klein, C. O. (1995). Comparative cancer potency for silica from extrapolations of human and animal findings. *Scandinavian Journal of Work, Environment & Health,* 21, 104-107.

GCRO (2018). Gauteng City-Region Observatory Report No. 07 Mining Landscapes of the Gauteng City-Region, January 2018.

Groen, J. C., Peffer, L. A. and Pérez-Ramírez, J. (2003). Pore size determination in modified micro-and mesoporous materials. Pitfalls and limitations in gas adsorption data analysis. *Microporous and Mesoporous Materials,* 60, 1-17.

Gulson, B. L., Davis, J. J., Mizon, K. J., et al. (1994). Lead bioavailability in the environment of children: blood lead levels in children can be elevated in a mining community. *Archives of Environmental Health: An International Journal,* 49, 326-331.

Gulumian, M. (1999). The ability of mineral dusts and fibres to initiate lipid peroxidation Part I: Parameters which determine this ability. *Redox Report,* 4, 141-163.

Gulumian, M. (2000). The ability of mineral dusts and fibres to initiate lipid peroxidation. Part II: relationship to different particle-induced pathological effects. *Redox Report,* 5, 325-51.

Halliwell, B. and Gutteridge, J. M. (2015). *Free radicals in biology and medicine,* Oxford University Press, USA, p 292.

Han, X., Gelein, R., Corson, N., et al. (2011). Validation of an LDH assay for assessing nanoparticle toxicity. *Toxicology,* 287, 99– 104.

Harrington, A. D., Tsirka, S. E. and Schoonen, M. A. (2012). Quantification of particle-induced inflammatory stress response: a novel approach for toxicity testing of earth materials. *Geochemical Transactions,* 13, 1-10.

Heinzerling, A., Hsu, J., Yip, F. (2016). Respiratory Health Effects of Ultrafine Particles in Children: A Literature Review. *Water Air Soil Pollution,* 227, 32.

Hershko, C. (2007). Mechanism of iron toxicity. *Food and Nutrition Bulletin,* 28, S500-S509.

Hnizdo, E., and Sluis-Cremer, G. K. (1991). Silica exposures, silicosis, and lung cancer: a mortality study of South African gold miners. British Journal of Industrial Medicine, 48, 53-60.

Hnizdo, E. and Sluis-Cremer, G. (1993). Risk of silicosis in a cohort of white South African gold miners. *American Journal of Industrial Medicine,* 24, 447-457.

Hnizdo, E. and Vallyathan, V. (2003). Chronic obstructive pulmonary disease due to occupational exposure to silica dust: a review of epidemiological and pathological evidence. *Occupational and Environmental Medicine,* 60, 237-243.

Holder, A. L., Goth-Goldstein, R., Lucas, D., et al. (2012). Particle-induced artifacts in the MTT and LDH viability assays. *Chemical Research in Toxicology,* 25, 1885-1892.

Hornung, R. W., Deddens, J. A. and Roscoe, R. J. (1998). Modifiers of lung cancer risk in uranium miners from the Colorado Plateau. *Health Physics,* 74, 12-21.

Howe, G. R. and Stager, R. H. (1996). Risk of lung cancer mortality after exposure to radon decay products in the Beaverlodge cohort based on revised exposure estimates. *Radiation Research,* 146, 37-42.

Hu, W., Zhang, Q., Su, W. C., et al. (2003). Gene expression of primary human bronchial epithelial cells in response to coal dusts with different prevalence of coal workers' pneumoconiosis. *Journal of Toxicology and Environmental Health Part A,* 66, 1249-1265.

Huang, X., Li, W., Attfield, M. D., et al. (2005). Mapping and prediction of coal workers' pneumoconiosis with bioavailable iron content in the bituminous coals. *Environmental Health Perspectives,* 113, 964-968.

Hughes, J. M., Weill, H., Checkoway, H., et al. (1998). Radiographic evidence of silicosis risk in the diatomaceous earth industry. *American Journal of Respiratory and Critical Care Medicine,* 158, 807-814.

Hussain, M., Madl, P., Khan, A. (2011). Lung deposition predictions of airborne particles and the emergence of contemporary diseases Part-I. *theHealth,* 2(2), 51-59.

Hwang, Y.-H., Bornschein, R. L., Grote, J., et al. (1997). Environmental arsenic exposure of children around a former copper smelter site. *Environmental Research,* 72, 72-81.

IARC (1990). *International Agency for Research on Cancer, Monographs on the Evaluation of Carcinogenic Risks to Humans, Chromium, Nickel and Welding, Volume 49*, IARC Publications, p 257-445.

IARC (2012a). *International Agency for Research on Cancer, Monographs on the Evaluation of Carcinogenic Risks to Humans: Silica dust, crystalline, in the form of quartz or cristobalite, Volume 100C,* IARC Publications, p 355-405.

IARC (2012b). *International Agency for Research on Cancer, Monographs on Chromium (VI) Compounds, Volume 100C,* IARC Publications, p 147-167.

ICRP (1994). ICRP. *Human Respiratory Tract Model for Radiological Protection. ICRP Publication 66. Ann. ICRP 24 (1-3).*

Ide, C. W. and Bullough, G. R. (1988). Arsenic and old glass. *Occupational Medicine,* 38, 85-88.

Imlay, J. A., Chin, S. M. and Linn, S. (1988). Toxic DNA damage by hydrogen peroxide through the Fenton reaction in vivo and in vitro. *Science,* 240, 640-642.

Imlay, J. A. and Linn, S. (1988). DNA damage and oxygen radical toxicity. *Science,* 240, 1302-1309.

IRIS (2002). Integrated Risk Information System, Arsenic, inorganic; CASRN 7440-38-2. United States Environmental Protection Agency.

IRIS (2005). Integrated Risk Information System, Nickel refinery dust, IRIS Summary. United States Environmental Protection Agency.

Jameson, C. and Walters, D. B. (2016). *Chemistry for toxicity testing, Methods for generation of test atmospheres,* Butterworth Publishers, p 125.

Janin, Y., Couinaud, C., Stone, A., et al. (1984). The" lead-induced colic" syndrome in lead intoxication. *Surgery Annual,* 17, 287-307.

Janssen, N. A., Yang, A., Strak, M., et al. (2014). Oxidative potential of particulate matter collected at sites with different source characteristics. *Science of the Total Environment,* 472, 572-581.

Jerrett, M., Burnett, R. T., Ma, R., et al. (2005). Spatial analysis of air pollution and mortality in Los Angeles. *Epidemiology,* 16, 727-736.

Jimenez, L., Thompson, J., Brown, D., et al. (2000). Activation of NF-κB by PM_{10} occurs via an iron-mediated mechanism in the absence of IκB degradation. *Toxicology and Applied Pharmacology,* 166, 101-110.

Journeay, W. S., Suri, S. S., Moralez, J. G., et al. (2009). Macrophage inflammatory response to self- assembling rosette nanotubes. *Small,* 5, 1446-1452.

Jung, H., Guo, B., Anastasio, C., et al. (2006). Quantitative measurements of the generation of hydroxyl radicals by soot particles in a surrogate lung fluid. *Atmospheric Environment,* 40, 1043-1052.

Kamunda, C., Mathuthu, M. and Madhuku, M. (2016). Health risk assessment of heavy metals in soils from Witwatersrand gold mining basin, South Africa. *International Journal of Environmental Research and Public Health,* 13, 663-674.

Kelly, F. J. and Fussell, J. C. (2012). Size, source and chemical composition as determinants of toxicity attributable to ambient particulate matter. *Atmospheric Environment,* 60, 504-526.

Khiroya, H., and Turner, A., M. (2015). The role of iron in pulmonary pathology. *Multidiciplinary Respiratory Medicine*, 10, 34.

Kitamura, F., Yokoyama, K., Araki, S., et al. (2003). Increase of olfactory threshold in plating factory workers exposed to chromium in Korea. *Industrial Health*, 41, 279-285.

Kneen, M. A., Ojelede, M. E. and Annegarn, H. J. (2015). Housing and population sprawl near tailings storage facilities in the Witwatersrand: 1952 to current. *South African Journal of Science,* 111, 1-9.

Kocyigit, A., Armutcu, F., Gurel, A., et al. (2004). Alterations in plasma essential trace elements selenium, manganese, zinc, copper, and iron concentrations and the possible role of these elements on oxidative status in patients with childhood asthma. *Biological Trace Element Research,* 97, 31-41.

Kolluru, R. V. (1996). *Health risk assessment: principles and practices. In: Risk Assessment and Management Handbook for Environmental, Health, and Safety Professionals*, McGraw-Hill, New York.

Kong, B., Seog, J. H., Graham, L. M., et al. (2011). Experimental considerations on the cytotoxicity of nanoparticles. *Nanomedicine,* 6, 929–941.

Krewski, D., Burnett, R. T., Goldberg, M. S., et al. (2004). Validation of the Harvard Six Cities Study of particulate air pollution and mortality. *New England Journal of Medicine,* 350, 198-199.

Krewski, D., Jerrett, M., Burnett, R. T., et al. (2009). Extended follow-up and spatial analysis of the American Cancer Society study linking particulate air pollution and mortality. *Research Report (Health Effects Institute),* 140, 5-114.

Kroll, A., Pillukat, M. H., Hahn, D., et al. (2012). Interference of engineered nanoparticles with *in vitro* toxicity assays. *Archives of Toxicology,* 86, 1123-36.

Kuo, H.-W., Lai, J.-S. and Lin, T.-I. (1997). Nasal septum lesions and lung function in workers exposed to chromic acid in electroplating factories. *International Archives of Occupational and Environmental Health,* 70, 272-276.

Laden, F., Schwartz, J., Speizer, F. E., et al. (2006). Reduction in fine particulate air pollution and mortality: extended follow-up of the Harvard Six Cities study. *American Journal of Respiratory and Critical Care Medicine,* 173, 667-672.

Lagerkvist, B., Linderholm, H. and Nordberg, G. F. (1986). Vasospastic tendency and Raynaud's phenomenon in smelter workers exposed to arsenic. *Environmental Research,* 39, 465-474.

Lee-Feldstein, A. (1986). Cumulative exposure to arsenic and its relationship to respiratory cancer among copper smelter employees. *Journal of Occupational and Environmental Medicine,* 28, 296-302.

Lehman, S. E., Morris, A. S., Mueller, P. S., et al. (2016). Silica nanoparticle-generated ROS as a predictor of cellular toxicity: mechanistic insights and safety by design. *Environmental Science: Nano,* 3, 56-66.

Lewis, D. and Copley, M. (2011). Inhaled product characterization: calculating particle-size distribution metrics. *Pharmaceutical Technology*, S33-S37.

Li, N., Wang, M., Oberley, T. D., et al. (2002). Comparison of the pro-oxidative and proinflammatory effects of organic diesel exhaust particle chemicals in bronchial epithelial cells and macrophages. *The Journal of Immunology,* 169, 4531-4541.

Liebenberg, W. (1956). A mineralogical approach to the development of the uranium extraction processes practised on the Witwatersrand. *Journal of the Southern African Institute of Mining and Metallurgy,* 57, 153-208.

Liebenberg, W. (1972). *Mineralogical features of gold ores in South Africa. In: Gold Metallurgy in South Africa* RJ Adamson, Chamber of Mines South Africa

Lilis, R., Miller, A. and Lerman, Y. (1985). Acute mercury poisoning with severe chronic pulmonary manifestations. *Chest,* 88, 306-309.

Lin, W., Huang, Y.-W., Zhou, X.-D., et al. (2006). *In vitro* toxicity of silica nanoparticles in human lung cancer cells. *Toxicology and Applied Pharmacology,* 217, 252-259.

Lipfert, F., Baty, J., Miller, J., et al. (2006a). $PM_{2.5}$ constituents and related air quality variables as predictors of survival in a cohort of US military veterans. *Inhalation Toxicology,* 18, 645-657.

Lipfert, F., Wyzga, R., Baty, J., et al. (2006b). Traffic density as a surrogate measure of environmental exposures in studies of air pollution health effects: Long-term mortality in a cohort of US veterans. *Atmospheric Environment,* 40, 154-169.

Lockwood, D. J. (2015). Rayleigh and Mie Scattering. In: Luo R. (eds) Encyclopedia of Color Science and Technology. Springer, Berlin, Heidelberg.

Loh, M. M., Sugeng, A., Lothrop, N., et al. (2016). Multimedia exposures to arsenic and lead for children near an inactive mine tailings and smelter site. *Environmental Research,* 146, 331-339.

Lubin, J. H., Pottern, L. M., Stone, B., et al. (2000). Respiratory cancer in a cohort of copper smelter workers: results from more than 50 years of follow-up. *American Journal of Epidemiology,* 151, 554-565.

MAK (2000). *MAK Value Documentation, Silica, crystalline: quartz dust, cristobalite dust and tridymite dust (respirable fraction), The MAK Collection for Occupational Health and Safety (Published in the series Occupational Toxicants, Vol. 14, 2000),* Weinheim, Germany: Verlag Wiley-VCH, p 205-271.

Malatse, M. and Ndlovu, S. (2015). The viability of using the Witwatersrand gold mine tailings for brickmaking. *Journal of the Southern African Institute of Mining and Metallurgy,* 115, 321-327.

Malcolm, D. and Barnett, H. (1982). A mortality study of lead workers 1925-76. *British Journal of Industrial Medicine,* 39, 404-410.

Mallon, W. (2016). Occupational exposure limits. *Occupational Health Southern Africa,* 22, 21.

Malo, J., Malo, J., Cartier, A., et al. (1990). Acute lung reaction due to zinc inhalation. *European Respiratory Journal,* 3, 111-114.

Martin, R., Dowling, K., Pearce, D., et al. (2014). Health effects associated with inhalation of airborne arsenic arising from mining operations. *Geosciences,* 4, 128-175.

McCarthy, T. S. (2011). The impact of acid mine drainage in South Africa. *South African Journal of Science,* 107, 01-07.

McDonald, J. A. and Potter, N. U. (1996). Lead's legacy? Early and late mortality of 454 lead-poisoned children. *Archives of Environmental Health: An International Journal,* 51, 116-121.

McFarland, R. B. and Reigel, H. (1978). Chronic mercury poisoning from a single brief exposure. *Journal of Occupational and Environmental Medicine,* 20, 532-534.

McNerney, J. M. and Schrenk, H. (1960). The acute toxicity of cyanogen. *American Industrial Hygiene Association Journal,* 21, 121-124.

Mercer, R. R., Scabilloni, J. F., Wang, L., et al. (2017). The Fate of Inhaled Nanoparticles: Detection and Measurement by Enhanced Dark-field Microscopy. *Toxicologic Pathology,* 46, 28-46.

Merkel, B. J. and Arab, A. (2014). *Uranium-Past and Future Challenges: In: Proceedings of the 7th International Conference on Uranium Mining and Hydrogeology*, Springer.

Michaels, D., Zoloth, S. R. and Stern, F. B. (1991). Does low-level lead exposure increase risk of death? A mortality study of newspaper printers. *International Journal of Epidemiology,* 20, 978-983.

Miller, K. A., Siscovick, D. S., Sheppard, L., et al. (2007). Long-term exposure to air pollution and incidence of cardiovascular events in women. *New England Journal of Medicine,* 356, 447-458.

Milnerowicz, H., Ściskalska, M. and Dul, M. (2015). Pro-inflammatory effects of metals in persons and animals exposed to tobacco smoke. *Journal of Trace Elements in Medicine and Biology,* 29, 1-10.

Monteiro-Riviere, N. A., Inman, A. O. and Zhang, L. W. (2009). Limitations and relative utility of screening assays to assess engineered nanoparticle toxicity in a human cell line. *Toxicology and Applied Pharmacology,* 234 222-235.

Moreno, M. E., Acosta-Saavedra, L. C., Meza-Figueroa, D., et al. (2010). Biomonitoring of metal in children living in a mine tailings zone in Southern Mexico: A pilot study. *International Journal of Hygiene and Environmental Health*, 213, 252-258.

Morgan, W. (1978). Industrial bronchitis. *British Journal of Industrial Medicine,* 35, 285-291.

Morton, W. E. and Caron, G. A. (1989). Encephalopathy: an uncommon manifestation of workplace arsenic poisoning? *American Journal of Industrial Medicine,* 15, 1-5.

Moya, J., Bearer, C. F. and Etzel, R. A. (2004). Children's behavior and physiology and how it affects exposure to environmental contaminants. *Pediatrics,* 113, 996-1006.

Mphephu, N., Viljoen, M. and Annegarn, H. Geochemistry of mine tailings and contribution to soil and water pollution on the Central Rand. Implementing sustainable development in mining: From talk to action. Chamber of Mines of South Africa, Mining and Sustainable Development Conference, Sandton, 2003. 3-5.

Mphephu, N. F. (2001). *Environmental issues related to the underground workings of the Central Rand gold fields, Johannesburg, South Africa.* MSc dissertation.

Mrost, M. (1974). Slimes disposal at South African gold mines. *Journal of the South African Institute of Mining and Metallurgy*, 285-291.

Murgueytio, A. M., Evans, R. G. and Roberts, D. (1997). Relationship between soil and dust lead in a lead mining area and blood lead levels. *Journal of Exposure Analysis and Environmental Epidemiology,* 8, 173-186.

Mylonas, C. and Kouretas, D. (1999). Lipid peroxidation and tissue damage. *In vivo (Athens, Greece),* 13, 295-309.

Nemery, B. (1990). Metal toxicity and the respiratory tract, *European Respiratory Journal*, 3, 202-219.

Nemmar, A., Hoet, P. M., Vanquickenborne, B., et al. (2002). Passage of inhaled particles into the blood circulation in humans. *Circulation,* 105, 411-414.

Nengovhela, A., Yibas, B. and Ogola, J. (2006). Characterisation of gold tailings dams of the Witwatersrand Basin with reference to their acid mine drainage potential, Johannesburg, South Africa. *Water SA,* 32, 499-506.

Nico, P. S., Kumfer, B. M., Kennedy, I. M., et al. (2009). Redox dynamics of mixed metal (Mn, Cr, and Fe) ultrafine particles. *Aerosol Science and Technology,* 43, 60-70.

Nij, E. T., Borm, P., Höhr, D., et al. (2002). Pneumoconiosis and exposure to quartz-containing dust in the construction industry. *Annals of Occupational Hygiene,* 46, 71-76.

NIOSH (1989). National Institute for Occupational Safety and Health, Iron Oxide Dust Report National Institute for Occupational Safety and Health.

NIOSH (2017). National Institute for Occupational Safety and Health, Current Intelligence Bulletin 68, NIOSH Chemical Carcinogen Policy, Department of Health and Human Services, Centers for Disease Control and Prevention.

NJDoH (2007). Hazardous Substance Fact Sheet: Iron Oxide. New Jersey Department of Health and Senior Services.

Norboo, T., Angchuk, P., Yahya, M., et al. (1991). Silicosis in a Himalayan village population: role of environmental dust. *Thorax,* 46, 341-343.

Nsimba, E. B. (2009). *Cyanide and cyanide complexes in the goldmine polluted land in the East and Central Rand Goldfields, South Africa.* MSc dissertation, University of the Witwatersrand, South Africa.

NSW (1993). New South Wales Government Lead Issues Paper. New South Wales Government.

NTP (2002). Tenth Report on Carcinogens. National Toxicology Program, US Department of Health and Human Services.

NTP (2005). Eleventh Report on Carcinogens National Toxicology Program, US Department of Health and Human Services.

Oberdörster, G., Sharp, Z., Atudorei, V., et al. (2004). Translocation of inhaled ultrafine particles to the brain. *Inhalation Toxicology,* 16, 437-445.

Ochieng, G. M., Seanego, E. S. and Nkwonta, O. I. (2010). Impacts of mining on water resources in South Africa: A review. *Scientific Research and Essays,* 5, 3351-3357.

OEHHA (2005). Office of Environmental Health Hazard Assessment (OEHHA) Adoption of chronic reference exposure levels for silica (crystalline, respirable).

Oguntoke, O. and Annegarn, H. J. (2014). Effectiveness of mediation in the resolution of environmental complaints against the activities of gold mining industries in the Witwatersrand region. *Clean Air Journal,* 24, 17-23.

Ohlwein, S., Kappeler, R., Kutlar, J. M., et al. (2019). Health effects of ultrafine particles: a systematic literature review update of epidemiological evidence. *International Journal of Public Health,* 64, 547-559.

Ojelede, M. (2012). *Risk assessment of atmospheric emissions from gold mine tailings on the Witwatersrand*. PhD thesis, University of Johannesburg, South Africa.

Olaguibel, J. and Basomba, A. (1988). Occupational asthma induced by chromium salts. *Allergologia et Immunopathologia,* 17, 133-136.

Oosthuizen, M., Wright, C., Matooane, M., et al. (2015). Human health risk assessment of airborne metals to a potentially exposed community: a screening exercise. *Clean Air Journal,* 25, 51-57.

Oostingh, G. J., Casals, E. and Italiani, P. (2011). Problems and challenges in the development and validation of human cell-based assays to determine nanoparticle-induced immunomodulatory effects. *Particle and Fibre Toxicology,* 8, 1-21.

OSHA (2016). *Permissible Exposure Limits for Silica* [Online]. Available: https://www.osha.gov/dsg/etools/silica/compare_to_limit/pel/pel.html [Accessed April 2016].

OSHA (2017a). Permissible Exposure Limits, Annotated Table Z-3 Mineral Dusts.

OSHA (2017b). Permissible Exposure Limits, Annotated Table Z-1.

Ostro, B., Hu, J., Goldberg, D., et al. (2015). Associations of mortality with long-term exposures to fine and ultrafine particles, species and sources: results from the California Teachers Study Cohort. *Environmental Health Perspectives,* 123, 549-556.

Ostro, B., Roth, L., Malig, B., et al. (2009). The effects of fine particle components on respiratory hospital admissions in children. *Environmental Health Perspectives,* 117, 475-480.

Øvrevik, J., Refsnes, M., Låg, M., et al. (2015). Activation of proinflammatory responses in cells of the airway mucosa by particulate matter: oxidant- and non-oxidant-mediated triggering mechanisms. *Biomolecules,* 5, 1399-1440.

Parmeggiani, L. (1983). Encyclopedia of Occupational and Health Safety, 3rd ed., vol. 2. International Labour Organization (ILO), Geneva, Switzerland.

Patial, R. K. (1999). Mountain desert silicosis. *Journal of the Association of Physicians of India,* 47, 503-504.

Pavan, C. and Fubini, B. (2016). Unveiling the variability of "Quartz Hazard" in light of recent toxicological findings. *Chemical Research in Toxicology,* 30, 469-485.

Perkins, T. N., Shukla, A., Peeters, P. M., et al. (2012). Differences in gene expression and cytokine production by crystalline vs. amorphous silica in human lung epithelial cells. *Particle and Fibre Toxicology,* 9, 2-18.

Petrilli, F., Rossi, G., Camoirano, A., et al. (1986). Metabolic reduction of chromium by alveolar macrophages and its relationships to cigarette smoke. *Journal of Clinical Investigation,* 77, 1917-1924.

Phakedi, S. S. N. (2011). *Population exposure to cyanide vapour from gold mine tailings dams.* MSc dissertation, University of Johannesburg, South Africa.

Pinto, S. and McGill, C. (1953). Arsenic trioxide exposure in industry. *Industrial Medicine and Surgery,* 22, 281-7.

Poland, G. A., Ovsyannikova, I. G., Kennedy, R. B., et al. (2014). A systems biology approach to the effect of aging, immunosenescence and vaccine response. *Current Opinion in Immunology,* 29, 62-68.

Polissar, L., Lowry-Coble, K., Kalman, D. A., et al. (1990). Pathways of human exposure to arsenic in a community surrounding a copper smelter. *Environmental Research,* 53, 29-47.

Pope, C. A., Burnett, R. T., Thurston, G. D., et al. (2004). Cardiovascular mortality and long-term exposure to particulate air pollution. *Circulation,* 109, 71-77.

Pope III, C. A., Burnett, R. T., Thun, M. J., et al. (2002). Lung cancer, cardiopulmonary mortality, and long-term exposure to fine particulate air pollution. *The Journal of the American Medical Association,* 287, 1132-1141.

Pope III, C. A., Rodermund, D. L. and Gee, M. M. (2007). Mortality effects of a copper smelter strike and reduced ambient sulfate particulate matter air pollution. *Environmental Health Perspectives,* 115, 679-683.

Pope III, C. A., Thun, M. J., Namboodiri, M. M., et al. (1995). Particulate air pollution as a predictor of mortality in a prospective study of US adults. *American Journal of Respiratory and Critical Care Medicine,* 151, 669-674.

Potkonjak, V. and Pavlovich, M. (1983). Antimoniosis: A particular form of pneumoconiosis. *International Archives of Occupational and Environmental Health,* 51, 199-207.

Pritchard, R. J., Ghio, A. J., Lehmann, J. R., et al. (1996). Oxidant generation and lung injury after particulate air pollutant exposure increase with the concentrations of associated metals. *Inhalation Toxicology,* 8, 457-477.

Prousek, J. (1995). Fenton reaction after a century. *Chemické Listy,* 89, 11-21.

Quent, V., Loessner, D., Friis, T., et al. (2010). Discrepancies between metabolic activity and DNA content as tool to assess cell proliferation in cancer research. *Journal of Cellular and Molecular Medicine,* 14, 1003-1013.

Rastogi, S. K. (2008). Renal effects of environmental and occupational lead exposure. *Indian Journal of Occupational and Environmental Medicine,* 12(3), 103–106.

Reddel, R. R., Yang, K., Rhim, J. S., et al. 1989. *Immortalized human bronchial epitherial mesothelial cell lines. US Patent Number: 4 885 238*

Rembuluwani, N., Dacosta, F. A. and Gumbo, J. R. (2014). Environmental risk assessment and risk management strategies for abandoned New Union Gold Mine in Malamulele, Limpopo, South Africa. *An Interdisciplinary Response to Mine Water Challenges - Sui, Sun & Wang (eds), China University of Mining and Technology Press, Xuzhou,* 367-373.

Renault, S., Sailerova, E. and Fedikow, M. (2001). Phytoremediation of mine tailings and bio-ore production: results from a study on plant survival at the Central Manitoba (Au) minesite (NTS 52L/13). *Report of Activities,* 138-149.

Renault, S., Szczerski, C., Sailerova, E., et al. (2004). Phytoremediation and revegetation of mine tailings and bio-ore production: progress report on plant growth in amended tailings and metal accumulation in seedlings planted at Central Manitoba (Au) minesite (NTS 52L/13). *Report of Activities,* 257-261.

RETSCH (2011). AS200 Air Jet Sieve User's Manual.

Rice, F., Park, R., Stayner, L., et al. (2001). Crystalline silica exposure and lung cancer mortality in diatomaceous earth industry workers: a quantitative risk assessment. *Occupational and Environmental Medicine,* 58, 38-45.

Rickard, D. (2015). *Pyrite: A Natural History of Fool's Gold,* Oxford University Press.

Rimola, A., Costa, D., Sodupe, M., et al. (2013). Silica Surface Features and Their Role in the Adsorption of Biomolecules: Computational Modeling and Experiments. *Chemical Reviews*, 113, 4216−4313.

Riss, T. L., Moravec, R. A., Niles, A. L., et al. (2016). *Cell viability assays*, Bethesda (MD): Eli Lilly & Company and the National Center for Advancing Translational Sciences.

Rodriguez, J. M. and Edeskär, T. (2013). Case of study on particle shape and friction angle on tailings. *Journal of Advanced Science and Engineering Research,* 3, 373-387.

Rohrs, L. C. (1957). Metal-fume fever from inhaling zinc oxide. *AMA Archives of Internal Medicine,* 100, 44-49.

Rosner, T. (1999). *The environmental impact of seepage from gold mine tailings dams near Johannesburg, South Africa.* PhD thesis, University of Pretoria, South Africa.

Rösner, T. (2001). A preliminary assessment of pollution contained in the unsaturated and saturated zone beneath reclaimed gold-mine residue deposits (WRC Report No 797/1/01). Water Research Commission, South Africa.

Rösner, T. and Van Schalkwyk, A. (2000). The environmental impact of gold mine tailings footprints in the Johannesburg region, South Africa. *Bulletin of Engineering Geology and the Environment*, 59, 137-148.

Rowens, B., Guerrero-Betancourt, D., Gottlieb, C. A., et al. (1991). Respiratory failure and death following acute inhalation of mercury vapor: a clinical and histologic perspective. *Chest,* 99, 185-190.

Ryu, J. E., Ziegler, E. E., Nelson, S. E., et al. (1983). Dietary intake of lead and blood lead concentration in early infancy. *American Journal of Diseases of Children*, 137, 886-891.

SA (2018). *South African Government Website, Constitution of the Republic of South Africa, 1996 - Chapter 2: Bill of Rights* [Online]. Available: https://www.gov.za/documents/constitution/chapter-2-bill-rights#24 [Accessed April 2018].

SAAQIS (2016). *The South African Air Quality Information System (SAAQIS) Home Page* [Online]. Available: http://www.saaqis.org.za/ [Accessed November 2016].

Sager, T. M. and Castranova, V. (2009). Surface area of particle administered versus mass in determining the pulmonary toxicity of ultrafine and fine carbon black: comparison to ultrafine titanium dioxide. *Particle and Fibre Toxicology*, 6, 15.

Sahaphong, S. and Trump, B. F. (1971). Studies of cellular injury in isolated kidney tubules of the flounder. V. Effects of inhibiting sulfhydryl groups of plasma membrane with the organic mercurials PCMB (parachloromercuribenzoate) and PCMB (parachloromercuribenzenesulfonate). *The American Journal of Pathology*, 63, 277-298.

Saiyed, H., Sharma, Y., Sadhu, H., et al. (1991). Non-occupational pneumoconiosis at high altitude villages in central Ladakh. *British Journal of Industrial Medicine*, 48, 825-829.

Samet, J. M., Graves, L. M., Quay, J., et al. (1998). Activation of MAPKs in human bronchial epithelial cells exposed to metals. *American Journal of Physiology-Lung Cellular and Molecular Physiology*, 275, L551-L558.

Samitz, M. (1970). Ascorbic acid in the prevention and treatment of toxic effects from chromates. *Acta Dermato-Venereologica*, 50, 59-64.

Samoli, E., Peng, R., Ramsay, T., et al. (2008). Acute effects of ambient particulate matter on mortality in Europe and North America: results from the APHENA study. *Environmental Health Perspectives*, 116, 1480-1486.

Sandström, A., Wall, S. and Taube, A. (1989). Cancer incidence and mortality among Swedish smelter workers. *British Journal of Industrial Medicine,* 46, 82-89.

Santarelli, L., Recchioni, R., Moroni, F., et al. (2004). Crystalline silica induces apoptosis in human endothelial cells *in vitro*. *Cell Biology and Toxicology,* 20, 97-108.

Sarsby, R. (2000). *Environmental Geotechnics*, Thomas Telford, London, p 440.

Schenker, M. B. (1998). Respiratory health hazards in agriculture. *American Journal of Respiratory and Critical Care Medicine,* 158(5 Pt 2), S1–S76.

Schindelin, J., Rueden, C. T., Hiner, M. C., et al. (2015). The ImageJ ecosystem: An open platform for biomedical image analysis. *Molecular Reproduction and Development,* 82, 518-529.

Schins, R. P., Knaapen, A. M., Weishaupt, C., et al. (2002). Cytotoxic and inflammatory effects of coarse and fine particulate matter in macrophages and epithelial cells. *Annals of Occupational Hygiene,* 46, 203-206.

Schneider, C. A., Rasband, W. S. and Eliceiri, K. W. (2012). NIH Image to ImageJ: 25 years of image analysis. *Nature Methods,* 9, 671-675.

Schober, S. E., Mirel, L. B., Graubard, B. I., et al. (2006). Blood lead levels and death from all causes, cardiovascular disease, and cancer: results from the NHANES III mortality study. *Environmental Health Perspectives,* 114, 1538-1541.

Schulte, E. (2004). Soil and Applied Iron. Understanding Plant Nutrients. A3554.

Schwartz, J., Landrigan, P. J., Baker Jr, E. L., et al. (1990). Lead-induced anemia: dose-response relationships and evidence for a threshold. *American Journal of Public Health,* 80, 165-168.

Scorgie, Y., Burger, L., Annegarn, H., et al. (2000). Background study for the development of an air quality management strategy for Gauteng: Characterisation of existing air quality and assessment of future trends and driving forces. Report compiled on behalf of the National Environmental Research Institute, Denmark, as part of a Danish Co-operation for Environment and Development (DANCED) project, Report No. MTX-00/NERI-01.

Sellamuthu, R., Umbright, C., Li, S., et al. (2011). Mechanisms of crystalline silica-induced pulmonary toxicity revealed by global gene expression profiling. *Inhalation Toxicology,* 23, 927-937.

Shi, T., Knaapen, A., Begerow, J., et al. (2003a). Temporal variation of hydroxyl radical generation and 8-hydroxy-2′-deoxyguanosine formation by coarse and fine particulate matter. *Occupational and Environmental Medicine,* 60, 315-321.

Shi, T., Schins, R. P., Knaapen, A. M., et al. (2003b). Hydroxyl radical generation by electron paramagnetic resonance as a new method to monitor ambient particulate matter composition. *Journal of Environmental Monitoring,* 5, 550-556.

Shirakawa, T., Kusaka, Y., Fujimura, N., et al. (1990). Hard metal asthma: cross immunological and respiratory reactivity between cobalt and nickel? *Thorax,* 45, 267-271.

Simoni, M., Baldacci, S., Maio, S., et al. (2015). Adverse effects of outdoor pollution in the elderly. *Journal of Thoracic Disease,* 7, 34-45.

SLR (2014). SLR Global Environmental Solutions. Air quality assessment *SLR Ref: 140826 501.00351.00002.Rev0*.

Smith, I. (2003). Mycobacterium tuberculosis pathogenesis and molecular determinants of virulence. *Clinical Microbiology Reviews,* 16, 463-496.

Snodgrass, W., Sullivan, J. B., Rumack, B. H., et al. (1981). Mercury poisoning from home gold ore processing: Use of penicillamine and dimercaprol. *The Journal of the American Medical Association,* 246, 1929-1931.

Song, S., Lee, K., Lee, Y.-M., et al. (2011). Acute health effects of urban fine and ultrafine particles on children with atopic dermatitis. *Environmental Research,* 111, 394-399.

Soni, J., Singhania, R., Bansal, A., et al. (1992). Acute mercury vapor poisoning. *Indian Pediatrics,* 29, 365-368.

Spech, R. W., Wisniowski, P., Kachel, D. L., et al. (2000). Surfactant protein A prevents silica-mediated toxicity to rat alveolar macrophages. *American Journal of Physiology-Lung Cellular and Molecular Physiology,* 278, L713-L718.

Stange, W. (1999). The process design of gold leaching and carbon-in-pulp circuits. *Journal of the South African Institute of Mining and Metallurgy(South Africa),* 99, 13-25.

Stanley, G. (1987). *The extractive metallurgy of gold in South Africa,* South African Institute of Mining and Metallurgy.

Steele, M. J., Beck, B. D., Murphy, B. L., et al. (1990). Assessing the contribution from lead in mining wastes to blood lead. *Regulatory Toxicology and Pharmacology,* 11, 158-190.

Steenhof, M., Gosens, I., Strak, M., et al. (2011). *In vitro* toxicity of particulate matter (PM) collected at different sites in the Netherlands is associated with PM composition, size fraction and oxidative potential-the RAPTES project. *Particle and Fibre Toxicology,* 8, 26.

Steenland, K. and Brown, D. (1995). Silicosis among gold miners: exposure--response analyses and risk assessment. *American Journal of Public Health,* 85, 1372-1377.

Steenland, K. and Goldsmith, D. F. (1995). Silica exposure and autoimmune diseases. *American Journal of Industrial Medicine,* 28, 603-608.

Stölzel, M., Breitner, S., Cyrys, J., et al. (2007). Daily mortality and particulate matter in different size classes in Erfurt, Germany. *Journal of Exposure Science and Environmental Epidemiology,* 17, 458-467.

Strober, W. (2001). Trypan blue exclusion test of cell viability. *Current Protocols in Immunology,* A3. B. 1-A3. B. 3.

Suciu, I., Prodan, L. and Lazar, V. (1981). Research on copper poisoning. *Medicina del Lavoro,* 72, 190-197.

Sundaram, P., Agrawal, K., Mandke, J., et al. (2001). Giant cell pneumonitis induced by cobalt. *Indian Journal of Chest Diseases and Allied Sciences,* 43, 47-50.

Sunderman Jr, F. W. and Horak, E. (1981). Biochemical indices of nephrotoxicity, exemplified by studies of nickel nephropathy. *Organ-Directed Toxicity,* 55-67.

Sundström, C. and Nilsson, K. (1976). Establishment and characterization of a human histiocytic lymphoma cell line (U- 937). *International Journal of Cancer,* 17, 565-577.

Sutton, M. and Weiersbye, I. Land use after mine closure–risk assessment of gold and uranium mine residue deposits on the Eastern Witwatersrand, South Africa. Proceeding of the Third International Conference on Mine Closure, Mine closure, 2008. 14-17.

Sutton, M. W. (2012). *Use of remote sensing and GIS in a risk assessment of gold and uranium mine residue deposits and identification of vulnerable land use.* MSc dissertation, University of the Witwatersrand, South Africa.

Swanepoel, A. J., Rees, D., Renton, K., et al. (2010). Quartz Exposure in Agriculture: Literature Review and South African Survey. *Annals of Occupational Hygiene*, 54, 281–292.

Swanepoel, A. J., Kromhout, H., Jinnah, Z. et al. (2011) Respirable dust and quartz exposure from three South African farms with sandy, sandy loam and clay soils. *Annals of Occupational Hygiene*, 55, 634–643.

Swanepoel, A. J. (2012) Exposure to respirable crystalline silica in central South African farm workers. PhD thesis, University of the Witwatersrand, South Africa.

Tamburlini, G., von Ehrenstein, O. S. and Bertollini, R. (2002). Children's health and environment: a review of evidence. World Health Organization Regional Office for Europe, European Environment Agency Copenhagen.

Tannenbaum, A., Silverstone, H. and Koziol, J. (1946). Tracer studies on the distribution and excretion of uranium in mice, rats, and dogs. U.S. Department of Energy Office of Scientific and Technical Information.

Taueg, C., Sanfilippo, D., Rowens, B., et al. (1992). Acute and chronic poisoning from residential exposures to elemental mercury-michigan, 1989–1990. *Journal of Toxicology: Clinical Toxicology,* 30, 63-67.

Thatcher, T. L. (1995). Deposition, resuspension and penetration of particles within a residence. *Atmospheric Environment*, 29, 1487-1497.

Thomas, B. (1968). The effect of the mining industry on public stream: Eighty years of mining and pollution prevention measures. *Association of Mine Managers (AMM) of South Africa,* 839-847.

Tomasek, L., Rogel, A., Tirmarche, M., et al. (2008). Lung cancer in French and Czech uranium miners: radon-associated risk at low exposure rates and modifying effects of time since exposure and age at exposure. *Radiation Research,* 169, 125-137.

TSI (2001). Product information sheet Model 3080 - Series Electrostatic Classifiers.

TSI (2004). Particle Instruments Model 3321 Aerodynamic Particle Sizer Spectrometer User's Manual.

TSI (2006). Aerosol Instrument Manager Software for APS Sensors User's Manual.

TSI (2007). Model 3772/3771 Condensation Particle Counter Operation and Service Manual

TSI (2010a). Aerosol Instrument Manager Software for Condensation Particle Counters, EPC Environmental Particle Counter Monitor, Water-based Condensation Particle Counters, and Electrical Aerosol Detector User's Manual.

TSI (2010b). Aerosol Instrument Manager Software for Scanning Mobility Particle Sizer (SMPS™) Spectrometer User's Manual.

TSI (2012). Small Scale Powder Disperser Model 3433 User's Manual.

TSI (2014). Data Merge Software Module Model 390069 User's Manual.

Turci, F., Pavan, C., Leinardi, R., et al. (2016). Revisiting the paradigm of silica pathogenicity with synthetic quartz crystals: the role of crystallinity and surface disorder. *Particle and Fibre Toxicology,* 13, 32.

Tutu, H., McCarthy, T. and Cukrowska, E. (2008). The chemical characteristics of acid mine drainage with particular reference to sources, distribution and remediation: The Witwatersrand Basin, South Africa as a case study. *Applied Geochemistry,* 23, 3666-3684.

USSilica (2010). Product data sheet - Min-U-Sil 5, USSilica Berkeley Springs, West Viginia.

Valavanidis, A., Fiotakis, K. and Vlachogianni, T. (2008). Airborne particulate matter and human health: toxicological assessment and importance of size and composition of particles for oxidative damage and carcinogenic mechanisms. *Journal of Environmental Science and Health, Part C,* 26, 339-362.

Vallyathan, V. (1994). Generation of oxygen radicals by minerals and its correlation to cytotoxicity. *Environmental Health Perspectives,* 102, 111-115.

Vallyathan, V. and Shi, X. (1997). The role of oxygen free radicals in occupational and environmental lung diseases. *Environmental Health Perspectives,* 105, 165-177.

van Maanen, J. M., Borm, P. J., Knaapen, A., et al. (1999). *In vitro* effects of coal fly ashes: hydroxyl radical generation, iron release, and DNA damage and toxicity in rat lung epithelial cells. *Inhalation Toxicology,* 11, 1123-1141.

Van Niekerk, H. and Viljoen, M. (2005). Causes and consequences of the Merriespruit and other tailings- dam failures. *Land Degradation & Development,* 16, 201-212.

Veranth, J. M., Moss, T. A., Chow, J. C., et al. (2006). Correlation of *in vitro* cytokine responses with the chemical composition of soil-derived particulate matter. *Environmental Health Perspectives,* 114, 341-349.

Veranth, J. M., Reilly, C. A., Veranth, M. M., et al. (2004). Inflammatory cytokines and cell death in BEAS-2B lung cells treated with soil dust, lipopolysaccharide, and surface-modified particles. *Toxicological Sciences,* 82, 88-96.

Vermeulen, N. J. (2007). *The composition and state of gold tailings.* PhD thesis, University of Pretoria, South Africa.

Verstraelen, S., Bloemen, K., Nelissen, I., et al. (2008). Cell types involved in allergic asthma and their use in *in vitro* models to assess respiratory sensitization. *Toxicology In Vitro,* 22, 1419-1431.

Vida, S., Pintos, J., Parent, M.-É., et al. (2010). Occupational exposure to silica and lung cancer: pooled analysis of two case-control studies in Montreal, Canada. *Cancer Epidemiology Biomarkers & Prevention,* 19, 1602-1611.

Vincent, J. H. (2005). Health-related aerosol measurement: a review of existing sampling criteria and proposals for new ones. *Journal of Environmental Monitoring,* 7, 1037-1053.

Vogelmeier, C., Bencze, K. and Fruhmann, G. (1987). Pulmonary involvement in zinc fume fever. *CHEST Journal,* 92, 946-948.

Volckens, J., Dailey, L., Walters, G., et al. (2009). Direct particle-to-cell deposition of coarse ambient particulate matter increases the production of inflammatory mediators from cultured human airway epithelial cells. *Environmental Science & Technology,* 43, 4595-4599.

Von Klot, S., Wölke, G., Tuch, T., et al. (2002). Increased asthma medication use in association with ambient fine and ultrafine particles. *European Respiratory Journal,* 20, 691-702.

Von Rahden, H. (1970). *Mineralogical and geochemical studies of some witwatersrand gold ores with special reference to the nature of the phyllosilicates.* PhD thesis, University of the Witwatersrand, South Africa.

von Schirnding, Y., Mathee, A., Kibel, M., et al. (2003). A study of pediatric blood lead levels in a lead mining area in South Africa. *Environmental Research,* 93, 259-263.

Vuong, N. Q., Goegan, P., De Rose, F., et al. (2017). Responses of A549 human lung epithelial cells to cristobalite and α- quartz exposures assessed by toxicoproteomics and gene expression analysis. *Journal of Applied Toxicology,* 37, 721-731.

Vupputuri, S., Parks, C. G., Nylander-French, L. A., et al. (2012). Occupational silica exposure and chronic kidney disease. *Renal failure,* 34, 40-46.

Wagener, F. (1997). The Merriespruit slimes dam failure: overview and lessons learnt: technical paper. *Journal of the South African Institution of Civil Engineering,* 39, 11-15.

Wedeen, R. (1991). Renal diseases of occupational origin. *Occupational Medicine,* 7, 449-463.

Welch, K., Higgins, I., Oh, M., et al. (1982). Arsenic exposure, smoking, and respiratory cancer in copper smelter workers. *Archives of Environmental Health: An International Journal,* 37, 325-335.

Wexler, J., Whittenberger, J. L. and Dumke, P. R. (1947). The effect of cyanide on the electrocardiogram of man. *American Heart Journal,* 34, 163-173.

WHO (2005). Air Quality Guidelines: Global Update 2005: Particulate Matter, Ozone, Nitrogen Dioxide, and Sulfur Dioxide. World Health Organization.

WHO (2010). World Health Organization. Childhood lead poisoning.

Wichmann, H.-E., Spix, C., Tuch, T., et al. (2000). Daily mortality and fine and ultrafine particles in Erfurt, Germany part I: role of particle number and particle mass. *Research report (Health Effects Institute),* 5-86; discussion 87-94.

Williams, P. R. and Paustenbach, D. J. (2002). Risk characterization: Principles and practice. *Journal of Toxicology and Environmental Health Part B: Critical Reviews,* 5, 337-406.

Woodward, A., Roder, D., McMichael, A. J., et al. (1991). Radon daughter exposures at the Radium Hill uranium mine and lung cancer rates among former workers, 1952–87. *Cancer Causes & Control,* 2, 213-220.

Wright, C., Matooane, M., Oosthuizen, M., et al. (2014). Risk perceptions of dust and its impacts among communities living in a mining area of the Witwatersrand, South Africa. *Clean Air Journal,* 24, 22-27.

Xenidis, A., Papassiopi, N. and Komnitsas, K. (2003). Carbonate-rich mining tailings in Lavrion: risk assessment and proposed rehabilitation schemes. *Advances in Environmental Research,* 7, 479-494.

Xiang-Zhen, X., Lubin, J. H., Jun-Yao, L., et al. (1993). A cohort study in southern China of tin miners exposed to radon and radon decay products. *Health Physics,* 64, 120-131.

Yáñez, L., García-Nieto, E., Rojas, E., et al. (2003). DNA damage in blood cells from children exposed to arsenic and lead in a mining area. *Environmental Research,* 93, 231-240.

Yoder, C. H. (2006). Appendix 4: Quartz. *Ionic Compounds: Applications of Chemistry to Mineralogy*, 173-175.

Young, D. S., Sachais, B. S. and Jefferies, L. C. (1993). The rietveld method.

Zalups, R. K. and Lash, L. H. (1994). Advances in understanding the renal transport and toxicity of mercury. *Journal of Toxicology and Environmental Health, Part A Current Issues,* 42, 1-44.

Zanelli, R., Barbic, F., Migliori, M., et al. (1994). Uncommon evolution of fibrosing alveolitis in a hard metal grinder exposed to cobalt dusts. *Science of the Total Environment,* 150, 225-229.

Zhang, Q., Dai, J., Ali, A., et al. (2002). Roles of bioavailable iron and calcium in coal dust-induced oxidative stress: possible implications in coal workers' lung disease. *Free Radical Research,* 36, 285-294.

Zhang, Q. and Huang, X. (2003). Induction of interleukin-6 by coal containing bioavailable iron is through both hydroxyl radical and ferryl species. *Journal of Biosciences,* 28, 95-100.